

Burr minimization of superalloys in micromilling

BY

Mohan Kumar

(Admission No: 16DR000230)



THESIS

SUBMITTED TO

**INDIAN INSTITUTE OF TECHNOLOGY
(INDIAN SCHOOL OF MINES) DHANBAD**

For the award of the degree of

DOCTOR OF PHILOSOPHY

JANUARY, 2022



Form No: PH13

INDIAN INSTITUTE OF TECHNOLOGY (INDIAN SCHOOL OF MINES) DHANBAD

CERTIFICATE FROM THE SUPERVISOR(S)

(To be submitted at the time of Thesis Submission)

This is to certify that the thesis entitled “**Burr minimization of superalloys in micromilling**” being submitted to the Indian Institute of Technology (Indian School of Mines), Dhanbad by Mr **Mohan Kumar**, Admission No **16DR000230**, for the award of Doctor of Philosophy (Ph.D.) Degree is a bonafide work carried out by him/her, in the Department of **mechanical engineering**, IIT (ISM), Dhanbad, under my/our supervision and guidance. The thesis has fulfilled all the requirements as per the regulations of this Institute and, in my/our opinion, has reached the standard needed for submission. The results embodied in this thesis have not been submitted to any other university or institute for the award of any degree or diploma.

Vivek Bajpai

Signature of Supervisor (s)

Name: ___Prof. Vivek Bajpai_____

Date: ___31/01/22_____



Form No: PH11

INDIAN INSTITUTE OF TECHNOLOGY (INDIAN SCHOOL OF MINES) DHANBAD

CERTIFICATE FOR CLASSIFIED DATA

(To be submitted at the time of Thesis Submission)

This is to certify that the thesis entitled “**Burr minimization of superalloys in micromilling**” being submitted to the Indian Institute of Technology (Indian School of Mines), Dhanbad by Mr **Mohan Kumar** for award of Doctor of Philosophy (Ph.D) Degree in **Mechanical Engineering** does not contains any classified information. This work is original and yet not been submitted to any institution or university for the award of any degree.

Vivek Singh

Signature of Supervisor (s)

Mohan Kumar

Signature of Scholar

Form No: PH10

INDIAN INSTITUTE OF TECHNOLOGY (INDIAN SCHOOL OF MINES) DHANBAD

COPYRIGHT AND CONSENT FORM

(To be submitted at the time of Thesis Submission)

To ensure uniformity of treatment among all contributors, other forms may not be substituted for this form, nor may any wording of the form be changed. This form is intended for original material submitted to the IIT (ISM), Dhanbad and must accompany any such material in order to be published by the ISM. Please read the form carefully and keep a copy for your files.

TITLE OF THESIS: Burr minimization of superalloys in micromilling

AUTHOR'S NAME & ADDRESS: Mohan Kumar, Vill + PO = Darihat, Dist-Rohtas,

Bihar, PIN-821306

COPYRIGHT TRANSFER

1. The undersigned hereby assigns to Indian Institute of Technology (Indian School of Mines), Dhanbad all rights under copyright that may exist in and to: (a) the above Work, including any revised or expanded derivative works submitted to the ISM by the undersigned based on the work; and (b) any associated written or multimedia components or other enhancements accompanying the work.

CONSENT AND RELEASE

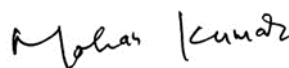
2. In the event the undersigned makes a presentation based upon the work at a conference hosted or sponsored in whole or in part by the IIT (ISM) Dhanbad, the undersigned, in consideration for his/her participation in the conference, hereby grants the ISM the unlimited, worldwide, irrevocable permission to use, distribute, publish, license, exhibit, record, digitize, broadcast, reproduce and archive; in any format or medium, whether now known or hereafter developed: (a) his/her presentation and comments at the conference; (b) any written materials or multimedia files used in connection with his/her presentation; and (c) any recorded interviews of him/her (collectively, the "Presentation"). The permission granted includes the transcription and reproduction of the Presentation for inclusion in products sold or

distributed by IIT(ISM) Dhanbad and live or recorded broadcast of the Presentation during or after the conference.

3. In connection with the permission granted in Section 2, the undersigned hereby grants IIT (ISM) Dhanbad the unlimited, worldwide, irrevocable right to use his/her name, picture, likeness, voice and biographical information as part of the advertisement, distribution and sale of products incorporating the Work or Presentation, and releases IIT (ISM) Dhanbad from any claim based on right of privacy or publicity.
4. The undersigned hereby warrants that the Work and Presentation (collectively, the "Materials") are original and that he/she is the author of the Materials. To the extent the Materials incorporate text passages, figures, data or other material from the works of others, the undersigned has obtained any necessary permissions. Where necessary, the undersigned has obtained all third party permissions and consents to grant the license above and has provided copies of such permissions and consents to IIT (ISM) Dhanbad.



Signature of Supervisor (s)



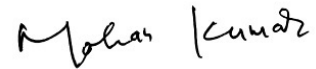
Signature of Scholar

GENERAL TERMS

- * The undersigned represents that he/she has the power and authority to make and execute this assignment.
- * The undersigned agrees to indemnify and hold harmless the IIT (ISM) Dhanbad from any damage or expense that may arise in the event of a breach of any of the warranties set forth above.
- * In the event the above work is not accepted and published by the IIT (ISM) Dhanbad or is withdrawn by the author(s) before acceptance by the IIT(ISM) Dhanbad, the foregoing copyright transfer shall become null and void and all materials embodying the Work submitted to the IIT(ISM) Dhanbad will be destroyed.
- * For jointly authored Works, all joint authors should sign, or one of the authors should sign as authorized agent for the others.



Signature of Supervisor (s)



Signature of the Author

Dedicated to my beloved parents

Shri. Madan Pal,

And

Smt. Kunti Devi

ACKNOWLEDGEMENTS

I am grateful to all people who provided me their colossal support during my doctoral study.

I wish to express my sincere thanks and deep sense of gratitude to my thesis advisor **Dr. Vivek Bajpai** for introducing me to this exciting topic. I would also like to thank him for his valuable guidance, encouragement and freedom they gave me throughout the course of my work. His constant energy and immense enthusiasm in research always motivated me. I experienced both ups and downs, good and bad times in my life during the stay in IIT (ISM), Dhanbad. He was always there for me to support and encourage. I am thankful to him for the excellent research facilities provided by him and also his willingness to spare his precious time for research discussions and clarifying my doubts. I acknowledge the constant encouragement and advice he has given me not only towards research but also for personal life.

I am extremely thankful to the members of my Doctoral Scrutiny Committee, **Dr. Nirmal Kumar Singh, Dr. R.R. Das**. I would also thank **Prof. S. Narayanan** Chairman, Doctoral Scrutiny Committee, for their constant encouragement and support. I also thank **Prof. Rajiv Shekhar**, Director, IIT (ISM), Dhanbad for providing the necessary infrastructure and facilities for the research work during the period of study.

I express my sincere thanks to **Prof. RK Das, Dr. Amit Dixit, Dr. Deepak Mandal** All of them have always been very kind and cooperative with me.

I also thank all **faculties** and **staff members** in the Department of Mechanical Engineering, IIT(ISM) who associated with me during this study directly and indirectly to support me during the preparation of the thesis.

I individually thank all of my lab mates **Rachit Ranjan, Deepak Kumar, Shashank Shukla, Ankit Jain, Ravi Shankar Rai, Arnab das, Rajesh Raj Sahoo** for their help and support during my research period.

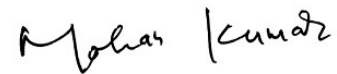
I individually thank my dearest friends Sawan Kumar, Vikas Kumar, Abhijeet Raj, Ramesh Kumar, Lukesh Kumar, Nikesh Sahoo, Chitransh Singh who shared their knowledge with me various aspects. I also thank all of my lab mates for their help and support during my research period.

This dissertation would have been impossible without the support of my family. I express my deepest gratitude to my family for their love and support throughout my life. I am indebted to my late uncle **Sri Shiv Mangal Pal**, father **Sri Madan Pal**, my mother **Smt. Kunti Devi**, my elder brothers **Sri Shasi Kant Pal & Mantu Pal** and for their care and love. I have no suitable word that can fully describe their everlasting love to me.

Last but not least, I thank almighty God for being with me all the times. May your name be honoured, and glorified.

Funding support:

This research work has been financially supported by Department of Science and Technology (DST), India under project number DST(SERB)/533/2017-18/Mechanical Engineering (File No. ECR/2016/001956). An instrument from the FIST grant has been used in the thesis: project sanction number: SR/FST/ET-II/2018/222(C) date: 14 March 2019 for the Mechanical Engineering Department.



(MOHAN KUMAR)

Place: IIT (ISM), Dhanbad

Date: 31-01-2022

Contents

Chapter: 1	INTRODUCTION	1
1.1	Need and scope of micromilling	1
1.2	Micromilling, issues and their applications	1
1.2.1	Burr formation	4
1.2.2	Need for burr minimization.....	4
1.3	Aim and objectives	5
1.4	Research novelty and originality.....	6
1.5	Industrial importance	6
1.6	Organization of thesis	6
Chapter: 2	LITERATURE SURVEY	9
2.1	Micromachining of Superalloys.....	9
2.1.1	Heat generation on micromachining superalloys.....	12
2.2	Burr minimization methods in micromilling:	14
2.2.1	Tool geometry and tool path optimizations	14
2.2.2	Mechanism of burr formation in Micromilling.....	15
2.2.3	Cooling and Lubrication:	18
2.2.4	High-speed micromachining	29
2.3	Literature outcome	31
2.4	Research methodology	31
Chapter: 3	EXPERIMENTAL SETUP.....	33
3.1	Basic setup (Model V-60).....	33
3.1.1	Design considerations for micro machining center have been done on the following points: 33	
3.2	Design methodology	33
3.2.1	Design and analysis of optimum prototype machine tool.....	43
3.3	High-speed micromachining setup (HSM)	52
3.4	Minimum quantity lubrication (MQL) assisted micromachining setup.....	53
3.5	Summary	54
Chapter: 4	MECHANISM OF TOP BURR FORMATION	56
4.1	Introduction.....	56
4.2	Motivation, objective, and approach.....	56
4.3	Top burr formation mechanism in micromilling (Theoretical approach)	57
	Initiation, propagation, and formation of top burr	58
4.4	Experimental Validation	61
4.4.1	Design of experiment (DOE)	61
4.5	Results and discussions.....	63
4.5.1	Mechanism of burr formation	63
4.5.2	Effect of radial depth of cut on down milling top burr	67

4.5.3	Effect of axial depth of cut and feed per tooth (ANOVA).....	68
4.6	Summary	70
Chapter: 5	HIGH-SPEED MICROMACHINING.....	71
5.1	Introduction.....	71
5.2	Motivation, objective, and approach.....	71
5.3	Experimental details.....	72
5.4	Experimental setup and procedure	74
	Results and discussions.....	75
5.4.1	Measurement of burr.....	75
5.4.2	Top burr characterization and analysis	76
5.4.3	Burr generation at traditional speed.....	76
5.4.4	Burr generation at high-speed cutting.....	76
5.4.5	Parametric study.....	77
5.5	Summary	80
Chapter: 6	BURR MINIMIZATION OF Ti6Al4V ALLOY USING COOLANT and LUBRICANT 82	
6.1	Introduction.....	82
6.2	Motivation, objective & approach	82
6.3	Experimental details.....	84
6.3.1	Characterization of emulsion-based cutting fluids.....	84
6.3.2	Characterization of nano lubricant based cutting fluid	86
6.3.3	Design of experiment for the first set of experiments (emulsion):	90
6.3.4	Design of experiment for the second set of experiments (nano lubricant):.....	91
6.3.5	Optimization Methodology	91
6.4	Results and Discussion.....	92
6.4.1	Effect of emulsion lubricant on the top burr formation	92
6.4.2	Effect of nanofluid on the top burr.....	97
6.4.3	Comparative analysis of the effect of emulsion and nanofluid:.....	101
6.5	Summary	102
Chapter: 7	BURR MINIMIZATION OF INCONEL718 USING COOLANT and LUBRICANT 103	
7.1	Introduction.....	103
7.2	Motivation, objective, and approach.....	103
7.3	Experimental details.....	104
7.3.1	Design of experiment for the first set of experiments (emulsion):	104
7.3.2	Design of experiment for the second set of experiments (nano lubricant):.....	105
7.4	Optimization Methodology	105
7.5	Results and Discussion.....	105
7.5.1	Effect of emulsion lubricant on the top burr formation	105
7.5.2	Effect of nano-fluid on the top burr	110

7.5.3	Comparative analysis of the effect of emulsion and nanofluid:.....	115
7.6	Summary	116
Chapter: 8	CONCLUSION AND FUTURE SCOPE	118
8.1	The main conclusion of the thesis.....	118
8.1.1	Experimental setup.....	118
8.1.2	Mechanism of top burr formation	119
8.1.3	High-speed micromachining	119
8.1.4	Application of COOLANT and LUBRICANT in the machining of superalloys.....	119
8.2	Contribution	121
8.3	Future scope	121

List of Figures

Figure 1.1: Schematic representation of milling process(Ref 5).....	2
Figure 1.2: Applications of micromilling(Ref 16–18)(Ref 19)	3
Figure 1.3: SEM image showing burr formation in micromilling	4
Figure 1.4: Assembly parts of gear(Ref 21).....	5
Figure 1.5: Thesis structure.....	8
Figure 2.1: Literature review topics.....	9
Figure 2.2: (a) Superalloy’s consumption (b) Distribution of difficult to machine metal alloys(Ref 22)	10
Figure 2.3: Comparison of machinability of superalloys with other metal alloys(Ref 38).....	12
Figure 2.4: Sources of heat generation in machining(Ref 30).	14
Figure 2.5: Tool path strategies for minimizing and preventing burrs in face milling(Ref 56).....	14
Figure 2.6: (a) Conventional tool path for face milling engine block face and resulting burrs at key locations (b) Modified tool path for part(c)Workpiece resulting from optimized tool path; Tool path length: old path – 209 mm, a new path – 524 mm, cycle time with increased feed rate remain at 5sec.	15
Figure 2.7: Types of burr based on mechanism of formation(Ref 58).....	16
Figure 2.8: Eight types of burr formed in milling operation(Ref 60).....	16
Figure 2.9: Burrs control mechanism in micromilling. (a) Extending workpiece boundaries with supporting material. (b) The crack grows on the support material. (c) Burrs formation on the support material. (e) The process of burr control(Ref 63)	17
Figure 2.10: Ti6Al4V machining experiments: Simulation(a,b) and experimental(c,d) results for conventional and vibration-assisted micro milling	18
Figure 2.11: Manufacturing cost distribution in the European automotive industry(Ref 74).....	19
Figure 2.12: Classifications of cutting fluids(Ref 77).....	20
Figure 2.13: Conventional cutting fluids life cycle with their impact on surroundings(Ref 83)	23
Figure 2.14: Schematic of cutting fluid supply system used in modern industry	24
Figure 2.15: Random supply of cutting fluid in flood cooling system(Ref 89).....	24
Figure 2.16: Schematic diagram representing MQL using cryogenic coolant(Ref 91)	25
Figure 2.17: 3D surface plot with SEM images of burr formation after micromilling ($a_p=0.15$ mm)(Ref 94).....	26
Figure 2.18: SEM images of burr formation after micromilling ($a_p=0.15$ mm)(Ref 91)	27
Figure 2.19: Hybrid micromachining setup(Ref 96)	28
Figure 2.20: SEM images of burr under different cutting conditions(Ref 96)	28
Figure 2.21: Recommended high-speed range for different materials(Ref 103)	30

Figure 2.22: Burr formation at cutting speed (rpm) (a) 50,000; (b) 1,00,000; (c) 1,50,000 (d) 2,00,000 with constant feed (5 mm/sec), depth of cut(10 μ m), tool diameter (0.5 mm)(Ref 68).....	31
Figure 3.1: Architecture of the machine tool	34
Figure 3.2: Design methodology of micromilling machine	35
Figure 3.3: View of Spindle.....	38
Figure 3.4: CAD drawing of linear X (or Y) stage	40
Figure 3.5: CAD drawing of linear z-stage.....	41
Figure 3.6: (a) Linearly motorized XY-stage (b) Linearly motorized Z-stage	41
Figure 3.7: Two different prototypes of the machine tool(a)Prototype-I (b) Prototype-I.....	42
Figure 3.8: Fishbone diagram for machine tool performance.....	43
Figure 3.9: CAD models of base(machine bed) and frame.....	44
Figure 3.10: CAD model and drawings of spindle holding mount(SHM).....	45
Figure 3.11: CAD model of assembled machine tool.....	46
Figure 3.12: (a)Total deformation(m) and (b)equivalent stress (Pa) of static structural analysis.....	47
Figure 3.13: Comparison of natural frequencies of the unassembled frame using natural granite and cast iron determined in modal analysis	47
Figure 3.14: Natural frequencies of the assembled micro-milling machine tool determined in modal analysis.....	48
Figure 3.15: Mode Shapes in modal analysis	49
Figure 3.16: Results of harmonic response analysis	50
Figure 3.17: Basic experimental setup of micromachining	50
Figure 3.18: Schematic of the experimental setup	51
Figure 3.19: MACH3 loader software(Ref 110).....	51
Figure 3.20:high-speed micromachining (HSM) setup	52
Figure 3.21: Syringe Pump	53
Figure 3.22: Nozzle for Mist Coolant Spray unit.....	54
Figure 3.23: MQL assisted micromachining setup.....	54
Figure 4.1: (a)Top view of the interaction of two flute end milling tool with workpiece (b) Detailed view of entry and exit of the flutes of end milling tool (c)Simplified view of entry with increasing depth of cut and exit with decreasing depth of cut.....	58
Figure 4.2: Stages of top burr formation: Initiation, propagation, and formation.....	60
Figure 4.3: (a) Experimental setup (b) Tool path planning.....	62
Figure 4.4: Mechanism of micromilling under different cutting depth conditions: (a & b) rubbing/burnishing (c) ploughing (d) cutting((Ref 13)).....	62
Figure 4.5: 3D profilometer image showing tool path interaction during the formation of top burr in up and down milling	63

Figure 4.6: SEM image showing the formation of curly burrs (V_c :10,000 rpm, f :4 $\mu\text{m}\cdot\text{tooth}^{-1}$, D_c :60 μm).....	65
Figure 4.7: SEM image showing the formation of longitudinal burrs(V_c :10,000 rpm, f :6 $\mu\text{m}\cdot\text{tooth}^{-1}$, D_c :60 μm).....	66
Figure 4.8: SEM image showing the formation of continuous serrated burrs (V_c :10,000 rpm, f :8 $\mu\text{m}\cdot\text{tooth}^{-1}$, D_c : 60 μm).....	67
Figure 4.9: Effect of radial depth of cut on top burr formation	68
Figure 4.10: Main effects plot for down milling burr width in comparison to process parameters.....	69
Figure 5.1: Flow chart of the experiment	72
Figure 5.2: Microstructure of Ti6Al4V alloy.....	73
Figure 5.3: Scanning electron microscopy (SEM) image of top burr generation in Ti6Al4V.....	75
Figure 5.4: Burr formation (a) traditional cutting speed (b) high-speed cutting.....	77
Figure 5.5: Variation in the equivalent width in up and down milling with (a) Cutting speed; (b) feed rate (c) depth of the cut.....	79
Figure 5.6: Variation in the equivalent width of up and down milling burr width by (a) Diameter of tool (b) No. of flute.....	80
Figure 6.1: Servo cut s lubricant with specification details	85
Figure 6.2: Variations of viscosity with increase in concentration (oil-water)	85
Figure 6.3: Morphology of nanoparticles (a) FESEM image at 120 k X (b) EDX analysis.....	86
Figure 6.4: XRD analysis of CuO nanoparticle.....	87
Figure 6.5: Schematic of preparation of nanofluid	87
Figure 6.6: Chronology of preparation of nanofluid.....	88
Figure 6.7: Zeta potential of CuO nanofluid (0.3%) versus frequency.....	89
Figure 6.8: Influence of nanoparticle concentration with variation in (a) Thermal conductivity (b) viscosity	90
Figure 6.9: Main effects plot for up milling.....	93
Figure 6.10: Main effects plot for down milling.....	93
Figure 6.11: SEM images of top burr formation in up and down micromilling at V_c =25.13 m/m, f =5 $\mu\text{m}\cdot\text{tooth}^{-1}$, D_c =40 μm	94
Figure 6.12: Main effects plot for OEC	95
Figure 6.13: SEM image at optimum condition.....	96
Figure 6.14 : The main effects plots of input parameters on equivalent top burr width (up milling)...	97
Figure 6.15: The main effects plots of input parameters on equivalent top burr width (down milling)98	
Figure 6.16: SEM images of top burr formation after up or down micromilling at v_c =25.13 m/min, f =5 $\mu\text{m}\cdot\text{tooth}^{-1}$, D_c =40 μm	98
Figure 6.17: variation of OEC with input parameters.....	100

Figure 6.18: SEM image at optimum condition.....	100
Figure 6.19: SEM image showing comparative analysis of equivalent top burr width with best (a) dry; (b) emulsion (1:20) and nanofluid (0.2%wt)	101
Figure 7.1: Main effects plot for up milling.....	106
Figure 7.2: Main effects plot for down milling.....	106
Figure 7.3: SEM images of top burr formation in up and down micromilling at $V_c=25.13$ m/m, $f=6$ $\mu\text{m}\cdot\text{tooth}^{-1}$, $D_c=50$ μm	107
Figure 7.4: Main effects plot for OEC	109
Figure 7.5: SEM image at optimum condition.....	110
Figure 7.6: Main effects plot for up milling.....	111
Figure 7.7: Main effects plot for down milling.....	112
Figure 7.8: SEM images of top burr formation after up or down micromilling at $v_c=25.13$ m/min, $f=6$ $\mu\text{m}\cdot\text{tooth}^{-1}$, $D_c=50$ μm	112
Figure 7.9: SEM image showing variation of top burr width with depth of cut (constant parameter: 0.1% NF, $f=6$ $\mu\text{m}\cdot\text{tooth}^{-1}$)	113
Figure 7.10: SEM image showing a variation of top burr width with feed rate (Constant Parameters: 0.1% NF, $D_c=50$ μm)	113
Figure 7.11: variation of OEC with input parameters.....	114
Figure 7.12: SEM image at optimum condition.....	115
Figure 7.13: SEM image showing comparative analysis of equivalent top burr width with best (a) dry; (b) emulsion (1:20)and nanofluid (0.3%wt)	116

List of Tables

Table 1: Comparison of material properties	35
Table 2: Comparison of capabilities of Bearings(Ref 109)	37
Table 3: Technical Specification of Spindle(Ref 44).....	38
Table 4: Desired specifications for the linear stages.....	39
Table 5: Stage selection requirement and solution	39
Table 6: Machine XYZ stage specifications	41
Table 7: Mechanical properties of the materials involved in FEA	46
Table 8: Input parameters and their levels	61
Table 9: Full factorial experiments with output response.....	68
Table 10: ANOVA table for down milling burr	69
Table 11: List of experimental parameters	74
Table 12: Detail of experiments	74
Table 13: Physical properties of copper oxide nanoparticles.....	86
Table 14: Input parameters and their levels	91
Table 15: Input parameters and their levels	91
Table 16: Response measures with QC and relative assigned weight along with OEC values	96
Table 17: Optimal test results	96
Table 18: Response measures with QC and relative assigned weight along with OEC values.....	99
Table 19: Optimal test results	100
Table 20: Comparison of output response of the two cutting fluids (optimum combination)	101
Table 21: Input parameters and their levels	104
Table 22: Input parameters and their levels	105
Table 23: Response measures with QC and relative assigned weight along with OEC values	110
Table 24: Response measures with QC and relative assigned weight along with OEC values....	114
Table 25: Optimal test results	115
Table 26: Comparison of output response of the two cutting fluids (optimum combination)	116

SYMBOLS AND ABBREVIATIONS

Abbreviations

ANOVA: Analysis of variance

BL: Base Lubricant (emulsion)

BUE: Built-up Edge

CAD: Computer Aided Design

CC: Cutting Condition

CR: Contribution Ratio

DOE: Design of Experiment

EM: Emulsion

FE: Finite Element

HSM: High-speed Micromachining

HSMM: High-speed Micromachine

LIGA: Lithographie, Galvanoformung, Abformung

MEMS: Micro-electro Mechanical System

MQL: Minimum Quantity Lubrication

MRR: Material Removal Rate

MSS: Mean sum square

MTL: Machine Tool Laboratory

NF: Nanofluid (nano lubricant)

NL: Nano-lubricant

OEC: Overall Evaluation Criteria

QC: Quality Characteristics

SDBS: Sodium Dodecylbenzene Sulphonate

SDS: Sodium Dodecyl Sulphate

SEM: Scanning Electron Microscopy

SS: Sum of square

WC: Tungsten Carbide

Symbols

CuO: Copper Oxide

Dc: Axial depth of Cut

f: Feed

fr: Feed rate

N: Spindle speed

Rc: radial depth of cut

re: Tool edge radius

SS_{res}: Residual Sum of square

SS_{total}: Total Sum of square

t_c: Minimum chip thickness

V_c : Cutting speed

W_b : Equivalent Burr Width

Y': The sample mean of i number of observations

Y_i: ith observation in the group where i=1,2,3.....n

Z: Number of flute

ABSTRACT

Superalloys have exceptional mechanical and chemical properties and therefore, they are extensively used in advanced machinery. Milling and Micromilling have been proven to be the most versatile mechanical micromachining to produce 3D-micro features on such material. Despite of the excellent material properties, superalloys possess poor machinability. Low thermal conductivity and diffusivity leads to high machining temperature, thus low tool life and burr formation with poor surface finish occur in machining. Burrs are extremely undesired and they become more critical in micro parts. In the current study the aim is to minimize the top burr formed during micromilling of super alloys. Literature showed that the high-speed cutting and lubrication may helpful in reducing the machining forces and thus beneficial for burr minimization. The high-speed cutting and lubrication/coolant are easy to apply in conventional cutting. Achieving high-speed cutting with a small diameter milling tool of few micro meter is difficult due to the limitation in the spindle speed. Therefore, to attain the objective a high-speed micro machining (10,000-60,000 rpm) centre has been designed and developed from the scratch in-house and used for the machining purpose with minimum vibration. The second issue was with the cooling and lubricating. The small size of the micro tool does not allow a liquid coolant to insert between the tool-chip interaction. Therefore, MQL has been designed with two cutting fluids: emulsion (oil-water) and nano fluid (nano particles-water). The MQL arrangement has been installed with the high-speed micro machining centre as a feature of the instrument. The experimental setup and instruments have been explained in chapter-3.

Three methods have been used to accomplish the task of burr minimization: By understanding the mechanism of top burr formation, high-speed micromachining (HSM), and MQL. The radial depth of cut has been varied continuously with the cutting path to understand the top burr formation on Ti6Al4V, which showed very less effect of the variation of radial depth of cut, although, analysis showed the top burr formation mechanism. In addition effect of axial depth of cut and feed per tooth has been analysed in the section. The high-speed micromilling has been performed on Ti6Al4V. It is found that the high-speed machining reduces the burr size. The burr size was reduced by up to 40% in high-speed cutting. MQL showed interesting results, where, the burrs have been reduced by up to 81%. The detailed effect of high-speed cutting and various concentrations of the cutting fluid is explored in the present work.

Keywords: Micromilling, Ti6Al4V, Inconel 718, Up milling, Down milling, Top burr, Equivalent burr width, Nanofluid, Overall evaluation criteria (OEC)

Chapter: 1 INTRODUCTION

This chapter gives a brief introduction about the basics of micromilling, research background, and motivation of issues relevant to burr formation of superalloys with an emphasis to minimize it to a maximum extent. Further, it also covers the aims and objectives, scope, and organization of this thesis.

1.1 Need and scope of micromilling

In today's scenario, Micromachining technology is one of the most advance manufacturing techniques which is great in demand and will remain active in upcoming years. Although this technology was initially originated from the electronics sector, currently it has been covering almost all fields ranging from aerospace, defence, automobiles, sensors to computation and control systems i.e., optical, MEMS (micro-electro-mechanical systems), magnetic, chemical, and biomedical fields(Ref 1). This is mainly due to the rising demand for miniaturization in these industries. Innovation of this technology has given the opportunities to scale down the three-dimensional shapes and structures from macro to micro(μm). There are several processes by which materials get removed in micromachining i.e., by mechanical force, by melting and vaporization, by ablation, by dissolution, plastic deformation, solidification, and lamination. Machines based on these are electric discharge machining, laser micro machining, lithography, electroplating and plating (LIGA), etc(Ref 2). Although these are capable of producing precise geometry with very little tolerance, still they have either limitation of having feature's ability (mainly 2d or 2.5d), material constraint limit, material removal rate (MRR), and costly. As an example, a laser can't produce microchannels with a controlled anisotropic profile and an isotropic chemical etching can't produce high aspect ratio channels(Ref 3). However, micromilling is the most versatile machining operation for fabrication for micro three-dimensional features like micro molds, micro masks, micro slots, micro grooves, micro channels, micro dimples, micro pillars with high aspect ratio irrespective of material hardness or toughness with high material removal rate.

1.2 Micromilling, issues and their applications

Micromilling (Micro end milling) is the most productive and cost-efficient micromachining process which is used to fabricate complex micro 3D features on any materials with high precision & accuracy, excellent surface finish, and high material removal rate(Ref 4). The size of the tungsten carbide end mill tool that is currently commercially available is small as $5 \mu\text{m}$. The schematic representation of the milling operation is shown in Figure 1.1. The cutting parameters that are controlled in micromilling operation are cutting speed, feed per tooth (chip

load), and depth of cut. In macromilling, where optimal cutting conditions have long been defined and documented and can be selected from reference books depends on different factors such as workpiece and tool materials, desired surface finish. However, the standard still needs to define in micromilling operation.

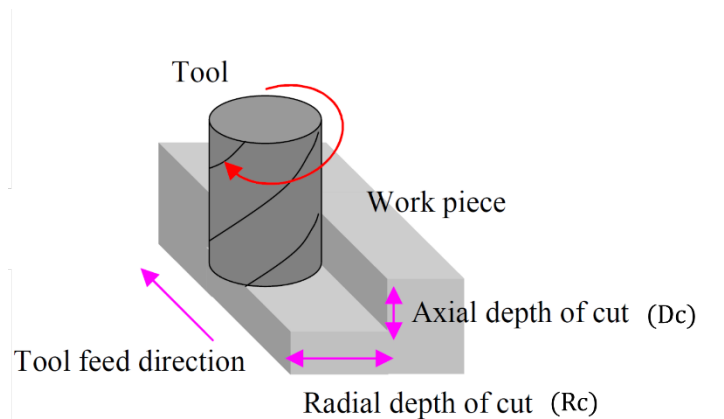


Figure 1.1: Schematic representation of milling process(Ref 5)

There are two types of depth of cut used in micromilling operation Axial depth of cut(D_c) along the rotation axis of the tool and radial depth of cut(R_c) normal to the rotation axis of the tool as shown in Figure 1.1. Their values depend on the diameter of the tool and workpiece material. Feed(f) which is usually known as chip load in micromilling can be defined as the thickness of the chip removed by the tool in one revolution (equation 1). The unit of chip load is micro meter per flute or micro meter per tooth($\mu\text{m}/\text{tooth}$).

$$f = \frac{fr}{NZ} \quad (1)$$

Where,

fr = feed(mm/min)

N = Spindle Speed(rpm)

Z = Number of flutes

Cutting speed(V_c) is the linear cutting velocity of the cutting edge. The unit of cutting speed is in m/min. The relationship between cutting speed, spindle speed, and diameter (mm) of the tool is given by equation 2-

$$V = \frac{\pi DN}{1000} \quad (2)$$

Although there are many similarities in kinematics to macro milling, it is associated with several other issues too. On scaling down of the dimensions, process dynamics change significantly as well. (i) The unfavorable size of the tool (25 μm to 50 μm) causes the length to diameter ratio to be often high which leads to tool run out and tool breakage. (ii) The uncut chip thickness and depth of cut are comparable to the tool edge radius or grain size of the workpiece material which leads to ploughing and poor surface quality(Ref 6). (iii) Deburring of micro-size burr is very difficult(Ref 7) (iv)The stiffness and accuracy of micromilling machines have a significant influence on the quality of the parts. There is the requirement of high-speed spindles which can achieve a speed of 4,50,000 rpm or more seems fit for proper machining(Ref 8). however, the current micromilling machine provides a maximum of 2,00,000 rpm spindle speeds(Ref 9). (v)Monitoring and diagnostic of the tool during micromilling has been recommended by many researchers as the worn cutting tool leads to inappropriate machining which results in high burr formation and poor surface finish(Ref 10–12). Although the aforementioned issues have been discussed and investigated by many researchers in the past, however, there are still many yet to be resolved(Ref 13–15). This thesis dealt with the issue of burr formation during micromilling and methodology to get rid of it. Micromilling has wide applications in the field of aerospace, biomedical, chemical, and electronics industry (Figure 1.2)

- **Aerospace:** For the fabrication of mold, die, and nozzles.
- **Biomedical:** Implants, surgery, drug delivery, and dentistry.

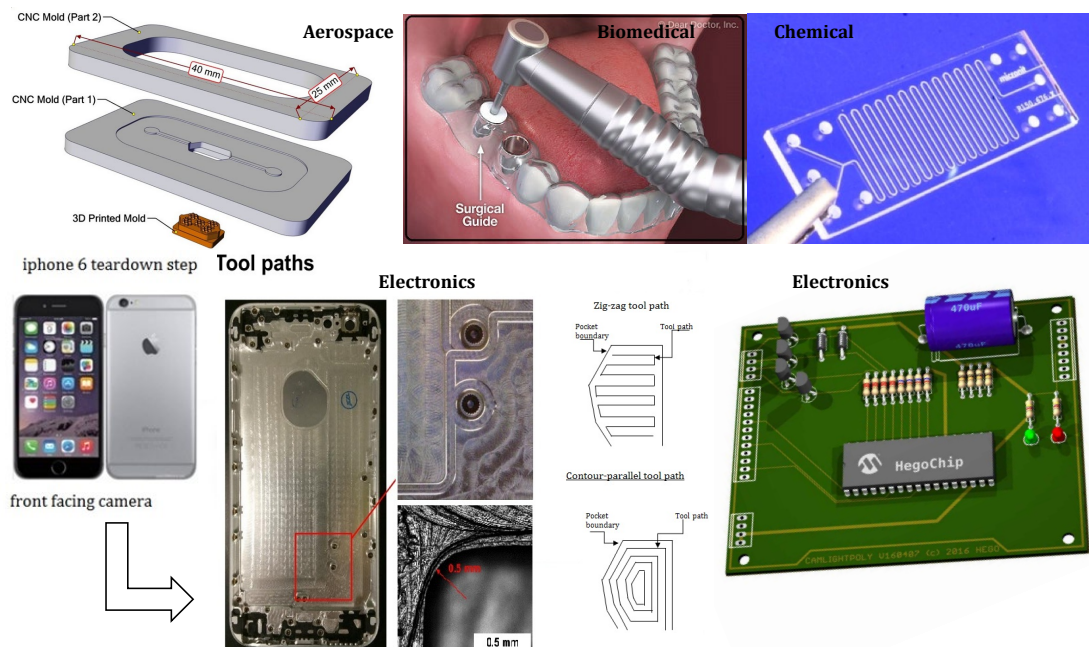


Figure 1.2: Applications of micromilling(Ref 16–18)(Ref 19)

- **Chemical industry:** Fabrication of Microreactor

- **Electronics:** 3D- microfeatures in the form of micro slots, microchannels, micro hole created by milling tool on display and housing part of the cell phone and Printed circuit board (PCB).

1.2.1 Burr formation

Burr gets formed when the cutting tool plastically deforms the uncut chip material instead of removing them. Thus, it can be defined as an unwanted plastic deformed material that remains stick to the workpiece after machining or shearing operation.

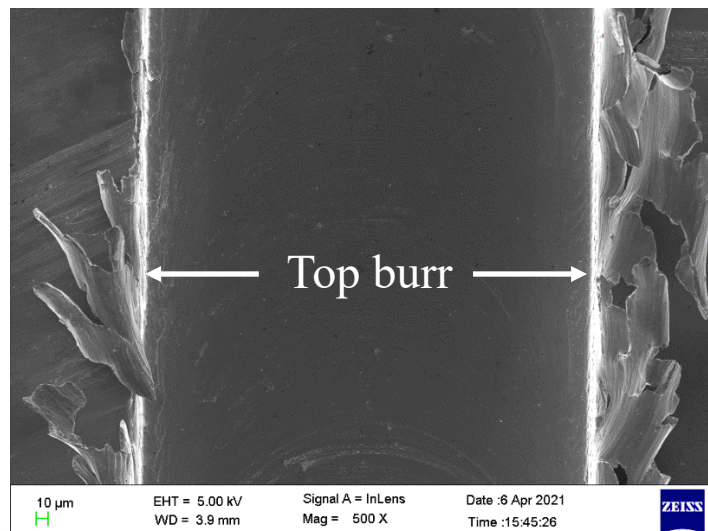


Figure 1.3: SEM image showing burr formation in micromilling

Any mechanical machining (milling, drilling, turning, or grinding) is always escorted by chip and burr whether it is macro or micro machining. Since the size of burrs is very less in comparison to macro machining, their removal is very difficult and challenging. There are eight types of burrs formed during micromilling operation (detailed explanation in next chapter section 2.2.2), among which top burr is the most critical burr that hamper the precision and accuracy of 3D micro features(Ref 20). As it can be seen from Figure 1.3 that the top burr formed on the top surface of the micromilling channel and its size is comparable to milling tool diameter. So, this thesis is focused on the analysis of top burr formation to minimize it to the maximum extent.

1.2.2 Need for burr minimization

Since the 20th century, demands for the fabrication of miniature components on complex geometry have risen drastically. These components/products should be portable, durable, and excellent in surface finish. Accordingly, challenges have been raised to increase productivity which can be attained with high machining performance. High machining performance can be

achieved if the cutting parameters (cutting speed, feed per tooth, and depth of cut) values are high, which results in excessive tool wear, high heat generations, high cutting forces, burr formation, and poor surface quality. Among all these factors, burr formation is one of the big threats that hinder the surface quality of any product. Some of its adverse effects on components/products have been mentioned below:

- (a) Decreasing the fit and ease of assembly of the mating part: Due to the formation of burr on one component, the wear gets accelerated and propagated on mating to another component due to the relative motion between the two. It can be clearly shown from Figure 1.4 that an absolutely fine surface finish requires for the mating of gears. Formation of any burr will lead to wear and tear of mating parts.

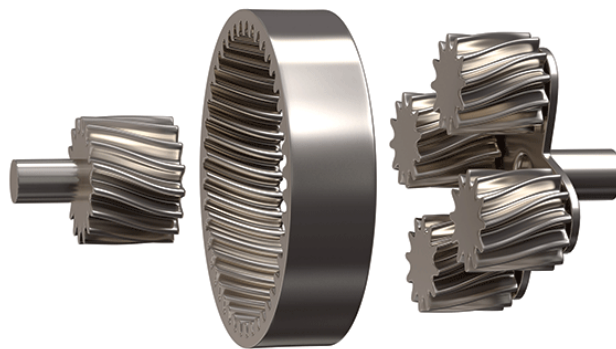


Figure 1.4: Assembly parts of gear(Ref 21)

- (b) Destroy dimensional accuracy and surface finish.
(c) Jeopardizing the safety of workers.
(d) Contributing to electrical short circuits.
(e) Reducing cutting performance and tool life.
(f) Increasing the time and cost of production: due to the formation of burr, an extra post-processing method called 'deburring' has to be applied to get rid of this and enhance the surface finish. Thus, it leads to an increase in lead time as well as the cost of production.

1.3 Aim and objectives

Deburring is quite complex and expensive in mechanical micromachining. Hence, burr minimizations are one of the major challenges in micromilling for better quality and smooth functioning of the equipment. The presented work aims to “**understand and minimize the mechanism of top burrs in micromilling**”.

Following objectives have been defined for achieving the aim of the work:

1. Development of a suitable machine tool for performing the micromilling operations

2. Understanding the mechanism of burr formation in down milling side of the top burr
3. Application of high-speed machining for burr minimization
4. Application of MQL for burr minimization

1.4 Research novelty and originality

The research carried out is significantly novel, since the mechanism of top burr formation in down milling of Ti6Al4V alloy to minimize is not explored so far. The effect of cutting parameters (speed, feed, and depth of cut) on the entry and exit burr of Ti6Al4V alloy in high-speed micromachining is already present in literatures, however, this study is novel in terms as it introduced a new technique (equivalent top burr width) to measure top burr width, comparative analysis of top burr formation at conventional and high-speed in up and down milling operation. Additionally, the effects of tool parameters (tool diameter and number of flute) have been analyzed. Application of MQL with micromilling is a novel task performed in the present work. Further, the introduction of a new cutting fluid (CuO nanofluid) for top burr minimization of superalloys is the successful outcome of the thesis.

1.5 Industrial importance

This project is important to the machining industry especially to the micro fabrication industry as it proposes a new economic and sustainable cutting fluid (copper oxide nanofluid) which helps in burr minimization and enhancing the surface quality of superalloys. In addition, high-speed micromilling has shown very promising results by diminishing the burr size and thus reducing the need for cutting fluids.

1.6 Organization of thesis

The thesis comprises Seven Chapters:

- **Chapter One** is the general Introduction, which deals with the basics of micromilling and its applications. It also includes burr formation, needs for burr minimization, aim and objectives of the work, novelty, and the industrial importance of the work.
- **Chapter Two** provides a chronological development in the technology for burr minimizations for superalloys. The chapter gives a brief overview of each method: conventional as well as recent to minimize burr to enhance surface quality. Conventional methods comprise deburring and flood cooling. While recent methods include high-speed micromachining (HSM), cooling and lubrication techniques: minimum quantity lubrication (MQL), MQL-using nanofluids, cryogenic micromachining.

- **Chapter Three** gives details about the development of the micromachining experimental setup. The experimental setup has been divided into four sections: Basic setup (varnica V-60), High-speed micromachining setup (HSM), MQL assisted micromachining setup, and cryogenic micromachining setup.
- **Chapter Four** deals with the mechanism of top burr formation in the down milling of Ti6Al4V alloy. The mechanism has been explained in various stages viz. initiation, propagation, and formation. Three types of top burr based on the behavior of material (Ti6Al4V) have been observed i.e., continuous serrated and longitudinal burr and curly burrs. Additionally, the effect of radial depth of cut, chip load, and depth of cut on top burr width has been analyzed.
- **Chapter Five** presents a recently developed method that is now in trend to reduce the burr size i.e., High-speed Micromachining (HSM). This chapter introduces a new technique to measure top burr width in terms of equivalent burr width. In this chapter, a comparative analysis of top burr formation in down milling at conventional and high-speed speed for titanium alloy(Ti6Al4V) has been analyzed. Further, the effect of cutting (speed, feed, and depth of cut) and tool parameters (tool diameter and the number of flutes) on the top burr formation has been analyzed.
- **Chapter Six** focuses on the investigation of top burr formation on Ti6Al4V alloy using cooling and lubrication techniques. Water-based emulsion and nanofluid (copper oxide nanofluid) have been used as a variant of coolant and lubricant. In this chapter, details about nano powder, preparation of emulsion and nanofluid, its characterization, and stability have been discussed. Effects of cutting parameters (feed and depth of cut) and nanofluid concentrations on the top burr formation have been analyzed. Further, multi optimization technique OEC (Overall evaluation criterion) has been applied to find the significant parameters that affect the output response (top burr) at optimum conditions.
- **Chapter Seven** provides another state of the art to minimize the top burr of INCONEL718 superalloy in up milling and down milling which is applied based on the successful outcome of chapter six.
- **Chapter Eight** provides a summary of the conclusion from each chapter of this thesis. Some suggestions regarding the scope of future work in this area are also given.
- The relevant references are appended at the end.

A schematic view of the thesis structure has been shown below in Figure 1.5.

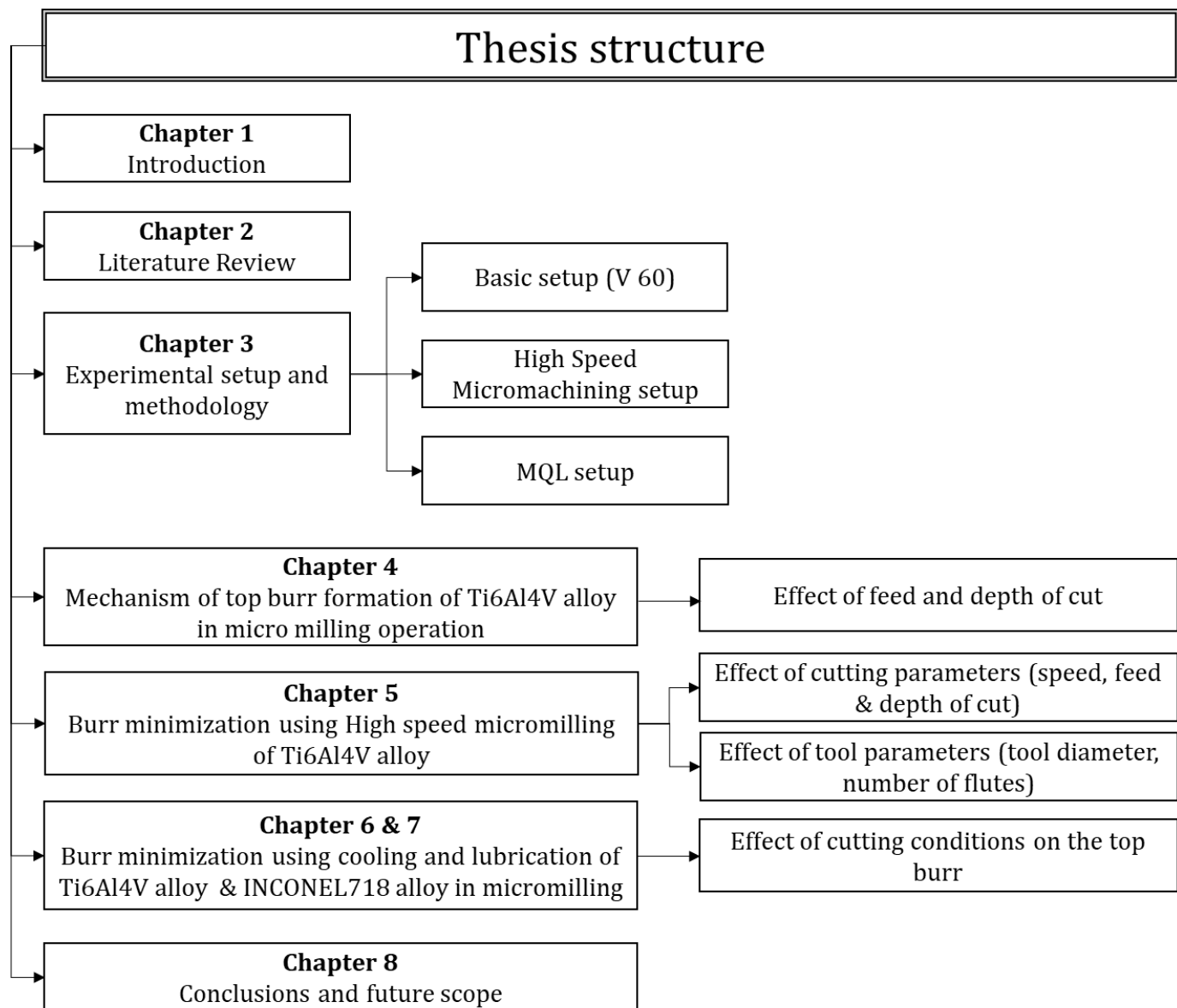


Figure 1.5: Thesis structure

Chapter: 2 LITERATURE SURVEY

A significant amount of work relevant to burr minimizations of superalloys using tool and tool path geometry optimization, coolant and lubricant, high cutting speed, Minimum quantity lubrication (MQL) is reported in the literature. These reports were based on conventional methods as well as recent techniques. Hence, the two aspects of the burr minimization method have been reviewed thoroughly in this chapter. Further, the chapter concludes with a brief discussion on the research gap, and methodology to achieve the objective. The outlines of this chapter have been enclosed in Figure 2.1 below.

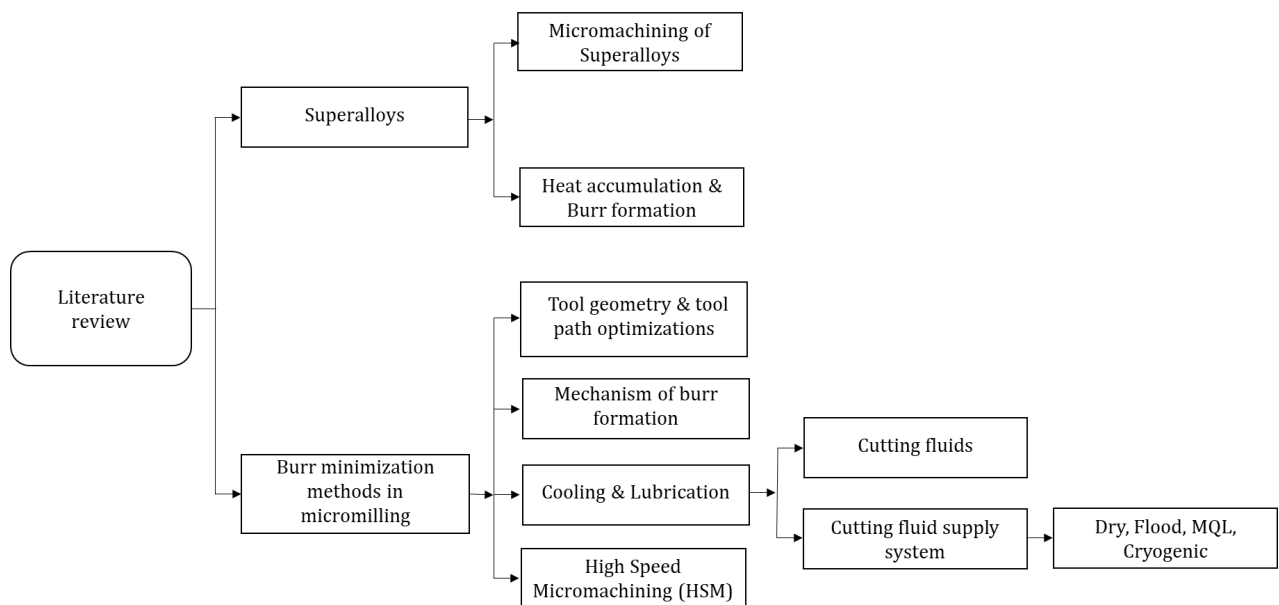


Figure 2.1: Literature review topics

2.1 Micromachining of Superalloys

Superalloys are mainly alloys of titanium, nickel, cobalt, tungsten, molybdenum, niobium, chromium, and magnesium alloys. However, based on the majority of constituents available, superalloys are mainly classified into four parts as titanium based, nickel based, cobalt based, and iron based(Ref 22,23)(Figure 2.2(b)).

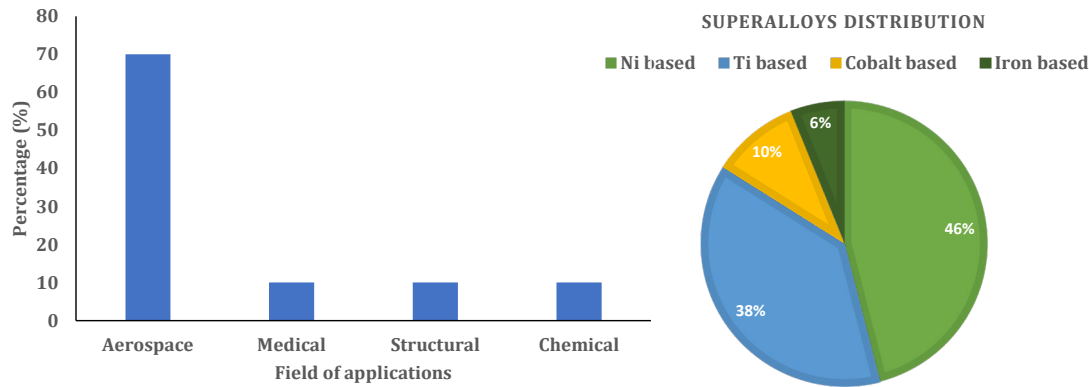


Figure 2.2: (a) Superalloy's consumption (b) Distribution of difficult to machine metal alloys(Ref 22)

Titanium based; Titanium is the 9th most abundant element while the 4th most abundant structural metal is found on the earth's crust. Pure titanium does not have remarkable mechanical properties. It is generally a soft element having very low density (approx. 60% of density of iron). However, it got strengthen significantly on alloying and deformation processing(Ref 24). Alloying titanium exhibits mechanical properties close to nickel alloys. Titanium and its alloys have the outstanding physical and mechanical property of ability to maintain hardness and strength at high temperatures, posing the highest strength to weight ratio between all common metals up to 550°C, toughness, wear resistance, corrosion resistance, and good biocompatibility(Ref 25). Resultantly, it has wide application in biomedical, aerospace, chemical, petrochemicals, automotive, and marine industries (Figure 2.2(a)). Both pure and alloyed have diverse application areas. Commercially pure titanium (CPTI) (ASTM grades 1-4, 7, 11) is used mostly for corrosion resistance. While high strength alloy grades (α , α - β , and β alloys) are used mostly for their superior strength to weight ratio, corrosion resistance in aerospace, automotive, and biomedical applications. Grade 5-Ti6Al4V (α - β alloy) which accounts for approx. 50% of actual use in the titanium industry, widely been used in aerospace and biomedical because of the high strength to weight ratio. However, many of these require machining for specific applications(Ref 26).

Nickel based; Nickel based alloys are more popular and in great demand because of their applications over titanium alloys. it covers the highest percentage (46%) among the superalloys based on constituent availability (Figure 9(b)). About 50% by weight aero-engine alloys are nickel-based alloys(Ref 27). It has broad applications in the marine, aerospace, and nuclear industries(Ref 28). Ni-based alloys have dominant property over Ti alloy at high temperatures. Among commercially available Ni alloy, Inconel-718 has high thermal fatigue resistance up to 700°C. It is highly resistant to creep and corrosion at elevated temperatures. Apart from this,

they are resistant to thermal shock and high melting temperatures (Ref 29). Unfortunately, being excellent properties superalloys are poor in terms of machinability (Figure 2.3). hence, its machining is very difficult (Ref 30), because of its inherent properties such as:

- Low thermal conductivity produces high cutting force and heat on machining due which poor heat dissipation in the machining zone between tool-work piece and chip. This creates a high thermal gradient which leads to high tool wear and catastrophic tool failure and poor machining(Ref 31).
- Low elastic modulus, (approx. 50% of steel) leads to deflections of work piece due to high cutting force which causes vibrations, chattering, and rubbing leading to elevated temperatures, resulting in the poor surface finish(Ref 32).
- The high chemical reactivity of titanium and nickel alloys leads to adhesion and diffusion wear at elevated temperatures. Thereby causing BUE(Built-up edge), chipping, and burr formation(Ref 33).
- High dynamic shear strength, causes adiabatic shear bending at the primary shear zone where the material suffers from the intense shear rate which leads to serrated or saw-tooth chip formation (which is the characteristics features of titanium machining) which results in machining instability, chattering, and force fluctuation which leads to chipping and burr formation on the cutting edge(Ref 34).
- The hardness and work hardening of nickel increase with an increase in temperature below 650°C. This is due to the presence of Y-participates in the material.
- Due to above mentioned characteristics of Ni alloys, very high temperature (>1000 °C) and stresses (>3450MPa) in the cutting zone lead to the accelerated crater and flank wear which results in burr formation, depending upon tool material and cutting condition used(Ref 35,36). Also,
- Strain hardening is the inherent property of Ni alloy due to the presence of molybdenum and niobium in the material. This is dominant in cutting operations as the hardness of chip produce increase after being subjected to deformation at the first shear zone. These strained hardened chips could notch the tool face(Ref 37).

So, the above peculiar properties reveal that superalloys possess higher chemical affinity at elevated temperature, low thermal conductivity, and lower elastic modulus. This resulted in built-up edge formation, adhesion of the workpiece material in the cutting tool, and work hardening of the work material. Therefore, rapid tool wear, surface degradation, elevated cutting force, and formation of burrs can be found during the machining process. These lead to the wastes of a large amount of materials. Therefore, the cost of the machining process increases. Additionally, the complexity of design of the

components of those materials added additional cost in machining process. Eventually, the cost of the machining of those materials is much higher. This is the deterministic feature to determine the machinability of the materials. In this thesis, machinability has been defined in terms of chemical reactivity, thermal conductivity, modulus of elasticity, shear strength, etc. These all parameters control the burr formation, surface quality, chip formation, cutting force, tool wear during machining process. Therefore, these are the major deterministic parameters to define the machinability of a material. In Figure 2.3, machinability has been defined in terms of the cost of machining.

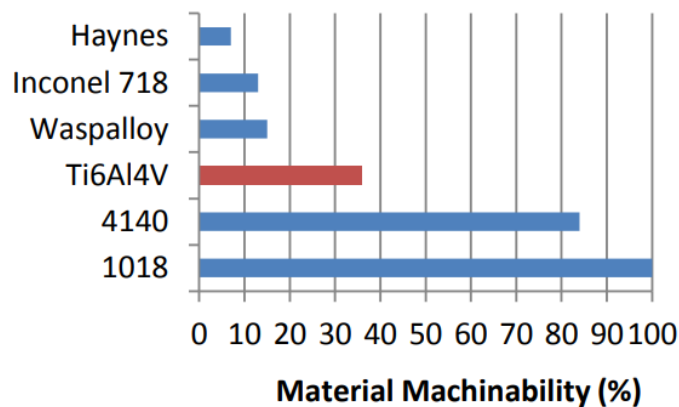


Figure 2.3: Comparison of machinability of superalloys with other metal alloys(Ref 38)

2.1.1 Heat generation on micromachining superalloys

Due to their peculiar properties, superalloys are easily prone to high heat generation at the tool-chip and tool-workpiece interface which results in poor machinability. Although about 80% of heat is carried away by chips, the remaining 20% is distributed to the tool and workpiece(Ref 39). Thus, it is determinantal to both tools as well as workpiece.

Effects on the tool:

- (a) Rapid tool wear occurs, which finally leads to low tool life(Ref 40,41).
- (b) Tool loses its hot hardness due to the plastic deformation of cutting edges(Ref 42).
- (c) Thermal shock may lead to thermal flaking and fracturing of cutting edges(Ref 43).
- (d) Built-up edge formation: For Titanium based superalloys, the chemical affinity of the workpiece materials towards the cutting tool increases at elevated temperature. Therefore, rapid heat generation may cause higher diffusion of the work material into the cutting tool resulting in strong adhesion at the tool work interface. As a result, the work material may weld into the tool material causing formation of the built-up edge (BUE)(Ref 44). Additionally, the lower thermal conductivity of these superalloys leads

to the accumulation of the cutting heat at the tool work interface which further increases the chances of BUE formation. In general, heat generation causes thermal softening which reduces the strain hardening and eases the material flow. However, for superalloys, strain hardening is more dominant than thermal softening.

Therefore, the heat generation does not provide any favourable condition to reduce the BUE formation rather than accelerate this(Ref 45).

Effects on the workpiece:

- (a) Dimensional inaccuracies of the specimen due to thermal expansion/contraction prior/after machining(Ref 46).
- (b) Tensile residual stresses and microcracks at the surface and sub surfaces(Ref 47–49).
- (c) Machined surface damage due to oxidation, burning, etc(Ref 50).
- (d) Burr formation(Ref 51–53)

Finally, it leads to adverse effects on productivity and performance. During machining operation, mainly three deformation zones are formed: primary, secondary, and tertiary deformation zones as shown in Figure 2.4. The heat generated in the first two zones i.e., primary and secondary deformation zones is mainly due to the cutting conditions. The heat generated in the primary deformation/shear zone by plastic deformation is transferred to the workpiece and chip via conduction(Ref 54). The secondary deformation zones transfer the heat to the tool by the conduction of frictional heat generated at the tool-chip interface. The heat is carried away by the chip by conduction, convection depending on the cooling method (dry or wet) used while machining. Superalloys mainly titanium and Inconel alloys being low thermal conductivity (Titanium alloys 6.7 W/mK and Inconel alloys 11.2W/mK) and specific heat produces excessive heat particularly in secondary deformation zones on machining(Ref 30). This leads to high heat generation at the tool tip. About 20% is retained to the tool-tip and the remaining 80% to the chip which results in low tool life. Further, the heat generated in the tertiary deformation zone i.e., tool flank face is due to the transfer of primary and secondary deformation zones heat(Ref 55).

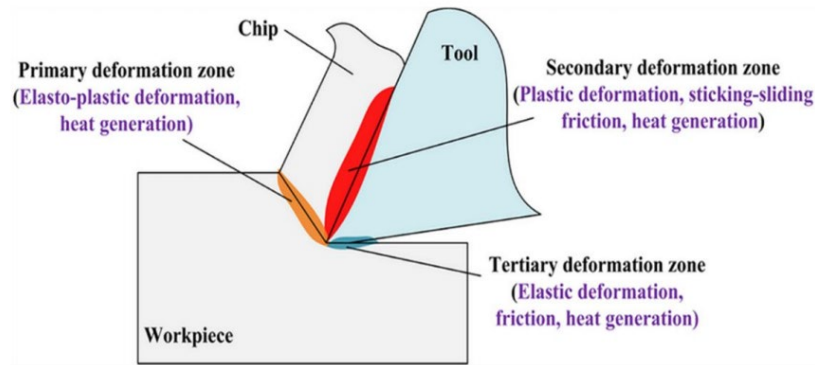


Figure 2.4: Sources of heat generation in machining(Ref 30).

2.2 Burr minimization methods in micromilling:

Numerous factors are responsible for the burr formation in the micromilling of superalloys. Its adverse effect has been discussed in section 1.2.2. So, a better strategy will be to minimize the burr formation to maximum extent. This will cut off the need for an extra additional process called deburring which is quite complex and costly. Hence, to minimize it, all the possible strategy, from raw materials to the manufacturing of the product has been considered (in terms of workpiece and tool geometry, tool path, mechanism of formation, process parameters, cooling, and lubrication) in this section.

2.2.1 Tool geometry and tool path optimizations

Aurich and Dornfeld(Ref 56), in their study, found that the main reason for the burr formation in face milling operation is the exit of the tool from the workpiece. So, they proposed a special tool path strategy(seen in Figure 2.5) by always machining on the part edge (I.e., avoiding the tool exit). They used criteria control of exit order sequence by tool geometry and path variation. Additionally, they maintain uniform chip loads over complex features.

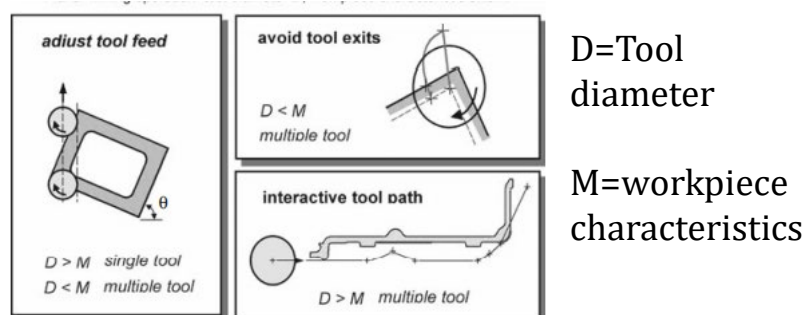


Figure 2.5: Tool path strategies for minimizing and preventing burrs in face milling(Ref 56)

Aurich and Dornfeld(Ref 56) further reduced the burr formed on AlSi surface by frequently changing the tool path with the additional deburring operation. Optimized tool path using the above criteria shown in Figure 2.6.

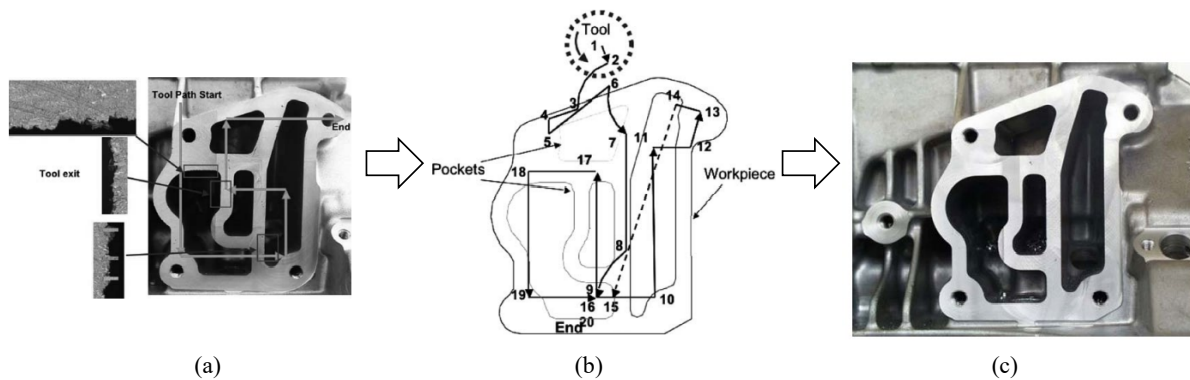


Figure 2.6: (a) Conventional tool path for face milling engine block face and resulting burrs at key locations (b) Modified tool path for part (c) Workpiece resulting from optimized tool path; Tool path length: old path – 209 mm, a new path – 524 mm, cycle time with increased feed rate remain at 5sec.

Aramcharoen and Mativenga(Ref 57) studied the effects of tool geometry and size effect on burr formation during micromilling of hardened tool steel. It was observed that lower burr size was obtained when undeformed chip thickness larger than cutting edge radius while cutting edge geometry has a significant effect on micromilling. Chamfered cutting edge geometry provides better surface finish with minimum burr size concerning round cutting edges.

2.2.2 Mechanism of burr formation in Micromilling

Deburring is quite easy in macromachining. However, it cannot be employed in micromachining because deburring may lead to ruptures of the micro features created on the surface of the machined workpiece. Hence, understanding the basic mechanism of burr formation is necessary for burr minimization. Based on the mechanism of formation, burrs are classified into four types(Ref 58): (Figure 2.7)

- a) Poisson burr: Lateral flow of materials occurs when a solid is compressed. Material is compressed until permanent plastic deformation occurs.
- b) Rollover burr: A chip pushed out of cutting tool's path on exit from workpiece rather than sheared.
- c) Tear burr and: Loose tearing of workpiece rather than shearing. It is similar to the burr formed in punching operations.

- d) Cut-off burr: projection of material left when work piece falls from the stock before the cut has been separating.

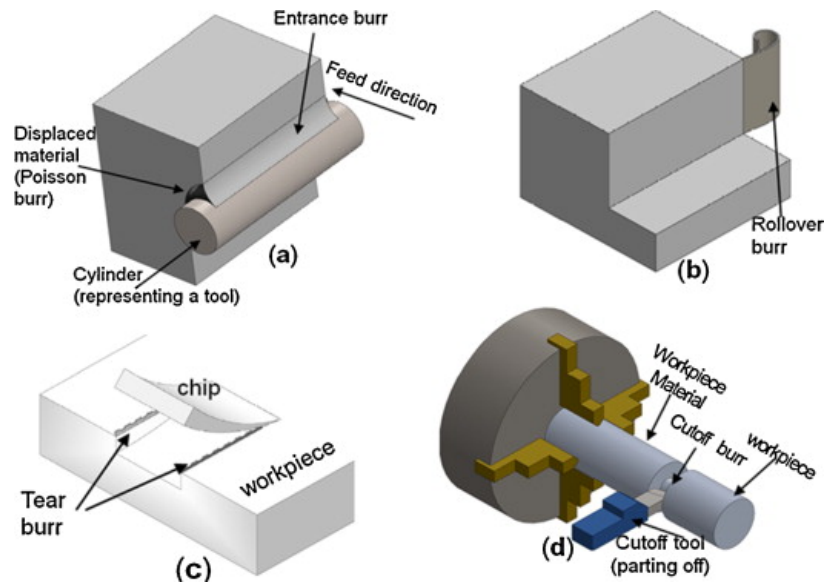


Figure 2.7: Types of burr based on mechanism of formation(Ref 58)

Nakayama and Arai(Ref 59) described machining burrs formed in various cutting operations, by the cutting edge, and by the mode and direction of burr formation. Hashimura et. al(Ref 60) classified burrs in face milling according to burr location, shape, and mechanism of formation (Figure 2.8).

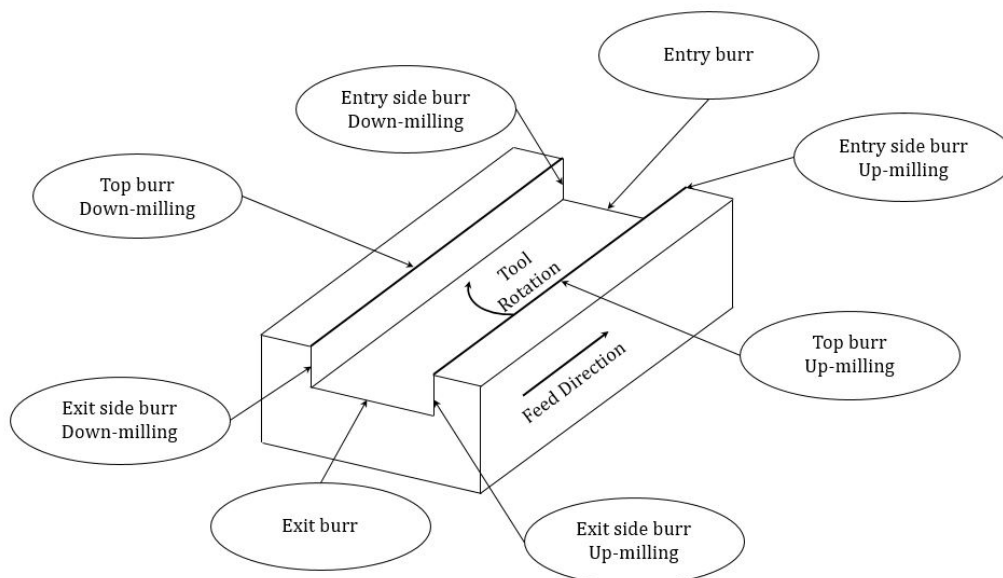


Figure 2.8: Eight types of burr formed in milling operation(Ref 60)

Lin(Ref 61) investigated burr formation during the face milling of stainless steel and found that five types of burr can be produced at the exit edge, viz. knife-type, saw-type, burr breakage, curl type, and wave-type(Ref 60). Chern investigated the mechanism of burr formation in face milling of aluminum alloys and observed five types of burrs in the experiments: knife-type, wave-type burr, curl-type, edge breakout, and secondary burr(Ref 62). Kou et. al(Ref 63) postulated a mechanism in which they used supporting material at the verge of the workpiece to minimize burr formation(Figure 2.9).

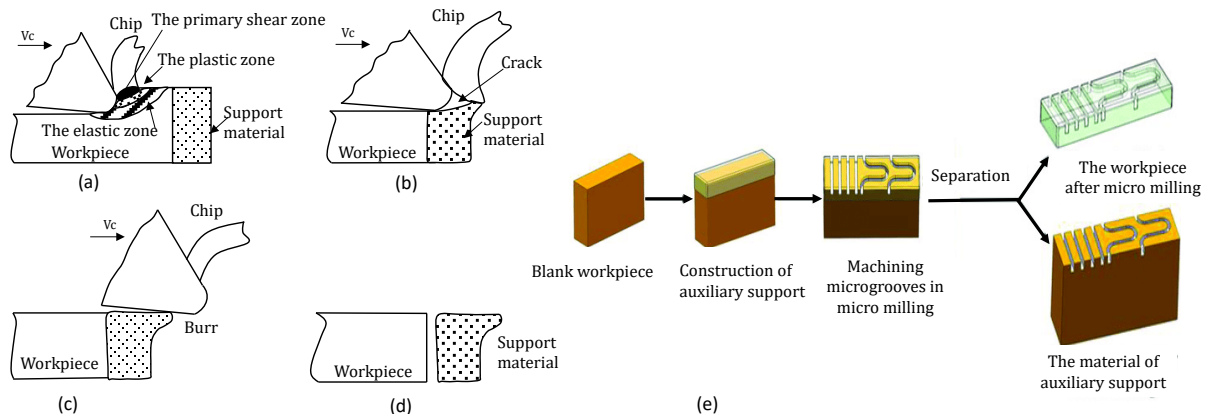


Figure 2.9: Burrs control mechanism in micromilling. (a) Extending workpiece boundaries with supporting material. (b) The crack grows on the support material. (c) Burrs formation on the support material. (e) The process of burr control(Ref 63)

Modeling of burr formation has been an important tool as well to understand and better control burr formation in micromilling(Ref 64).

Numerical Approach:

Many researchers tried to analyze the mechanism of burr formation in micromilling using a finite element approach. They used various software to model the burr and simulate the results. Chen et.al(Ref 65) simulated the burr formation during micro ball end milling operation of Ti6Al4V alloy. they found massive burrs at the slot base in comparison to the flat end mill tool. Correlation the FEA and experimental results they found that the ratio of axial depth of cut to the cutter radius has a significant effect on the top burr. Ozel et.al(Ref 66) used 3D DEFORM software for finite element modeling of burr formation in micromilling of Ti6Al4Valloy. Davoudinejad(Ref 67) used AdvantEdge® FEM software for finite element modeling of aluminum alloy 6061-T6 in micro end milling. Yadav et.al(Ref 68) used abacus explicit software to model exit burr in micromilling of Ti6Al4Valloy. Further, they simulate the results with experimental ones and find good agreements. Chen et.al(Ref 69) proposed burr reduction mechanism in vibration-assisted micromilling. they compared the top burr obtained with and

without vibration (conventional milling) on Ti6Al4V alloy using same parameters as for FE simulation as shown in Figure 2.10. In conventional micromilling, top burrs forms in down milling were larger than up milling burrs. However, they obtain less burr size while slot machined by vibration assisted micromilling. They observed burr size in downmilling got reduced by 87%.

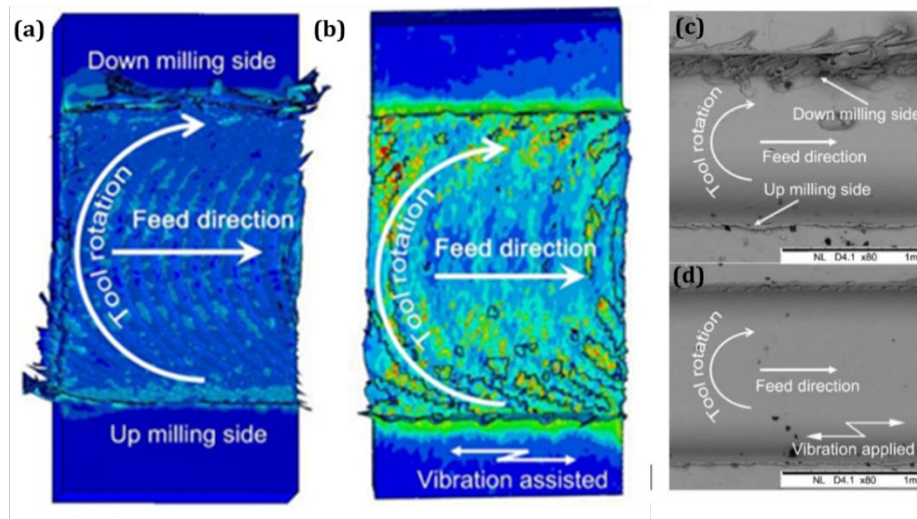


Figure 2.10: Ti6Al4V machining experiments: Simulation(a,b) and experimental(c,d) results for conventional and vibration-assisted micro milling

Wu et.al(Ref 15) fabricated high aspect ratio micro slots (1.5:1 and 3:1) on Ti6Al4V alloy to evaluate burr morphology. They analyse burr formation mechanism comprehensively proposing a theoretical model assisted with simulation. They find that top burr formed during chip removal process due to the pushing outwards of the material connecting the chip and workpiece. Sidewall burr and sidewall bottom burr composed of adhesion and microcavity. the formation of adhesion is due to the extrusion and residual of chip material whereas microcavity is due to the tearing failure of material at chip root. Zhang et.al(Ref 70) analyses burr formation mechanism in high aspect ratio(2:1) grooves of harden steel (SKD 11). They used to deform 3D model finite element modeling and simulation. of entrance, exit, side, and bottom burr. The average error found was 9.5% and 2.1% considering the size effect of materials in the modeling process.

2.2.3 Cooling and Lubrication

2.2.3.1 Cutting Fluids & their importance in industry

In today's manufacturing industry, the demand is rising for high productivity, low cost, and excellent surface quality. So, to meet these demands, naturally, the cutting parameter's value

has to be increased significantly which leads to the rise in temperature and high heat generation at the tool-workpiece and tool-chip interface. Subsequently, this will result in tool wear, burr formation, and poor surface finish. Therefore, the use of cutting fluid is a must today, to achieve the desired productivity with better dimensional accuracy and excellent surface finish. It dissipates the heat, removes chips away from the machining zone, reduces built-up edge (BUE) and burr formation(Ref 71). It was observed that cutting speed could be increased up to 40 % without reducing the tool life with a sufficient supply of water(Ref 72),(Ref 73). However, it is considered to be a poor lubricant for machining as it causes serious corrosion issues in machine tool parts and components. After that, a new formulation for cutting fluid has been developed which is specific for specific materials (detailed has been explained in next section)(Ref 71). Petroleum/mineral oil-based, semi-chemical, and chemical-based cutting fluids are very commonly used nowadays by the metal cutting industry on a wide scale. Due to which consumption rates increased and it has been predicted that the consumption of cutting fluid may increase 1.2 % globally by the next decade(current use ~38 million metric tons)(Ref 23). Further, its cost is significant as well concerning tooling cost and manufacturing cost of the product and it accounts for 17.9% and 7.5% respectively(Ref 71).

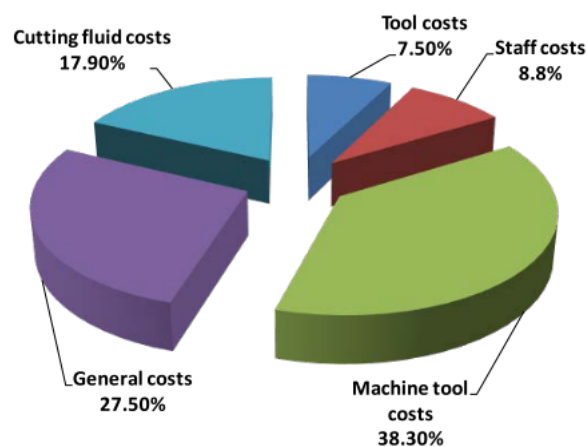


Figure 2.11: Manufacturing cost distribution in the European automotive industry(Ref 74)

However, the misuse of cutting fluids leads to an addition of an extra maintenance cost particularly with the use of non-biodegradable cutting fluids (Figure 2.11). This is mainly due to the presence of highly toxic ingredients such as chemical agents and hydrocarbons. Further, it depends on various factors like workpiece material, machining process, and method of supplying it.

2.2.3.2 Functions and actions of cutting fluids

Cutting fluids perform two roles in machining operations. It provides lubrication to the machining zone by decreasing the heat generated due to the friction at a lower speed and acts as a coolant by dissipating the heat generated at relatively higher speeds(Ref 75). Thus, at low speed, it decreases the rake frictional force at the rake face and thus increases shear angles. Due to which thinner and tightly curled chips are produced reducing the temperature in the shear zone and thus power consumption. It has been reported that low lubrication is more beneficial concerning cooling at low-speed machining. High lubrication cutting fluids are not preferred at high speed as these go on vaporize at high temperatures before reaching the machining zone. For high-speed machining, the cutting fluids should have significant thermal properties as well as appropriate wettability, such as having a high specific heat coefficient and low surface tension to ensure its capacity to transfer contact with the tool/chip and workpiece material(Ref 76). To fulfill such functions cutting fluids should have significant properties like tribological and thermal.

2.2.3.3 Classifications and properties of cutting fluids

Cutting fluids were mainly classified into three sections as seen in Figure 2.12. All these fluids have their significance and limitations as per the applications required. Some are specific to specific materials and machining operations.

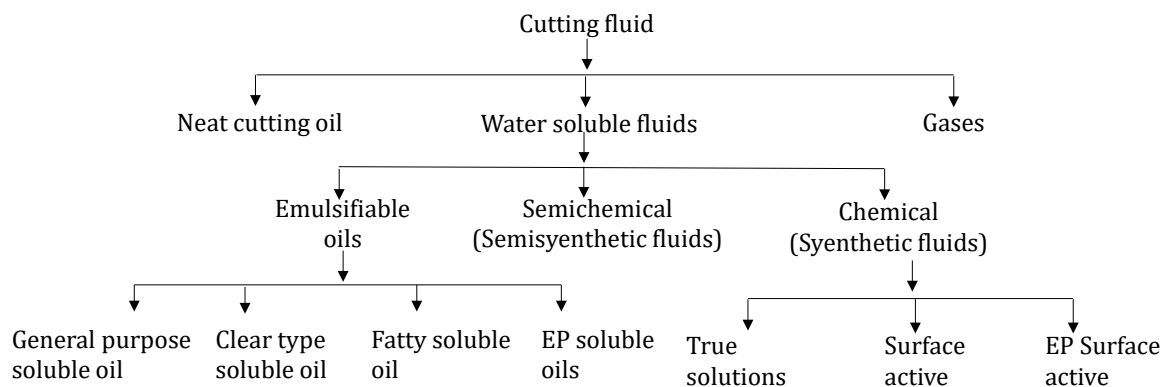


Figure 2.12: Classifications of cutting fluids(Ref 77)

Neat cutting oils

Neat cutting oils are straight oils generally used in their purest form. These are mainly straight mineral oil or vegetable or animal-based oils(fats). Such oils are preferred where the sole purpose is lubrication and hence supplied on machine shop floors where cutting pressures between tool-chip interface require is very high. However, the drawback is that they have poor

cooling characteristics being low in specific heat capacity ($\sim 2.10\text{J/g K}$) and thermal conductivity(Ref 78). Its thermal conductivity is approximately one-third of the water. Generally, they are preferred to use at low cutting speed in conventional machining operations such as deep hole drilling, gear hobbing, broaching, tapping, threading, etc. Since at high-speed machining they tend to form a high mist and smoke formation being high flammability(Ref 79),(Ref 80).

Water-soluble fluids

Water-soluble cutting fluids are mainly used where the machining operations are performed at high-speed and pressure on the tool is low and thus it is preferred over neat oil(Ref 81). Such cutting fluid forms an emulsion on mixing with oil and hence is a combination of both properties cooling as well as lubrication properties. Further, water-soluble cutting fluids are classified into three sections: emulsifiable oils, Semichemical(semi-synthetic), and chemical(synthetic) fluids.

Emulsified Oils

The primary purpose of emulsifiers is to ensure better dispersion of oil in water to form a stable emulsion. Such oils are often used to dissipate the heat and provide lubricity on high-speed machining operations with low cutting pressure(Ref 82). These fluids are mainly oil-based concentrates which contain emulsifiers like soap, wetting agents, and couplers. Thus, the characteristics of such fluids are they have good lubricity and cooling ability, adequate wettability, moderate viscosity, and low flammability. the key property of the soluble oil is the stability of the emulsion(Ref 83). Soluble oil also contains additives similar to those found in straight oils to improve their lubrication properties as per desirability of application. However, it also has some drawbacks like misting, rancidity, bacterial growth, and thus low stability. These oils are further classified into four main categories as follows: general type emulsions (milky fluids) are those having oil droplets of diameter less than 200 microns. They are usually mixed at a concentration in the range of 1- 40 liters of base fluid for conventional machining. Clear-type fluids are more emulsifiers in comparison to milky emulsions as less oil (higher proportion is rust inhibitors). These oils are generally used during light-duty machining like grinding. Fatty soluble oils have vegetable fats or animal fat or other esters which are added with mineral oils to provide a variant of fluids with excellent lubricating properties. Extreme pressure (EP) oils are fluids, known as extreme pressure additives, mainly contains sulfur, chlorine, or phosphorous additives to improve the machining performance at high cutting conditions of pressure and temperature. Generally, it is employed during heavy-duty machining.

Semi chemical fluids

Semi chemical or Semisynthetic cutting fluids are formed by the combination of synthetic fluids and soluble oils (emulsified oil in water). However, here the concentration of emulsified mineral oil is small (5-30 % of the base fluid)(Ref 80). With the incorporation of EP additives, the lubricating performance can be altered as per the desirability of moderate and heavy-duty machining. These fluids have better characteristics concerning chemical fluids.

Chemical fluids

Chemical fluids are formed from alkaline organic and inorganic compounds sources. Further, it can be used on a wide scale with the inclusion of various additives like amines and nitrite to prevent corrosion, borates, and phosphates for water softening, nitrates for nitrite stabilization, and soap and wetting agents for lubrication and reducing surface tension. They do not contain mineral or petroleum-based oil. These cutting fluids have good cooling characteristics but are poor in lubrication (due to a lack of oiliness) i.e., why they are restricted to grinding operations where cooling is a priority(Ref 84). Chemical fluids are further sub-divided into three parts:

- True solutions are those chemical solutions having good corrosion inhibitors property as it does not contain wetting agents. True solutions having dilutions in the range of 1:50 to 1:100 are generally used for grinding operations for ferrous metals.
- Surface active fluids are used with concentrations of 1:10 to 1:40 while grinding of ferrous as well as nonferrous metal alloys.
- EP surface-active fluids have similar properties as extreme pressure additives. These are used with concentrations of 1:5 to 1:30 for heavy machining operations.

Gas-based fluids

Gaseous-based fluids are either remain in gaseous forms or cooled pressurized liquid forms. Air, liquid nitrogen (LN₂), carbon dioxide, argon, and helium are some of the good biodegradable gas-based fluids. They have high oxidation and rust resistance at elevated cutting temperatures. Apart from this, gas-based fluids can be used in the mist as well form in combination with conventional cutting fluids using minimum quantity lubrication (MQL) to enhance their lubrication performance. These types of cutting fluids are superior for heavy machining conditions where conventional cutting fluid supply techniques fail to penetrate the tool-chip and tool-workpiece interface(Ref 85). For example, liquid nitrogen at -196 °C is used as a cutting fluid for machining superalloys where chip formation and chip breaking are major issues due to the accumulation of high heat. Now, after discussion of all types of cutting fluids, the attention needs to focus on sustainability which has been discussed in the next section.

2.2.3.4 Environmental effect of conventional cutting fluids

About 85% of the cutting fluids used globally are mainly mineral oil (petroleum) based fluids. Such conventional fluids are potentially hazardous to the health as well as the environment as these affect significantly ecological cycles with air, soil, and water, and their toxicity may affect and damage the ecosystems(Ref 83)(seen in Figure 2.13). A survey in US and EU reveals that approximately 32% and 13% of all fluids used are disposed to the environment(Ref 86). Among these, most of the fluids need to have additional treatment before disposal. Furthermore, these fluids on evaporation at high temperature go on merge with the vapor and microparticles, and thus it may cause serious health matters like respiratory and lungs diseases. It has been found from the report that about 80% of all industrial diseases of machine tool operators are due to direct physical contact with conventional fluids. Moreover, being these hazardous fluids are complex in their composition they may be allergenic, irritants, and suspected cancerous agents(Ref 87). Various microbial toxins can be produced as well by aerobic/anaerobic bacteria/fungi present mostly in emulsion fluids, which can pose another threat issue to workers' health. For these reasons, various regulations and policies have been imposed for the use of hazardous cutting fluid(Ref 88).

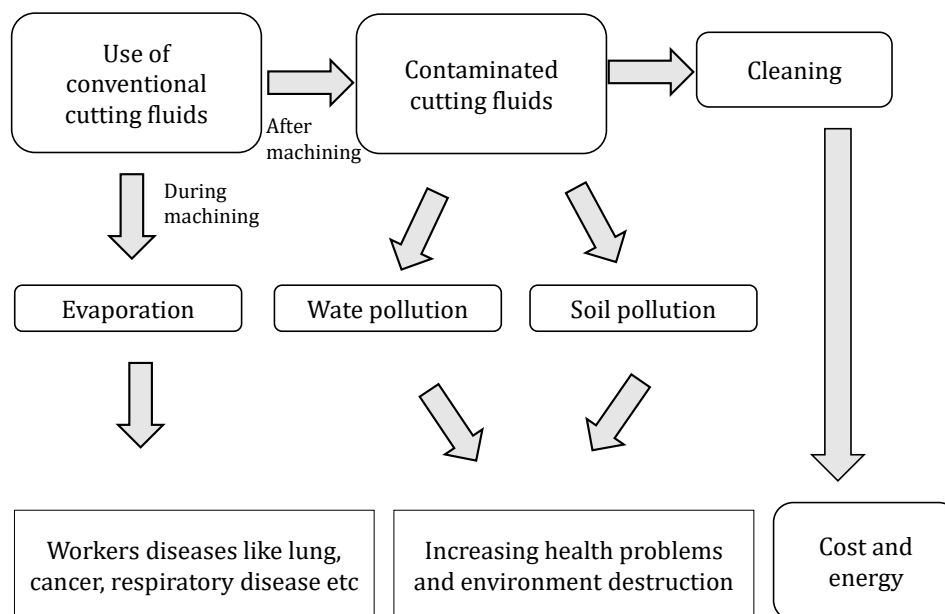


Figure 2.13: Conventional cutting fluids life cycle with their impact on surroundings(Ref 83)

2.2.3.5 Cutting fluid supply system

The cutting fluid supply system has been classified into four sections: dry cutting, flood cooling, compressed coolant, and MQL system (Figure 2.14).

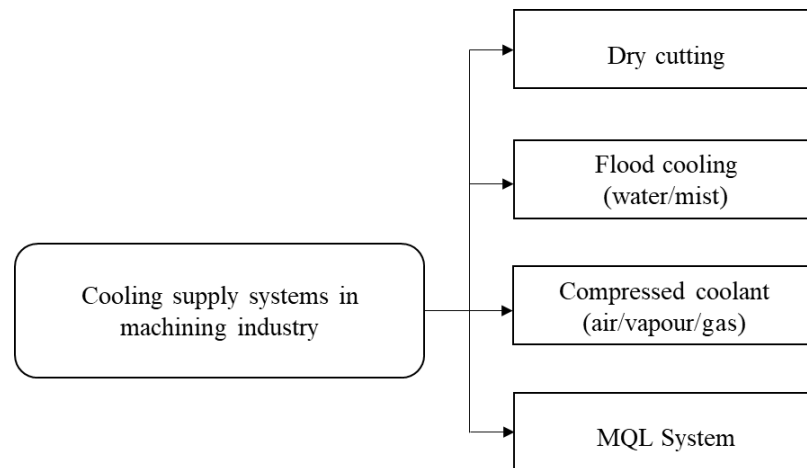


Figure 2.14: Schematic of cutting fluid supply system used in modern industry

Dry, flood cooling, HPC

Traditionally, flood cooling is the most important process used to remove the heat generated during the standard machining process. In this supply system, an enormous amount of cutting fluid (at pressure >3 bar and flow rates up to 225 L/min) is supplied through randomized nozzles (Figure 2.15) in the machining zone (Ref 89). However, it is hazardous in terms economically, environmentally, and hygienically. As it consumes very high fluid consumption, low penetrating ability, and high machine setup maintenance cost. It was found that cutting fluid and tool accounts for 17% and 4% respectively of total machining cost. It also causes serious pollution problems like dermatitis and respiratory disease among workers on the machining floor. It was found that in high-speed milling, flood cooling shows premature tool failure by thermal fatigue wear and several thermal gradients loading. Hence to get rid of this MQL provides an ideal solution.

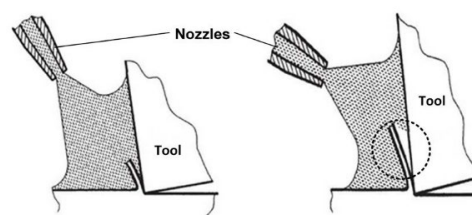


Figure 2.15: Random supply of cutting fluid in flood cooling system (Ref 89)

High-pressure cooling (HPC)

A high-pressure cooling supply system is preferred mainly during high-speed machining due to the generation of high heat. In these methods, coolant is supplied generally at very high pressure (up to 200 bar) through customized designed nozzles at the tool-chip interface (Ref

90). This cutting fluid supply system offers excellent penetration ability to tool-chip and tool-workpiece regions, thereby reducing tool wear and increasing tool life. Mainly discontinuous chips formed on supply of such fluid which is easy to remove away from machining zone via hydraulic jack. The applications of such a supply system are mainly in heavy industry. However, high fluid consumption rate, pumping and filtering cost, and finally, the installation setup cost are limitations of such a fluid supply system.

Minimum quantity lubrication (MQL)

MQL is generally regarded as the best alternative to conventional flood cooling particularly for micromachining(Ref 83). In this method, a minuscule amount of lubricant is sprayed through a special design nozzle (having a diameter approximately 1mm)at high air pressure(up to 6 bar)and flow rates (ranging from 10 to 500 ml/hr) on tool-chip/tool-workpiece interface in a mist form which provides essential lubricity that's lacking in dry as well as wet machining(schematic view of MQL system shown in Figure 2.16). It is preferred over flood supply system as it offers low oil consumption in mL/h instead of L/min(flood supply system).

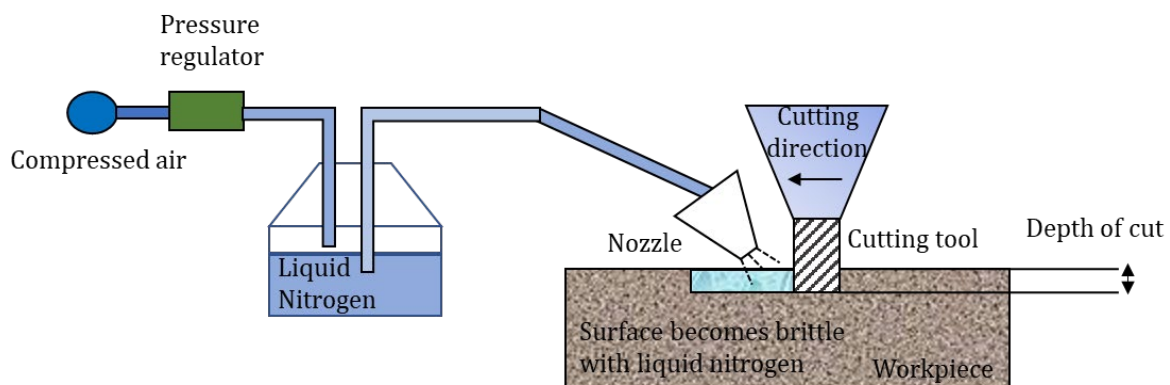


Figure 2.16: Schematic diagram representing MQL using cryogenic coolant(Ref 91)

Percin et.al(Ref 92) performed a micro drilling operation on Ti6Al4V alloy to investigate the effects of various machining conditions: dry, flooded, MQL, and cryogenic on burr formation. An uncoated tungsten carbide drill of dia 700 μm was used for the experiment. Coolant and lubrication were delivered at pressure ≤ 3 bar. Supplying pressure more than 3 bar causes the chip to jam and the tool may break. Among all the cutting conditions, it was observed that minimum burr height was obtained under cryogenic conditions. Spraying liquid nitrogen causes the workpiece material to brittle, due to which material undergoes less plastic deformation and hence burr height also decreases. A wide range of research has been reported in micromachining to analyze tool wear, tool life, and surface roughness. However, very few

researchers have tried to analyze the effects of MQL on burr formation. Biermann and Steiner(Ref 93) investigated the effect of MQL on burr formation during micromilling of austenitic stainless steel X5CrNi18-10. They found that top burr width gets increases if constant lubricant is not supplied. Vazquez et.al(Ref 94) observed the burr formation using dry, conventional emulsion and MQL as cutting fluid. Conventional Emulsion taken was vegetable oil (1:10 oil-to-water ratio emulsion) MAK KIT10 ES-AL by LUBRICORP with viscosity 1.3 cSt while MQL was vegetable oil TRI –cool MD1 by TRICO with viscosity of 34cSt. It was found that burr height gets reduced by three times in comparison to machining with conventional emulsion. Additionally, it was shown that when the nozzle orientation of MQL was in the direction of feed, no burr formation was visible. Whereas when the nozzle was oriented against the feed direction, burr formation appears similar to be under dry condition (as shown in Figure 2.17).

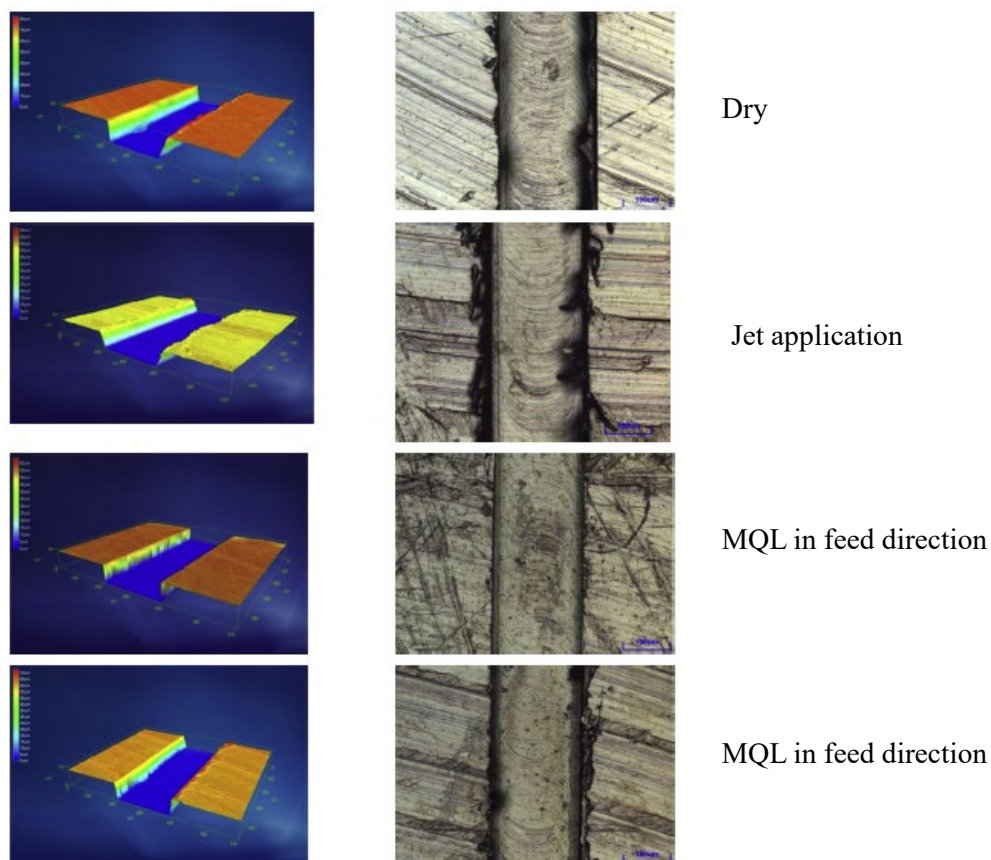


Figure 2.17: 3D surface plot with SEM images of burr formation after micromilling ($a_p=0.15$ mm)(Ref 94)

Lauro et al.(Ref 95)found that burr length decreases by 48.5% (dry) and 65.8% (MQL) with the increase of speed while it increases as 124.9% (dry) and 100.3%(MQL) with an increase of feed rate during orthogonal microcutting of biocompatible ti alloy Ti-6Al-7Nb. They used Coolube 2210 as biodegradable oil and the flow rate was constant 2.6 mL/min with the pressure of 6

bar. Uzun et.al.(Ref 91) analyzes the burr formation on Inconel 718 under the different cutting condition: Dry, MQL, and Cryo precooling. A vegetable liquid lubricant (coolube2210) at a flow rate of 150 ml/h was sprayed during the MQL process. However, to perform cryo precooling operation, liquid nitrogen was sprayed onto the cutting zone at pressure <1 bar. They observed that cryogenic minimizes burr more significantly with respect to dry and MQL. Inconel 718 being high toughness undergoes intense burr formation. However, with the use of cryogenic precooling its hardness increases and toughness decreases, due to which less plastic deformation and hence minimum burr was observed (Figure 2.18).

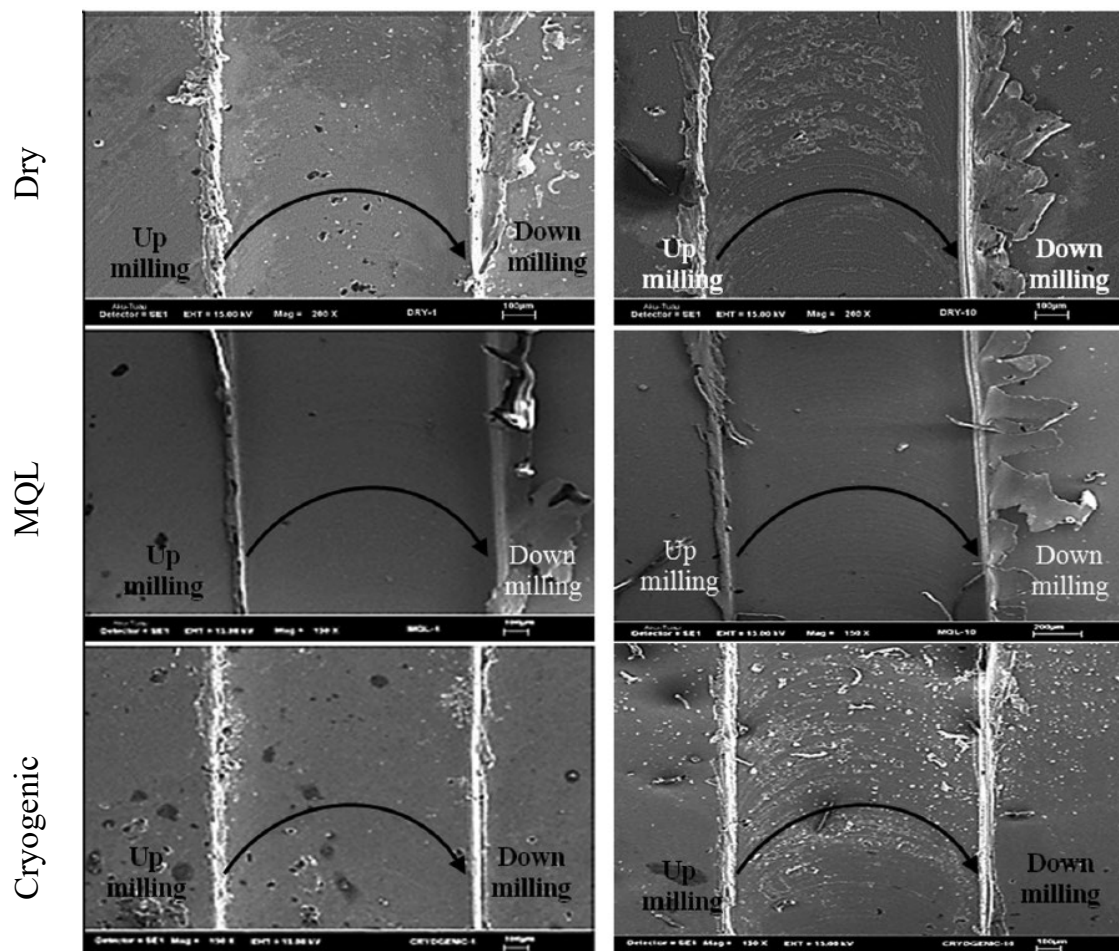


Figure 2.18: SEM images of burr formation after micromilling ($a_p=0.15$ mm)(Ref 91)

Aslantas et.al.(Ref 96) performed a comparative analysis of burr formation on Ti6Al4V in different cooling conditions and a hybrid of cooling and lubrication (cryogenic and MQL). A vegetable-based liquid lubricant and carbon dioxide were used for the MQL process and cooling agent respectively (see Figure 2.19 below). The mixture was sprayed onto the cutting zone at a pressure of 3 bar, a flow rate of 25 l/h and the temperature recorded at nozzle was -10 °C. They observed that the hybrid process minimizes burr more significantly with respect to other

cooling conditions (see Figure 2.20). It was also observed that burr size formed was greatest with air-cooled at -30°C due to the embrittlement of the tool at low temperature.

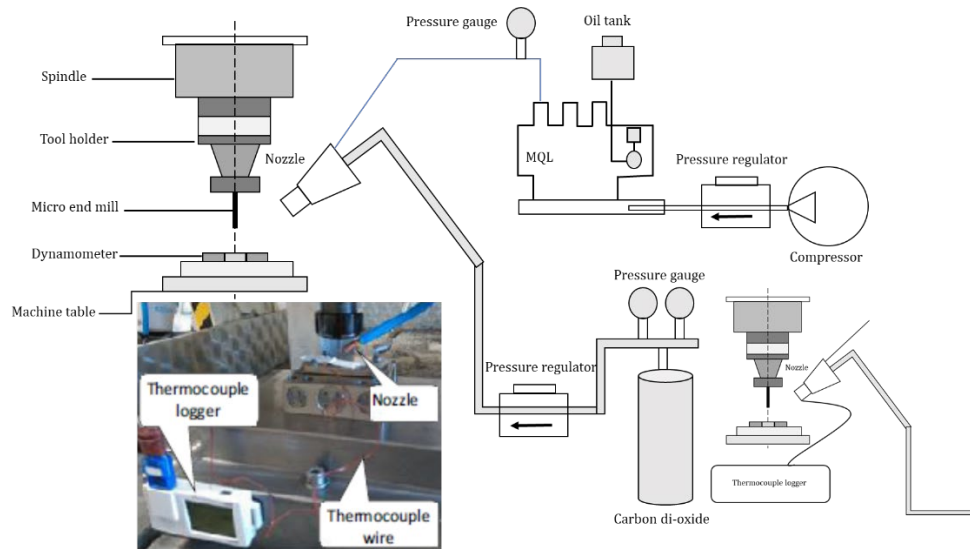


Figure 2.19: Hybrid micromachining setup(Ref 96)

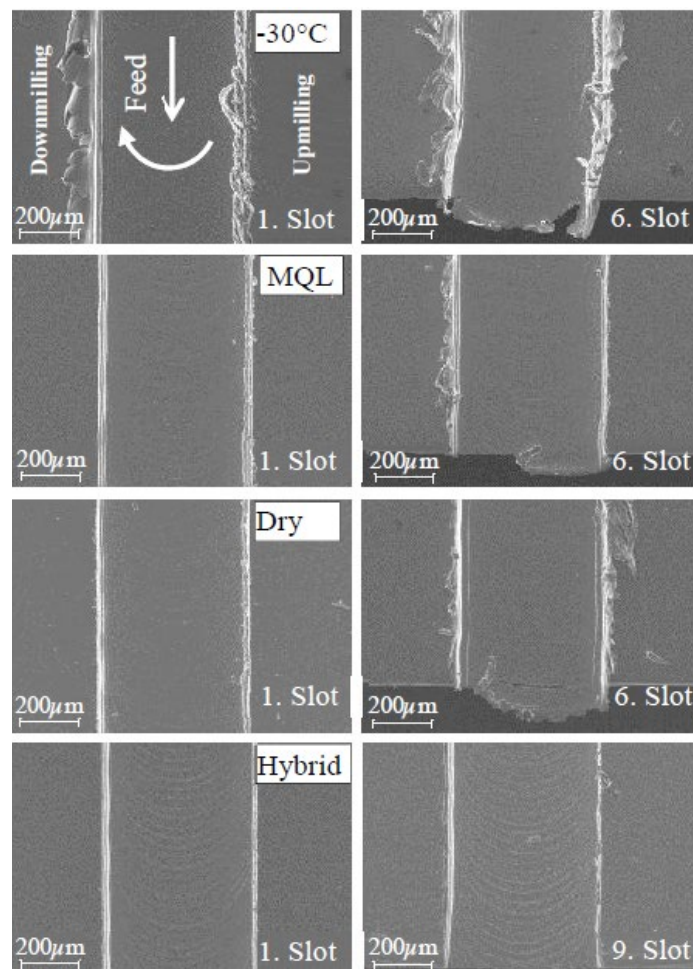


Figure 2.20: SEM images of burr under different cutting conditions(Ref 96)

2.2.4 High-speed micromachining

Workpiece sizes are decreasing, while part versions increase. Miniaturization in the manufacturing world demands changes in the manufacturing process. These increased demands require rethinking to work more efficiently with smaller tool diameters, which require higher rpm speeds that most conventional spindles cannot achieve. Even if they can, it puts undue stress on them by constantly red-lining the spindles. Conventional CNC equipment using tools smaller than 1/2" diameter at 10,000 rpm or less usually results in unfavorable feed rates and costly tool breakage(Ref 97). The traditional method of machining involves comparatively large tools at fairly low speeds. Inherent to its design, a larger tool is often unsuitable for intricate machining(Ref 98). To attempt machining with micro-tooling, conventional machines must run very slowly and tend to easily break the fragile tools. Large tools, by their mass, are resilient to the effect of chips. Smaller tools, on the other hand, are fragile and more susceptible to breakage(Ref 99). Improper chip evacuation is a major cause of tool breakage. More small tools break because of inadequate chip removal than they do for incorrect machining parameters. Chips must be removed from the cutting channel to minimize breakage possibilities. Small tools require high spindle speeds, but they need to go even faster to kick the chips out. recently, One of the best machining techniques trending nowadays with small size tooling is high-speed micromachining(HSM). The smaller the size of the tool, the higher the spindle speed required for precise machining of the parts. Recent researches have shown that high-speed spindles with speed ranging from 6,000 to 2,00,000 rpm are ideal for micromachining like drilling, milling, thread milling, and engraving(Ref 34). This technique uses high rotational speed, taking a smaller step-over, but with significantly increased feed rates. In HSM with micro-tooling, since the spindles move fast, there's insufficient time for heat to feed back into the part and cause issues. During the machining process, the tool continuously removes the chips from the surface of the workpiece. about 10% heat is generated due to the friction on each side of the tool while 10% is from the bending(deformation) of the chip. Therefore, about 80 % of the heat is inside the chip. HSM tries to evacuate the bulk of the heat with the chip, providing for a cleaner cut. The better machining quality is based on cooler tooling, lower machining forces and less vibration. The high spindle speed reduces the chip load to less than 127 μ m(Ref 100). Such a low chip load significantly reduces the forces between the tool and the material. High-speed/low-force machining develops less heat, reduces tool deflection, and allows machining of thinner-walled workpieces. This results in better surface quality, cooler machining, easier work holding, and better accuracy. Bajpai et. al(Ref 101) investigated the burr formation in high-speed micromilling of Ti6Al4V. They observed that with the increase of tool rotation from 10,000 to

50,000 rpm and 50,000 to 90,000 rpm, burr height decreases by 5% and 25 % whereas burr thickness decreases by 5% and 25 % respectively. The reason for the decrease in burr size was primarily due to a decrease in uncut chip thickness with an increase of spindle speed. Jahanmir(Ref 102) analyses the burr formation on aluminum alloy (6061-T6) using ultra high-speed micromilling and found that the best surface quality with minimum burr was obtained while machining at recommended speed(3,50,000 rpm).

List of recommended high-Speed machining for difficult-to-machine metal alloys:

Recommendations for high-speed machining are based on the type of materials to be machined. It goes on varies with the softness and hardness of the material. A broad range of cutting speed for difficult to machine metal and its alloys has been shown below in Figure 2.21.

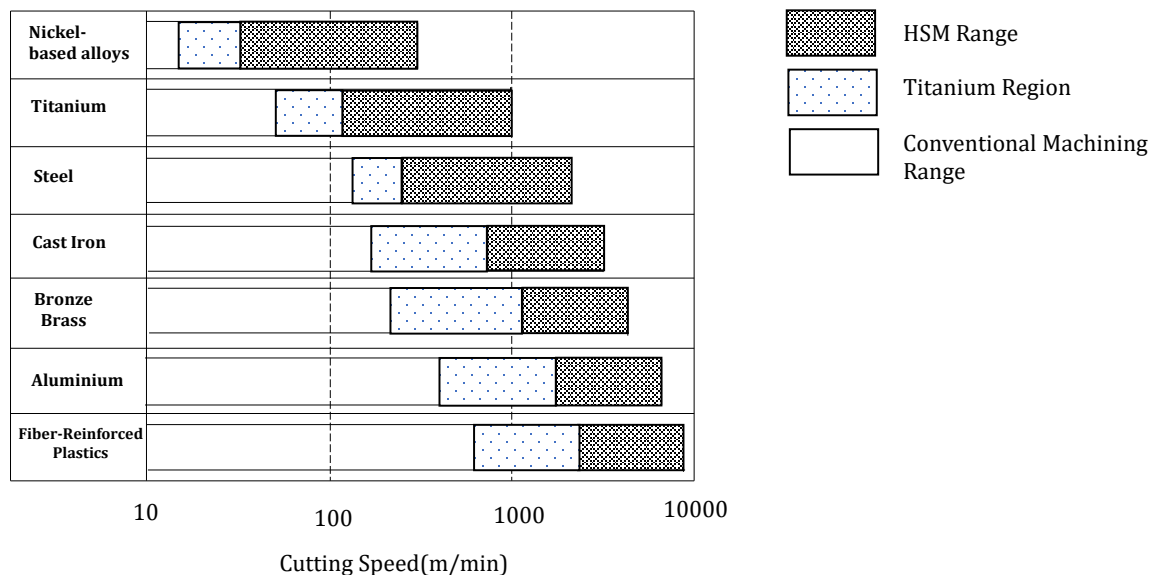


Figure 2.21: Recommended high-speed range for different materials(Ref 103)

Kuppuswamy and Yui(Ref 104) conducted high-speed micromilling on nitinol alloy to minimize the burr. They observed that cutting speed was the most influencing parameter that reduced the burr more significantly followed by feed per tooth and depth of cut. The optimum speed at which they got minimum burr size was 15 m/min. Finite element modeling of burr formation in high-speed micromilling of Ti6Al4V was done by Yadav et.al.(Ref 68). On simulation they concluded, burr height and width decrease by 96% as the speed increases from 10,000 rpm to 2,00,000 rpm. Comparison of burr formation with varying speed from 50,000 rpm to 2,00,000 rpm at constant parameter: feed (5 mm/sec), depth of cut(10 μ m), tool diameter (0.5 mm) has been shown below in Figure 2.22.

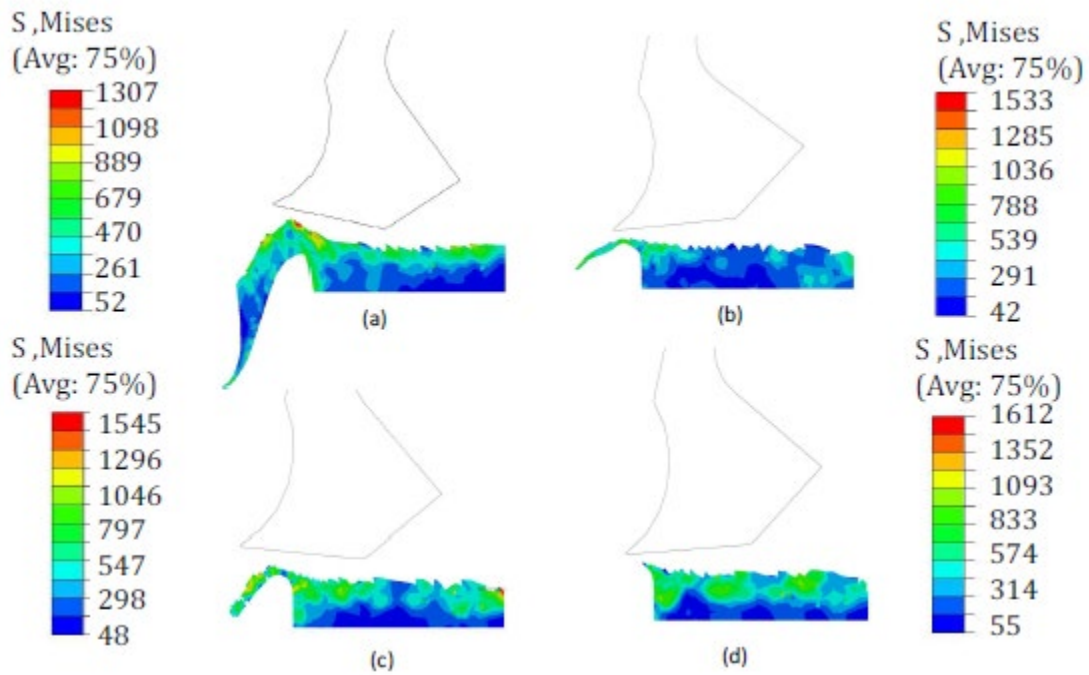


Figure 2.22: Burr formation at cutting speed (rpm) (a) 50,000; (b) 1,00,000; (c) 1,50,000 (d) 2,00,000 with constant feed (5 mm/sec), depth of cut($10\mu\text{m}$), tool diameter (0.5 mm)(Ref 68)

2.3 Literature outcome

The following research gap has been finalized from the study of the literature

- 1) It was found that researchers were mainly focused on minimizing entry and exit burr in micromilling. Limited work has been reported to minimize the top burr in super alloys.
- 2) Application of nanofluids and nano lubrication in MQL and cryogenic need to be explored for the micromilling process and its effect in minimizing the burr formation.
- 3) Effects of nanofluid on machining output response still needs to be flourished, as it's gaining a very promising field in the micromachining area.
- 4) Limited research has been found on high-speed micromachining for superalloys.

The research outcome discussed above provided formulation of the research problems and are addressed accordingly in the present study.

2.4 Research methodology

The following methodology has been implemented to accomplish the research gap:

- 1) Mechanism of top burr formation: A comprehensive experimental work with varying process parameters viz. chip load and cutting speed has been performed to understand the burr formation mechanism in the down milling side.

- 2) High-speed micromilling: Due to a decrease in the size of the tool, there is a drastic loss in the cutting speed of the tool. To achieve the high cutting speed the spindle speed has to be increased significantly. Experiments have been performed at conventional and high cutting speed to explore the effect of high-speed cutting on the burr formation and its size.
- 3) MQL using coolant and lubricant: Since difficult to machine metal alloys leads to heat accumulation on machining operation due to low thermal conductivity due to less heat dissipation at the tool-chip interface. The problem becomes more serious in the case of micro-milling due to the very small heat zone and tool chip interface. This leads to high temperature in the machining zone which leads to burr formation and poor surface finish. Conventional cooling and lubrication methods may not be useful due to the narrow gap between the tool chip interface zone. Hence, a new methodology has been adopted in the form of MQL. Nano lubricant and nanofluid have been used for cooling and lubrication purposes. It is expected that it will be helpful in burr minimization.

In the next chapter, brief details about the development of micromilling setup have been discussed. The experimental setup has been divided into three sections: Basic setup (Varnica V-60), High-speed micromachining setup (HSM) and MQL assisted micromachining setup.

Clarification: Varnica Precision Pvt. Ltd. is a company incubated in the Institute for the development of high-speed machines and other machine tools. At present, one high-speed micro machining center has been developed with the highest spindle speed of 60,000 rpm (model V-60) and another is under development with a maximum spindle speed of 1,40,000 rpm. The model V-60 has features of MQL and cryogenic machining.

Chapter: 3 EXPERIMENTAL SETUP

This chapter focussed on the development of micromilling setup. It includes all the analysis relevant from design, modelling and simulation further their validation to achieve the desired precision and accuracy. The whole experimental setup has been classified in three sections viz., basic setup model V-60, high-speed micromachining (HSM) setup, minimum quantity lubrication (MQL) assisted micromachining setup. The basic setup **Model V-60** was developed for dry machining which further assisted with MQL for wet machining. The high-speed machine was borrowed from IIT Bombay for the high-speed machining.

3.1 Basic setup (Model V-60)

3.1.1 Design considerations for micro machining center have been done on the following points:

- Design Methodology
- Machine bed material selection
- Spindle Selection
- Linear Stages Selection
- Design principles
- Parameters affecting machine tool performance
- Structural loop stiffness of the machine tool

3.2 Design methodology

A generic flow chart has been prepared, which was followed for designing the machine setup (Figure 3.2). In the beginning, based on the literature survey, some specific design considerations were followed, which helped in deciding the structural configuration of the structure. The selection of locations of the components in the structure was intuitive. Machine architecture was decided. Machine architecture is shown in Figure 3.1 as well. It helped further in determining the structural loop of the machine tool. Desired goals were decided beforehand. CAD models were prepared for FE analysis of the machine tool. FE analysis had to be conducted to find out the behavior of the structure. If the results of a particular FE analysis were found satisfactory then only the next analysis was conducted, otherwise, the design has to be improved intuitively according to the response of the machine tool. Here, static analysis was conducted first to know the static behavior of the machine tool under static load at the tip of the shaft and due to rotation of the shaft of the spindle. If satisfactory results were found in static structural analysis, subsequent analyses were performed. If the static results were unsatisfactory then geometric optimization was done to optimize the dimensional values. After

the geometric optimization, an optimal design was selected. Modal analysis was done to know the natural frequencies of the machine tool. The reason for conducting modal analysis was to define the resonant frequencies for the machine tool with the spindle operating frequency. The operating speed of the spindle was the set of values from the range of 10,000 to 60,000 RPM excluding the speed corresponding to resonant frequencies. If the no of frequencies was large before the excitation frequency (1000 Hz, equivalent of top speed of spindle), design changes were made to reduce the number of frequencies encountered before excitation frequency. Since, Modal analysis does not provide information about the amplitude of vibration, hence harmonic response (also known as frequency response) analysis was performed. Frequency response used input forces with different frequencies ranging from 0 to 1000 Hz to calculate the amplitude of vibration in the machine tool with change in frequency. If the frequency response curves of the machine tool were having a smaller number of peaks and smooth performance at a high-frequency range (low amplitude), the model has been finalized. Otherwise, design changes were made. After these detailed analyses, the final design of the machine tool was obtained. Once the final design was ready, then it was fabricated. After fabrication, the error budgeting of the machine tool had to be computed at the subcomponent level. Now, integration of components has to be done to make the machine operational. Finally, features have to be created for further analysis, which will determine the limitations of the machine. In the following subsections, the details of the reasons behind the selection of different components of the machine tool have been reported.

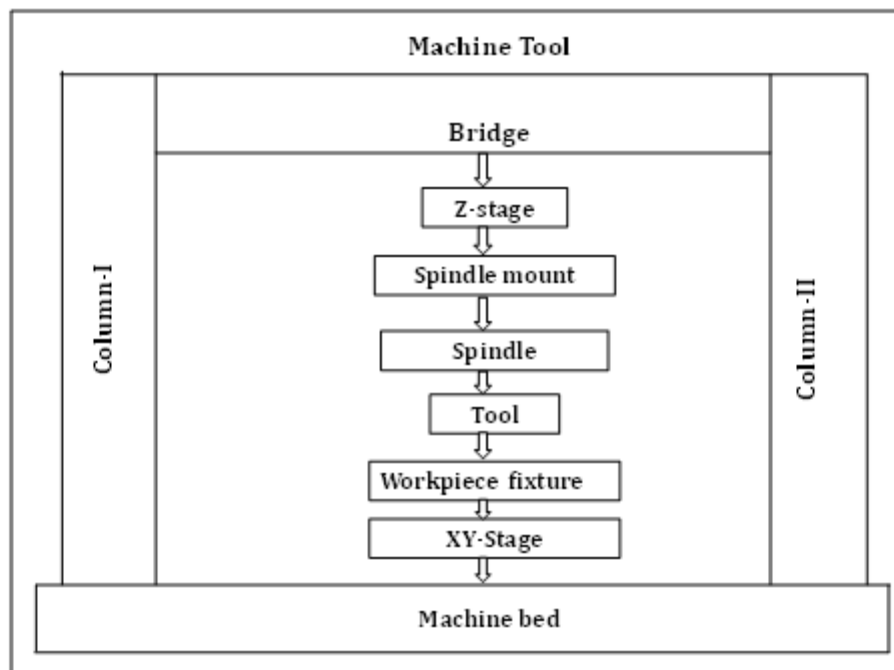


Figure 3.1: Architecture of the machine tool

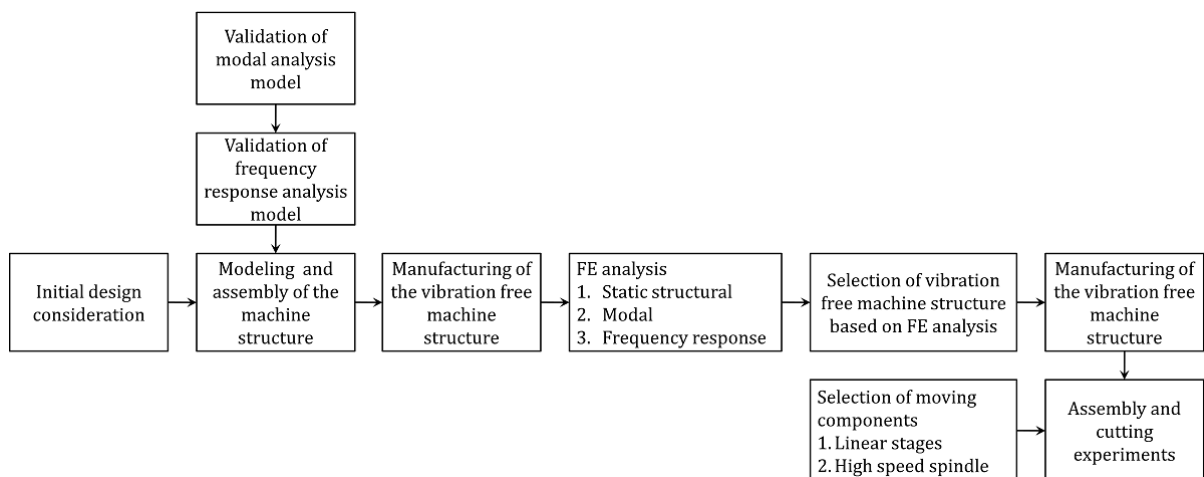


Figure 3.2: Design methodology of micromilling machine

Machine bed material selection

The machine material has to be highly thermally stable because of requirements of high accuracy and high surface quality. This can be only achieved with a material having a low thermal expansion coefficient and low specific heat capacity. To meet the goal of high surface quality, a material with good damping properties is needed.

Table 1: Comparison of material properties

	Granite	Cast iron	Slate	Marble
Density	2.54-2.66	5.54-7.81	2.6-2.9	2.37-3.2
Moisture expansion	0.00500	NA	NA	0.0025
Elasticity	20-60	621-240	NA	60
CYS	965-310	331-2520	138-207	68.9-241
LCTE	3.7-11.0	7.75-19.3	4.5-10	2.7-9
SHC	0.21-0.35	0.506	0.3-1.83	0.54-1.61
TC	1.20-4.20	11.3-53.3	1.3-3.8	1.3-2.9

On comparing the data given in Table 1, Cast iron and granite are good options for machine parts (Ref 105,106) Granite is the most suitable choice for machine bed because best damping property out of all materials available(Ref 107,108).

Spindle selection

The major factor affecting the properties of a spindle is the type of bearing. The following criteria were considered for the selection of the type of bearing for the spindle(Ref 109).

- a) Speed limit: - For measuring the speed capabilities of bearings, the product of bearing diameter in mm (D) and a top speed in rpm (N), called DN number is considered.

Ceramic balls have a low density as compared to those made of steel; as a result, these exhibit a low magnitude of centrifugal force. Air bearings experience only viscous friction forces. Magnetic bearings do not have any speed limitations.

- b) Applied Load: - Air bearings can support very high loads compared to ceramic and steel bearings. Magnetic bearings can also support very high loads if required.
- c) Accuracy: - The smoothness of the bearings affects the accuracy of the motion. Smooth finishing of bearings allows higher speeds by reducing spindle deflection. Ceramic (silicon nitride) balls have a better finish than steel balls. Air bearings have the advantage of averaging out all irregularities, which make their running smoothest.
- d) Magnetic bearings have the best accuracy due to the availability of a close-loop servo system and position sensors.
- e) Stiffness: - High modulus of elasticity implies high rigidity resulting in better stiffness. Ceramics have 1.5 times the modulus of elasticity (resistance to deformation) of steel. Air bearings do not have the problem of loss of contact. They can achieve a stiffness value as high as 100 N/ μm . The steady-state stiffness of magnetic bearings can be essentially infinite, but their dynamic stiffness depends on the frequency of the applied load and the bandwidth of the control system.
- f) Damping Capability: - Due to a highly smooth finish, ceramics have good damping capability. The thin, low viscosity air film in the bearing gap gives air bearings moderate to low damping capabilities. Due to the advantage of a closed-loop control system, magnetic bearings have very good damping capacity.
- g) Friction: - Friction is reduced drastically in ceramic bearings due to anti-friction properties, Air bearings and magnetic bearings have zero friction due to noncontact characteristics.
- h) Thermal Performance: - The hardness and strength of ceramics do not deteriorate at high temperatures as compared to steel. Due to the low viscosity of air, air bearings are tolerant to small changes in the bearing gap. The air cools as it expands and so, the flow and refrigeration effect have a significant effect on the performance of air bearings. Magnetic bearings heat early due to the high current in their coils.
- i) Size and Configuration: - Ceramics have a smaller size than steel bearings. The plumbing system of air bearings takes up a lot of space. Magnetic bearings are 5-10 times larger than ceramics bearings.
- j) Weight: - Ceramic balls are lighter than steel balls. Air bearings have moderate to high performance-to-weight ratios. Magnetic bearings are very heavy as compared to rolling element bearings.



Figure 3.3: View of Spindle

l)Cost: - Ceramic bearings and steel bearings have relatively low and comparable prices. Air bearings are relatively higher priced. Magnetic bearings are the costliest.

m)Control: - Two basic types of control available are open loop and closed loop (also referred to as “vector controlled”). Open-loop spindles typically are used when cutting forces are relatively low, as in micromilling. An open-loop spindle operates at maximum power (P) only at a peak rotation speed, whereas a closed-loop unit has maximum power at low-to-peak speeds.

Hence, based on Table 2, spindle model ‘AG62-60-0.24-P-DS’ (Precise high-speed spindle service private limited, GMBH, Germany) is selected. The image of the selected spindle with drawing is shown in Figure 3.3. The technical specifications of the spindle are given in Table 3.

Table 3: Technical Specification of Spindle(Ref 44)

Parameter	Value(unit)	Parameter	Values(unit)
Speed	60,000rpm	Lubrication type	Grease
Driven type	Motor	Collet run out	Static-2 μm Dynamic-8 μm
Motor power	1.5 kW	Radial stiffness	
Bearing type	Angular contact	Axial stiffness	
Torque	0.24 Nm	Cooling system	Water cooling
Motor type	Asynchronous	Mass	4 kg

Linear Stages Selection

The machine as a prototype is envisaged as an assembly of a stacked XY stage and a Z-axis unit, which holds a spindle unit at the end. The Z-axis unit is mounted on the center of the machine frame. Linear stages were selected after taking into consideration of requirements for a

precision machine tool. Requirements and the corresponding solution for them have been listed down in Table 5. A goal was set for the resolution, accuracy, and repeatability of the machine stages, as given in Table 4.

Table 4: Desired specifications for the linear stages

Property	XY stages	Z stage
Accuracy	< 5 μm	< 5 μm
Resolution	1 μm	1 μm
Repeatability	1 μm	100 μm

Table 5: Stage selection requirement and solution

Requirement	Solution
High accuracy high resolution and repeatability	Good servo control, optical limit switches, and end stops
Jerk free ride at a high linear speed	Good actuation system
High strength to weight ratio exceptional stiffness and long-term stability	Aluminum as the material
Free from backlash	Pre-loaded precision ground ball screw
Free from axial play	Duplex bearing
Good cantilever load capacity and high stiffness	Linear motion guide bearing
Free from contamination	Anodized finish surface

Hence, based on the above criteria linear stages (Model: LMS-150-200) have been bought from HOLMARC Opto-mechatronics Pvt Ltd, India. These stages have stepper motor control, which can provide high acceleration for extremely smooth motion and accuracy without any wear, heating, and cogging. They use crossed roller guides and precision ground lead screws, which are driven by directly coupled stepper motors. The motion is ruled in a way so that guiding errors of each element are absorbed in elastic components of the elements. This design provides sufficient structural stiffness and thermal symmetry. The platform is made of Aluminium alloy B51S and is anodized. The dimensional drawing of X, Y, and Z stages are given below in Figure 3.4 and Figure 3.5. Figure 3.6 shows the images of the linear stages. Table 6 contains the values

of dimensions shown in Figure 3.4.

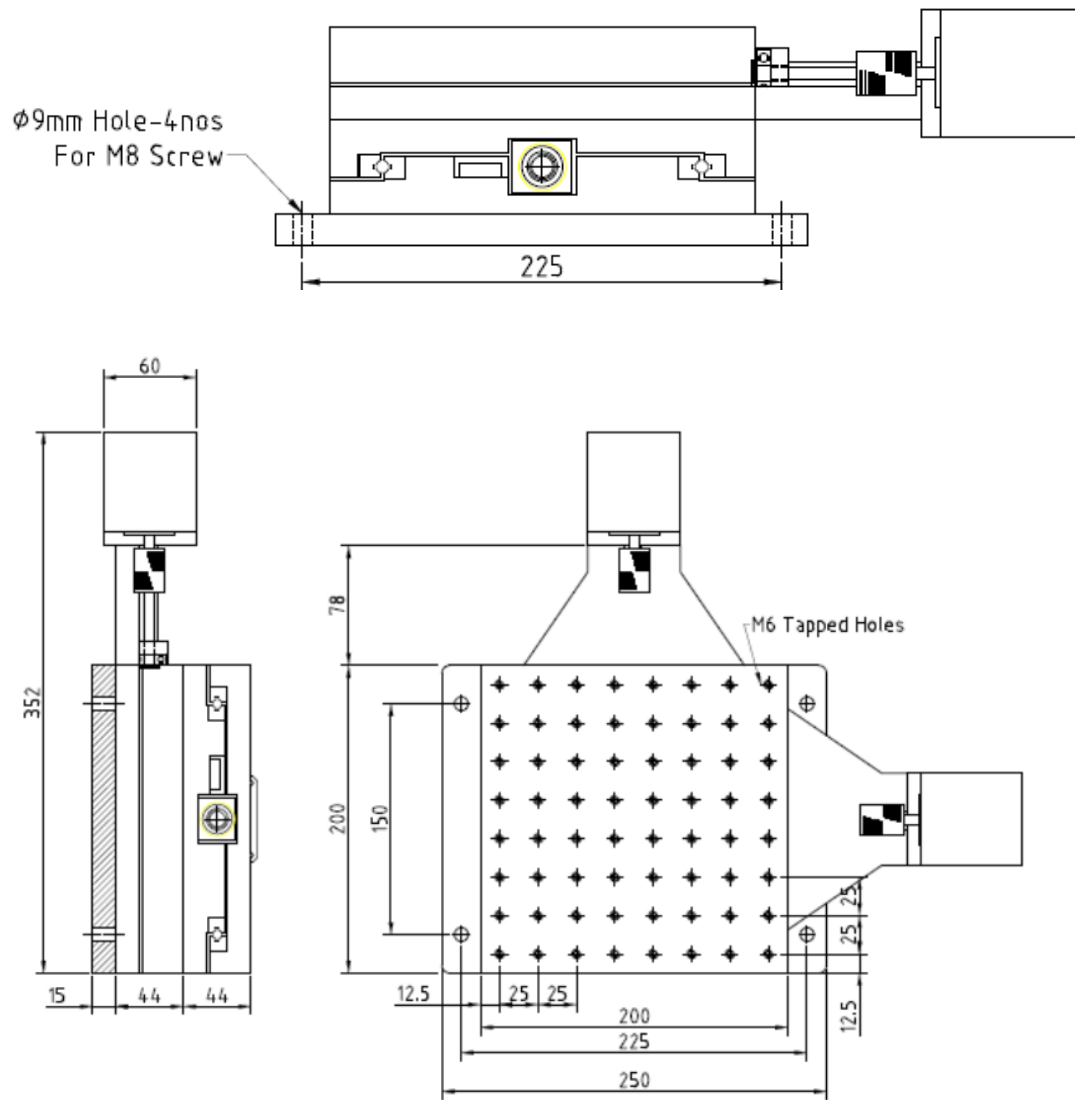
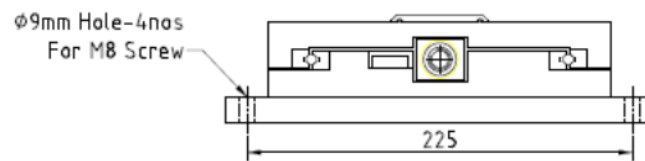


Figure 3.4: CAD drawing of linear X (or Y) stage



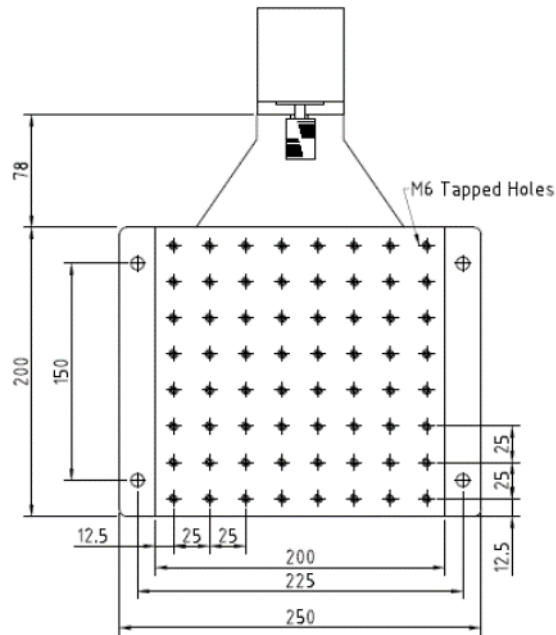


Figure 3.5: CAD drawing of linear z-stage

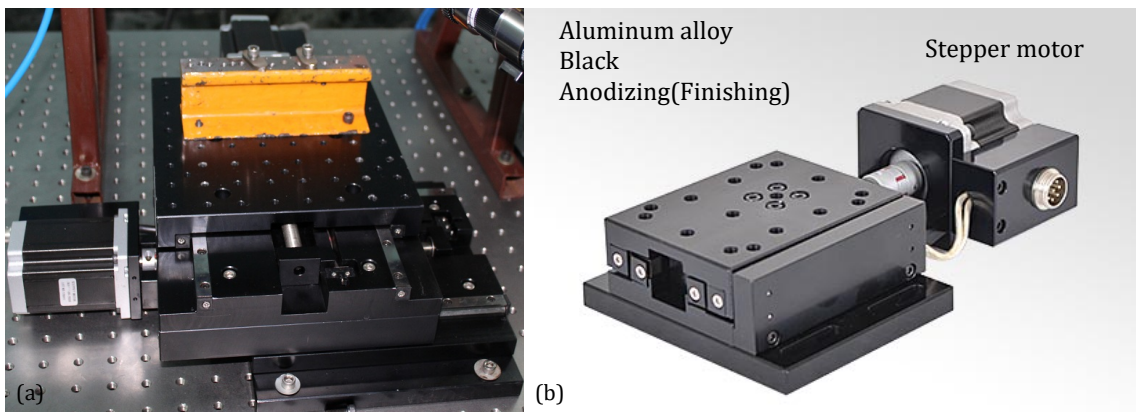


Figure 3.6: (a) Linearly motorized XY-stage (b) Linearly motorized Z-stage

Table 6: Machine XYZ stage specifications

Parameters	Value of x and y stage	Value for Z-stage
Total travel	150 mm	150 mm
Maximum travel speed	220 mm/min	220 mm/min
Accuracy	$\pm 2.5 \mu\text{m}$	$\pm 2.5 \mu\text{m}$
Repeatability	$2.5 \mu\text{m}$	$2.5 \mu\text{m}$
Resolution	$0.3125 \mu\text{m}$	$0.3125 \mu\text{m}$
Maximum load	Axial-20 Kg Transverse-20Kg	Axial-50 Kg Transverse-50Kg

Design principles

The machine tool has been designed based on two different design principles. Two different prototypes of the machine tool have been designed. According to the first principle, the machine tool has to be the best functional design feasible as per the requirement. This prototype of the machine tool is based on the optimal functionality approach. It is considered to be a highly ambitious design, studied purely for research purposes. In this design, the components were selected initially for validation purposes. This version of the machine tool has been named 'Prototype-I'. According to the second principle, the machine tool manufacturability is the desired aspect. The functionality of the machine tool has to be optimized but the design should be simple, which can be easily implementable in reality. Configuration of the design has been optimized geometrically to match the performance up to the level of 'Prototype-I'. This new version of the machine tool has been named 'Prototype-II'. Figure 3.7 shows the basis of two versions of the machine tool graphically.

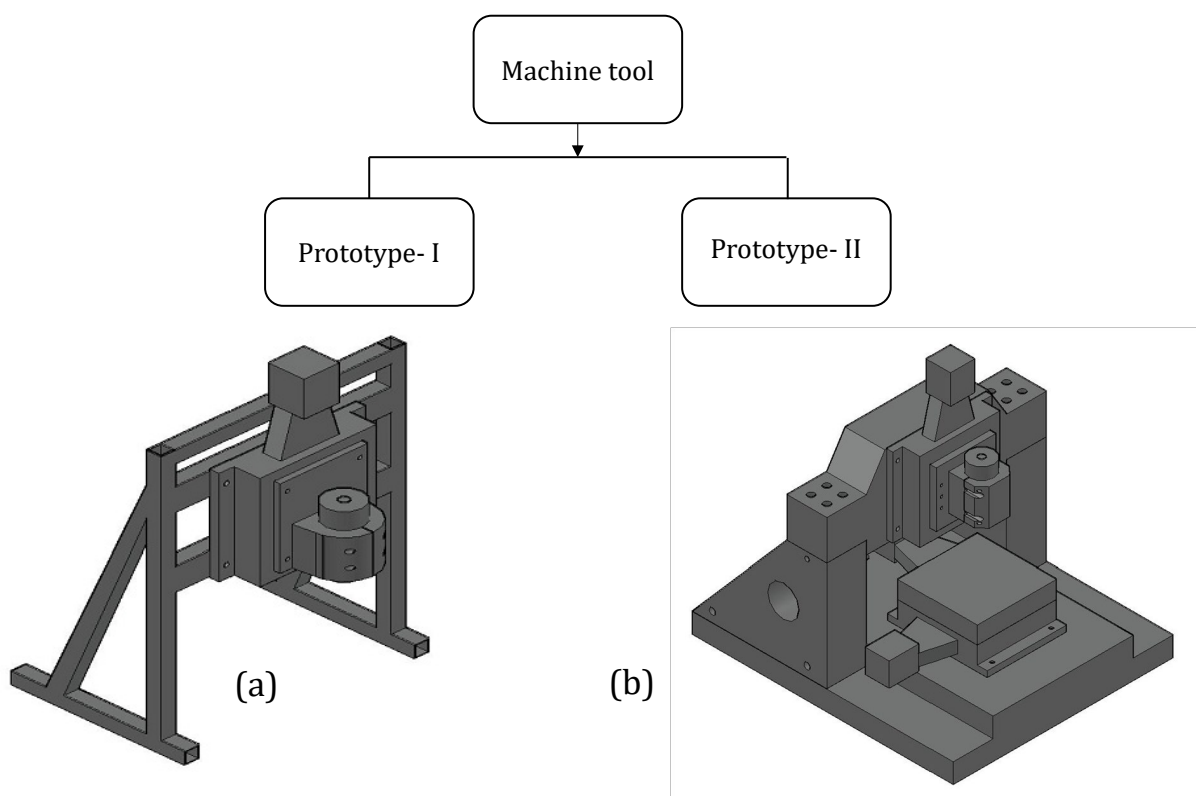


Figure 3.7: Two different prototypes of the machine tool (a) Prototype-I (b) Prototype-II

Parameters affecting machine tool performance

Parameters that can affect the performance of the machine tool have to be listed so that the machine tool components can be designed according to the most influencing parameters. A Fishbone diagram was drawn for finding out all the parameters affecting the machine tool performance. The Fishbone diagram for the machine tool is shown in Figure 3.8.

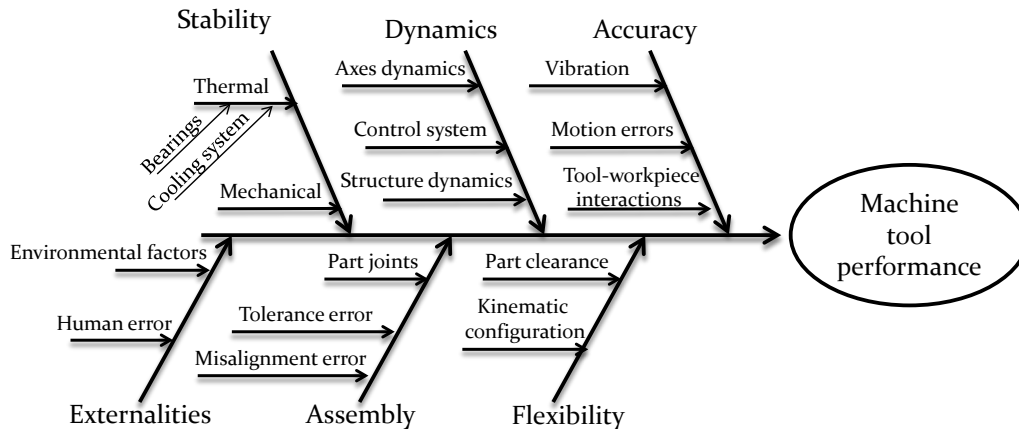


Figure 3.8: Fishbone diagram for machine tool performance

To decide the structural configuration of a machine tool, the structural loop has to be strong. The structural loop is the curve, which depicts the connectivity of different components of the machine tool. Action and reaction forces travel along this curve. The structural loop for the current machine tool is shown in Figure 3.7(a). Every component of the machine tool has its stiffness value. The stiffness of the parts of the machine tool can affect the accuracy of the machine tool significantly. A lumped mass approach can be followed to find the static loop stiffness of the second prototype of the machine tool.

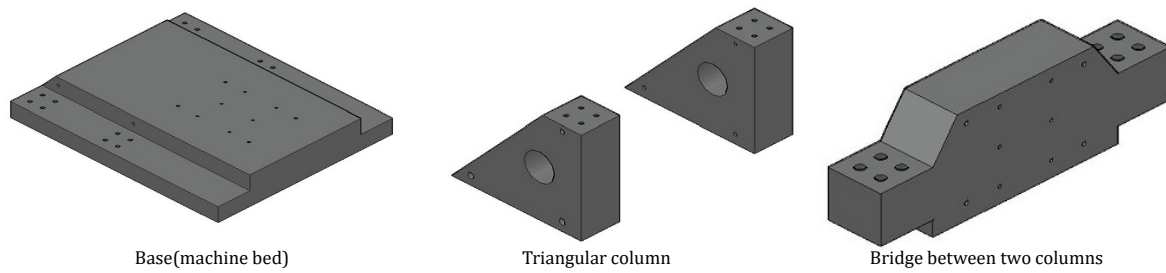
3.2.1 Design and analysis of optimum prototype machine tool

This section describes the approach applied for designing different components for the machine tool. Machine tool consists of the machine bed, two triangular columns connected with a bridge, linear stages, spindle mount, spindle, and tool.

3.2.1.1 Machine bed and Machine frame

The machine bed is the element, on which the whole machine is kept on. The machine frame is the supporting structure, which supports the components of the machine. Machine frame consists of both columns and bridge connecting them. The machine bed and frame both are made of granite (Figure 3.9). The machine bed has two shallow slots along both edges. These slots are to fix the side columns of the machine properly. Hence, both slots will be made highly flat by grinding. There is one linear pattern of holes at the center made for fixing the base plate of XY stages. The Frame structure consists of two side triangular columns and one connecting upper block. These columns have a larger bottom area and their bottom surface is highly flat. This design is made considering less material has to be used. The upper block has a trapezoidal shape. The backplate of the upper block is highly flat with a flatness of 5 microns. It's 207.5 mm

high surrounding walls are for holding Z-stage. These components are made of different materials.



Length of machine bed: 660 mm
Width of bed: 556 mm
Thickness of bed: 100 mm
Thickness of bridge: 100 mm
Thickness of peripheral walls: 207.5 mm
Thickness of triangular column walls: 100 mm
All the parts are interconnected through bolts

Figure 3.9: CAD models of base(machine bed) and frame

3.2.1.2 Spindle holding mount (SHM)

The spindle holding fixture is the critical part that is going to fix the spindle. Since the spindle is a major source of vibration in the structure; it has to be properly fixed relative to the machine frame. This prototype has various advantages over earlier models. It has extra ribs to support the hang of the spindle. It also includes additional rings, which provide support to the top of the spindle. CAD models and drawings of SHM and external rings are shown in Figure 3.10.

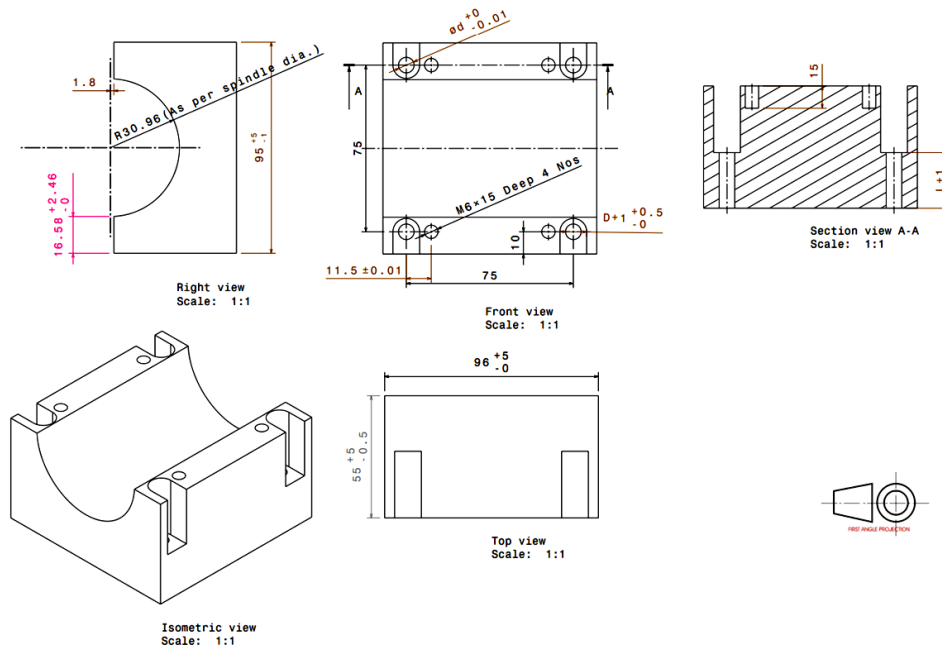


Figure 3.10: CAD model and drawings of spindle holding mount (SHM)

3.2.1.3 LINEAR MOTORIZED STAGE

The images of linearly motorized stages X, Y, and Z are already shown in Figure 3.6. To simplify the analysis and reduce the mesh number, these stages have been modeled accordingly without compromising on their physical behavior. CAD models and drawings are provided in Figure 3.4 and Figure 3.5.

3.2.1.4 SPINDLE:

Spindle modeling has been difficult due to a lack of information about its inner components. Still, from general information about spindle components, its major components have been modeled. Shaft, bearings, rotor, and casing are important parts of a spindle. Various configurations of spindle have been analyzed to match the actual spindle performance. CAD models of optimum configuration have been shown in Figure 3.3.

3.2.1.5 MACHINE TOOL ASSEMBLY

Integration of the components of the machine tool has been performed. Z-axis unit is bolted on z stage holding fixture. SHF holds the spindle. XY stage has been positioned on the machine bed accordingly. The assembled machine tool is shown in Figure 3.11.

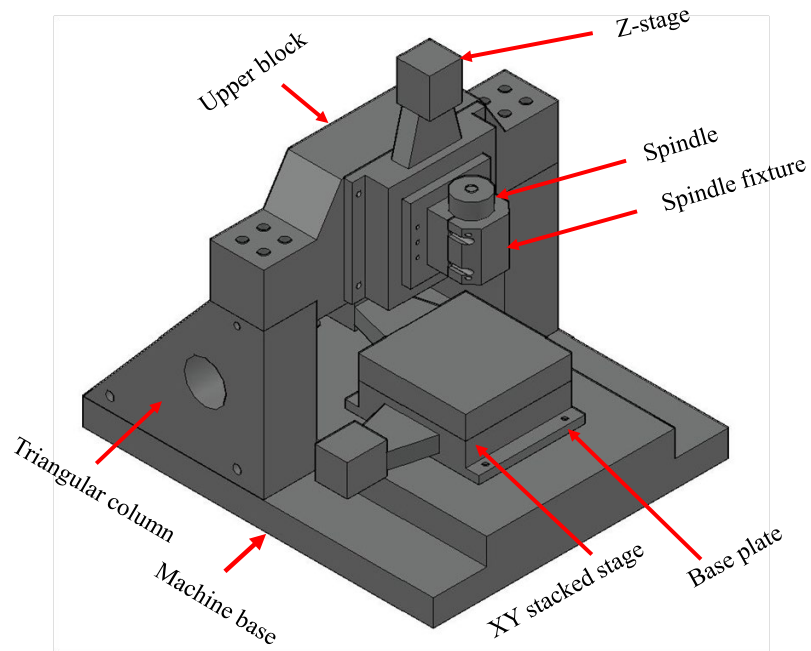


Figure 3.11: CAD model of assembled machine tool

Static analysis

The whole machine is analyzed for the static case. The Solid model was imported from AutoCAD and then analyzed. Material is defined as per requirement. Property values considered for the analysis are given in Table 7.

Table 7: Mechanical properties of the materials involved in FEA

Sl. No.	Materials	Density (kg/m ³)	Young's modulus (GPa)	Poisson's ratio	Damping characteristics(Log decrements)
1.	Natural granite	2900	90	0.25	0.015
2.	Cast iron	7200	120	0.26	0.0045
3.	Mild steel	7850	210	0.3	0.0023
4.	Stainless steel	8000	193	0.3	0.0023
5.	Aluminium alloy(B51S)	2800	80	0.033	0.0003

The bottom of the machine base is fixed. A force of magnitude 5N each is applied in x, y, z directions on the tool holder tip. The shaft of the spindle is given a rotational velocity of 60,000 rpm. The total deformation and von-mises stresses are found. Different configurations of the

machine are analyzed to calculate the maximum deformation in the structure. The design of the machine base is iterated by incorporating changes. Machine base without slots has been tested. It has been found that a base with slots provides a good amount of rigidity to the structure. Their results have been shown in Figure 3.12. The effect of the bearings in the spindle and the joints in the linear stages have been considered in the FEM analysis. The bearing parameters like axial and radial bearing stiffness, damping coefficients have been selected based on the original bearing parameters of the spindle. The parameters have been incorporated in the FEA simulation. The maximum deformation, as well as stress, have been found at the tip of the tool holder in the spindle. It can be seen that the proposed model of machine structure has provided superior rigidity to the assembled high-speed micro-milling machine tool.

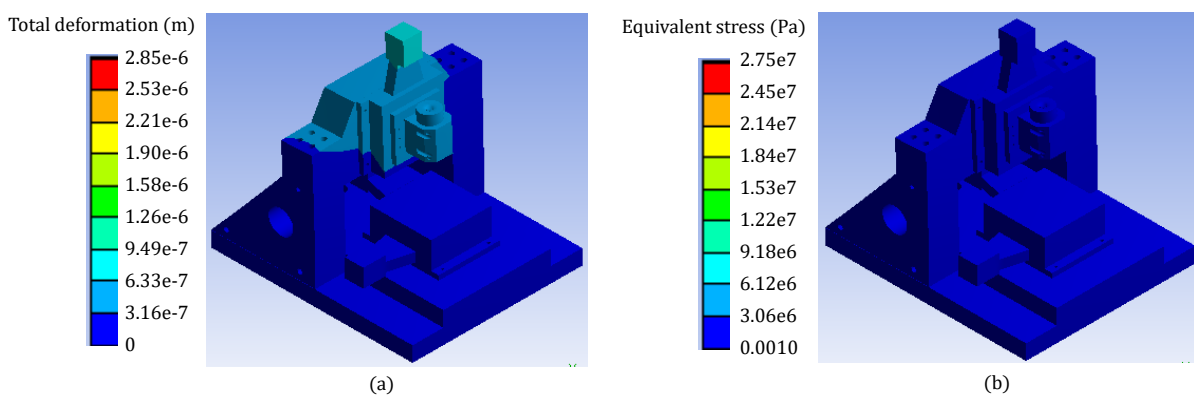


Figure 3.12: (a) Total deformation(m) and (b) equivalent stress (Pa) of static structural analysis

Modal analysis of unassembled frame

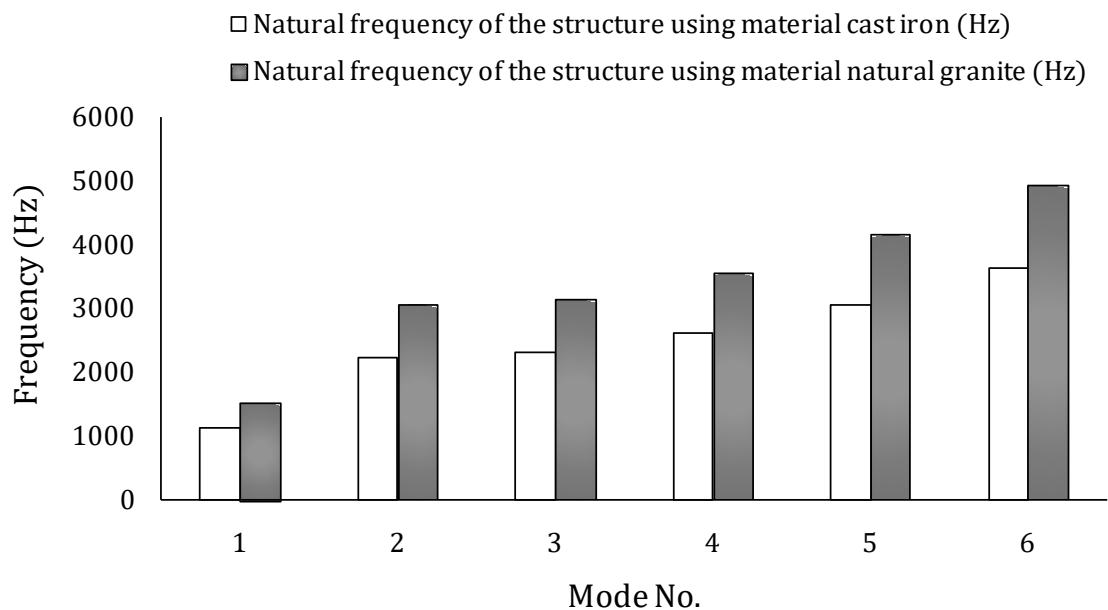


Figure 3.13: Comparison of natural frequencies of the unassembled frame using natural granite and cast iron determined in modal analysis

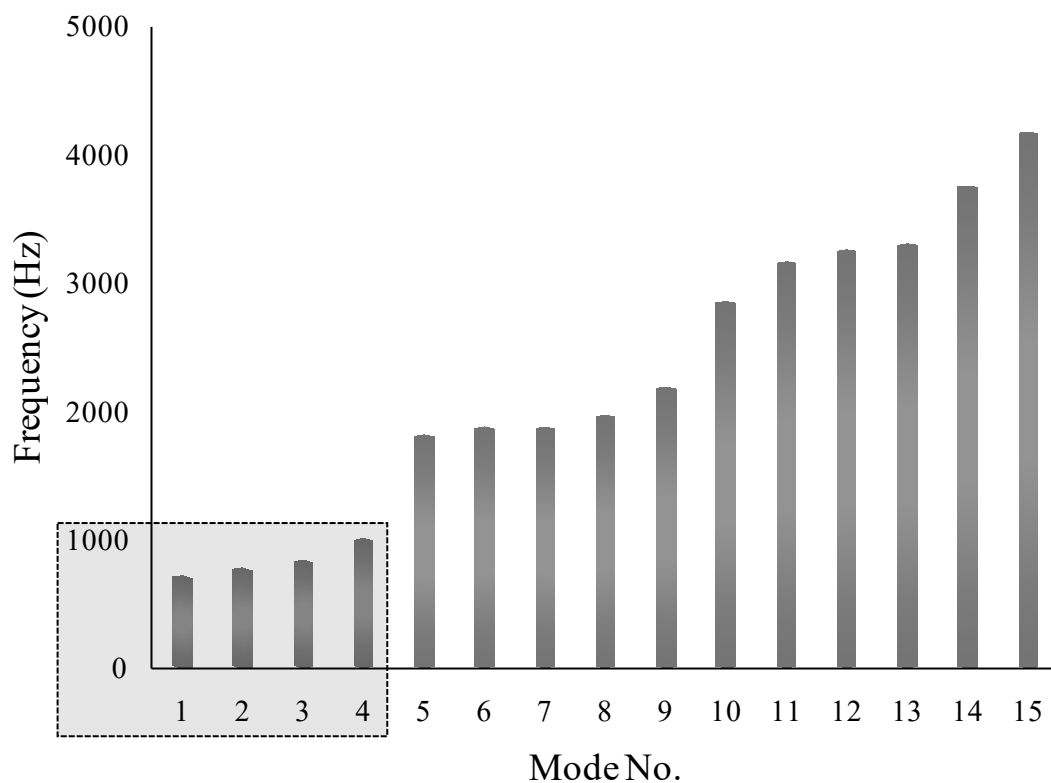


Figure 3.14: Natural frequencies of the assembled micro-milling machine tool determined in modal analysis

Mode shapes in modal analysis

Modal analysis has been performed on the individual unassembled structure with materials choosing natural granite and cast iron. The model with natural granite created a fewer number of resonances as shown in Figure 3.13. Hence, natural granite has been finalized for machine structure. Further, the machine structure has been assembled with spindle assembly and linear stages and modal analysis has been performed on the assembled micromilling machine tool. The bottom of the machine base is constrained and the bottom of the column structure is fixed. The plots of natural frequencies are given in Figure 3.14. The maximum value of excitation frequency is $(60,000/60 = 1000)$ 1000 Hz. As per the plot shown in Figure 3.15, only four resonances have occurred with the working frequency of the spindle. However, the deformation in the 2nd and 3rd mode shapes shows that the deformation was found in the motor of the linear stages (as shown in Figure 3.15). Hence, there are only two natural frequencies where the structure is creating resonance with the working frequencies of the spindle. Therefore, the structure is highly reliable for vibration isolation.

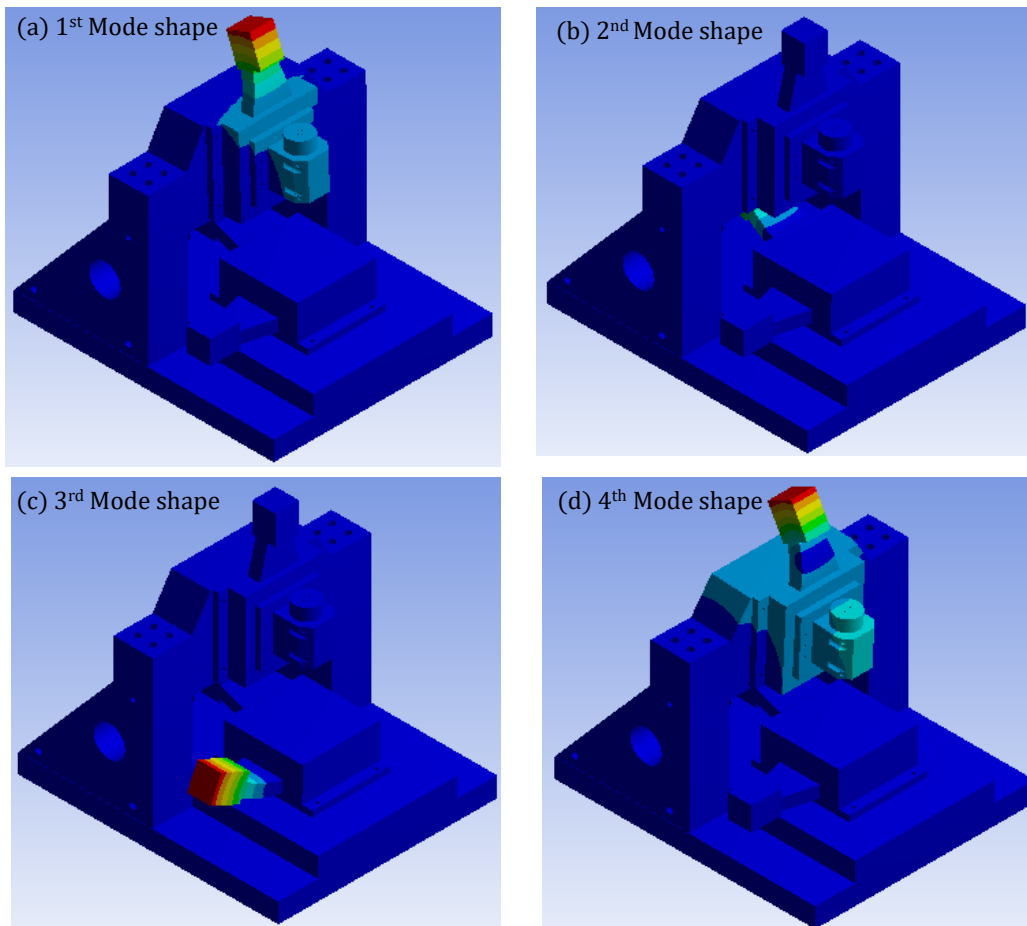


Figure 3.15: Mode Shapes in modal analysis

Harmonic response analysis

Frequency response analysis is needed to know the response of the machine tool under harmonically varying cutting forces. It is done using the harmonic response module of ANSYS. During this analysis, the same force is applied identically as in the case of static analysis. To include rotational velocity load, the equivalent amount of moment is applied on the shaft of the spindle. The amplitude of the deformation and at critical points with respect to frequency is plotted in Figure 3.16. During frequency response analysis, an amplitude vs. frequency plot is obtained for shaft tip in all directions. Peaks can be seen in all these plots near modes. The amplitudes of vibration for the machine tool were approaching towards nanometer level for both Y and Z axis. Hence, the structure shows high dynamic rigidity. The striking feature found is that the response has a lower value at higher frequencies in almost all cases. This is a good indication of the rigidity of the structure at high-speed operation. After seeing the mode shapes, 235 Hz is found as the most dominant frequency for both the Y and Z axis. The analysis has been performed along the Y and Z axes only because the deformation along X-axis was negligible as per the mode shapes.

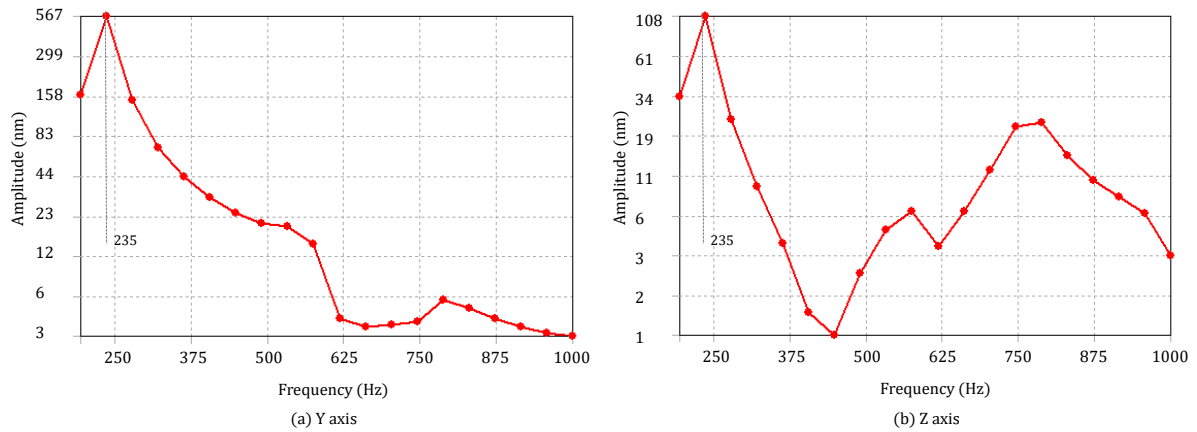


Figure 3.16: Results of harmonic response analysis

Thus, after all the experimental and FEA analysis, the final developed machine tool (varnica V-60) which is also named as basic setup in this thesis has been shown in Figure 3.17.

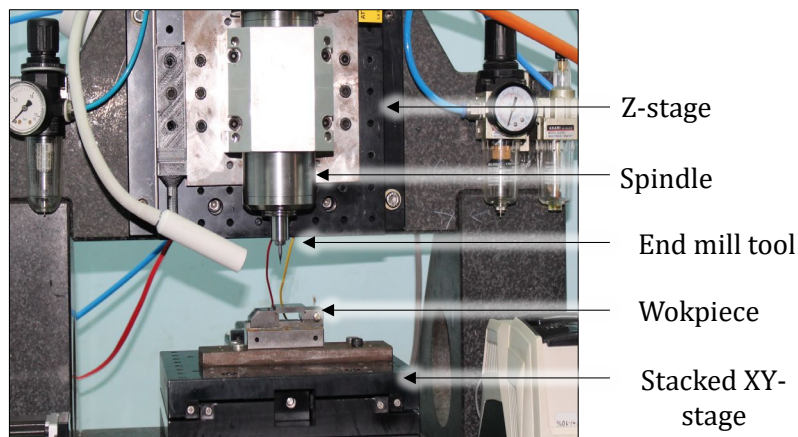


Figure 3.17: Basic experimental setup of micromachining

Machine operation

The three axes of micromilling machine have a stacked XY stage while the Z stage is mounted on a granite frame. All these three stages are connected to the dedicated computer (PC) through a controller (Mach3 micro position controller) which is further configured through software MACH3 loader (Figure 3.18).

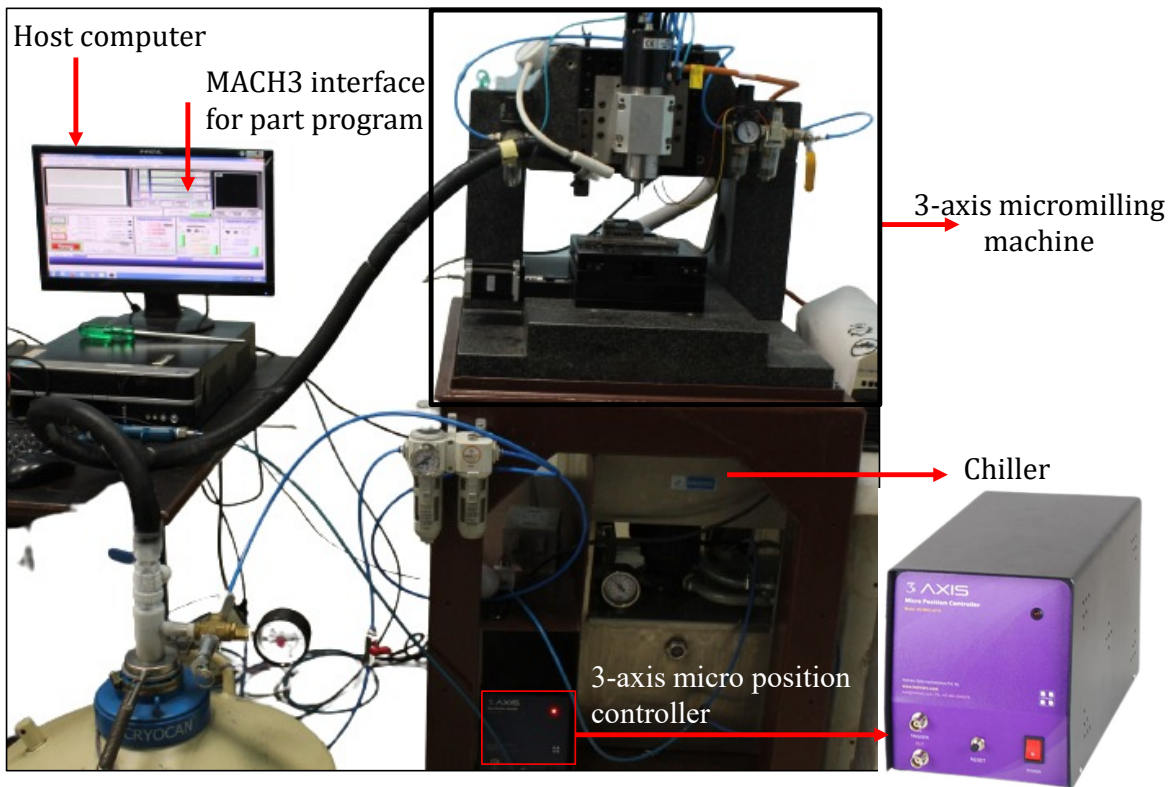


Figure 3.18: Schematic of the experimental setup

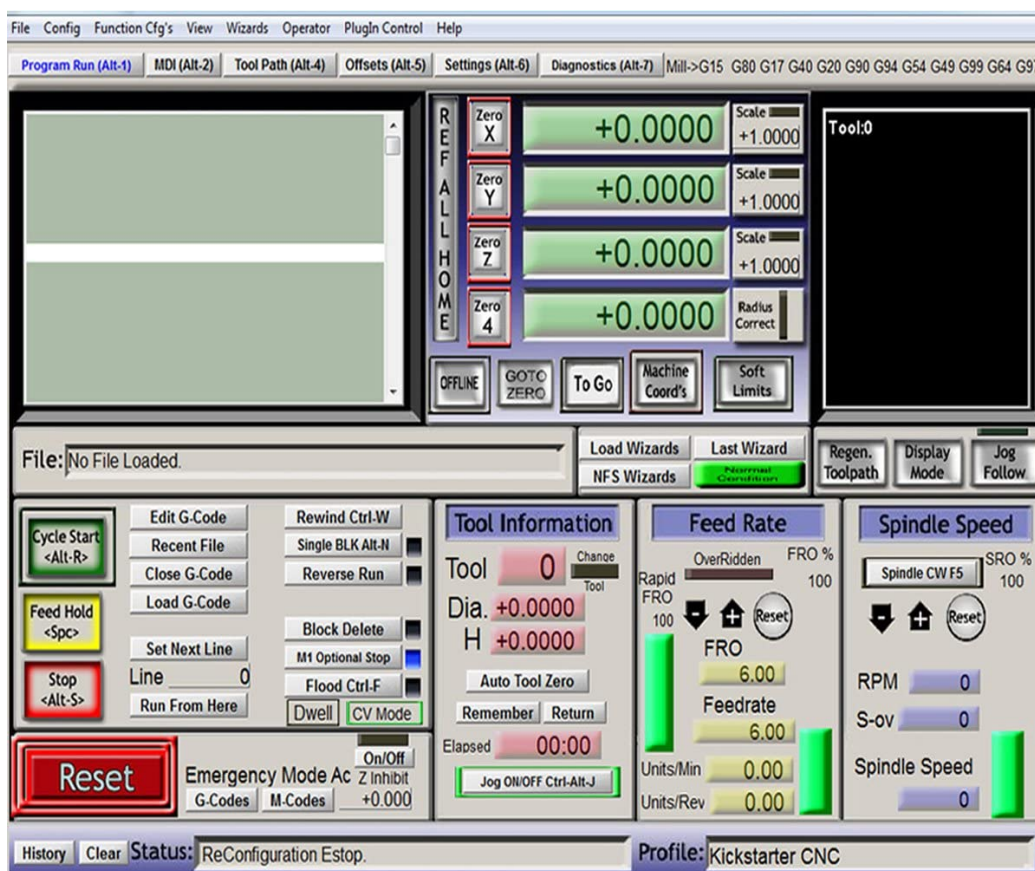


Figure 3.19: MACH3 loader software(Ref 110)

Here the input is fed in the form of part program G and M code. The output of code is transferred to the micro position controller which is responsible for the interpretation of program to machine language and thus executes the motion of the tool. Software is having the capability to execute motion profiles like the arc, circle, etc. Although, auto CAD, DXF files can be directly inserted using CAM software(Figure 3.19).

3.3 High-speed micromachining setup (HSM)

The ultra-high-speed micromachining center was developed and installed in the machine tool Laboratory (MTL) at Indian Institute of Technology (IIT) Bombay(Figure 3.20). The setup has the versatility of milling as well as drilling. The three-axis micromilling machine has stacked X-Y stages while the Z stage which is pneumatically counterbalanced is mounted on a granite frame. It has a ceramic bearing spindle having a torque of ~ 4.3 N-cm, which is sufficient to cut superalloys.

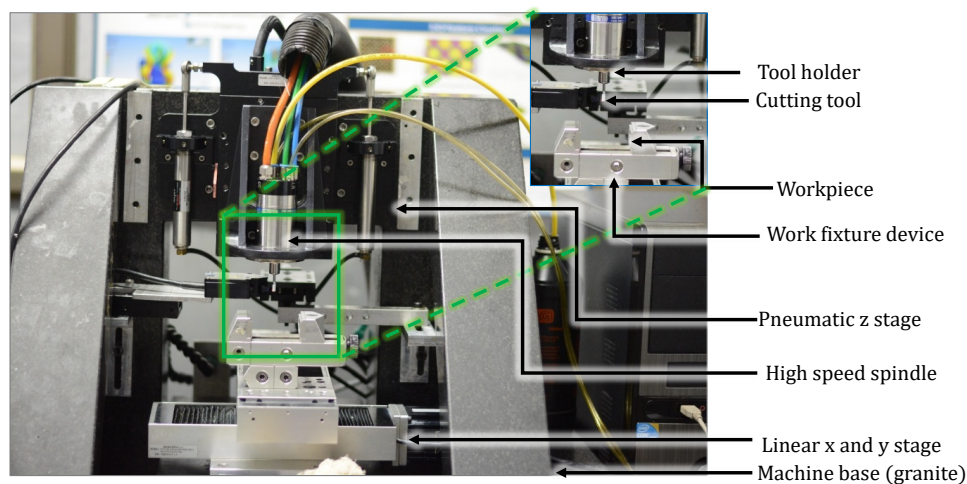


Figure 3.20:high-speed micromachining (HSM) setup

The technical description of the setup has been illustrated below:

AXES X, Y

- Travel distance: 100 mm
- Drives: precision ground ball screw/brushless DC servomotor
- Range of feed rate: 0.06-6000 mm/min
- Loading capacity: horizontal:25 kg, vertical:10kg, side:10kg
- Resolution:0.5 μm
- Accuracy: ± 0.5 μm

AXIS Z

- Travel distance: 60 mm
- Drives: non-contact direct drive /brushless linear servomotor
- Range of feed rate: 0.06-6000 mm/min
- Loading capacity: vertical:10kg
- Resolution: 1 nm
- Accuracy: $\pm 0.3 \mu\text{m}$

SPINDLE

- Spindle speed: 5000 -1,70,000 rpm with a variable frequency drive.
- Tool holder: Mega 4S (High-accuracy collet system with a runout in the collet of $1 \mu\text{m}$).
- Tool shank diameter: 3 mm

All three components are mounted on a granite frame to dampen the vibration and give dynamic stability. Further, the whole setup was assembled on a vibration isolation table.

3.4 Minimum quantity lubrication (MQL) assisted micromachining setup

Minimum quantity lubrication (MQL) assisted micromachining setup was developed on the basic setup model varnica V-60 with the integration of compressed air and lubrication supply system(Figure 3.23). Syringe pump arrangement was used for the controlled supply of lubricant(Figure 3.21) while compressor for the supply of desired pressure.



Figure 3.21: Syringe Pump

Technical specification details of syringe pump:

- Make and model: COMEN made, MODEL M200A
- Syringe capacity range: 10-60 ml
- Maximum flow rate: 2000 ml per hour

Delivery of the syringe is connected to the mist spray unit via a pipe as shown in Figure 3.22. Mist coolant spray unit is a simple nozzle having two holes.

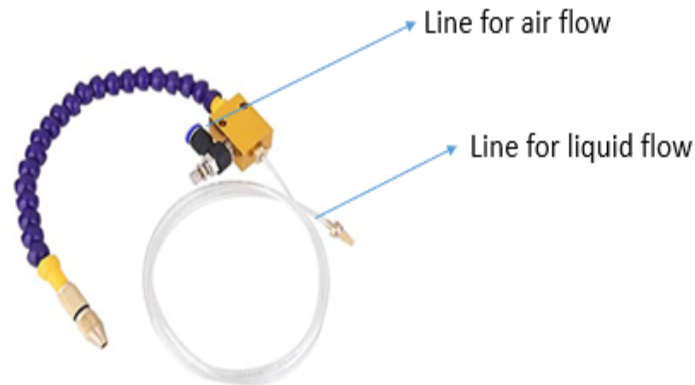


Figure 3.22: Nozzle for Mist Coolant Spray unit

The hole is used to supply CuO nanofluid at the desired flow rate had a diameter of 1 mm while at the periphery was another hole with a diameter of 8mm to supply compressed air at designed pressure.

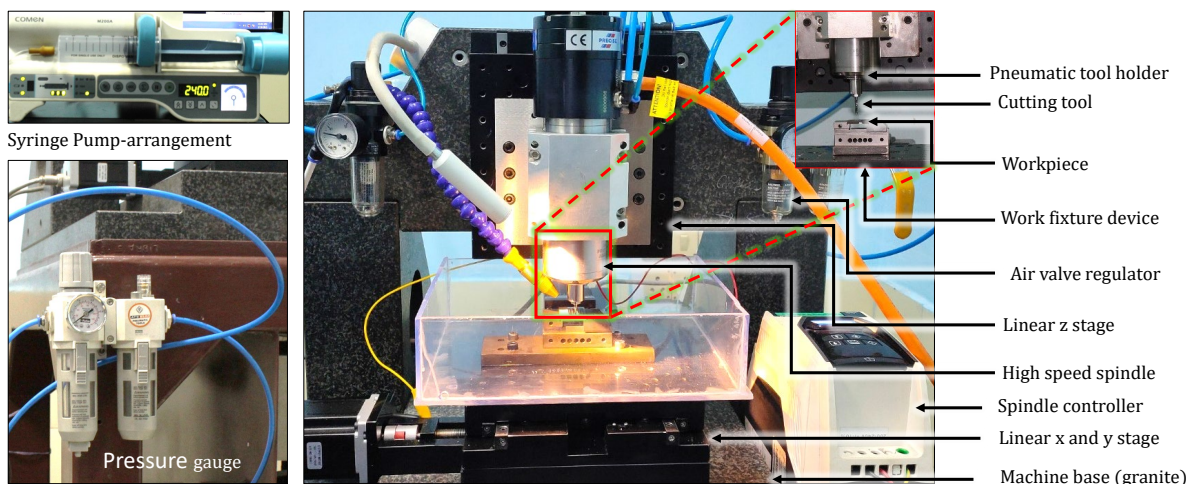


Figure 3.23: MQL assisted micromachining setup

3.5 Summary

The micromachining center has been designed, developed, and fabricated in-house. It is a granite structure fit with linear stages in three axes. The XY has less loading capacity than the Z-axis, all other specifications are the same in the X, Y, and Z axes. The developed micromachining center is capable of doing micro turning, micro drilling, and micromilling. It can use cooling arrangement of MQL and cryogenic coolant. A high-speed micro machining center up to 1,70,000 rpm has been borrowed from IIT Bombay for the machining at high cutting speed.

The next chapter deals with the mechanism of burr formation in micromilling on the down milling side. This will help in understanding the problems and issues and may help provide a way of solution for the minimization or removal of the burrs.

Chapter: 4 MECHANISM OF TOP BURR FORMATION

4.1 Introduction

This chapter deals with the study of the top burr formation mechanism in down milling operation on Ti6Al4V. Detailed and simplified flute locus in the milling operation has been elaborated with varying uncut chip areas during the entry and exit of the flute. Furthermore, various shapes of top burr formation at different cutting parameters have been explored based on the mechanism of formation. Three types of burr formation during down milling (Serrated, longitudinal and curly burrs) were found during milling operation. Also, the effect of feed per tooth and depth of cut on the top burr formation has been analyzed through the statistical technique ANOVA.

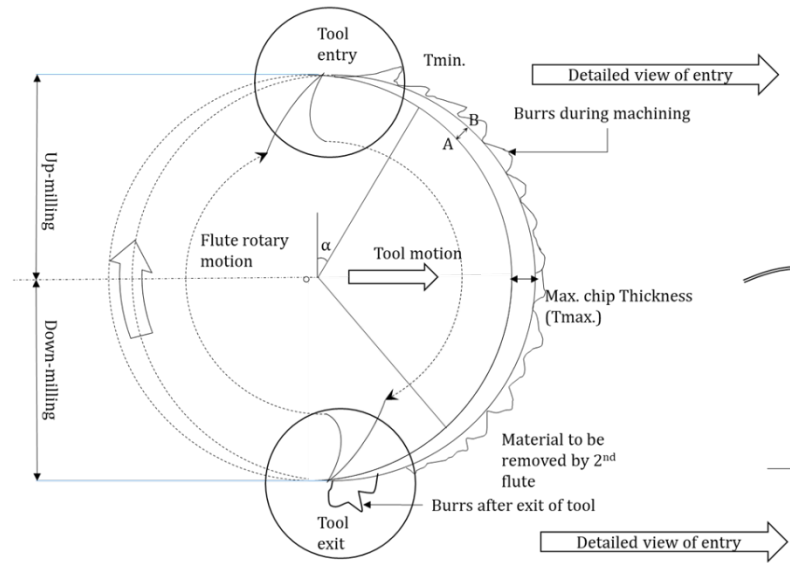
4.2 Motivation, objective, and approach

The top burr formed in the down milling is larger than the up milling side thus more dangerous for safety, surface quality, and productivity of product(Ref 111). Various approaches have been used in the past to minimize the top burr formation. However, minimizing the top burr is an intensive area of research. Many researchers were focused on the optimization of appropriate cutting parameters (cutting speed, feed per tooth, and depth of cut), tool parameters (tool dimensions/design and a number of flutes), tool material, tool geometry, and tool paths to analyze the performance of top burrs in micromilling operations(Ref 111). Additionally, various researchers were focused on cooling (low temperature compressed air, water, and cryogenic)(Ref 112) lubrication (water and oil soluble) and hybrid process (MQL)(Ref 113) to minimize burr size up to a maximum extent. Cheng et.al(Ref 114) had used resin coating on Ti6Al4V to minimize the top burr formation during micromilling. Although, understanding the burr formation mechanism theoretically was quite complicated because of three-dimensional plastic and elastic deformation with a high degree of freedom(Ref 59). Various models were developed analytically numerically(Ref 115) and through the finite element method(Ref 68) to understand Poisson burr and exit burr formation mechanisms more precisely in micromilling process. Zhang et.al(Ref 116) have proposed an analytical model to visualize the mechanism of Poisson and exit burr in micromilling operation considering size effect, minimum chip thickness, and cutting edge radius. They found an error of 16.8% while validating the analytical model with experimental in terms of burr width and height. Analysis of size effect and minimum chip thickness phenomenon on the cutting process in micromilling has been explained in literature(Ref 117). However, the literatures have clearly revealed that very limited research was done to understand the mechanism of burr formation on titanium alloys especially top burr. Hence, still further research needs to be performed to understand the various mechanisms

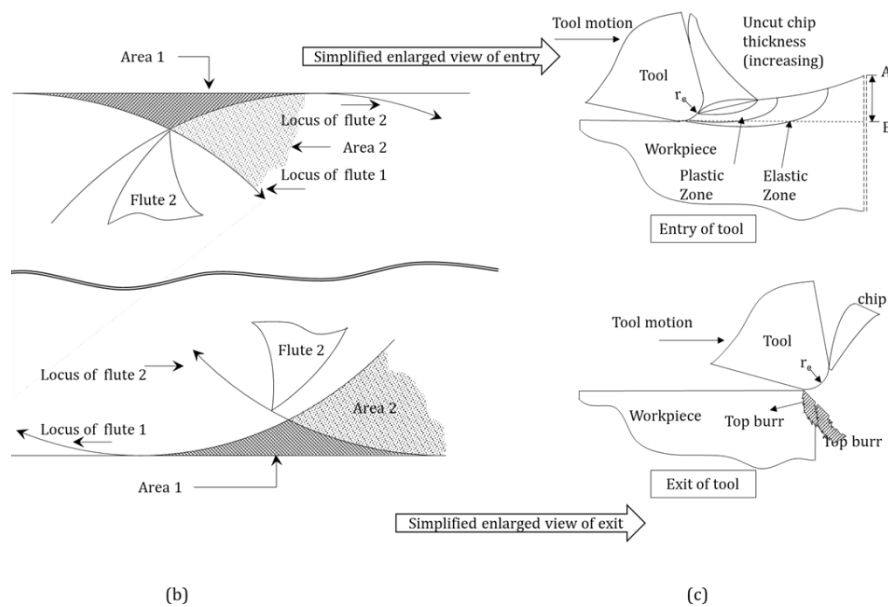
precisely to diminish burr formation. This paper presents the basic mechanism and statistical analysis of variable parameters like feed per tooth and depth of cut on top burr formation on Ti6Al4V alloy.

4.3 Top burr formation mechanism in micromilling (Theoretical approach)

Top burr formation in the micromilling operation has been studied. Figure 4.1(a) showed a typical diagram of milling operation. The top burrs in the up-milling side are a kind of entry burr and the top burrs in the down milling side are a kind of exit burrs. The only difference between the conventional entry and exit burr analysis is that the uncut chip area is not constant in the case of milling. Figure 4.1(b) shows the detailed entry and the exit of the flute. The flute enters with an increasing uncut chip area and exists with decreasing uncut chip area. Therefore, burrs form at two locations: Entry and Exit. Entry burrs are small in size and therefore, the mechanism of exit burr has been explained in detail. Figure 4.1(c) is the simplified view of entry and exit i.e. top burrs on the up milling side and top burrs on down milling side. When the tool completes one cutting stroke and exits at the end, it makes a chip as well as burrs. Burr formed in the direction above the plane of the paper (see Figure 4.1(c)).



(a)



(b)

(c)

Figure 4.1: (a) Top view of the interaction of two flute end milling tool with workpiece (b) Detailed view of entry and exit of the flutes of end milling tool (c) Simplified view of entry with increasing depth of cut and exit with decreasing depth of cut

Initiation, propagation, and formation of top burr

In down milling operation, as the tool exit from the edge of the workpiece during the successive pass, it leaves different types of chips and burrs on the periphery of the workpiece which varies

as per the material properties. However, mainly two factor leads to the top burr formation in down milling. Aurich et.al(Ref 118)in their research has studied the mechanism of Poisson burr formation through indentation of the cylindrical tool into the workpiece. As the cylindrical tool is displaced into the workpiece in the direction of cutter rotation, accumulation of materials occurred at the edges of the workpiece, and this side bulging is known as Poisson burr (Figure 2.7 (a)). A similar phenomenon has been observed here in up milling, as the tool enters the surface of the workpiece it starts removing the material with chip thickness varying from zero to maximum leaving chips and burrs on the surface of the workpiece. Although when the second pass has advanced over the first pass, it removes the up burrs formed at the edge (entry part) and it couldn't remove deform material (tear burr) of curved surface path hence up burrs were small in size. Thus, as the tool engages (entry) of the down milling operation, it has carried away the torn material which was left during the up milling operation (Figure 4.1 (c)). This torn material has stacked and redeposited on the top surface as a tool exit from the workpiece. In down milling, as the tool approaches the workpiece, it starts removing the material with uncut chip thickness varying from maximum at the point of engagement to minimum at the point of disengagement (Figure 4.1 (c)). So as the tool approaches, the workpiece experiences a sudden impact load; therefore, the contact area undergoes compression from all sides followed by several deformation shearing zones viz. shearing, primary shear, plastic deformation, and elastic deformation zones respectively (Figure 4.2 (a)).

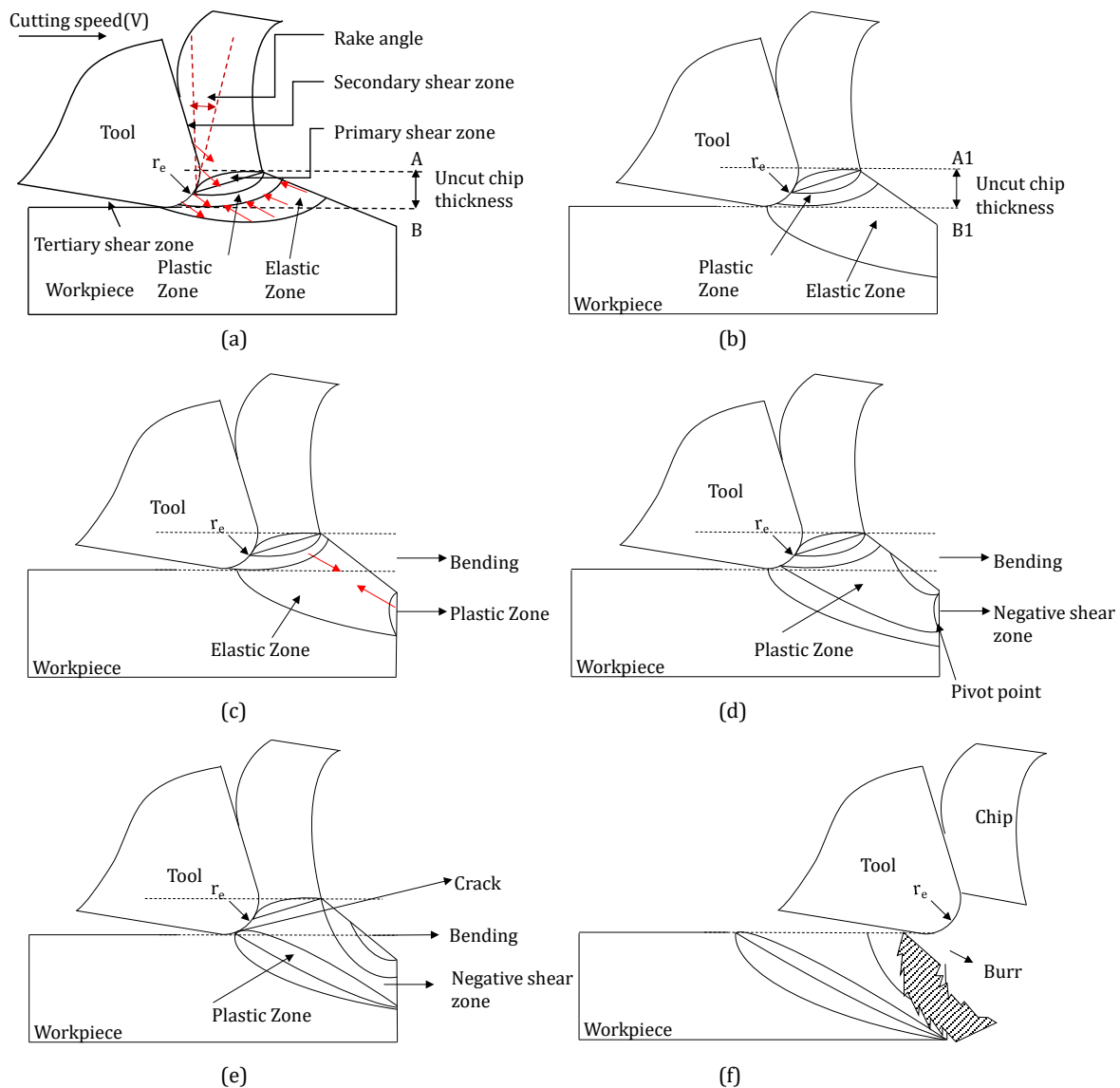


Figure 4.2: Stages of top burr formation: Initiation, propagation, and formation

As the tool has penetrated in the direction of cutting velocity; deformation zones propagate further in the direction of the least resistance region i.e., elastic zones until it has reached the workpiece edge (Figure 4.2 (b)). As the cutting tool continues to move forward in the cutting direction, plastic bending occurs at the edge (AB) of the workpiece due to which another plastic deformation zone is created at the verge of the workpiece (Figure 4.2 (c)). This zone is merged with the primary one and this phenomenon is known as nucleation. As the tool has advanced further very large deformation (pivoting) occurred at the edge; hence, one more shear zone (negative shear zone) was developed at the bending edge of the workpiece (Figure 4.2 (d)). The tool has proceeded further in the cutting direction; the force was diminished since the decrement in the area of resistance (uncut chip thickness) and crack initiated at the primary shear zone. Titanium alloy has a large critical fracture strain and negative shear zone which was

smaller than the permissible strain of material; hence, cracks propagated in the direction of cutting velocity (Figure 4.2(e)). Finally, a transition stage has come when the tool passed through the end of the workpiece with separation of chip and burr (Figure 4.2(f)). Therefore, during down milling top burr was formed due to side bulging as well as redeposition of tearing the material. Hence, down milling top, burr is larger with respect to up milling burr.

4.4 Experimental Validation

To study the mechanism of top burr formation, experiments have been performed on indigenously developed micromachining center “Varnica” model V60(Ref 119) at IIT(ISM) Dhanbad (See Fig 3(a)). The workpiece and tool can move in the lateral direction and vertical direction respectively. All three linear stages have positional resolution & accuracy of 100 nm & $\pm 2.5 \mu\text{m}$ respectively in a travel range of 150 mm.

4.4.1 Design of experiment (DOE)

A one mm diameter two flute coated (Al-Ti-N) end mill tool having a cutting edge radius of $6 \mu\text{m}$ and helix angle of 30° was used in the dry machining on Ti6Al4V. Full factorial experiments were designed considering two factors (Feed per tooth and axial depth of cut) and three levels have been selected based on literature survey, manufacturer’s recommendations, and machine limitations to experiment with details mentioned in Table 8.

Table 8: Input parameters and their levels

Factors	Level 1	Level 2	Level 3
Spindle speed, rpm	10,000		
Feed f , $\mu\text{m. tooth}^{-1}$	4	6	8
Axial depth of cut a , μm	40	50	60

Apart from this, an independent analysis of the radial depth of cut has been analyzed setting the tool path in such a manner that, the radial depth of cut starts from the maximum value (tool diameter) and ends at the negligible radial depth of cut (See Figure 4.3 (b)).

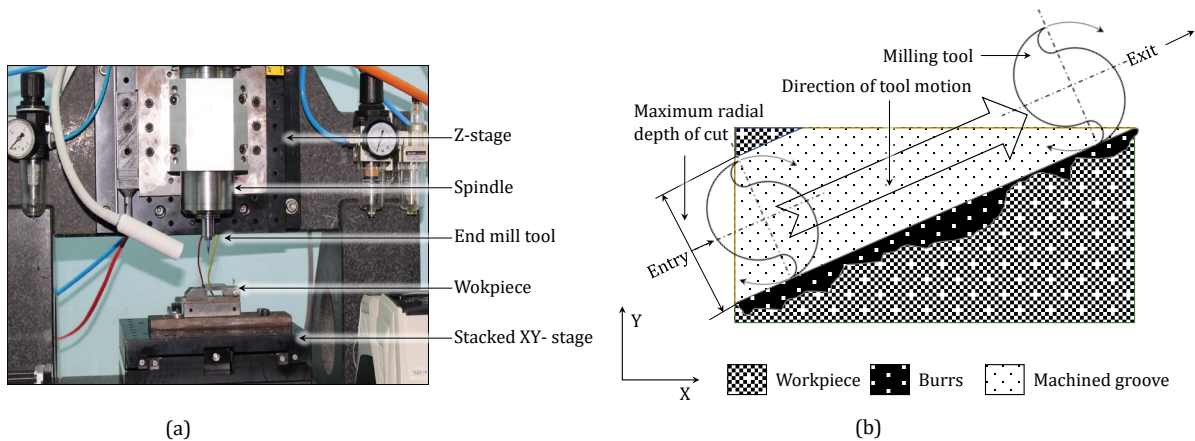


Figure 4.3: (a) Experimental setup (b) Tool path planning

Figure 4.3 (b) shows the tool rotation and the feed direction with top burr formed during up milling (a very small portion) and down milling operation (throughout the machining length). Top burr during up milling and down milling are shown. Oliveira et al (Ref 117) had investigated that mechanism of chip formation in micromilling depends on four situations as shown in Figure 4.4. If the axial depth of cut is less than the tool edge radius then either rubbing or burnishing will occur Figure 4.4(a). If it is taken close to tool edge radius but still below the tool edge radius then plowing (cutting) initiates but with a negative rake angle Figure 4.4(b).

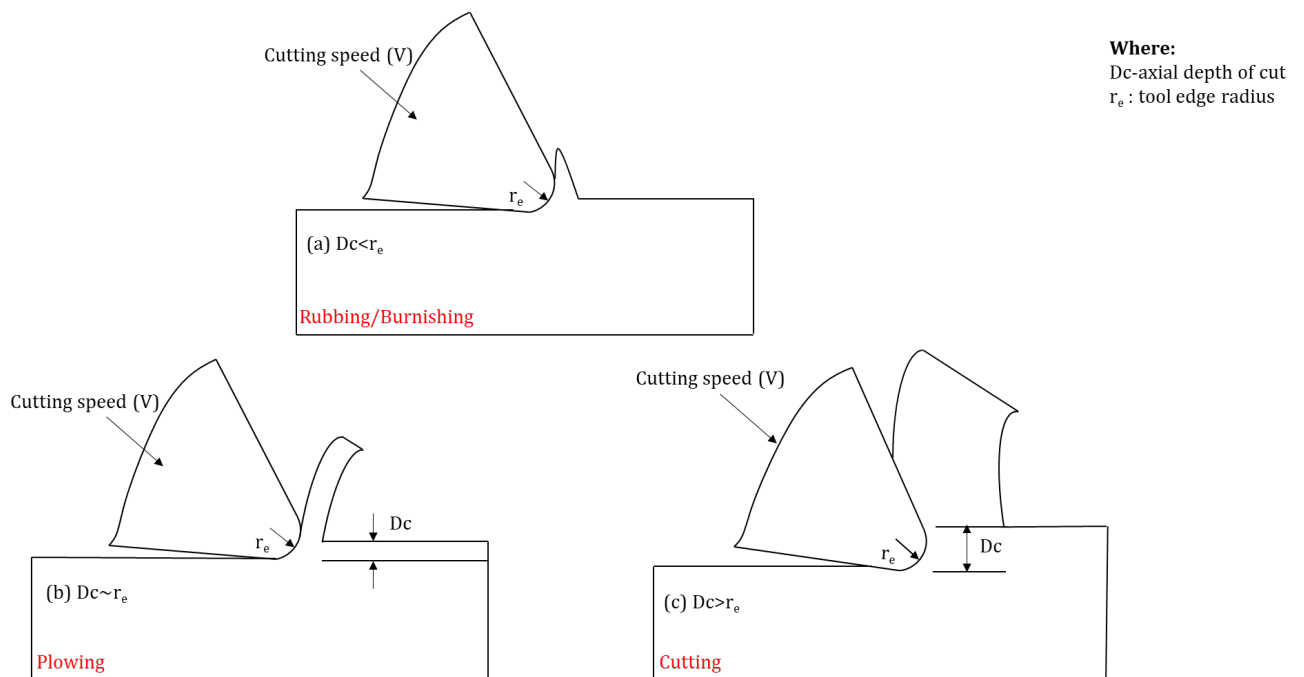


Figure 4.4: Mechanism of micromilling under different cutting depth conditions: (a) rubbing/burnishing (b) plowing (c) cutting ((Ref 13))

However, as it goes beyond tool edge radius then actual cutting starts, since the conversion of rake angle from negative to positive Figure 4.4(c). Hence, axial depth of cut is taken more than

the tool edge radius to ensure the cutting and not rubbing/plowing. In the experimental process, a slot was made with a variable radial depth of cut with a cutting length of 25 mm and axial depth of cut 40 μm . A second cut was done for the repetition of the experiment. The setup was not disturbed to ensure the same axial depth of cut in the first and second cut onto the workpiece.

4.5 Results and discussions

4.5.1 Mechanism of burr formation

3D Profilometer and Scanning electron microscope (SEM) were used to characterize the top burr to validate the theoretical approach proposed in section 4.3 and further to classify the top burr based on shapes formation.

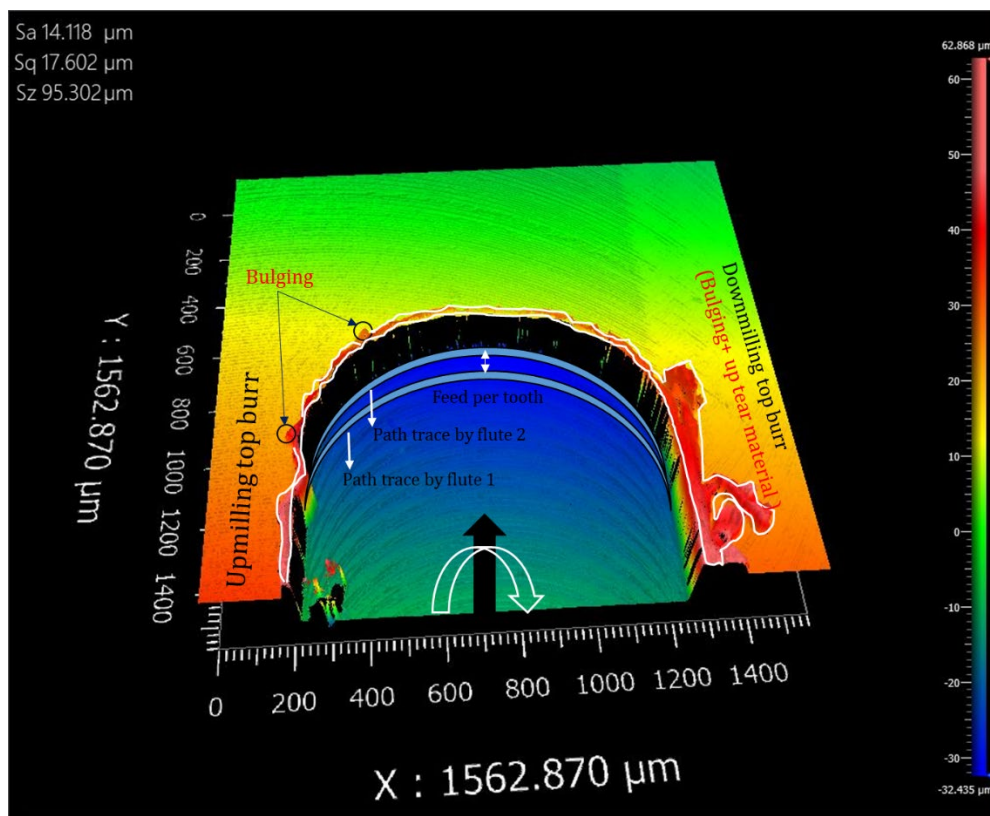


Figure 4.5: 3D profilometer image showing tool path interaction during the formation of top burr in up and down milling

As it can be seen from the 3d profilometer Figure 4.5, as the tool(path trace by flute 1) enters the surface of the workpiece in up milling, it has started removing the material with uncut chip thickness varying from zero at the entry to the maximum at the end of up milling (i.e., uncut chip area increasing) and then maximum at the entry of downmilling to a minimum at the exit(uncut chip area decreasing), leaving chips and burrs on the surface of the workpiece.

Although when the second pass (path trace by flute 2) has advanced over the first pass it removes the up burrs formed at the edge (entry part) and it couldn't remove deform material (tear burr) formed due to bulging action (Figure 4.5) of curved surface path hence up burrs were small in size. Thus, as the tool engages (entry) in the down milling operation, it has carried away the teared material which was left during the upmilling operation. This teared material has stacked and redeposits on the top surface as a tool exit from the workpiece. Thus, downmilling burr formed is a combination of tear material(upmilling) plus side bulging material hence, larger. As it can be seen from the 3d profilometer image shown above, as the tool(path trace by flute 1) enters the surface of workpiece in up milling, it has started removing the material with uncut chip thickness varying from zero at the entry to the maximum at the end of up milling (i.e., uncut chip area increasing) and then maximum at the entry of downmilling to a minimum at the exit(uncut chip area decreasing), leaving chips and burrs on the surface of the workpiece. Although when the second pass (path trace by flute 2) has advanced over the first pass it removes the up burrs formed at the edge (entry part) and it couldn't remove deform material (tear burr) formed due to bulging action of curved surface path hence up burrs were small in size. Thus, as the tool engages (entry) in the down milling operation, it has carried away the teared material which was left during the upmilling operation. This teared material has stacked and redeposits on the top surface as a tool exit from the workpiece. Thus, downmilling burr formed is a combination of tear material(upmilling) plus side bulging material and hence larger with respect to up milling top burr which is in agreement with the theory proposed in section 4.3. Further, Various kinds of top burrs form on the workpiece during micromilling and their classification is necessary to easily understand and differentiate between them. many researchers in the past used different names and classify such burrs on various aspects like burr location, burr shapes, and burr formation mechanism(Ref 59,62,120). Although, the burr formation mechanism is often unknown. In this study, top milling burrs (specific to titanium alloy) were classified considering all these factors. Also, the analysis is specific to down milling as larger burr formation in down milling side. Figure 4.6, Figure 4.7, and Figure 4.8 shown below clearly reveal that down milling top burr sizes are larger than up milling top burr which supports the theory proposed above. The nomenclature of top burr formation based on the mechanism of its formation has been explained based on three aspects:

4.5.1.1 Case I: If the ratio of feed per tooth to cutting-edge radius is less than 1

It can be observed from Figure 4.6 that curly top burr has been formed if the ratio of feed per tooth to cutting edge radius is less than 1. This shape is formed due to the rubbing and burnishing action which predominates when the tool edge radius is less than the minimum chip thickness(Ref 121).

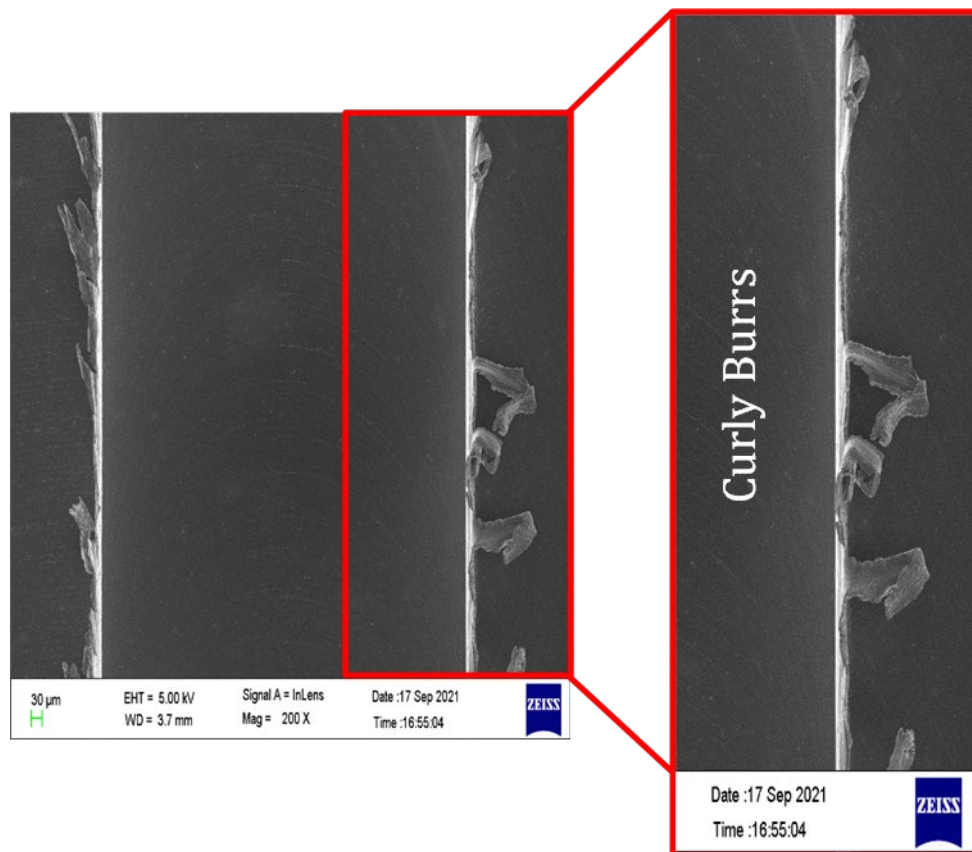


Figure 4.6: SEM image showing the formation of curly burrs (V_c :10,000 rpm, f :4 μm . tooth⁻¹,
 D_c :60 μm)

4.5.1.2 Case II: If the ratio of feed per tooth & cutting-edge radius equal to 1

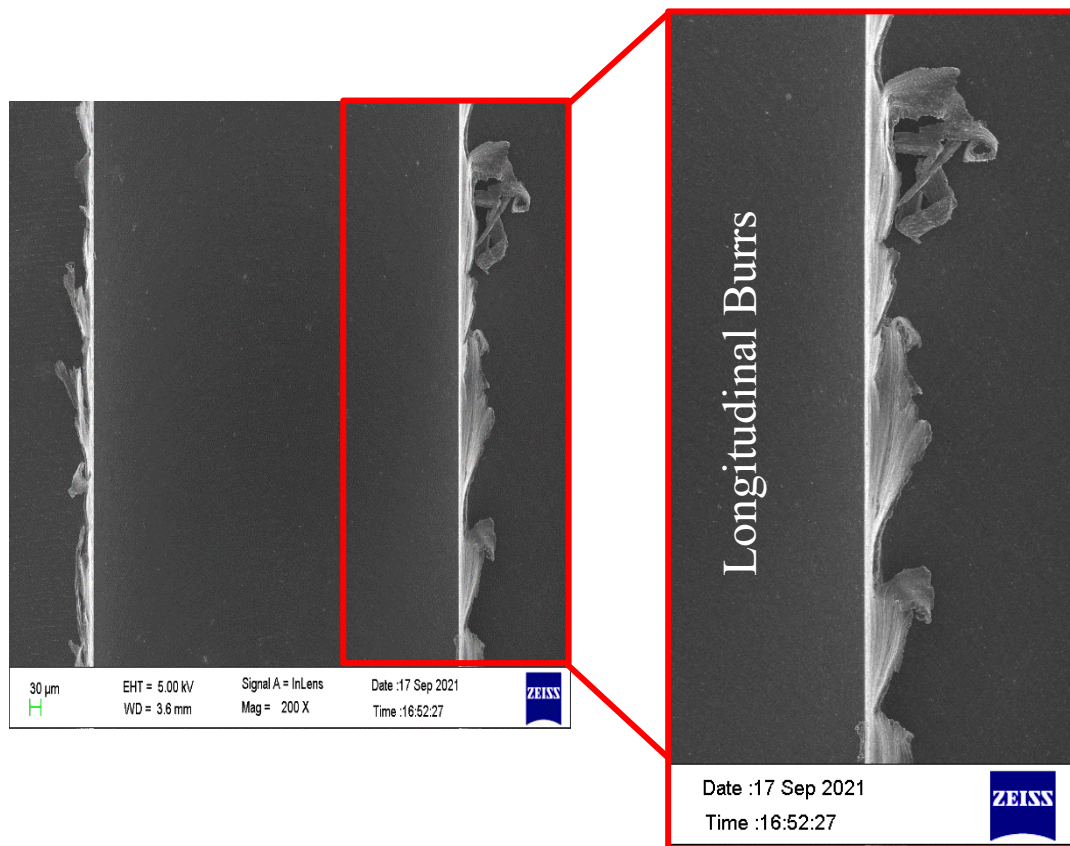


Figure 4.7: SEM image showing the formation of longitudinal burrs($V_c:10,000$ rpm, $f:6$ μm .
 tooth^{-1} , $D_c:60$ μm)

Longitudinal top burr (Figure 4.7) was a Poisson burr, which was formed on the surface of the machined workpiece caused by the combination of carried over torn chips of up milling and side bulging deformation at the tool exit. This type of burr can be easy if observed if the feed per tooth is close to the tool edge radius.

4.5.1.3 Case III: If the ratio of feed per tooth & cutting-edge radius is greater than 1

When feed per tooth is greater than tool edge radius then shearing phenomenon predominates over rubbing and ploughing which results in the formation of continuous serrated burrs. This shape(Figure 4.8) has been observed since titanium alloy has the inherent ability to form adiabatic shearing. These were formed at the edge of the workpiece and it has exhibited continuity longer than the cutting thickness of a one tool pass(Ref 122).

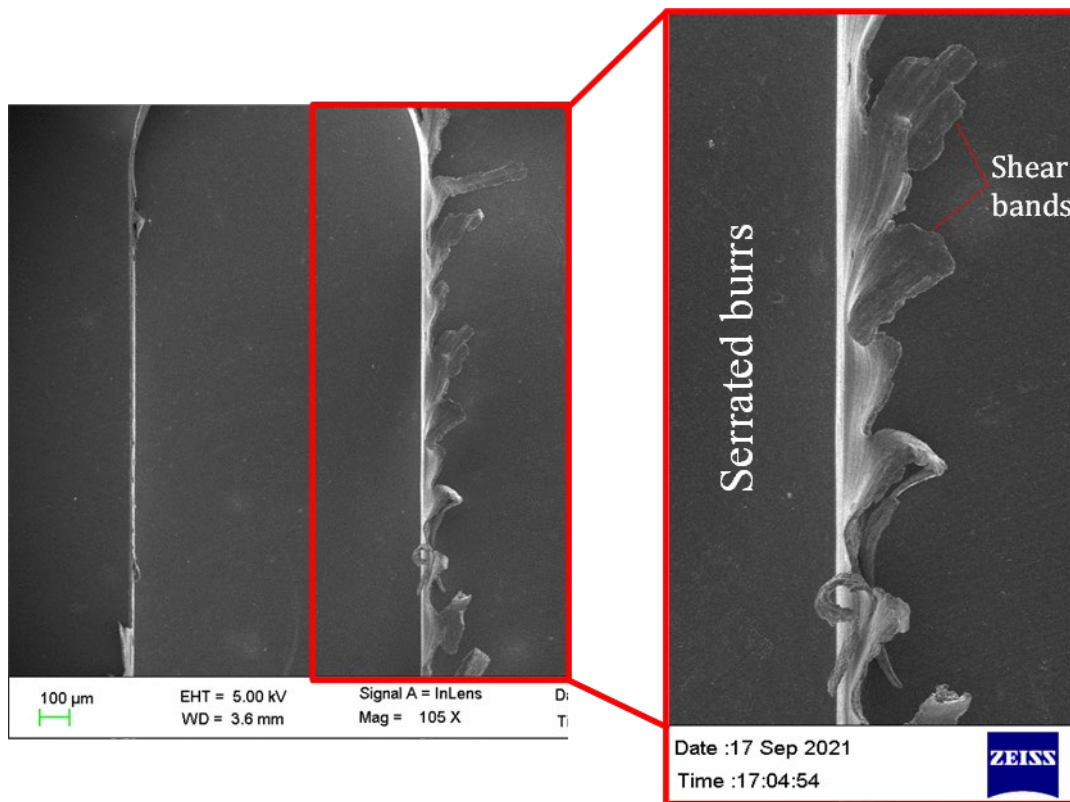


Figure 4.8: SEM image showing the formation of continuous serrated burrs (V_c :10,000 rpm, f :8 $\mu\text{m. tooth}^{-1}$, D_c : 60 μm)

4.5.2 Effect of radial depth of cut on down milling top burr

The radial depth of cut decreases with the tool feed and reaches a value of zero during the exit of the tool. Equivalent burr height(Ref 111) has been measured at every 0.05 mm distance two times and the two iterations are showing similar results. It is found that the variation of the radial depth of cut does not have any significant effect on the equivalent burr width (Figure 4.9). The above analysis was not explored at varying parameters due to insignificant results.

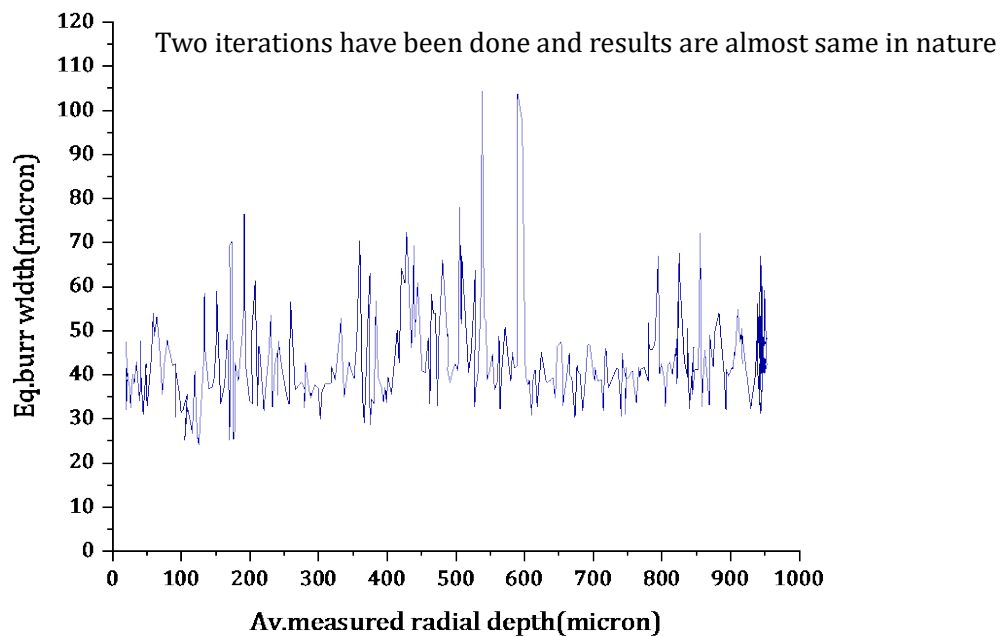


Figure 4.9: Effect of radial depth of cut on top burr formation

4.5.3 Effect of axial depth of cut and feed per tooth (ANOVA)

After the completion of the experiment, characterization was done using SEM to find the equivalent top burr width. After obtaining results, the data were statistically analyzed using ANOVA. It is a statistical technique to find the significance of input variables on the output responses (Ref 121). This was done by calculating the sequencing sum of squares (SS) for each parameter using equation 3.

$$SS = \sum_{i=1}^{i=n} (Y_i - Y')^2 \quad (3)$$

where n is the number of observations.

A high value of F-ratio for a given factor denotes the high influence on the outcome. Further, the magnitude of influence of each input parameter has been observed in terms of contribution ratio (%CR) which is given by equation 4. ANOVA results carried out at the level of confidence of 95% are given in Table 9 & Table 10. All parameters having P-value lower than 0.05 indicate statistical and physical significance on the down milling top burr and surface roughness.

$$\% CR = \frac{MSS - SS_{res}}{SS_{total}} \times 100 \quad (4)$$

Table 9: Full factorial experiments with output response

Process parameters			Output Response
Sl. no.	Feed ($\mu\text{m}/\text{tooth}$)	Depth of cut	Burr width (w_b)
1	4	40	131

2	4	50	107
3	4	60	80
4	6	40	92
5	6	50	95
6	6	60	50
7	8	40	86
8	8	50	54
9	8	60	42

Table 10: ANOVA table for down milling burr

SOURCE	DF	SS	MSS	F-ratio	P-value	CR (%)
Feed/tooth	2	3120.2	1560.1	14.82	0.014	46.41
Depth	2	3181.6	1590.8	15.11	0.014	47.32
Error	4	421.1	105.3			6.26
Total	8	6722.9				100

ANOVA was carried out to measure the impact of input parameters on the output response i.e., burr width in down milling side. From Table 10, it can be observed that depth of cut is a slightly more significant parameter contributing 47.32% causing top burr formation while feed per tooth has a contribution of 46.41 % which shows that both are significant in the formation of top burr.

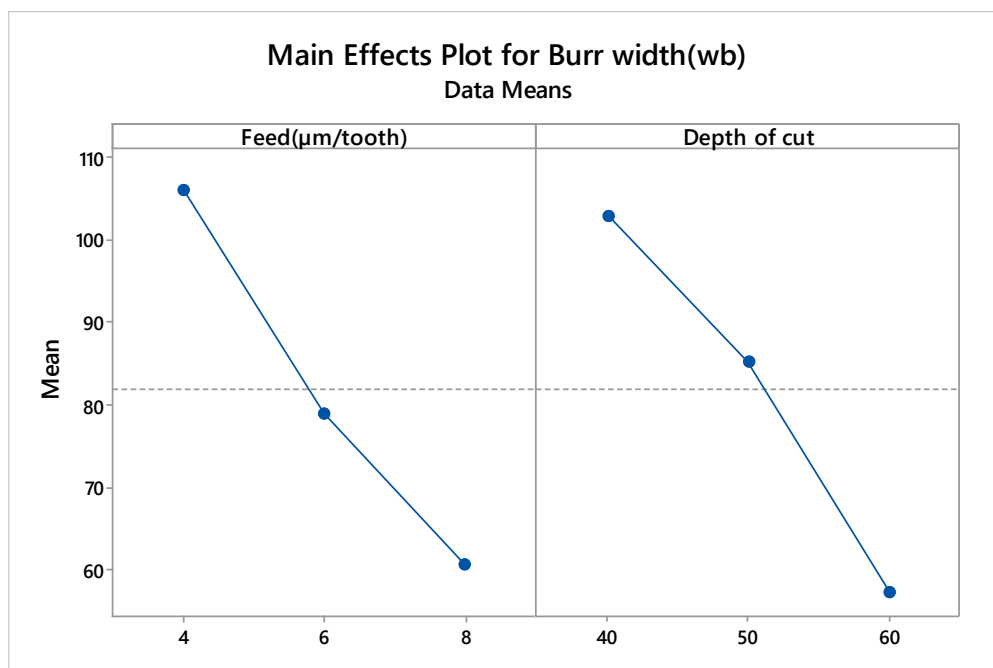


Figure 4.10: Main effects plot for down milling burr width in comparison to process parameters

In the main effects plot (Figure 4.10), one can be observed that each point shows mean/average equivalent top burr width for a particular level of feed per tooth and depth of cut. As feed per tooth increases from 4 to 6 and from 4 to 8 equivalent burr width decreases by 25.47 % & 42.7% respectively i.e., there is an inverse relationship between feed per tooth and depth of cut with equivalent burr width. at low feed per tooth equivalent, burr width form is very large. this is because the plowing effect is more pronounced and materials deform plastically to form larger burr(Ref 123). further, from the main effect plot, it can also be observed that equivalent burr width goes on decreasing with the increase of depth of cut. at a higher depth of cut, more heat is diffused into the chips due to which less heat remains forms on the surface of the workpiece(Ref 124).

4.6 Summary

Statistical analysis technique ANOVA has been employed to investigate the effects of depth of cut and feed per tooth on to the burr size. The axial depth of cut has taken an independent parameter due to the inclined tool path which gives continuous variation in the axial depth of cut from the tool diameter to zero. The basic mechanism of top burr formation in down milling has been explored. The down milling top burrs were classified for Ti6Al4V based on the mechanism of formation. Three types of top burr based on the behavior of material (Ti6Al4V) have been observed i.e., continuously serrated, longitudinal, and curly burrs. It is found that the down milling burrs were formed mainly due to the redeposition of material and side bulging action. The down milling top burrs are much larger than up milling top burrs regardless of other process parameters. ANOVA showed that the chip load (axial depth of cut and feed/tooth) are significant parameters for the burr size, an increase in the chip load reduced the burr size. The independent analysis of the effect of the radial depth of cut showed that there is no effect of changing the axial depth of in continuation on to the burr size. The burr formation mechanism may help in selecting the methods of reducing the burr size.

The next chapter is the second objective of the work. High-speed micro machining has been performed to see the effect on the burr size. It is expected that the high-speed cutting may exhibit low cutting forces that may help reduce the burr size.

Chapter: 5 HIGH-SPEED MICROMACHINING

(Kumar, M. and Bajpai, V. Experimental investigation on top burr formation in high-speed micromilling of Ti6Al4V alloy Proceedings of the Institution of Mechanical Engineers, Part B: Journal of Engineering Manufacture 234(4), 730-738)

5.1 Introduction

In this chapter, Experimental investigation and characterizations of top burr formation on Ti6Al4V alloy using end milling process were carried out. A scanning electron microscopy (SEM) identifies the burr formed on the machined surface. A new technique has been introduced to measure the top burr width (i.e. equivalent burr width) accurately. Equivalent burr width was calculated as the ratio of the total area of burr generated to the total height. Further, parametric analysis of cutting parameters and tool parameters has been investigated in detail.

5.2 Motivation, objective, and approach

Micromachining of difficult to cut metals as Ti and Ni alloys have always been challenging, as the low stiffness of micro end tool makes it very prone to failure(Ref 125)(Ref 126). High-speed micromilling (HSMM) can be a way through which chip load and stiffness can be reduced; however, at the same time, it creates chatter too. Previous researchers have investigated chatter instability and stability in micromilling process using finite element modeling and numerical approach(Ref 127)(Ref 128). Apart from chattering and damage to the tool, burr formation is a big threat in HSMM of Ti64 alloys. Burr generation is a common problem arising in machining. However, it predominates when machining of difficult-to-cut metal alloys is done. This is due to the generation of high temperatures at high cutting speed. Various analytical studies have been done to analyze cutting temperature and force in machining(Ref 129). The HSMM of aluminum and titanium alloy leaves a higher amount of burrs on the machined part as compared to conventional machining. Experiments have been performed on the micro-milling machine to find the effect of machining time on burr formation of Aluminum Alloy 1100(Ref 130). It has been observed that burr size increases with an increase in machining time because the tool got worn by increasing the machine time. A mathematical model to predict the exit burr height was developed and validated successfully by experimental results in high-speed micromilling of Ti64 alloy. It was observed that the burr height decreases by 90% as the speed increases from 50,000 to 2,00,000 rpm(Ref 131). Kizhakken(Ref 132)and Mathew developed mathematical model to predict the burr thickness in micromilling of Ti6Al4V alloy. They observed that the hyperbolic tangent material model gave better prediction over the johnson-cook material

model. Removal of micro burrs especially the top burr has been a challenging problem due to varying chip thickness, complex interactive effects among cutting parameters, and tool run out. Efforts had been taken for the elimination of burrs; however, it was value added, time-consuming, damaging close tolerances, and very expensive process(Ref 133,134). Effect of various parameters like cutting speed, feed rate, tool geometry, and the depth of cut on burr formation was analyzed for different work materials(Ref 135–137). Many researchers have successfully developed finite element 3D and 2D models of chip and burr size on Ti64 alloy in HSMM to simulate experimental results(Ref 138),(Ref 139). In micromilling of Ti64, the influence of different parameters has been studied on the formation of burrs and built-up edge (BUE)(Ref 140). It has been found that there was no connection between built-up edge and burr formation and large forces generated larger burrs. From the critical literature review, it was found that very little work has been done in the field of burr characterization and their minimization in the HSMM process of the Ti64 alloy. However, there was still a need to optimize cutting parameters using recent methods of optimizations to machine burr-free surfaces. Therefore, this experimental work was done to estimate the effect of process and tool parameters in burr formation at HSMM of the Ti64 alloy. A schematic flow chart of the experimental work has been shown below in Figure 5.1. The experiments have been executed on the HSMM to investigate and characterize the top burr generation. Meanwhile, the consequence of process parameters upon the equivalent size of top burr has been studied.

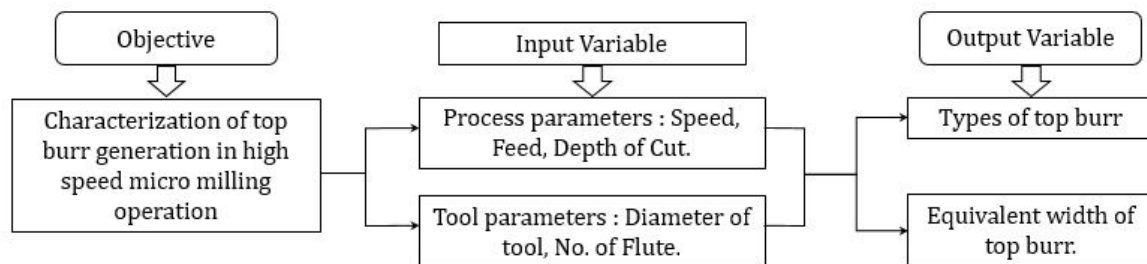


Figure 5.1: Flow chart of the experiment

5.3 Experimental details

The experimental work was conducted on Ti6Al4V alloy which consists of 90% titanium, 6% aluminum, and 4% vanadium. Its microstructure before machining shows α - β phase with an average grain size of 14 μm (Figure 5.2).

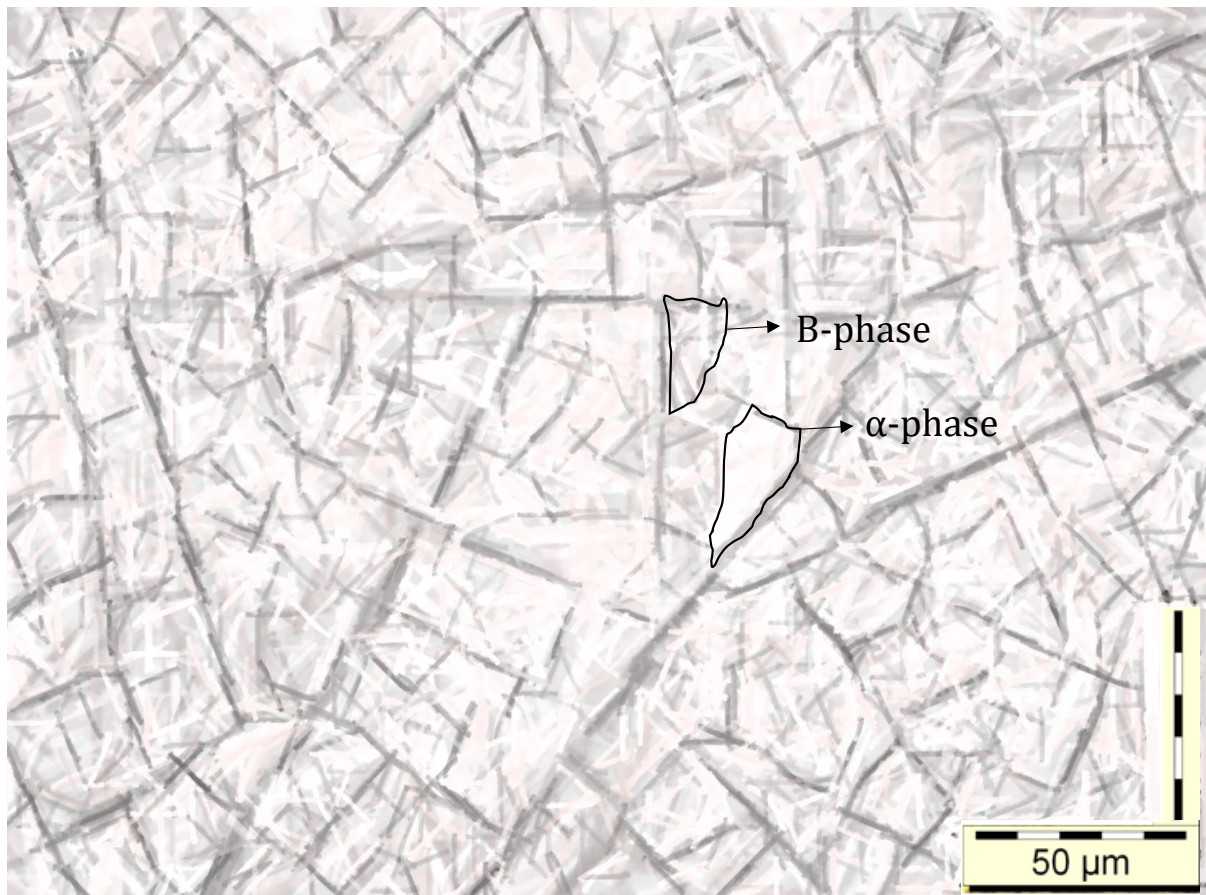


Figure 5.2: Microstructure of Ti6Al4V alloy

A specimen of dimension 25 mm × 25 mm × 3 mm was used for the experiment. Two uncoated tools (IND-SPHINX Precision Ltd. unit-B, Himachal Pradesh, India) having diameter 300μm and 500μm were used to investigate the consequences of different process parameters on the top burr generation at a conventional and high-speed cutting. The appropriate range of the process parameters was found by Initial experiments. Table 11 shows the set of process parameters, which may affect the mechanism of burr formation. A wide range of spindle speed and feed rates were recognized. The cutting speed of the spindle ranges between 16 m/min and 141 m/min. While the feed rate ranges between 1mm/sec to 5mm/sec which precipitates in maximal thickness of chip of 0.3μm to 15μm. So, the investigations are certainly reasonably aimed at a variety of parameters. Table 11 shows the sequence of machining operations performed with three repetitions to minimize the experimental errors.

Table 11: List of experimental parameters

Parameters	Diameter of tool (μm)	No. of flute	Cutting speed (m/min)	Feed rate (mm/sec)	Depth of cut (μm)
Level 1	300	2	16	1	10
Level 2	500	4	79	3	20
Level 3	—	—	141	5	50

Simultaneously, parametric studies have been performed by varying each parameter at the same time keeping other parameters constant. Three levels of cutting speed, depth of cut, and feed rate have been used. In the experiments, two sets of tools with different diameters and numbers of flutes have been studied (Table 12). The characterizations of top burrs have been investigated through scanning electron microscopy (SEM).

5.4 Experimental setup and procedure

The experiments have been carried out on the high-speed micro-milling machine setup. The details about the specifications have been mentioned in section 3.3, Figure 3.20. The uncoated end-milling cutters of tungsten carbide (WC) with a helix angle of 30° were used in the experiment. Tungsten carbide micro tool (manufactured by Axis tool® India) of two different sizes such as $500 \mu\text{m}$ (2 flutes) and $300 \mu\text{m}$ (2 and 4 flutes) along with a fine grain of less than $0.4 \mu\text{m}$ have been used in the study. Micro slots have been machined on the workpiece with a length of 5 mm and a width equivalent to the diameter of the tool.

Table 12: Detail of experiments

Sr. No.	Tool parameters		Process parameters		
	Diameter of tool (μm)	No. of flute	Cutting speed (m/min)	Feed rate (mm/sec)	Depth of cut (μm)
1	500	2	16	5	50
2	500	2	79	5	50
3	500	2	141	5	50
4	500	2	141	1	50
5	500	2	141	3	50
6	500	2	141	5	20
7	500	2	141	5	10
8	300	2	141	5	10
9	300	4	141	5	10

Results and discussions

5.4.1 Measurement of burr

To eliminate or scale down burrs successfully, the measurement of burr must be done with high accuracy. The sharp and uneven shape burrs are generated in the machining process, which is hard to measure. The secondary operation of burr removal such as deburring is mainly dependent upon the size and geometry of the burr (Ref 141). The accuracy of burr measurement affects the selection of an appropriate method for its removal and power consumption in deburring operations. The SEM image of burr formation in the HSMM of the Ti6Al4V alloy is shown in Figure 5.3. It can be observed from Figure 5.3 that the burr width is varying significantly, the variation between width 2 and width 1 is measured to be around 50%. Therefore, it is very difficult to consider the exact width of burr generated in up milling as well as in the down milling machining process. There may be a chance to get an incorrect reading. Therefore, a new term was introduced to find the top burr width i.e., Equivalent width. Equivalent width is calculated as the ratio of the total area of burr generated to the total height. MATLAB® has been used to measure the area and height of the SEM image of top burrs.

Mathematically,

$$\text{Equivalent width of burr in up milling} = \frac{\text{The total area of burr in up milling}}{\text{Total height}} \dots\dots\dots (1)$$

$$\text{Equivalent width of burr in Down milling} = \frac{\text{Total area of burr in Down milling}}{\text{Total height}} \dots\dots\dots (2)$$

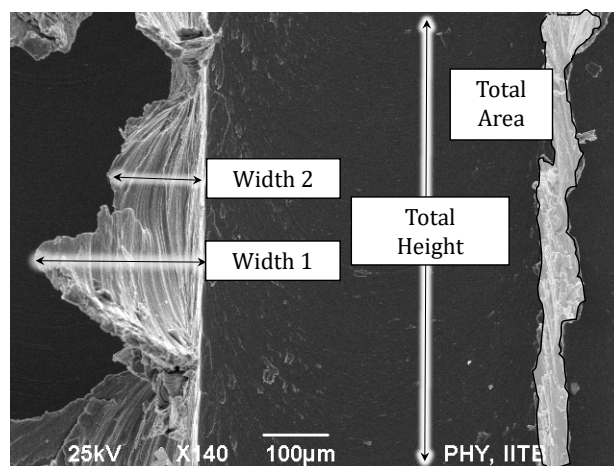


Figure 5.3: Scanning electron microscopy (SEM) image of top burr generation in Ti6Al4V

5.4.2 Top burr characterization and analysis

Burr generation in machining has been identified at three main locations: top surface on machined groove, entry, and exit of the tool. Top burr has two types i.e., up and down milling top burr. The up-milling burrs are generated on the up-milling side, where cutting and feed direction are opposite to each other. While down milling burrs are formed on the down-milling side, where both cutting and feed are in the same direction. Since the study is mainly focused on the top burr formation and its characterization. Therefore, the influence of process parameters upon the top burr size in up and down milling at traditional and high-speed cutting has been studied. Figure 5.4 (a) and (b) shows the top burr formation at traditional cutting speed (16 m/min at 10,000 rev/min) and at high-speed machining (141 m/min at 90,000 rev/min) respectively.

5.4.3 Burr generation at traditional speed

Figure 5.4 (a) illustrates the top burr formation at a traditional cutting speed of 16m/min at 10,000 rev/min, the linear feed rate of 5mm/sec, depth of cut 50 μm . It is obvious from the figure that the down milling operation produces more burr than the up-milling operation. The burr area evaluated in down milling is between 67600-81220 μm^2 with a height of 700 μm . The burrs are generated on the down milling side due to squeezing and accumulation of uncut chips in milling operation(Ref 142). These burrs are discrete in nature and thick in size. In comparison, very fewer burrs are generated in the up-milling. In similar conditions, the burr area evaluated in up milling is between 7348-12420 μm^2 with a height of 700 μm .

5.4.4 Burr generation at high-speed cutting

In HSMM, the mechanism of burr formation is examined at cutting speed of 141 m/min (spindle rotation 90,000 rev/min), feed rate of 5mm/sec, and depth of cut 50 μm . The measured burr area in down milling ranges from 20000 μm^2 to 53000 μm^2 with an average height of 600 μm . In similar conditions, the measured burr area in up milling ranges from 22000 μm^2 to 33000 μm^2 . Figure 5.4 (b) illustrates the formation of the top burr at high-speed cutting. It can be observed from Figure 5.4 (b) that longer burrs are formed in up milling side as compared to down milling side. The burr formed in high-speed cutting completely differs from the traditional cutting. It shows a small burr in down milling region and a bigger thin burr in up milling region as compared to traditional cutting. In up milling operation, thicker burrs are found at bottom side compared to the top side and they are facing towards the milled slot. These thin and long burrs show the material removal mechanism at high cutting speeds. In HSMM of Ti6Al4V alloy

adiabatic shear band is generated because of low thermal conductivity and heat accumulation, which results in burr formation and discrete chip generation(Ref 101),(Ref 143).

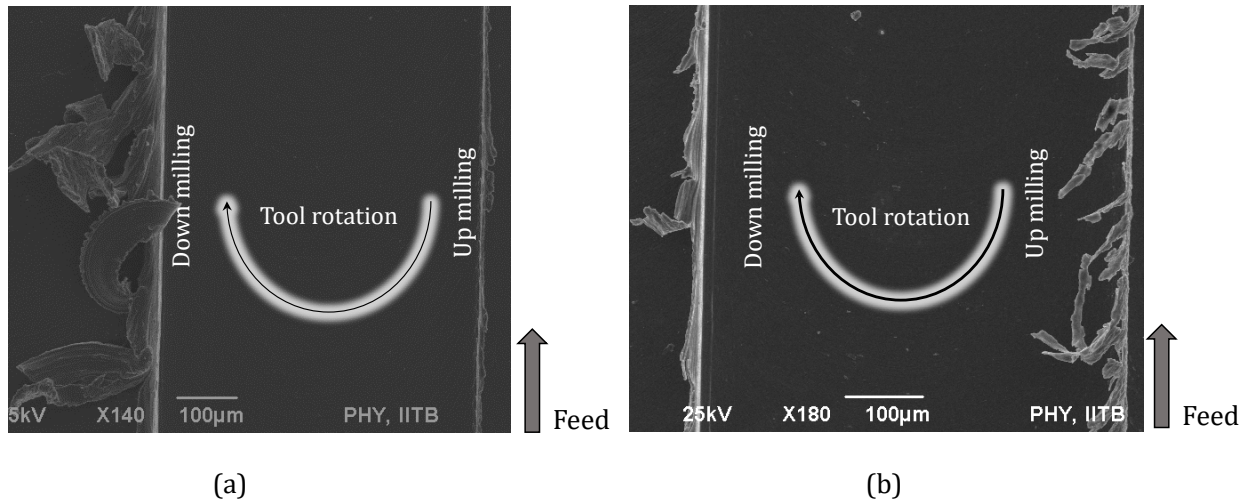


Figure 5.4: Burr formation (a) traditional cutting speed (b) high-speed cutting

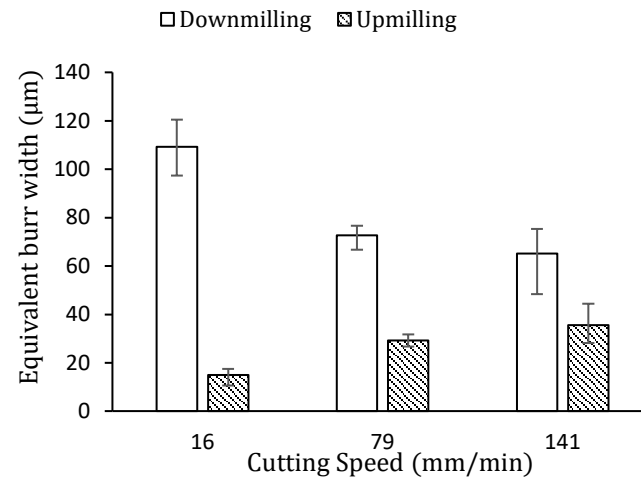
5.4.5 Parametric study

The top burr in micromilling is the most critical, as it is formed due to squeezing and bulging of uncut chip material and affects the overall performance of the component or machined part. For burr minimization, parametric studies have been carried out to investigate the consequence of different parameters on burr formation. An analysis of the equivalent width of up and down milling has been carried out to examine the influence of process and tool parameters. Figure 5.3 illustrates the top burr formation and measurement of the equivalent width of up and down milling.

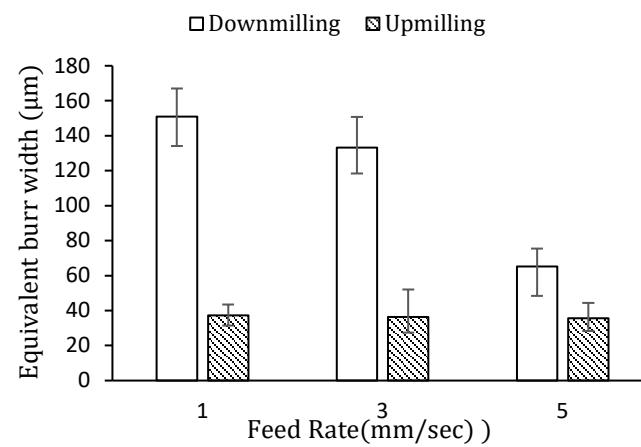
5.4.5.1 Influence of process parameters on equivalent burr width

Figure 5.5 (a) to (c) shows the influence of process parameters on the equivalent width of the top burr in up as well as in down milling. Figure 5.5(a) illustrates the influence of cutting speed on the equivalent width of top burr in up as well as down milling. The depth of cut and feed rate is taken as $50\ \mu\text{m}$ and $5\ \text{mm/sec}$. In up milling, the cutting speed is directly proportional to top burr equivalent width. As cutting speed increases from $16\ \text{m/min}$ to $79\ \text{m/min}$ and further from $79\ \text{m/min}$ to $141\ \text{m/min}$, the corresponding equivalent width increased by 95% and 22% respectively. It has been found that the reason for the increment in equivalent width is the higher strain rate hardening of the material(Ref 144).In down milling as the cutting speed increases, the top burr equivalent width decreases. The equivalent burr width decreased by

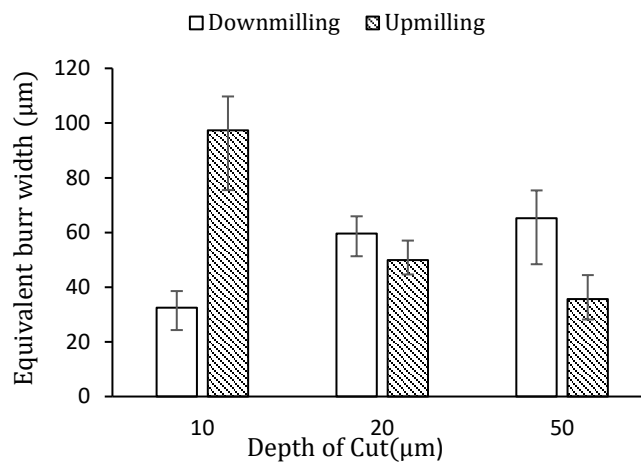
33% and 10% under the same variation of cutting speed. The decrement in burr size has been found due to an increase in material plastic strain rate and decrement in the uncut chip thickness with an increment in the cutting speed(Ref 145). Figure 5.5 (b) illustrates the influence of feed rate on the equivalent width in up milling as well as in down milling processes. The equivalent width of up milling decreases by 3% with changes in feed rate from 1 mm/sec to 3 mm/sec at 141 m/min and depth of cut 50 μ m. Similarly, if the feed rate varies from 3 mm/sec to 5 mm/sec there is a negligible decrement of 2% in equivalent burr width. On down milling side, the equivalent width is decreased by 12% and 51% with changes in feed rate from 1 mm/sec to 3 mm/sec and 3 to 5 mm/sec respectively. Figure 5.5(c) illustrates the influence of the depth of cut on equivalent width in both the cases at cutting speed 141 m/min and feed rate 5mm/sec. In up milling side, equivalent width gets decreased by 49% and 29% if the depth of cut increased from 10 μ m to 20 μ m and 20 μ m to 50 μ m. In high-speed up milling process more heat is diffused to the workpiece which causes the change in metal properties i.e. increase ductility. The material easily elongated along the direction of force applied by the tooth of the milling cutter. If the material has a low area for resistance to deform then more burr is produced. The depth of cut increases the uncut chip area for resistance to deformation hence, less burr produces. On down milling side, equivalent burr width increases with an increase in depth of cut. The equivalent burr width of down milling increases by 83% and 9% for a similar condition. In down milling, less heat is diffused so there is less influence of thermal softening. In the process of down milling more, an uncut chip area is produced; as a result, more burr formed.



(a)



(b)



(c)

Figure 5.5: Variation in the equivalent width in up and down milling with (a) Cutting speed; (b) feed rate (c) depth of the cut

5.4.5.2 Influence of tool parameters on equivalent burr width

Figure 5.6 (a) and (b) illustrate the influence of variation in tool parameters on the top burr size. As shown in Figure 5.6 (a) equivalent burr width increased by 64% and 15% in up and down milling with changes in the diameter of the tool from 300 μm to 500 μm respectively. The small tool diameter has to remove less material; therefore, small burr produce vice versa happened in larger tool diameter(Ref 146). In Figure 5.6 (b), 65% and 44% reduction were observed in the equivalent burr width in up and down milling, when the number of flutes increased from two to four. The reason for the decrement in the burr formation might be a reduction in feed per tooth and uncut chip area.

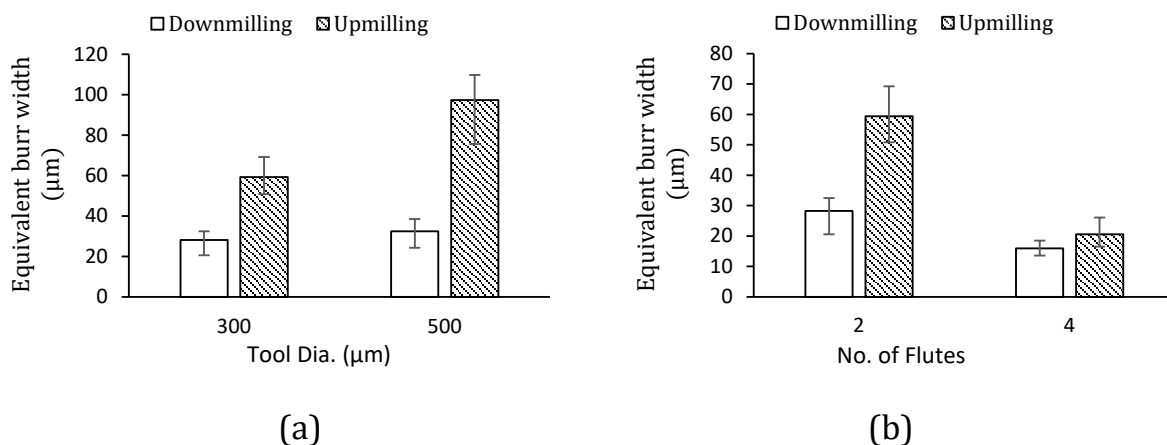


Figure 5.6: Variation in the equivalent width of up and down milling burr width by (a) Diameter of tool (b) No. of flute

5.5 Summary

The experimental study reveals the characterizations of burr formation at high-speed micromilling. Micro grooves have been fabricated on Ti6Al4V. MATLAB[®] has been used to measure the average burr size by considering the overall area of the formed burr and total height. The measured top burr is termed as “equivalent width”. Burrs were observed in all micro-milled grooves. The measured width of the top burr illustrates that the up-milling burrs are bigger in HSMM and the down milling burrs are bigger in conventional speed. As in HSMM up milling burr formed due to increase in strain rate hardening of material while at conventional speed, down milling burrs are bigger due to squeezing and accumulation of uncut chip. The equivalent burr width in up milling increases with an increase in the cutting speed, whereas, decreases with an increase in the cutting speed in down milling. An increment in the

feed rate reduces the down milling burr whereas no effect is seen in the up milling burrs. The depth of cut has opposite effects in up milling and down milling burrs. An increase in the depth of cut increases the down milling burrs and it decreases the up milling burrs.

It is observed that the top burrs in down milling have been reduced by 40.36% in high-speed machining. Hence, another methodology called minimum quantity lubrication (MQL) has been introduced in the next chapter to minimize the up and down milling burr to the maximum extent. Two types of lubricants: water based emulsion and copper oxide nanofluid (new been introduced) have been used in minimum quantity to examine the effects on the top burr.

Chapter: 6 BURR MINIMIZATION OF Ti6Al4V ALLOY USING COOLANT and LUBRICANT

6.1 Introduction

This chapter introduces another methodology called MQL using coolant and lubricant to minimize the top burr of Ti6Al4V alloy. The purpose of using coolant and lubricant is to reduce the friction and dissipate the heat accumulated at the interface of the tool-chip and tool-workpiece interface. Effects of different lubricants viz., an emulsion of water-based and copper oxide-based nanofluid have been investigated. Furthermore, OEC (overall evaluation criteria) has been employed to optimize the input process parameters for better output response.

6.2 Motivation, objective & approach

In general, two approaches have been proposed in the literature to overcome the poor machining of superalloys, namely (I) minimizing the excess heat produced at the tool-workpiece interface by introducing lubrication and cooling liquids in the cutting zone and (II) increasing the heat transfer rate in the vicinity of the cutting zone utilizing nanofluids. The first option is mostly applied in micro-milling, where the cutting zones are very minute and the precise delivery of lubricant is of paramount importance. The flow of lubricant may act to the tiny endmill with a relatively high force, which may deflect or even break, both resulting in a poor surface finish and low machining accuracy. The best alternative for precise delivery of lubricant is the minimum quantity lubrication (MQL) that has shown to be very beneficial and efficient in terms of sustainability and economy (Ref 147),(Ref 148). By this technique, lubricant (most often oil in water emulsion) is sprayed at high pressure in the machining zone using a nozzle of a small diameter. The flow rates are in the range of 50-500 ml·h⁻¹. Vazquez et.al (Ref 94) used vegetable oil TRI-Cool MD1 (Trico, USA) with a viscosity of 34 cSt. The MQL was applied in the feed direction and against the feed direction when machining Ti6Al4V alloy. Lower burr height and better surface roughness were obtained when the cutting fluid was applied in the direction of feeding. Percin et.al(Ref 92) investigated the effect of flooded, MQL, and cryogenic conditions on the exit burr formation and surface roughness in micro-drilling of Ti6Al4V alloy. They observed the smallest exit burr size in cryogenic conditions, followed by flood cooling, and the biggest burr was observed when the MQL technique was used. The results reported in the literature do not agree and the methods and parameters of cooling need to be further investigated. The second approach (II), i.e., the increase of the heat transfer rate in the vicinity of the machining zone, is achieved by cooling and lubricating the machining zone by nanofluids. Nanofluid contains a colloidal suspension of solid nanoparticles of a size smaller

than 100 nm. The purpose of adding nanoparticles is to increase the thermal properties of base fluid so that it can dissipate heat from tool-workpiece interface. Additionally, some nanoparticles could improve lubrication, e.g., MoS₂ (Ref 149). Nanoparticles can be either metal or non-metal but it should have high thermal conductivity, sustainable and user friendly. Surfactants may also be added in base fluids to reduce the surface tension of base fluid for proper dispersion of nanoparticles. Commonly used surfactant is Sodium dodecyl sulphate (SDS), sodium dodecylbenzene sulphonate (SDBS), Tween20 (Sigma-Aldrich, Germany). Adding copper oxide in deionised water and mixing it for 4 hours using mechanical vibrator increases thermal conductivity of nanofluid by 12.4% (Ref 150). Zhou et.al (Ref 151) prepared copper nanofluids by dispersing copper nanoparticles of size 50nm in DI water. They prepared by two stage technique, first of all copper nanoparticles were added in DI water and stirred for 15 minutes using magnetic stirrer and then sonicated for 2hr using sonicator. This procedure is repeated for 3 times and ensures complete dispersion of copper nanoparticles in DI water and it is observed that prepared nanofluids remain stable for 24 hrs with no noticeable sedimentation. Pashmforoush and Bagherinia (Ref 152) used silver coated copper nanoparticles of 7nm mixed in DI water to form a colloidal solution. Nanofluid was prepared using a magnetic stirrer for 4 hrs at 1000rpm and then sonicated for 30 minutes for proper dispersion. Tween 20 was used as a surfactant. In this study, they observed that with an increase in concentration, surface roughness value and wheel loading ratio decrease up to a certain limit after that with increasing concentration surface roughness value and wheel loading ratio increases due to agglomeration of nanoparticles at a higher concentration which reduces the efficiency of nanofluids because of changing heat transfer region from line to surface. Yi et.al (Ref 153) has used GO of size 50nm for preparing nanofluids by adding them into base fluids to study on Ti6Al4V workpiece. GO nanoparticles are added in base fluids with a concentration of 0.1%wt., 0.3%wt. and 0.5%wt. of base fluids during the experiment and it has been observed that cutting forces decreases in comparison with the conventional coolant method and also forces decrease with an increase in GO concentration. Tool wear and cutting vibration have also been reduced with the use of nanofluids in comparison with conventional coolants. These recent researches have shown that nanofluid lubricant is the best alternative to machining/micromachining of difficult-to-machine metal alloys. However, Nam et.al (Ref 154) reported having the first to use nanofluid as a lubricant in micromachining. They used nano diamond particles having a size of 30 nm, with base fluids paraffin oil and vegetable oil in the concentrations of 1%, 2%, and 3% by volume. They observed fewer torques, thrust force, burr size using 1% nanofluid in comparison to 2% while microdrilling of aluminium alloy 6061. Kim et.al (Ref 155) reduces coefficient of friction, tool wear, milling forces and surface roughness using nanofluid MQL with chilly CO₂. They concluded that 0.1% wt. nano diamond nanofluid is more effective for reducing milling force,

tool wear and coefficient of friction while 1% wt. for better surface roughness. Kumar et.al(Ref 156) performed micromilling experiment on Ti6Al4V alloy using variants of water based nanofluids viz water based alumina,HBN,WS2 and MoS2 and commercial lubricant (UNILUB2032). They found that the commercial lubricant and alumina nanofluids have greater performance in reducing burr width. By studying above-mentioned researches, it has been observed that numerous experiments have been executed on difficult-to-machine metal alloys to minimize cutting force, tool wear, surface roughness and burr formation using nanofluids in macro machining. However, very limited research has been reported for micro-milling of Ti6Al4V alloy using nanofluids. Hence, the current study focused on comparative analysis of the effects of various lubricants viz., emulsions (water based) and copper oxide nanofluid on the output response i.e., top burr. Full factorial has been used for design of experiment and OEC (overall evaluation criteria) for optimization.

6.3 Experimental details

Experiments have been performed on the high-speed micromachining center (V60) (the detail of the experimental setup is given in Chapter 3). The workpiece in the study is Ti6Al4V and a two flute WC coated (AlTiN) tool of diameter 400 μm has been used. Since the objective of the work is to analyze the effect of lubricant and coolant in the burr formation, lubrication has been selected carefully. Two types of cutting fluids have been selected 1. Emulsion (water-oil) and 2. Nano lubricants (Water-nanoparticles) are discussed as follows:

6.3.1 Characterization of emulsion-based cutting fluids

The base oil selected for the preparation of water-based emulsion was servo cut s produced by Indian oil corporation limited (IOCL), India. As a performance standard, it meets the specifications (details mentioned below) IS: 1115-1986 (Reaffirmed 1996). Servocut S is a soluble type-high quality cutting oil which yields rich milky emulsion with water. The emulsion formed is homogeneous and stable and does not split during usage or routine machine shut down periods, under normal conditions. It contains rust inhibitors, which impart anti-rust and anti-corrosive properties to the emulsion. Carefully selected biocide is incorporated to prevent bacterial growth in the emulsion. It is recommended for a variety of cutting operations on ferrous and non-ferrous metals. The grade is especially suitable for metal working operations where the cooling property is more desirable compared to the lubricating characteristics.

Characteristics of lubricant servo cut 'S'(Figure 6.1)

- Kinematic Viscosity, cSt @ 40°C
(Typical): 20
- Flash Point (COC), °C Min.: 150
- Copper strip corrosion @ 100°C:1
- Cast Iron corrosion test, 0/1-1: Pass



Figure 6.1: Servo cut s lubricant with specification details

The emulsion has been prepared in four ratios 1. 1:5, 2. 1:10, 3. 1:20, 4. 1:20 (Oil-water). Since viscosity is an important parameter which directly responsible for the machining performance. Hence, after the preparation of water-based emulsions viscosities of all the samples were characterized using a Rheometer in CRF IIT(ISM). (MAKE and MODEL: Malvern Instruments, UK, Bohlin Gemini 2)

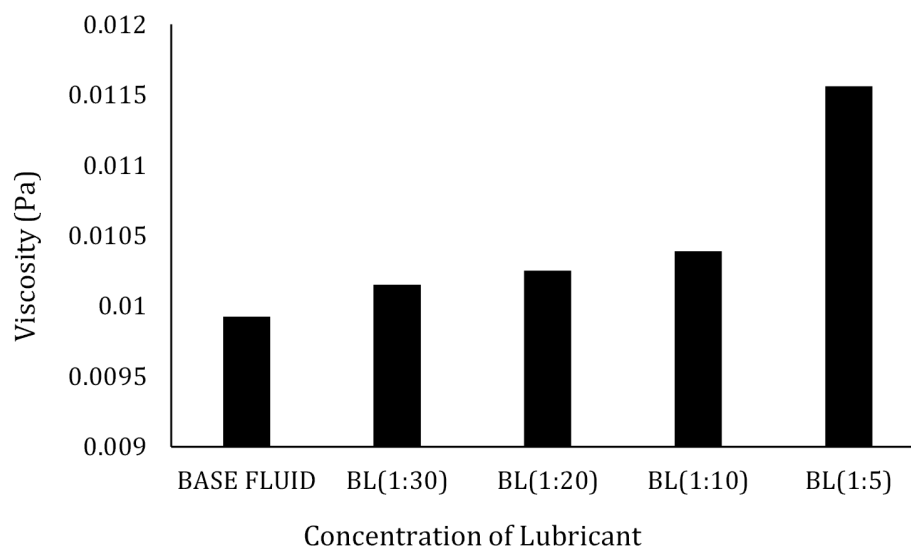


Figure 6.2: Variations of viscosity with increase in concentration (oil-water)

It can be observed from Figure 6.2 that as the ratio of oil-water increases, viscosity corresponding to each concentration increased approximately in the same proportions with respect to the base fluid (distilled water).

6.3.2 Characterization of nano lubricant based cutting fluid

To prepare nanofluid to be used as MQL in micro end milling, copper oxide nanoparticles were added to distilled water that served as the base fluid. Physical properties are listed in Table 13; detailed morphology and elemental compositions are provided in Figure 6.3.

Table 13: Physical properties of copper oxide nanoparticles.

Material	Appearance	Average size	Purity (%)	Density (g/cm ³)	Molecular Weight	Melting Point (°C)
CuO	Black	40 nm	99	6.3	74.55	1326

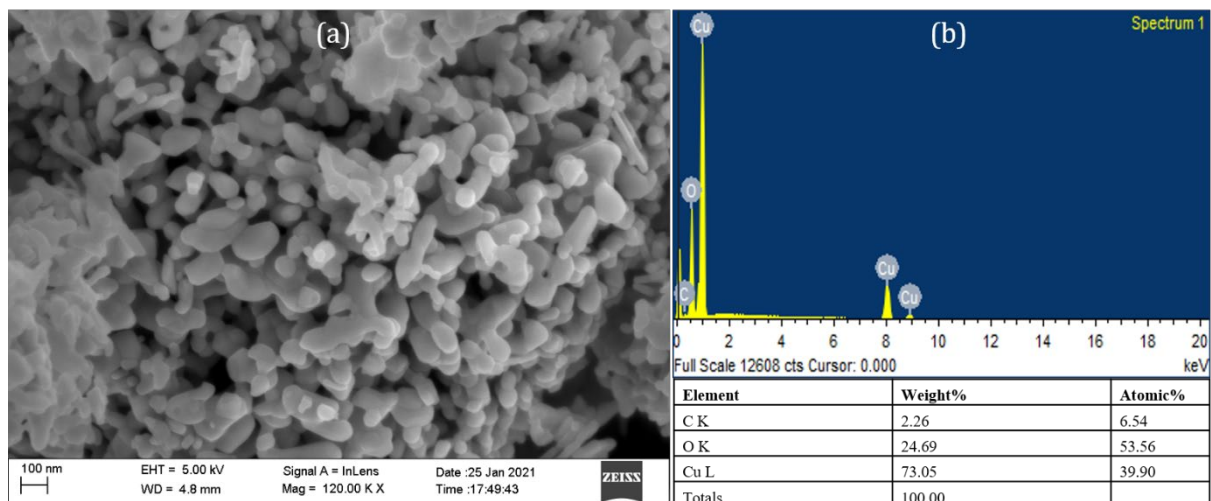


Figure 6.3: Morphology of nanoparticles (a) FESEM image at 120 k X (b) EDX analysis.

The crystalline structure and phase pure composition of the CuO nanoparticles were tested through XRD analysis (Make and Model: Rigaku, Smart-lab). The diffractogram peak of the CuO nanoparticle is indicated in Figure 6.4. The exhibited diffraction peak at 35.6°, 38.7°, 48.75°, 53.5°, 58.4°, 61.6°, 66.21°, 68.10° can be indexed to miller indices (111), (111), (202), (020), (202), (-113), (310), (220) (JCPDS File no.01-080-1916). The existence of a strong and sharp peak at 38.8° corresponding to a plane (100) indicates the highly crystalline nature of CuO nanoparticles. The unavailability of any unwanted peak in the diffraction pattern confirms the phase pure crystal structure of the nanoparticles.

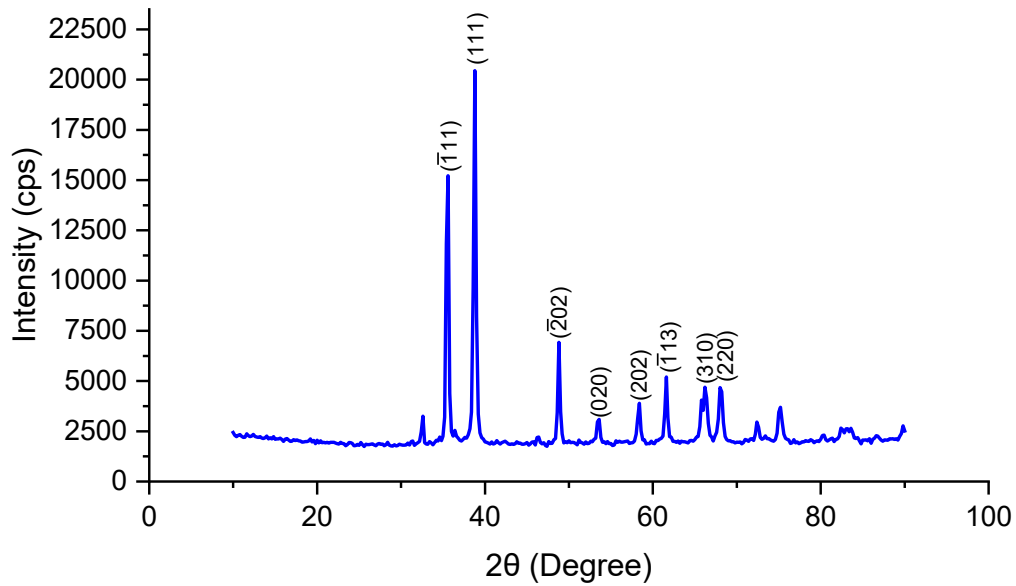


Figure 6.4: XRD analysis of CuO nanoparticle.

Preparation of nano lubricant

Nanofluids were prepared by a two-step method consisting of magnetic stirring followed by ultrasonication (Figure 6.5). A surfactant was added while preparing nanofluids to reduce the surface tension of the base fluid and to additionally affect the thermal conductivity of nanofluids being prepared.

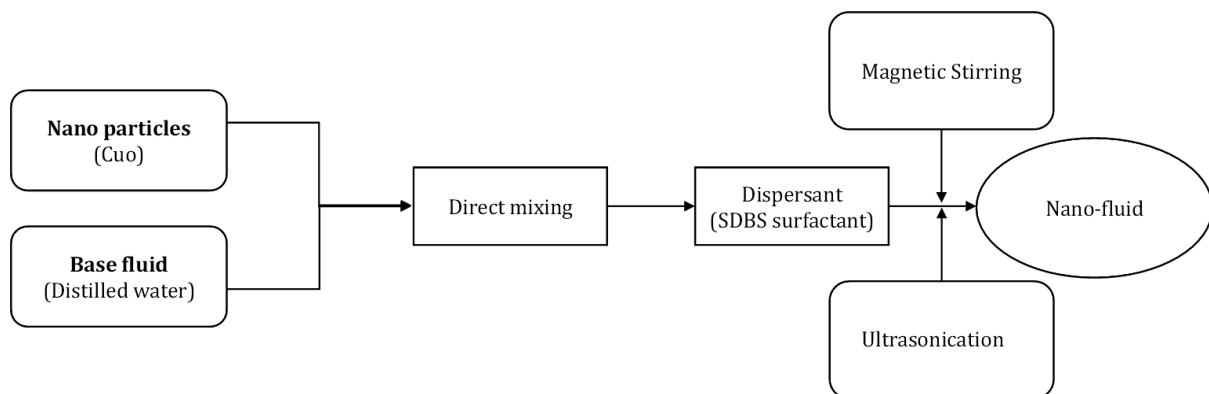


Figure 6.5: Schematic of preparation of nanofluid

Nanoparticles were added in 100 ml of distilled water in three concentrations, namely 0.1%wt, 0.2%wt, and 0.3%wt. In the first step, CuO nanoparticles were added in distilled water and stirred for 2 h at 1000 rpm using a magnetic stirrer. The second step was ultrasonic stirring for 3.5 h using a bath sonicator (Figure 6.6).

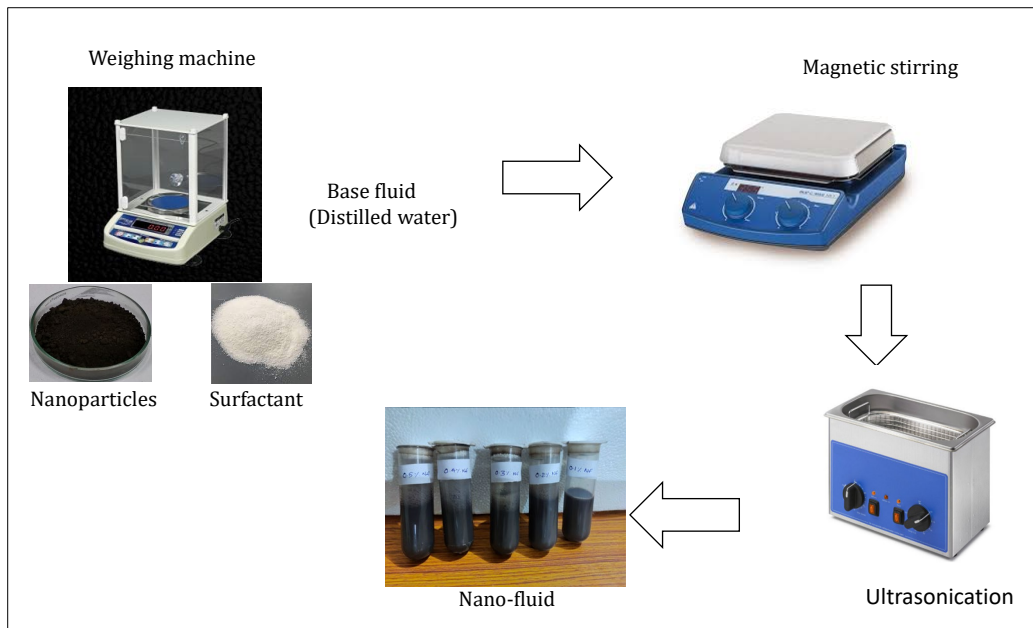


Figure 6.6: Chronology of preparation of nanofluid

To avoid heating of sonicator due to continuous operation, it has been stopped for 2 min after every 15 min of use. To avoid agglomeration of nanoparticles and ensure a proper dispersion, a 0.5 %wt of sodium dodecylbenzene sulphonate (SDBS) surfactant was added to the base fluid. The nano based cutting fluid has been prepared in weight % of CuO. Five weight % have been used for the preparation of the nano lubricant: 0.1%, 0.2%, 0.3%, 0.4%, 0.5%. The zeta potential test has been performed using instrument (Litesizer 500, Antan-par) to analyze the stability of nanofluid based on electrophoretic behavior. As per stabilization theory, if zeta potential has high stability, electrostatic repulsion between the nanoparticles increases which indicates good stability suspensions. Generally, a suspension with a measured zeta potential above 30 mV is considered to have good stability. In Figure 6.7, the zeta potential value for 0.3% nanofluid is 41.25 mV, which shows the solution is stable.

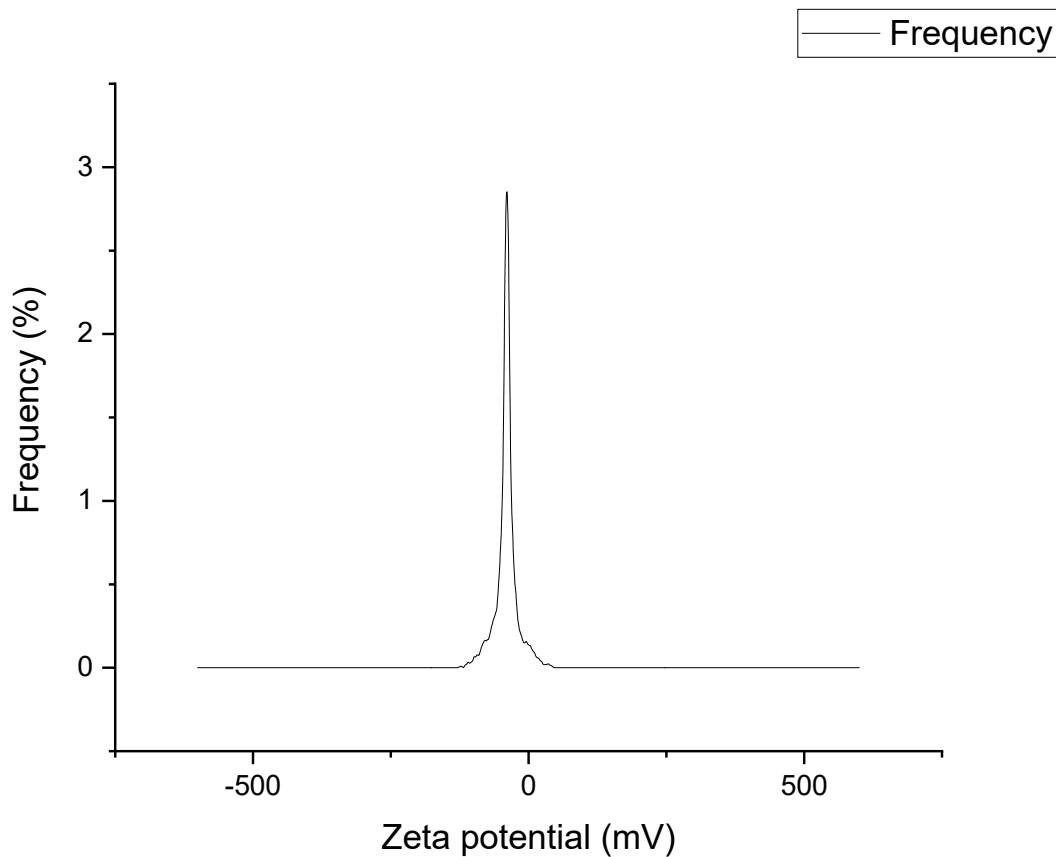


Figure 6.7: Zeta potential of CuO nanofluid (0.3%) versus frequency

The thermal conductivity and viscosity of the cutting fluid are the two most significant parameters affecting the top burr formation. A good thermal conductivity is required for the effective removal of heat from the cutting zone. Figure 6.8 shows a significant increase in the nanofluid thermal conductivity at different concentrations of nanoparticles. When compared to base fluid, the CuO at concentrations of 0.1%wt, 0.2%wt, and 0.3%wt, 0.4%wt, 0.5%wt attained an increase in thermal conductivity of 3.73%, 3.9%, 4.24%, 4.75% and 5.43% respectively. The viscosity of the cutting fluid ensures the ability to form thin film during machining and consequently reduces friction. In the case of low cutting fluid viscosity, the thin film required during machining does not form whereas in the case of high viscosity the cutting fluid does not penetrate in the tool-workpiece interface. Hence, optimum viscosity is desired for the best machining results. The viscosity of nanofluid depends on the concentration of nanoparticles (Figure 6.8b). Compared to base fluid, the CuO at concentrations of 0.1%wt, 0.2%wt, and 0.3%wt, 0.4%wt, 0.5%wt attained an increase in viscosity of 2.11%, 2.31%, and 2.62%, 2.92% and 3.12% respectively. Concentration and type of nanoparticles, base fluid, and temperature may alter the viscosity of nanofluid. Kinematic viscosity measurement by rheometer Bohlin Gemini 2 (Malvern Instruments, UK) located at CRF Lab in IIT (ISM) Dhanbad has been used to measure

kinematic viscosity of each concentration of nanofluid at fixed room temperature 25 °C and a shear rate 1480 sec⁻¹.

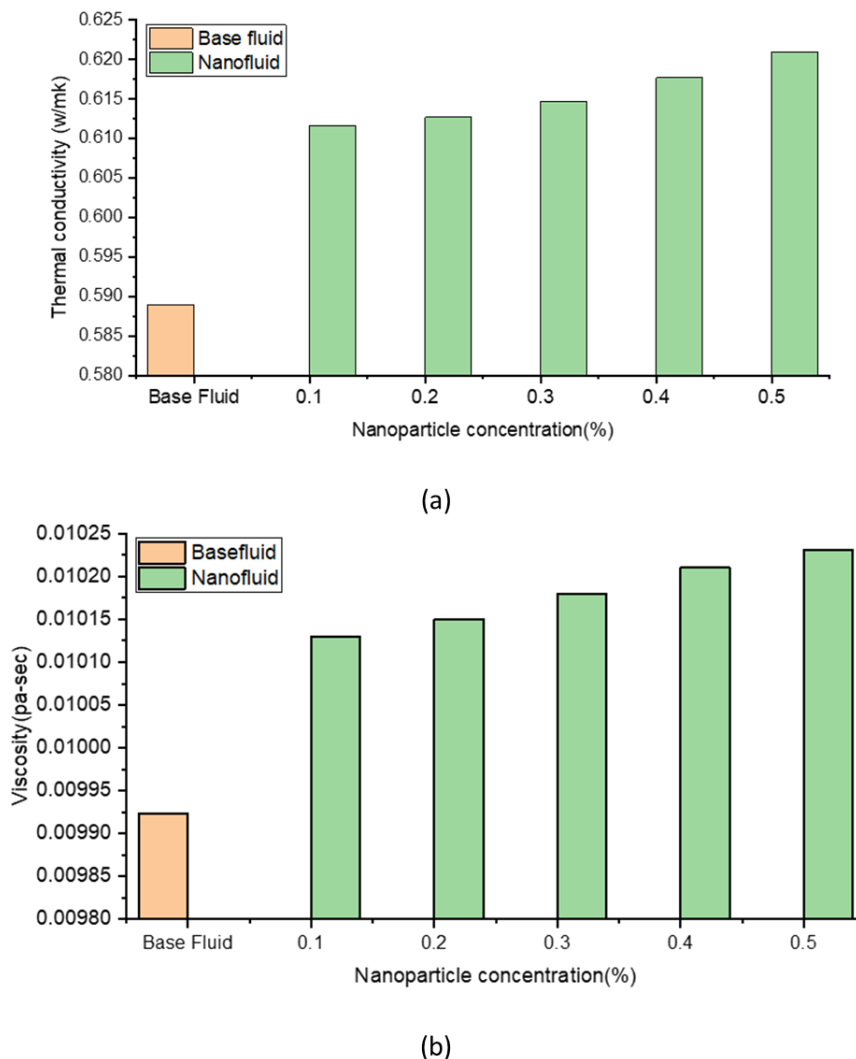


Figure 6.8: Influence of nanoparticle concentration with variation in (a) Thermal conductivity
(b) viscosity

6.3.3 Design of experiment for the first set of experiments (emulsion):

This design of experiment consists of all possible combinations of factors (variables) at all levels i.e., full factorial experimental design is used. Table 14 shows the level and process parameters, five levels of cutting conditions, two levels of feed, and two levels of depth of cut that have been used. Since the main objective of the study is to see the effect of the lubricant, therefore five levels of lubrication ratio have been taken. The levels (values) were selected based on the literature survey, preliminary experiments, manufacturer's recommendation, and machine capability. Each experiment was repeated thrice to get a mean value and minimize any error.

The spindle speed of $25.13 \text{ m}\cdot\text{min}^{-1}$ was kept constant throughout all the experiments. The full factorial design has been analyzed using Minitab 18 (Minitab, USA).

Table 14: Input parameters and their levels

Factors	Level 1	Level 2	Level 3	Level 4	Level 5
Emulsion concentration	Dry*	1:5	1:10	1:20	1:30
Feed f , $\mu\text{m}\cdot\text{tooth}^{-1}$	5	6			
Depth of cut D_c , μm	40	50			

* Dry means no cutting fluid was used

6.3.4 Design of experiment for the second set of experiments (nano lubricant):

Six levels of cutting conditions and two levels each of feed and depth of cut have been considered for full factorial interactions of all combinations. Their levels were selected based on the literature survey, preliminary experiments, manufacturer's recommendation, and machine capability; and these are gathered in Table 15. The spindle speed of $25.13 \text{ m}\cdot\text{min}^{-1}$ was kept constant throughout all the experiments. The full factorial design has been analyzed in Minitab 18 (Minitab, USA).

Table 15: Input parameters and their levels

Factors	Level 1	Level 2	Level 3	Level 4	Level 5	Level 6
Nanofluid concentration, % wt.	Dry*	0.1	0.2	0.3	0.4	0.5
Feed f , $\mu\text{m}\cdot\text{tooth}^{-1}$	5	6				
Depth of cut D_c , μm	40	50				

* Dry means no cutting fluid was used

6.3.5 Optimization Methodology

OEC (overall evaluation criteria) has been employed further to optimize the input process parameters for better output response(Ref 157). A particular output response may have

different weights, units, and quality characteristics (QC). QC can be either 'nominal is best', 'smaller is better, or 'larger is better. Considering 'X' as the larger is better and 'Y' as the smaller is better, OEC can be expressed as per equation:

$$OEC_{ij} = \left(\frac{X_{ij} - X_{minj}}{X_{maxj} - X_{minj}} \right) w_j \quad (5)$$

$$OEC_{ij} = 1 - \left(\frac{Y_{ij} - Y_{minj}}{Y_{maxj} - Y_{minj}} \right) w_j \quad (6)$$

$$OEC_i = \sum_{j=1}^{n=2} OEC_{ij} \quad (7)$$

Where:

- $i = 1, 2, 3, \dots, m$, $m = 24$: Number of experiments.
- $j = 1, 2, \dots, n$, $n = 2$: Number of quality characteristics or process responses.
- Y_{minj} and Y_{maxj} : smallest and largest values of Y_{ij} for the j th response, respectively.
- w_j is a weighting coefficient, which can be adjusted based on the practical need of the system.
- A and B are relative weightage of X and Y, respectively.

6.4 Results and Discussion

6.4.1 Effect of emulsion lubricant on the top burr formation

After the completion of the experiment, scanning electron microscopy (SEM) and optical microscopes were used to analyze the top burr size. Further, Minitab used to analyze the results and corresponding to the main effects plots have been shown in Figure 6.9 and Figure 6.10 for the up and down milling operation.

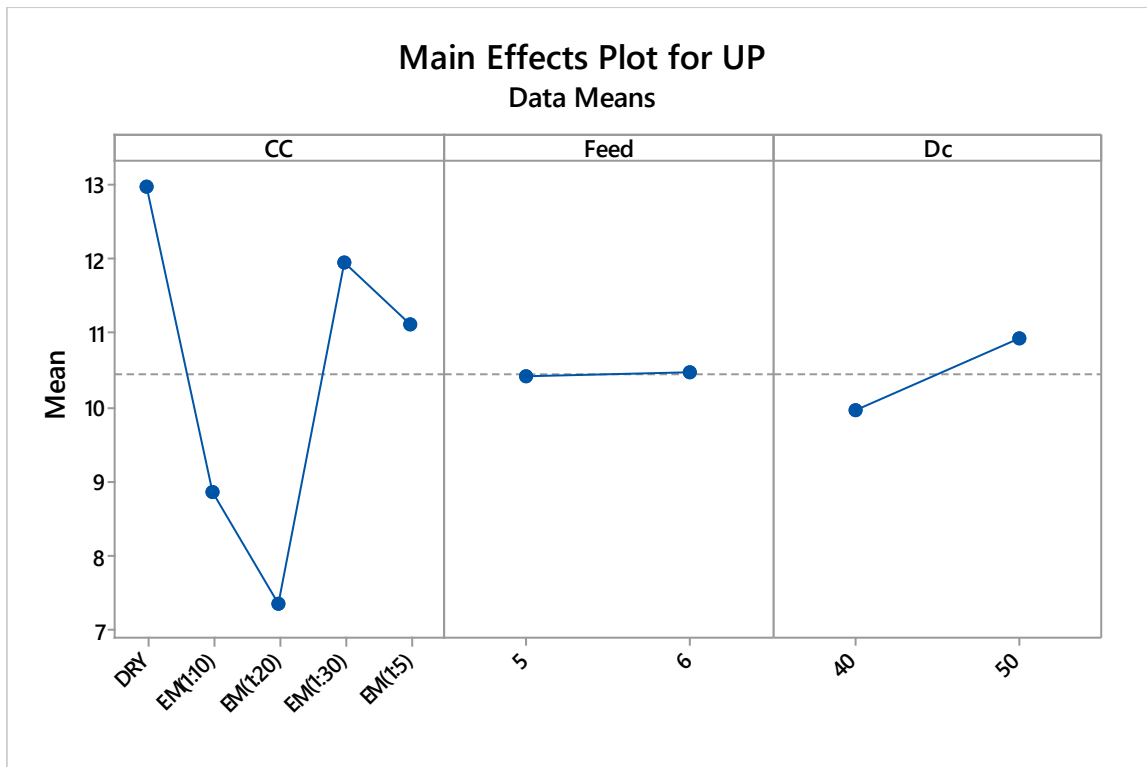


Figure 6.9: Main effects plot for up milling

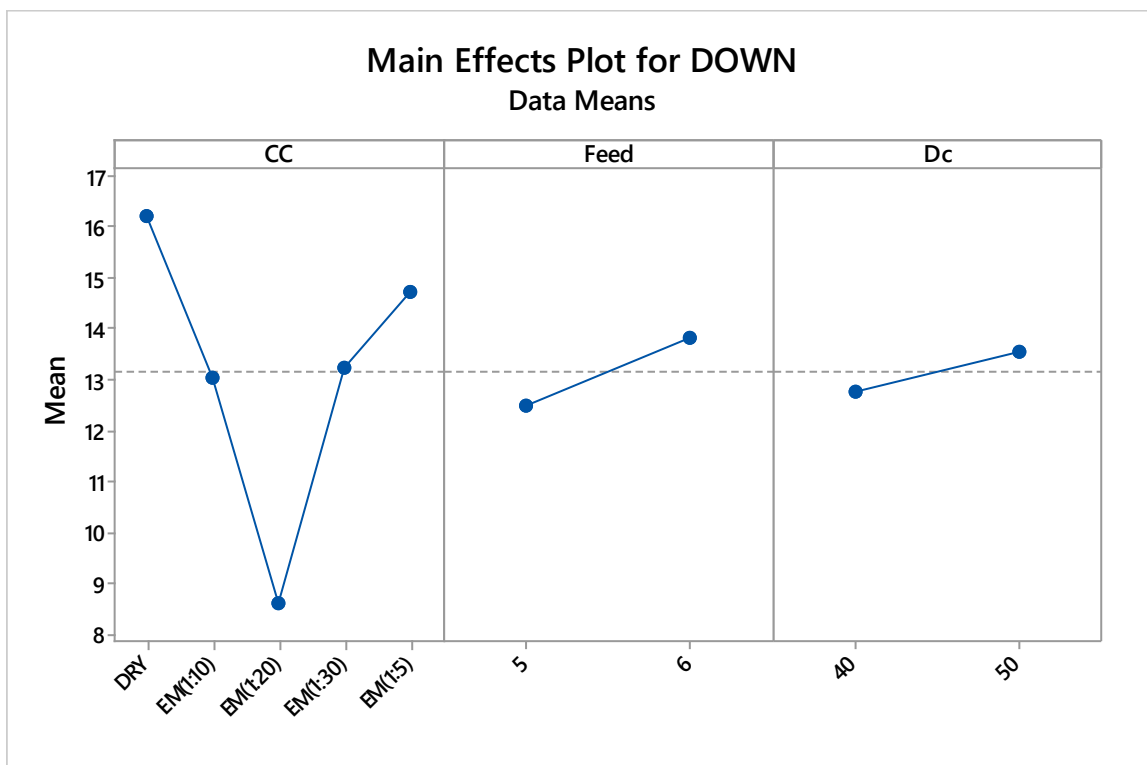


Figure 6.10: Main effects plot for down milling

It can be seen from Figure 6.9 and Figure 6.10 that the least burr size is obtained while using an emulsion with a concentration of EM(1:20) in both up as well as down milling, while the largest burr is formed in dry cutting. It was observed that EM(1:5), EM(1:10), EM(1:20), and EM(1:30) reduces the burr sizes by 14.35%, 31.63%, 43.44%, and 7.79% respectively in up milling operation while 9.25%, 19.62%, 47.03% and 18.39% respectively in down milling with respect to dry machining. The comparative analysis of SEM images at constant parameters of $V_c=25.13$ m/min, $f=5$ $\mu\text{m}/\text{tooth}$, $D_c=40$ μm (Figure 6.11) shows clear variations in size at different concentrations. However, it resembles the same trend at other parameters too.

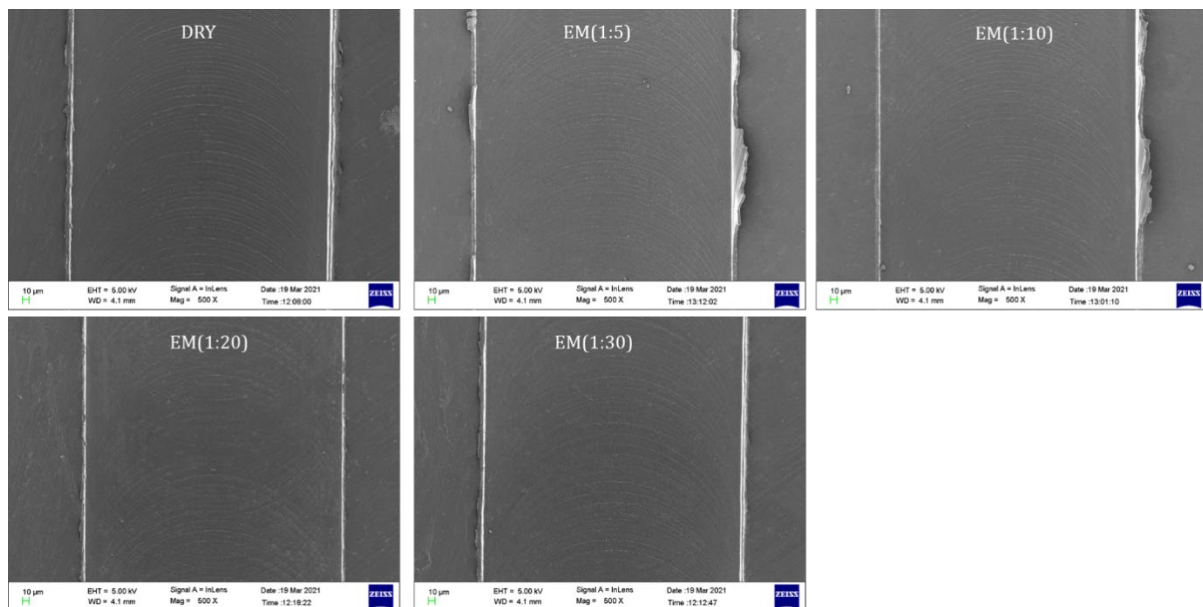


Figure 6.11: SEM images of top burr formation in up and down micromilling at $V_c=25.13$ m/m, $f=5$ $\mu\text{m}\cdot\text{tooth}^{-1}$, $D_c=40$ μm

As the concentration of fluid decreases (from EM(1:5) TO EM(1:20)) equivalent burr width is decreasing and finally a saturation stage (optimum condition) is reached where the effect is insignificant at tool-chip and tool-workpiece interface and hence, equivalent burr width is increasing (EM(1:30)). This is due to the better interaction of tool and workpiece with the use of cutting fluid at optimum concentration. At low concentration, a cutting fluid does not form a thin film of lubrication which is required for smooth machining whereas at higher concentration it is not able to penetrate the tool-workpiece interface(Ref 94). In addition to the effect of lubrication, the effect of depth of cut and the feed rate has been analysed. It was observed that the effect of depth of cut and feed per tooth is negligible as the feed per tooth values changed(increase) just by a marginal percentage of 0.57% and 10.74% with the increase of feed per tooth values from 5 to 6 in up and down milling respectively. While depth also changed(increase) by 9.94% and 6.03% in up and down milling. hence, their effect is insignificant with the increase in concentrations of emulsions from EM(1:5) to EM(1:30).

Optimization technique:

OEC (overall evaluation criteria) (section 6.3.5) has been used further to optimize the input process parameters for better output response. As per this technique, equal relative weightage (50% each) is assigned to both the output responses i.e., up milling top burr and down milling top burr. In this study, considering 'Y' as the smaller is better for both the output responses, OEC values have been evaluated for each experimental run (using equations 5, 6 & 7, section 6.3.5). Table 16 shows the values of the output response respective both the worst and best ones with their respective quality characteristics and relative weightage along with OEC values for each run.

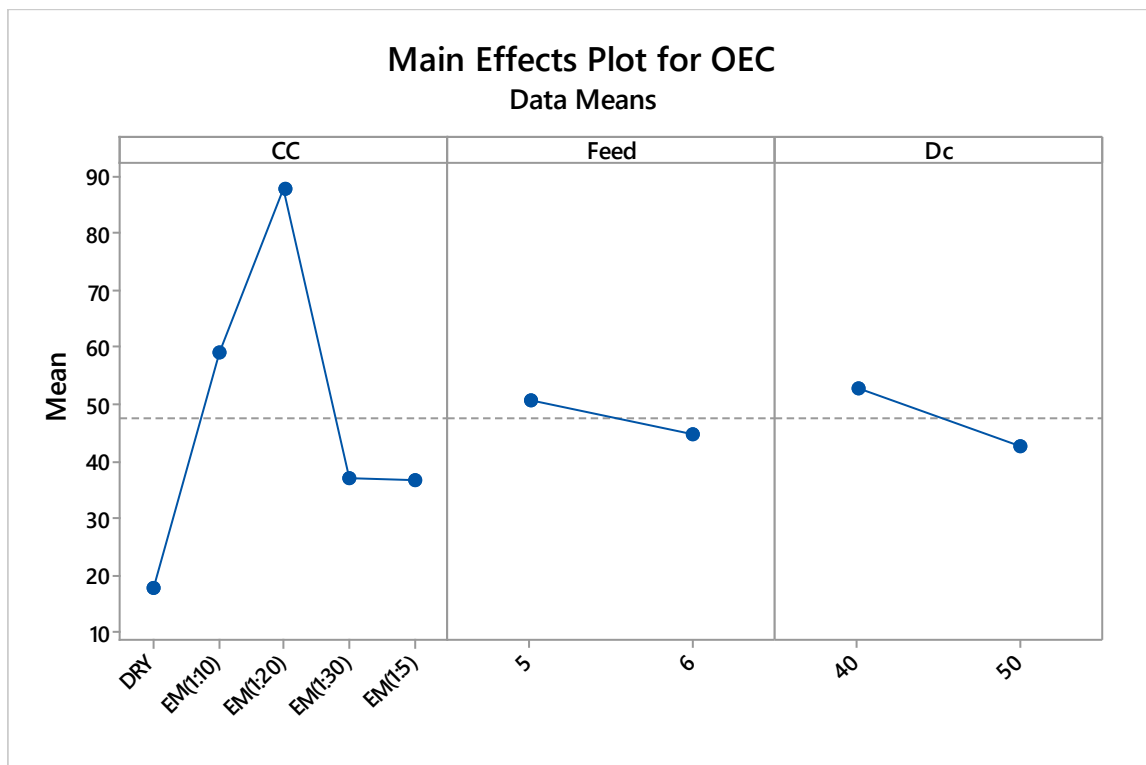


Figure 6.12: Main effects plot for OEC

Table 16: Response measures with QC and relative assigned weight along with OEC values

(a) Response and measure with QC relative assigned weight																				
Response Measure		Worst output					Best output					QC					Relative assigned Weight (%)			
Up W_b		13.42					6.2					Smaller is better					50			
Down W_b		19.7					7.58					Smaller is better					50			
Ex. No	1	2	3	4	5	6	7	8	9	10	11	12	13	14	15	16	17	18	19	20
OEC	76	15	70	39	50	51	54	19	95	27	27	26	38	0.48	68	29	86	34	93	46

From the main effect plot of OEC(Figure 6.12), it is found that the optimal value of input parameters is cutting condition(cc): EM(1:20), Feed:6 $\mu\text{m}\cdot\text{tooth}^{-1}$, depth of cut: 40 μm (Table 17). The SEM image corresponding to which has been shown in Figure 6.13.

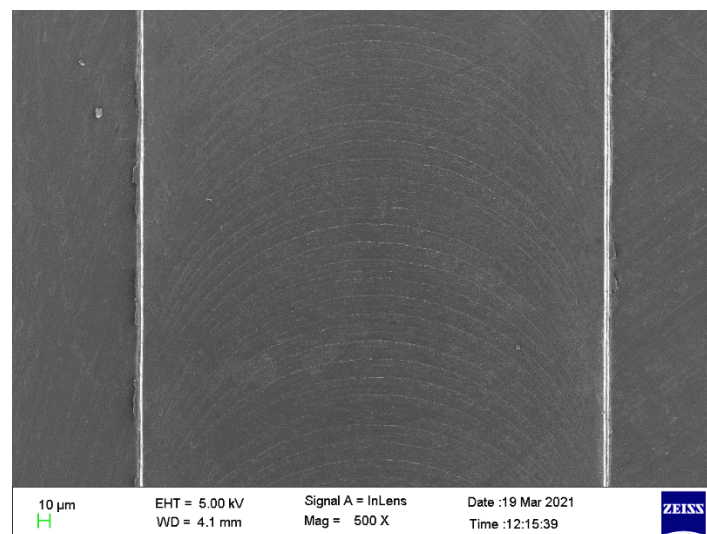


Figure 6.13: SEM image at optimum condition

Table 17: Optimal test results

Exp.	CC	Dc(μm)	Feed($\mu\text{m}/\text{tooth}$)	Up W_b (μm)	Down W_b (μm)
OEC	BL (1:20)	40	6	6.2	8.63

6.4.2 Effect of nanofluid on the top burr

After the experiment, a field emission scanning electron microscope (FESEM) (ZEISS made, model: supra55) and optical microscope were used to capture the images of microchannels. The smallest burr size is obtained using nanofluid with a concentration of CuO nanoparticles $\omega=0.2\%wt$, while the largest burr is formed in dry cutting. It was observed that 0.5%wt, 0.4%wt, 0.3%wt, 0.2%wt, and 0.1%wt of CuO reduces the burr sizes by 8.02%, 33.41%, 35.10%, 42.43% & 5.24% respectively in up milling operation while 5.24%, 33.88%, 28.14%, 60.24% and 26% respectively in down milling (Figure 6.14, Figure 6.15). There is a gradual decrease in the burr size as the concentrations of nanoparticles increases. However, a very drastic change has been seen when a concentration of 0.2%wt was used; the increase in the concentration of nanoparticles dissipates heat faster while penetrating the tool-workpiece interface. Again, after the higher concentrations above 0.2%wt, the effect is insignificant and the top burr equivalent width goes on increasing. This is due to the poor instability of nanofluid at higher concentrations (increase in viscosity and nanoparticles concentration) which adhere to dissipate the heat from the machining zone(Ref 158).

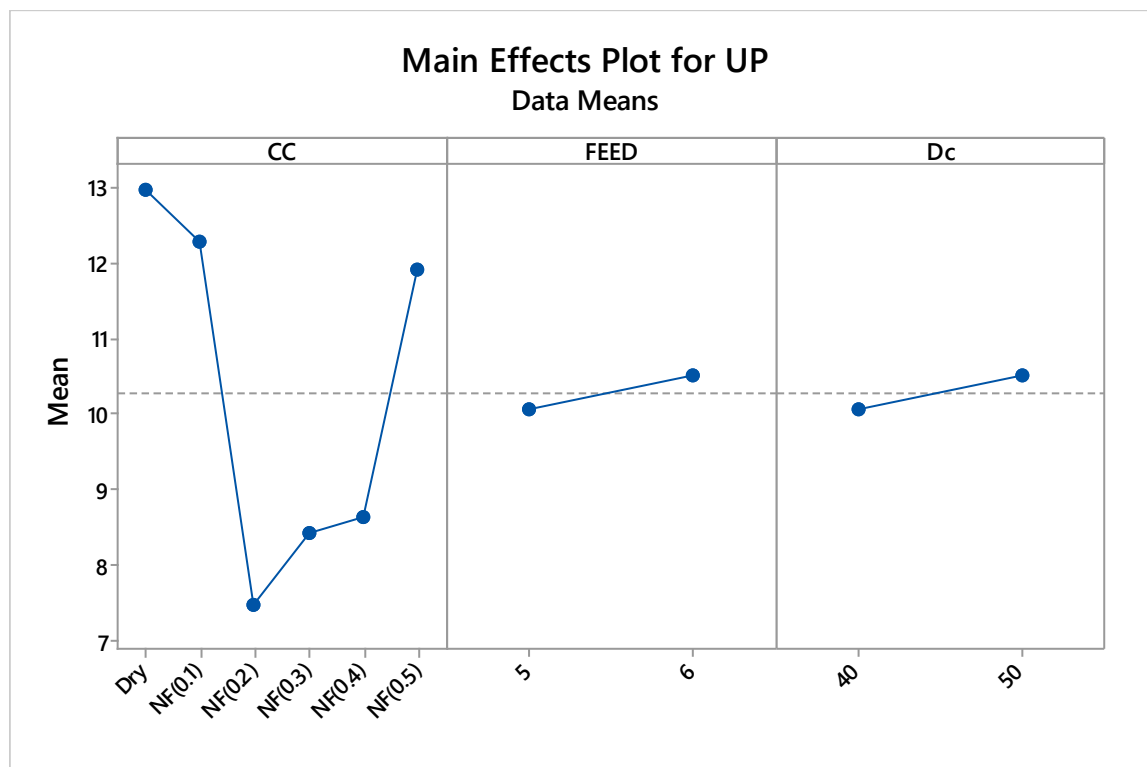


Figure 6.14 : The main effects plots of input parameters on equivalent top burr width (up milling)

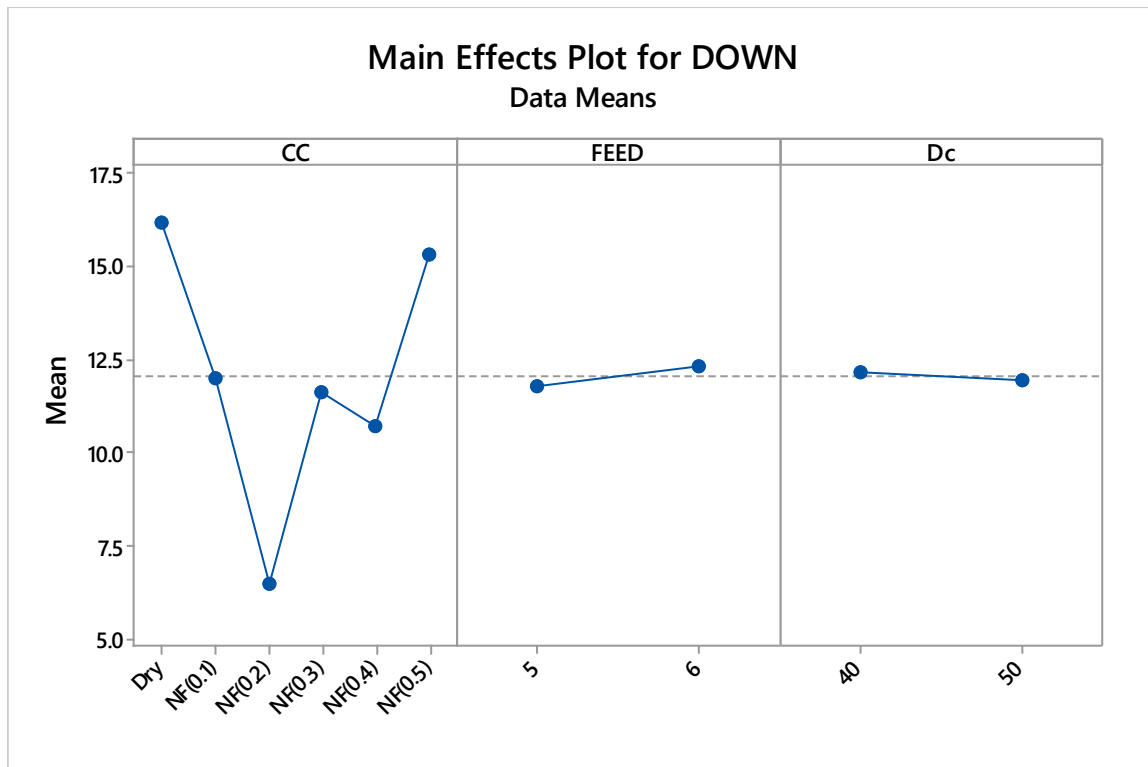


Figure 6.15: The main effects plots of input parameters on equivalent top burr width (down milling)

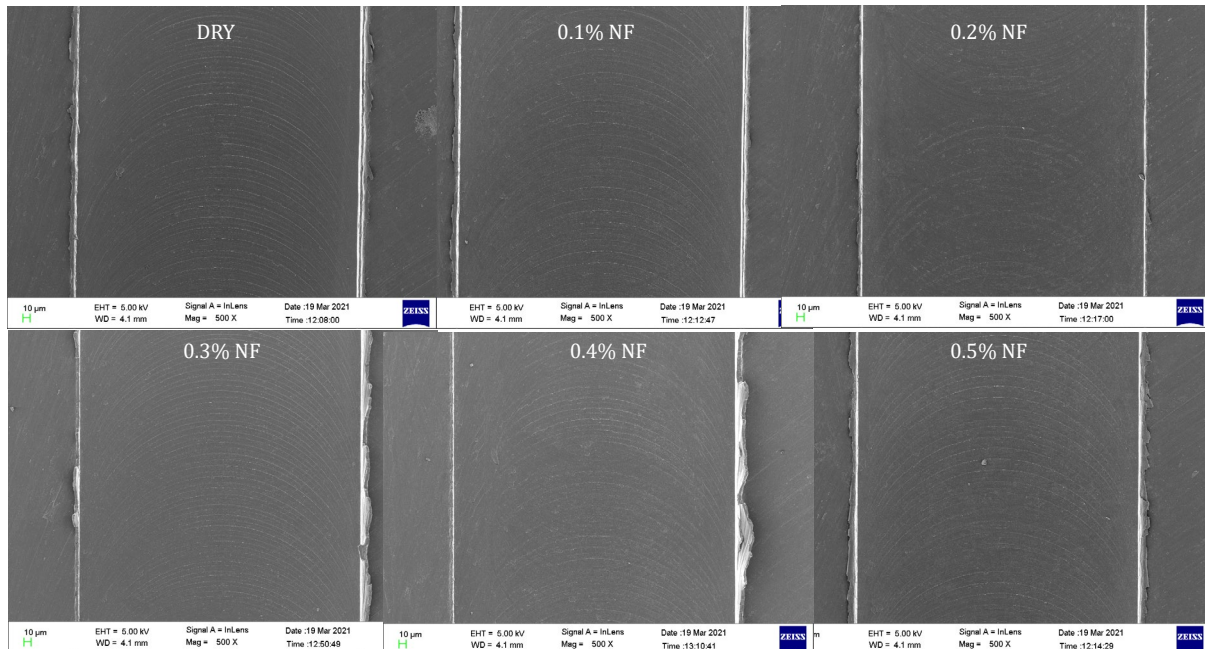


Figure 6.16: SEM images of top burr formation after up or down micromilling at $vc=25.13$ m/min, $f=5 \mu\text{m}\cdot\text{tooth}^{-1}$, $Dc=40 \mu\text{m}$

The comparative analysis of equivalent top burr width in up and down milling with various nanofluid concentrations at fixed cutting speed V_c , feed f , and depth of cut D_c are shown in (Figure 6.16). The same trend resembles other cutting conditions as well. As the depth of cut increases from 40 to 50 micron, the equivalent burr width increases by 4.57% and decreases by 1.64% in up and down milling respectively (Figure 6.14 and Figure 6.15). The percentage change is very less which shows that the effect of depth of cut is insignificant as the concentrations of nanofluid increase. This may be due to the edge tool effect which got sharper and better with MQL using nanofluid and results in better chips formation and hence less burr. While as feed increases from $5 \mu\text{m}\cdot\text{tooth}^{-1}$ to $6 \mu\text{m}\cdot\text{tooth}^{-1}$, equivalent burr width increases by 4.37% and 4.41% in up and down milling respectively. This is mainly because as feed/per tooth increases more than tool edge radius then the cutting phenomenon predominates over plowing action.

Optimization methodology

OEC (overall evaluation criteria) has been employed further to optimize the input process parameters for better output response. (Details have been mentioned above in section 6.3.5). Here, again equal relative weightage (50% each) assigned to both the output responses. Considering 'Y' as the smaller is better (for both the output responses), OEC values have been evaluated for each experimental run (using equations 5,6&7, section 6.3.5).

Table 18: Response measures with QC and relative assigned weight along with OEC values

(a) Response and measure with QC relative assigned weight																								
Response Measure		Worst output							Best output				QC						Relative assigned Weight (%)					
Up W_b		13.78							6.48				Smaller is better						50					
Down W_b		19.7							4.93				Smaller is better						50					
Ex. No.	1	2	3	4	5	6	7	8	9	10	11	12	13	14	15	16	17	18	19	20	21	22	23	24
OEC	47	66	80	21	25	30	35	25	100	77	2	26	66	73	94	18	58	67	62	50	40	34	15	72

Table 18 denotes the values of the output measures both the worst and the best ones with their respective quality characteristics and the relative weightage. It also shows the respective OEC value for each experimental run.

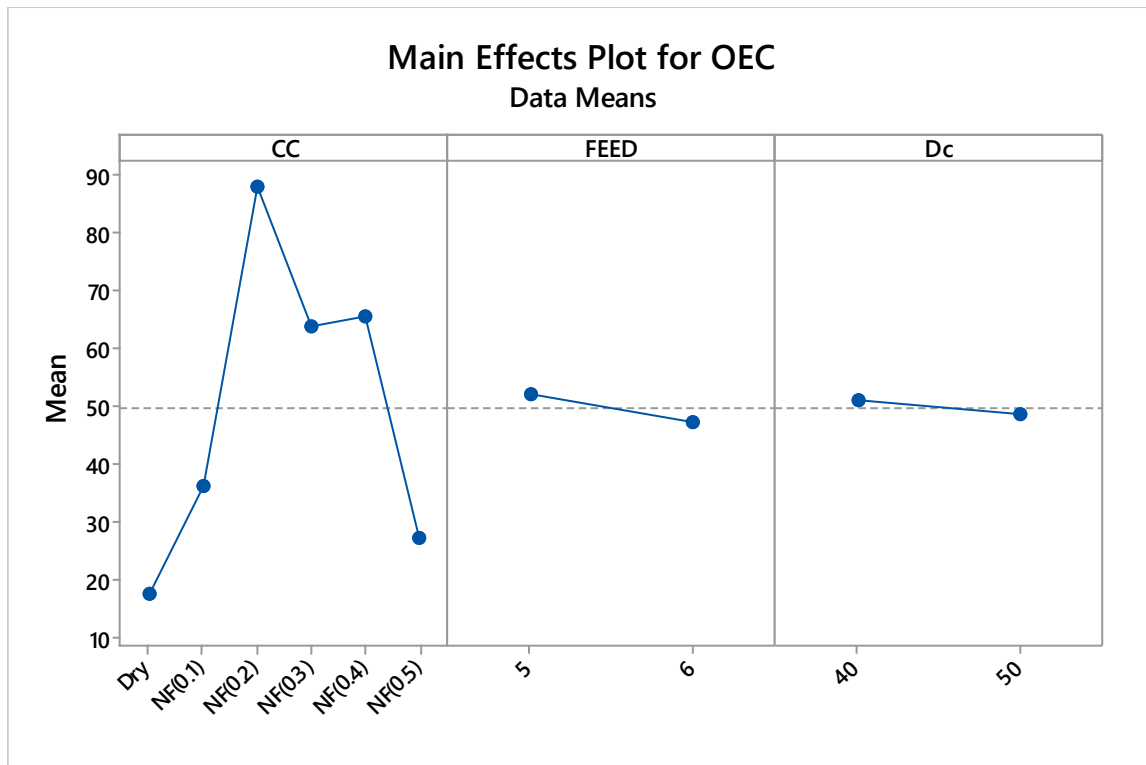


Figure 6.17: variation of OEC with input parameters

From the mean effect plot (as shown in Figure 6.17) of OEC, it is found that the optimal value of input parameters is CC: NF (0.2%), Depth of cut: 40 μm , and feed: 5 $\mu\text{m}\cdot\text{tooth}^{-1}$. From the OEC Table 18, it has been seen that experiment number 9 gives the highest value of OEC. Figure 6.18 depicts the SEM image of the top burr at optimum condition.

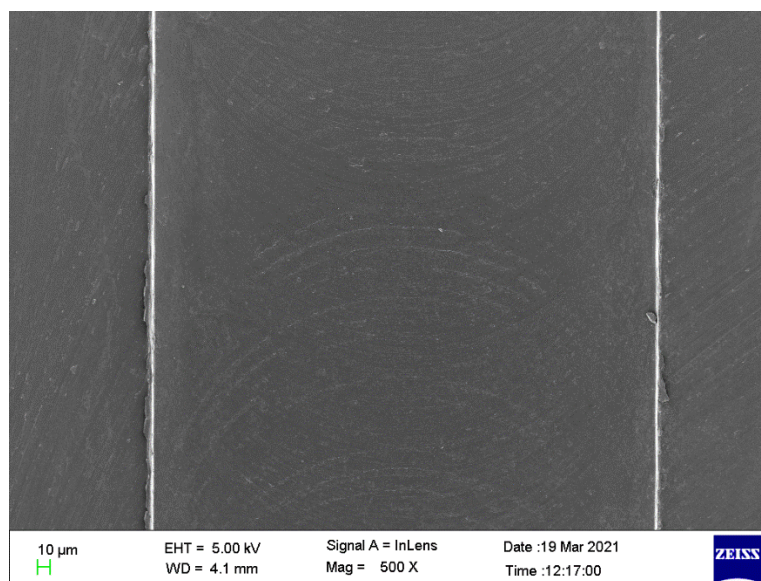


Figure 6.18: SEM image at optimum condition

Table 19: Optimal test results

Exp.	CC	Dc(μm)	Feed(μm)	Up Wb(μm)	Down Wb(μm)
OEC	NF (0.2)	40	5	6.48	4.93

6.4.3 Comparative analysis of the effect of emulsion and nanofluid:

The previous sections have dealt with the effect of the application of emulsion with different concentrations and the effect of nanofluid on burr minimization. In addition to the individual study, the effect of both the cutting fluids has been done with the best results obtained in each case. It is found that the emulsion is giving minimum burrs with an oil-water ratio of 1:20 whereas, the nanofluid gives the best result with 0.2%wt of nanoparticles. Results of the best conditions are shown in Figure 6.19. The table shows the percentage reduction in the burr size in up and down milling with EM and NF. EM is showing the same reduction of 47% in up and down milling burrs. The NF is showing a 45% reduction in up milling burrs and a 70% reduction in down milling burrs. Therefore, it can be seen that the effectiveness of the NL is much higher in down milling burrs than in the application of EM. The high cooling and heat dissipation abilities) characteristics of NF may be responsible for the more reduction of the burrs in the NF application. In addition, qualitative analysis is shown in Table 20. It is found from this figure that nanofluid cooling is more effective in down milling.

Table 20: Comparison of output response of the two cutting fluids (optimum combination)

Cutting condition	Dry machining	Nanofluid	Emulsion	NF%	EM%
Up milling	11.71	6.48	6.2	45%	47%
Down milling	16.21	4.93	8.63	70%	47%

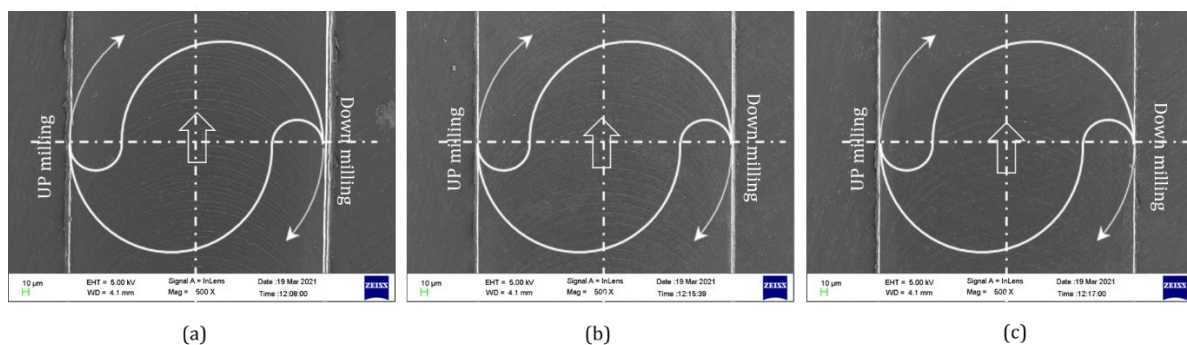


Figure 6.19: SEM image showing comparative analysis of equivalent top burr width with best (a) dry; (b) emulsion (1:20) and nanofluid (0.2%wt)

6.5 Summary

The effect of two types of cutting fluids of different strength has been seen on the size of top burrs in up milling and down milling in comparison with dry machining. The first cutting fluid is an emulsion or base lubricant (EM) with oil and water with four different ratios. The second cutting fluid used in this study is a nanoparticle (CuO) added nano lubricant with different wt% of nanoparticles at five levels. The lowest burr size is obtained using base lubricant, EM(1:20) cutting fluid while the larger burr is formed in dry machining. It was observed that EM(1:5), EM(1:10), EM(1:20), and EM(1:30) reduces the burr sizes by 14.35%, 31.63%, 43.44%, and 7.79% respectively in up milling operation while 9.25%, 19.62%, 47.03% and 18.39 % respectively in down milling with respect to dry machining. It showed that the effect of EM is very less in up milling burrs whereas it is effective in reducing the size of down milling burrs. Further, the effect of depth of cut and feed per tooth is negligible as the change is marginal. Optimum parameters at which the best output response obtained using base lubricant is-

CC: EM(1:20), Cutting speed:25.13 m/min, feed: $6 \mu\text{m}\cdot\text{tooth}^{-1}$, Dc: 40 μm .

The lowest burr size is obtained using nano-lubricant with 0.2 wt.% CuO, while the larger burr formed in dry machining. It was observed that 0.5%wt, 0.4%wt, 0.3 %wt, 0.2 %wt, and 0.1%wt of CuO reduces the burr sizes by 8.02%, 33.41%, 35.10%, 42.43% & 5.24% respectively in up milling operation while 5.24%, 33.88%, 28.14%, 60.24% and 26% respectively in down milling. Therefore, similar to the EM the nano lubricants are less effective in the up-milling burrs whereas effective in down milling burrs. Furthermore, the effect of depth of cut (Dc) and feed per tooth is not significant while using nanofluid. Further, a comparative analysis of the two cutting fluids i.e., water-based emulsion lubricant and nanofluid with the best results was done. It was found that 0.2% NF reduces the equivalent burr width by 45% and 70% in up and down respectively. Whereas, EM(1:20) decreases the equivalent burr width by 47% and 47% in up and down respectively. Minimum quantity lubrication (MQL) using CuO-based nanofluid has shown very promising results in mechanical micromachining to set an alternative to the conventional coolant.

The application of the cutting fluid showed positive results and a reduction in the burr formation has been observed. This technique has been utilized for another superalloy for the broad application. Inconel 718 has been selected for machining with the same type of cutting fluids. Experimental work and results of machining Inconel 718 are described in the next section.

Chapter: 7 BURR MINIMIZATION OF INCONEL718 USING COOLANT and LUBRICANT

7.1 Introduction

The successful outcomes of chapter 6 motivate the author to explore the effectiveness of lubricants on another superalloy INCONEL718. So, this chapter analyses the effects of variants of lubricants viz., a water-oil-based emulsion and copper oxide-based nanofluid on the top burr formation. OEC (overall evaluation criteria) has been employed further to optimize the input process parameters for better output response.

7.2 Motivation, objective, and approach

Among the two approaches discussed in section 6.2, many researchers used approach one to minimize the burr formation, tool wear and enhance surface finish for INCONEL alloys. Uzun et.al(Ref 159) have not found any significant effect on the burr formation and surface roughness using cryogenic pre-cooling in combination with MQL when machining INCONEL718. Aslantas & Cicek(Ref 160) used different cooling & lubrication techniques (MQL, ethanol, and oil-water emulsion) to investigate the burr formation. They found minimum burr using MQL technique but the change was not much significant. So, the results reported in the literature do not agree and the methods and parameters of cooling need to be further investigated. The second approach (II), i.e., the increase of the heat transfer rate in the vicinity of the machining zone, is achieved by cooling and lubricating the machining zone by nanofluids. Sirin and Kivak(Ref 161) studied the effect of different nanofluid lubricants effect on INCONEL X-750 superalloy in milling. Base fluids used as vegetable-based oil and hBN, Graphite, MoS₂ used as nanoparticles of size 80nm and concentration 0.25, 0.50, 0.75, 1.00 vol%. It has been noticed that thermal conductivity and viscosity follow the order hBN<Graphite<MoS₂. Surface roughness was observed lower for hBN nanofluids and the optimum concentration of all nanoparticles is at 0.50 vol%. Cutting temperatures lowest for MoS₂nanofluids among all other different nanofluids used; and out of all concentration, ratio better result observed at 0.25 vol%. This study shows hBN has the lowest cutting force of all and 0.50 vol% concentration ratio shows the best result. These recent researches have shown that nanofluid lubricant is the best alternative to machining/micromachining of difficult-to-machine metal alloys. However, very limited research has been reported for micro-milling of INCONEL 718 using nanofluids. Hence, the current study focused on comparative analysis of the effects of various lubricants viz., emulsions (water-based), copper oxide nanofluid, and nano lubricant (mixture of nanoparticle and emulsion) on

the output response i.e., top burr. A full factorial has been used for the design of the experiment and OEC (overall evaluation criteria) for optimization.

7.3 Experimental details

Experiments have been performed on the high-speed micromachining center (V60) (the detail of the experimental setup is given in Chapter 3). The workpiece in the study is Inconel 718 and a two-flute WC coated (AlTiN) tool of diameter 400 μm has been used. Since the objective of the work is to analyze the effect of lubricant and coolant in the burr formation, three cutting conditions have been implemented. 1: Dry machining for comparison. 2: Emulsion cooling for the effect of lubrication in micromachining and 3: Cooling with nanofluid for the effect of cooling and lubrication together. A novel MQL assisted micromachining setup has been used to experiment. The details about parts, specifications & their functions have been shown in chapter 3 Figure 3.23. The lubricant (both base fluid & nanofluid) was supplied at a constant flow rate of 2 l·h⁻¹ at 0.35 MPa pressure.

Two sets of experiments have been performed separately. 1: To see the effect of lubrication different ratios of emulsion have been used in comparison with the dry machining. 2. To see the effect of lubrication and coolant, different weight ratios of nanofluid/lubricant have been compared with dry machining. Before moving to the experimental work with the above said two sets of experiments, it is necessary to characterize the in-house prepared coolant and lubricants.

7.3.1 Design of experiment for the first set of experiments (emulsion):

(Similar to the experimental design of chapter 6)

This design of experiment consists of all possible combinations of factors (variables) at all levels i.e., full factorial experimental design is used. Table 21 shows the level and process parameters, five levels of cutting conditions, two levels of feed, and two levels of depth of cut that have been used. Since the main objective of the study is to see the effect of the lubricant, therefore five levels of lubrication ratio have been taken. The levels (values) were selected based on the literature survey, preliminary experiments, manufacturer's recommendation, and machine capability. The spindle speed of 25.13 $\text{m}\cdot\text{min}^{-1}$ was kept constant throughout all the experiments. The full factorial design has been analyzed using Minitab 18 (Minitab, USA).

Table 21: Input parameters and their levels

Factors	Level 1	Level 2	Level 3	Level 4	Level 5

Emulsion concentration	Dry*	1:5	1:10	1:20	1:30
Feed f , $\mu\text{m. tooth}^{-1}$	5	6			
Depth of cut D_c , μm	40	50			

* Dry means no cutting fluid was used

7.3.2 Design of experiment for the second set of experiments (nano lubricant):

(Similar to the experimental design of chapter 6)

Six levels of cutting conditions and two levels each of feed and depth of cut have been considered for full factorial interactions of all combinations. Their levels were selected based on the literature survey, preliminary experiments, manufacturer's recommendation, and machine capability; and these are gathered in Table 22. The spindle speed of $25.13 \text{ m}\cdot\text{min}^{-1}$ was kept constant throughout all the experiments. The full factorial design has been analyzed in Minitab 18 (Minitab, USA).

Table 22: Input parameters and their levels

Factors	Level 1	Level 2	Level 3	Level 4	Level 5	Level 6
Nanofluid concentration, % wt.	Dry*	0.1	0.2	0.3	0.4	0.5
Feed f , $\mu\text{m. tooth}^{-1}$	5	6				
Depth of cut D_c , μm	40	50				

* Dry means no cutting fluid was used

7.4 Optimization Methodology

(Similar to the optimization methodology of chapter 6)

7.5 Results and Discussion

7.5.1 Effect of emulsion lubricant on the top burr formation

After the completion of the experiment, scanning electron microscopy (SEM) and optical microscopes were used to analyze the top burr size. Further, Minitab used to analyze the results and corresponding to the main effects plots have been shown in Figure 7.1 for the up and down milling operation.

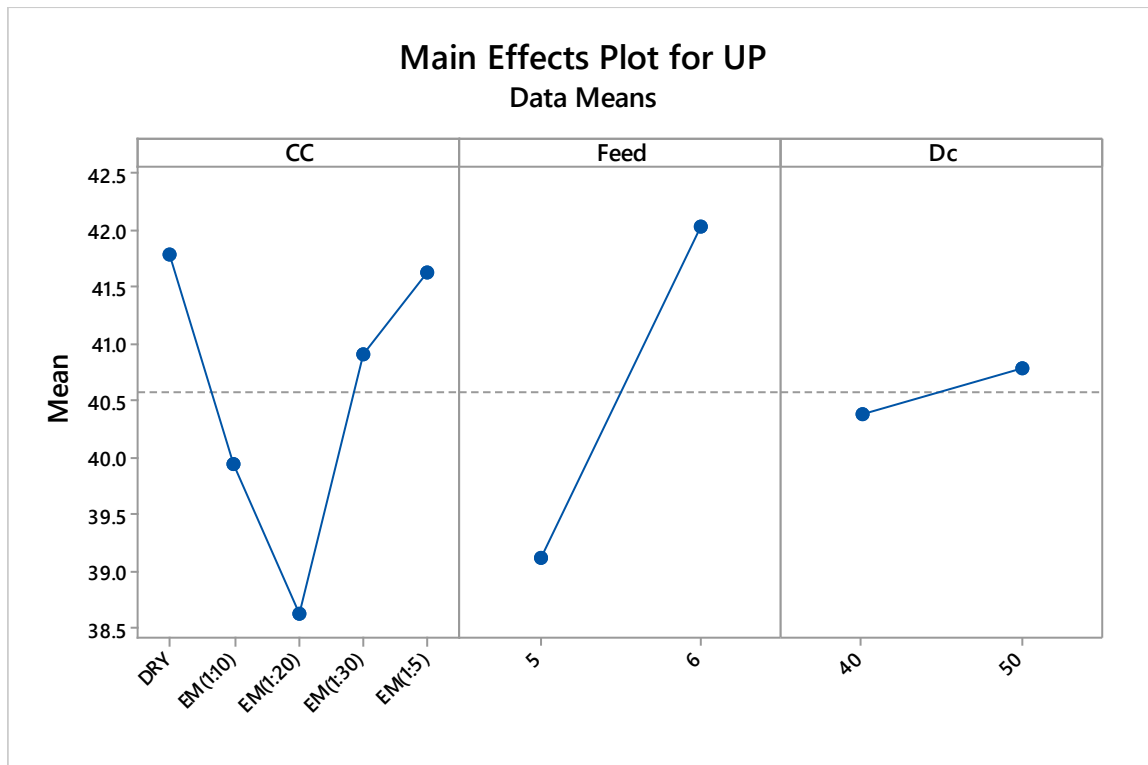


Figure 7.1: Main effects plot for up milling

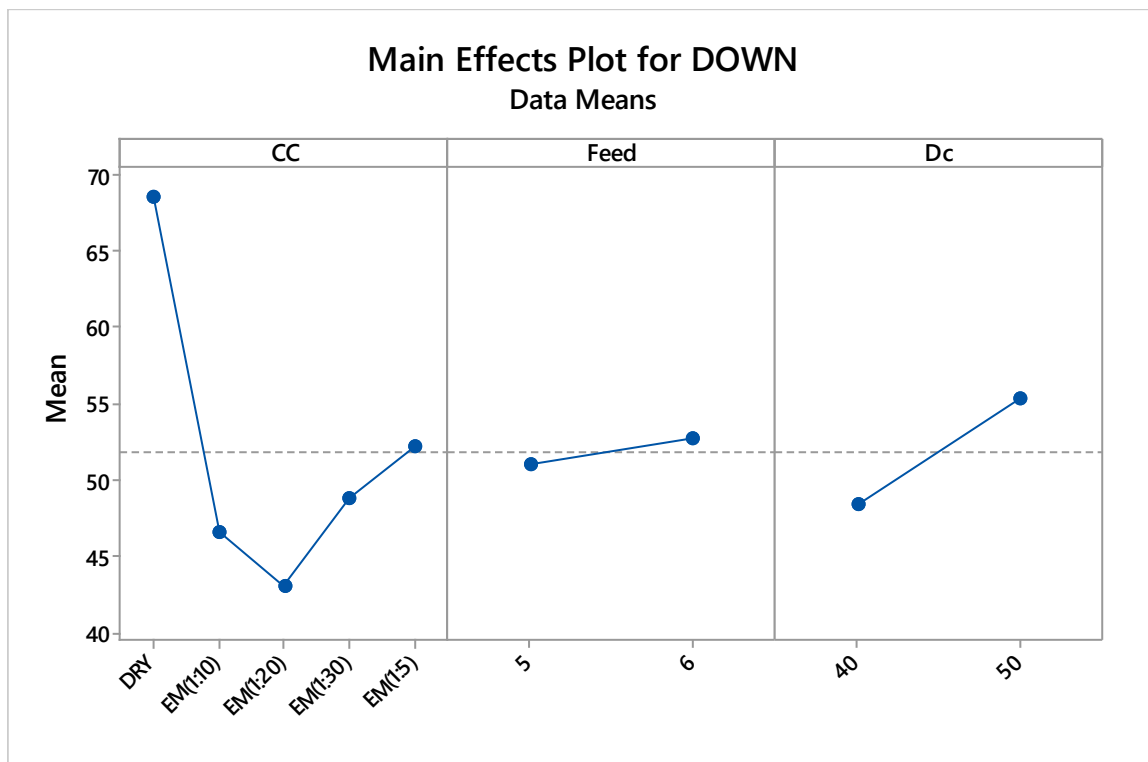


Figure 7.2: Main effects plot for down milling

It can be seen from Figure 7.1 and Figure 7.2 that the least burr size is obtained while using an emulsion with a concentration of EM(1:20) in both up as well as down milling, while the largest

burr is formed in dry cutting. It was observed that EM(1:5), EM(1:10), EM(1:20), and EM(1:30) reduces the burr sizes by 0.38%, 4.4%, 7.5%, and 2.1% respectively in up milling operation while 23%, 31.98%, 37.14% and 28.88% respectively in down milling with respect to dry machining. The comparative analysis of SEM images at constant parameters of $V_c=25.13$ m/m, $f=6$ $\mu\text{m}/\text{tooth}$, $a=50$ μm (Figure 7.3) shows clear variations in size at different concentrations. However, it resembles the same trend at other parameters too.

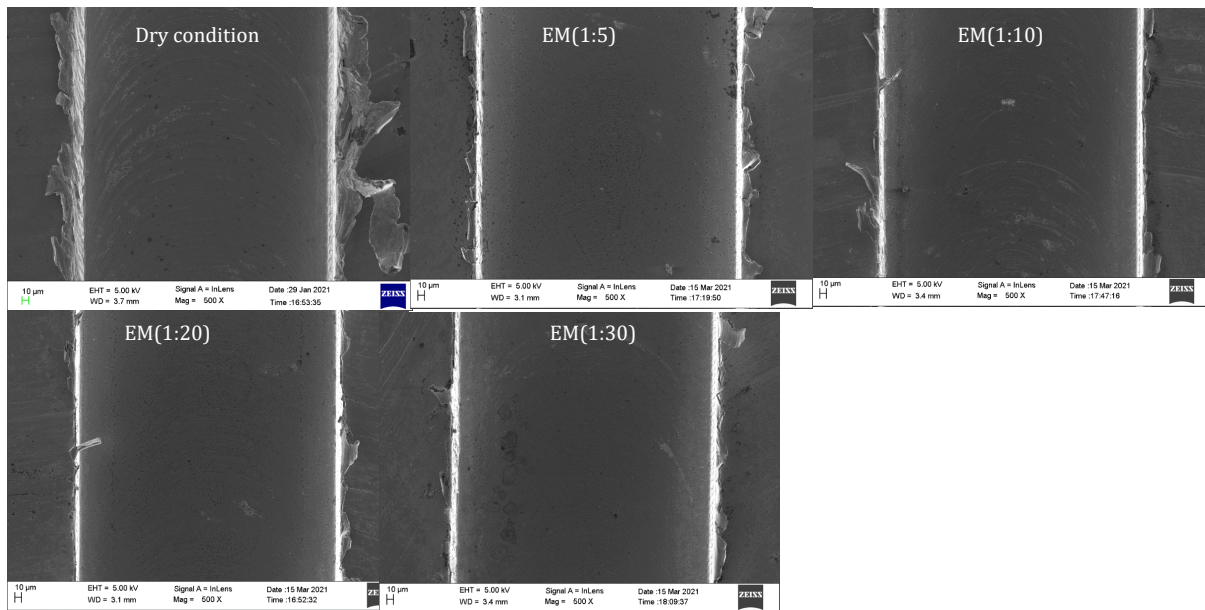


Figure 7.3: SEM images of top burr formation in up and down micromilling at $V_c=25.13$ m/m, $f=6$ $\mu\text{m}\cdot\text{tooth}^{-1}$, $D_c=50$ μm

As the concentration of fluid decreases (from EM (1:5) TO EM (1:20)) equivalent burr width is decreasing and finally a saturation stage (optimum condition) is reached where the effect is insignificant at tool-chip and tool-workpiece interface and hence, equivalent burr width is increasing (EM (1:30)). This is due to the better interaction of tool and workpiece with the use of cutting fluid at optimum concentration. At low concentration, a cutting fluid does not form a thin film of lubrication which is required for smooth machining whereas at higher concentration it is not able to penetrate the tool-workpiece interface(Ref 94).

In addition to the effect of lubrication, the effect of depth of cut and the feed rate has been analyzed. As feed rate is increasing from 5 to 6 microns per flute, equivalent top burr width is increasing in both up as well as down milling due to the decrease in uncut chip thickness with an increase in chip load. However, as the depth of the cut is increasing, equivalent top burr width increases as well due to the accumulation of large heat which leads to a change in material property to ductile which further leads to the decrease in the area of resistance and hence more burr formed(Ref 111).

Optimization technique:

OEC (overall evaluation criteria) (6.3.5) has been used further to optimize the input process parameters for better output response. As per this technique, equal relative weightage (50% each) is assigned to both the output responses i.e., up milling top burr and down milling top burr. In this study, considering 'Y' as the smaller is better for both the output responses, OEC values have been evaluated for each experimental run (using equations 5,6&7, section 6.3.5).

Table 23 shows the values of the output response respective both the worst and best ones with their respective quality characteristics and relative weightage along with OEC values for each run.

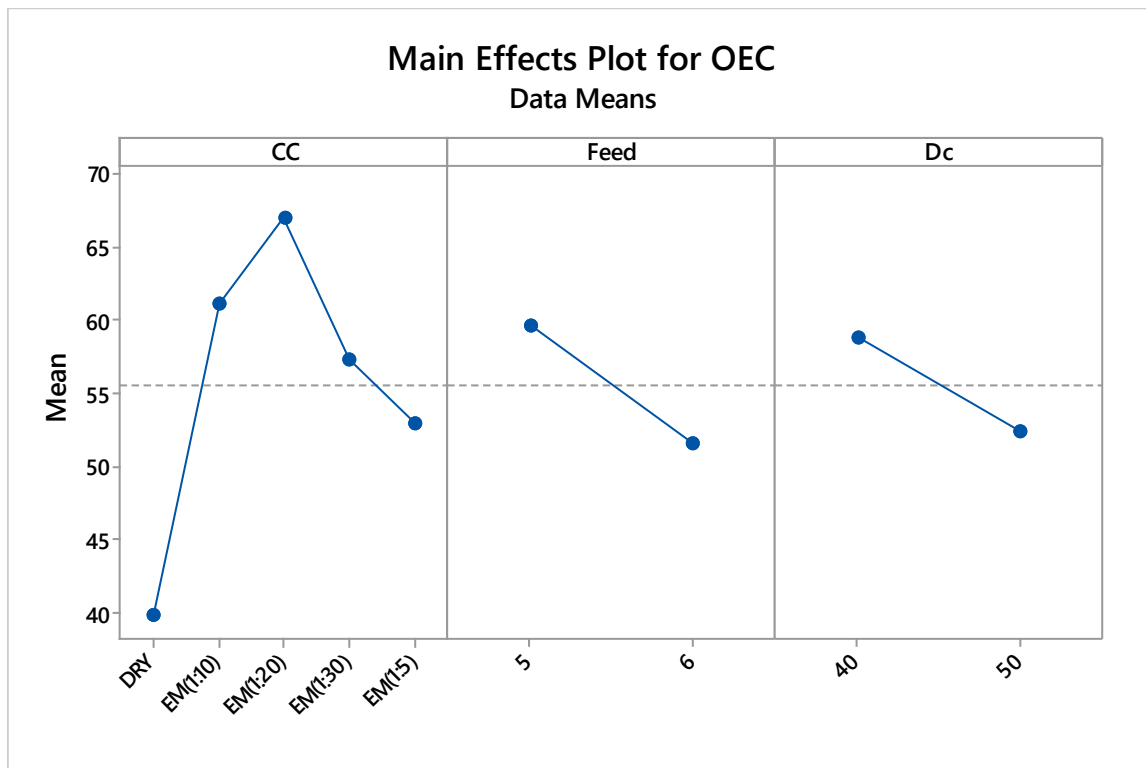


Figure 7.4: Main effects plot for OEC

Table 23: Response measures with QC and relative assigned weight along with OEC values

(a) Response and measure with QC relative assigned weight																				
Response Measure	Worst output			Best output			QC											Relative assigned Weight (%)		
Up W_b	49.307			27.615			Smaller is better											50		
Down W_b	97.359			33.205			Smaller is better											50		
Ex. No	1	2	3	4	5	6	7	8	9	10	11	12	13	14	15	16	17	18	19	20
OEC	23	65	58	88	41	28	35	50	58	75	74	72	34	61	44	65	50	62	55	63

From the main effect plot of OEC, it is found that the optimal value of input parameters is cutting condition(cc): EM(1:20), Feed: $6 \mu\text{m}\cdot\text{tooth}^{-1}$, depth of cut: $50 \mu\text{m}$. The SEM image corresponding to which has been shown in Figure 7.5.

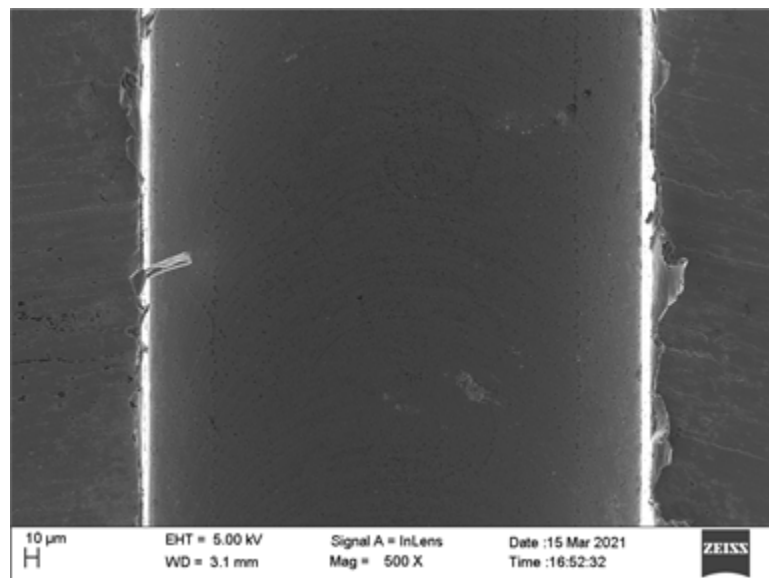


Figure 7.5: SEM image at optimum condition

7.5.2 Effect of nano-fluid on the top burr

After the experiment, a field emission scanning electron microscope (FESEM) (ZEISS made, model: supra55) and optical microscope were used to capture the images of microchannels. The smallest burr size is obtained using nanofluid with a concentration of CuO nanoparticles $\omega=0.3$ % wt, while the largest burr is formed in dry cutting. It was observed that 0.5%wt, 0.4%wt,

0.3%wt, 0.2 %wt, and 0.1%wt of CuO reduces the burr sizes by 28.86%, 43.7%, 66.22%, 18.07% and 7.8% respectively in up milling operation while 44.68%, 58.85%, 79.11%, 49.19% and 48.39% respectively in down milling (Figure 7.6, Figure 7.7). The use of nanofluid of concentrations 0.2 %wt and below has no significant effect on burr formation compared to dry cutting. However, a very drastic change has been seen when a concentration of 0.3%wt was used; the increase in the concentration of nanoparticles dissipates heat faster while penetrating the tool-workpiece interface. Again, after the higher concentrations above 0.3%wt, the effect is insignificant and the top burr equivalent width goes on increasing. This is due to the poor stability of nanofluid at higher concentrations (increase in viscosity and nanoparticles concentration) which adhere to dissipate the heat from the machining zone(Ref 158).

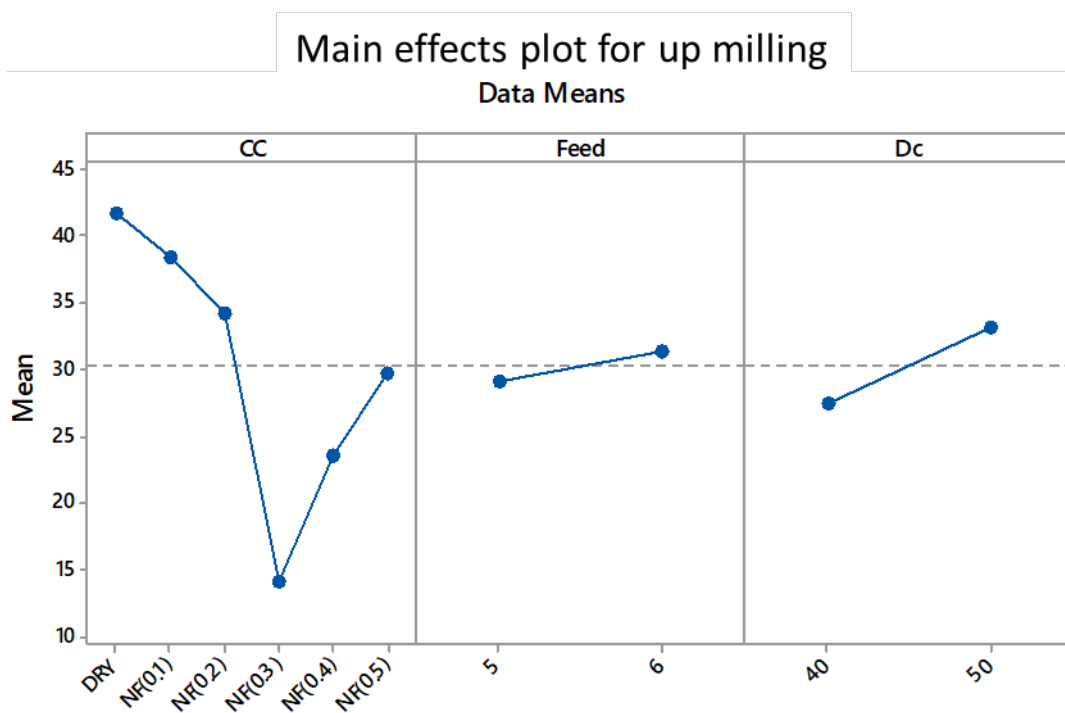


Figure 7.6: Main effects plot for up milling

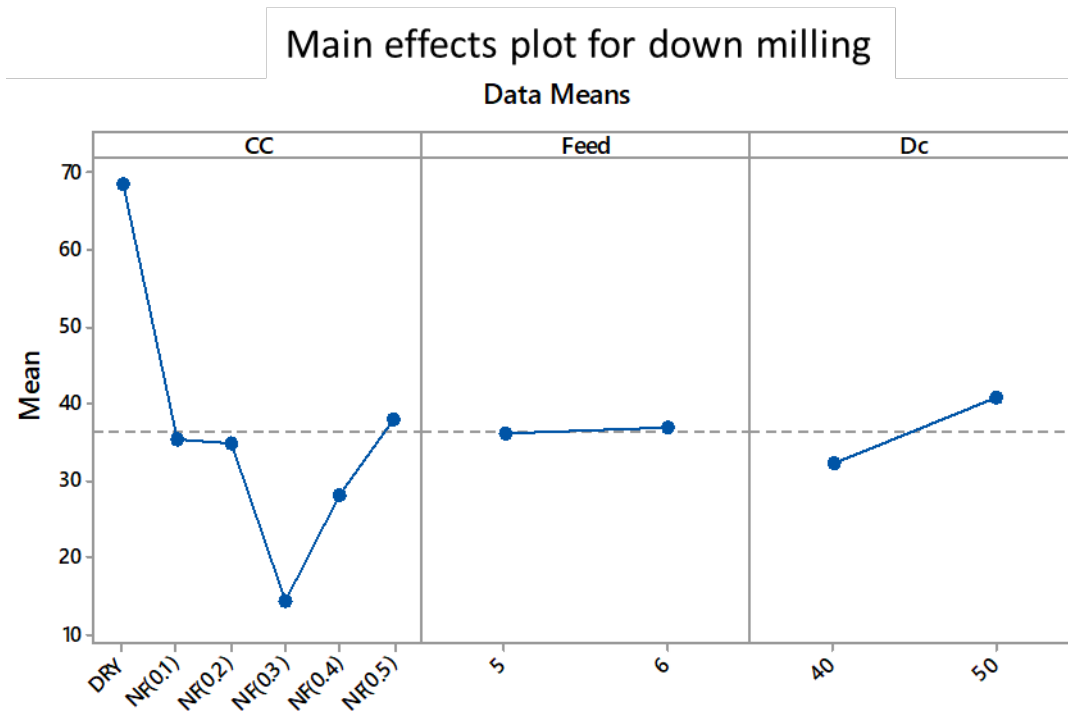
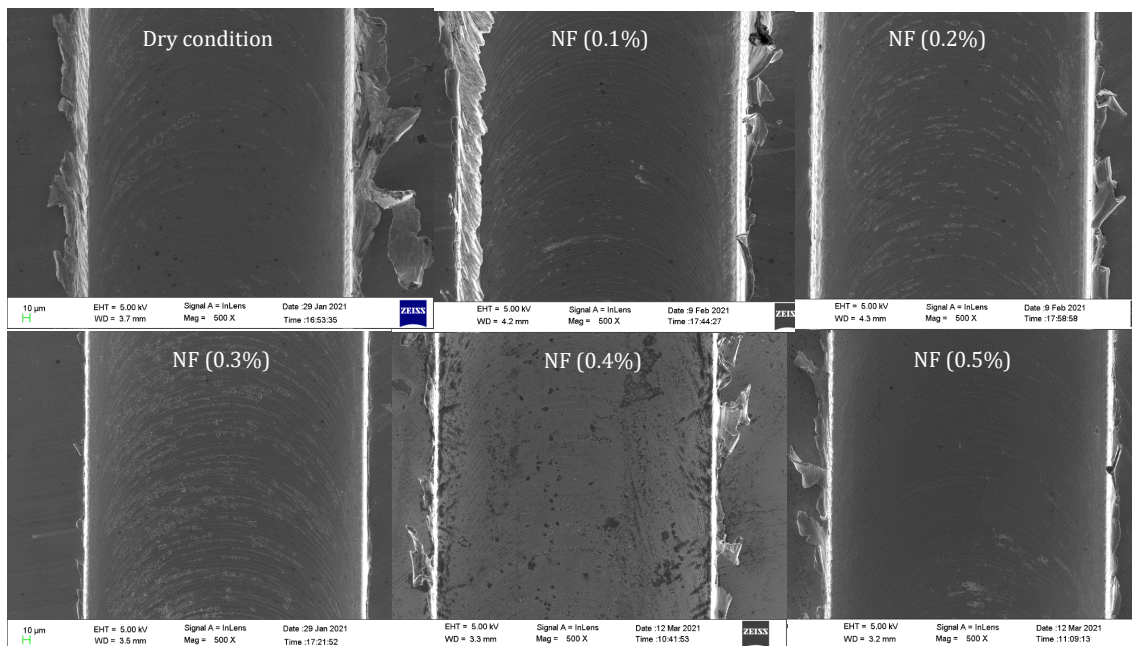


Figure 7.7: Main effects plot for down milling

Figure 7.8: SEM images of top burr formation after up or down micromilling at $v_c=25.13$ m/min, $f=6 \mu\text{m}\cdot\text{tooth}^{-1}$, $D_c=50 \mu\text{m}$

The comparative analysis of equivalent top burr width in up and down milling with various nanofluid concentrations at fixed cutting speed V_c , feed f , and depth of cut D_c are shown in (Figure 7.8). The same trend resembles other cutting conditions as well. As the depth of cut

increases from 40 to 50 micron, the equivalent burr width increases by 20.79% and 26.94% in up and down milling respectively (Figure 7.9).

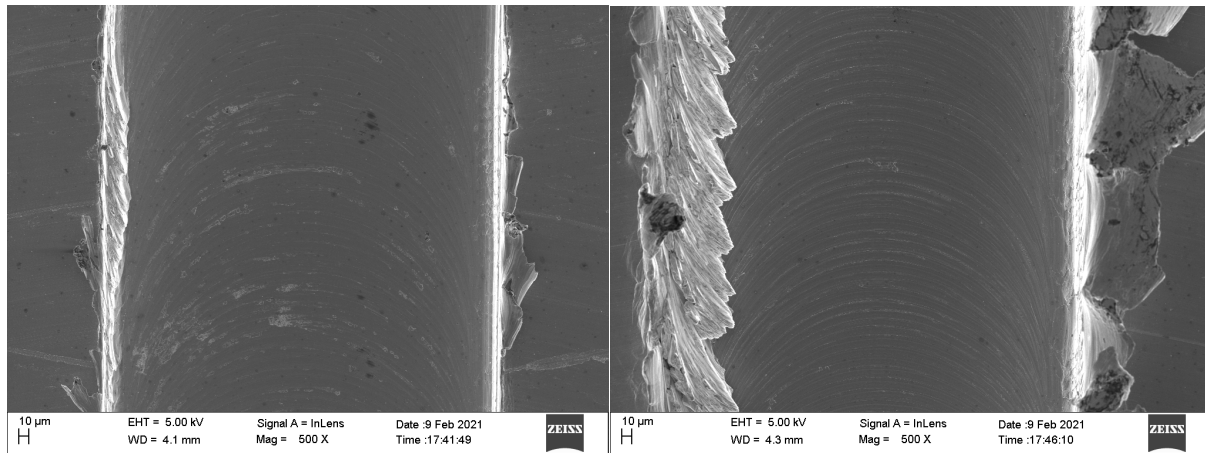


Figure 7.9: SEM image showing variation of top burr width with depth of cut (constant parameter: $0.1\% \text{ NF}$, $f = 6 \mu\text{m}\cdot\text{tooth}^{-1}$)

When the depth of cut increases, more heat is diffused to the workpiece due to which material property changes and hence ductility increases. Thus, the area to get resist decreases, and hence more burr is produced. While feed increases from $5 \mu\text{m}\cdot\text{tooth}^{-1}$ to $6 \mu\text{m}\cdot\text{tooth}^{-1}$, equivalent burr width increases by 7.77% and 2.29% in up and down milling respectively (Figure 7.10). This is mainly because as feed/per tooth increases more than tool edge radius then cutting phenomenon predominates over plowing action.

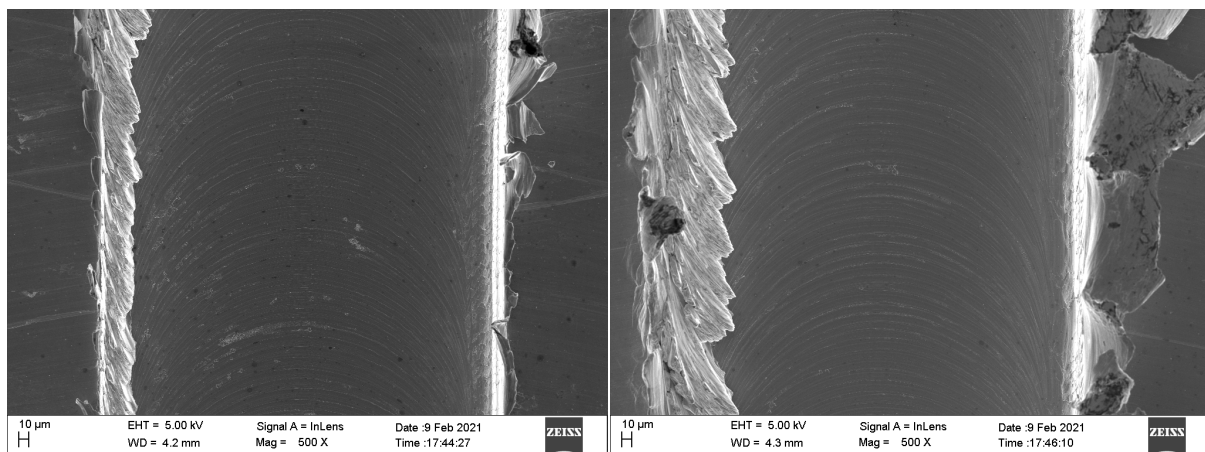


Figure 7.10: SEM image showing a variation of top burr width with feed rate (Constant Parameters: $0.1\% \text{ NF}$, $D_c=50 \mu\text{m}$)

Optimization methodology

OEC (overall evaluation criteria) has been employed further to optimize the input process parameters for better output response. (Details have been mentioned above in section 6.3.5).

Here, again equal relative weightage (50% each) assigned to both the output responses. Considering 'Y' as the smaller is better (for both the output responses), OEC values have been evaluated for each experimental run (using equations 5,6&7, section 6.3.5).

Table 24: Response measures with QC and relative assigned weight along with OEC values

(a) Response and measure with QC relative assigned weight																								
Response Measure		Worst output					Best output					QC					Relative assigned Weight (%)							
Up W_b		59.946					11.995					Smaller is better					50							
Down W_b		97.359					11.18					Smaller is better					50							
Ex. No.	1	2	3	4	5	6	7	8	9	10	11	12	13	14	15	16	17	18	19	20	21	22	23	24
OEC	19	71	81	79	59	76	64	62	69	75	56	62	23	86	36	33	86	66	95	95	28	64	100	92

Table 24 denotes the values of the output measures both the worst and the best ones with their respective quality characteristics and the relative weightage. It also shows the respective OEC value for each experimental run.

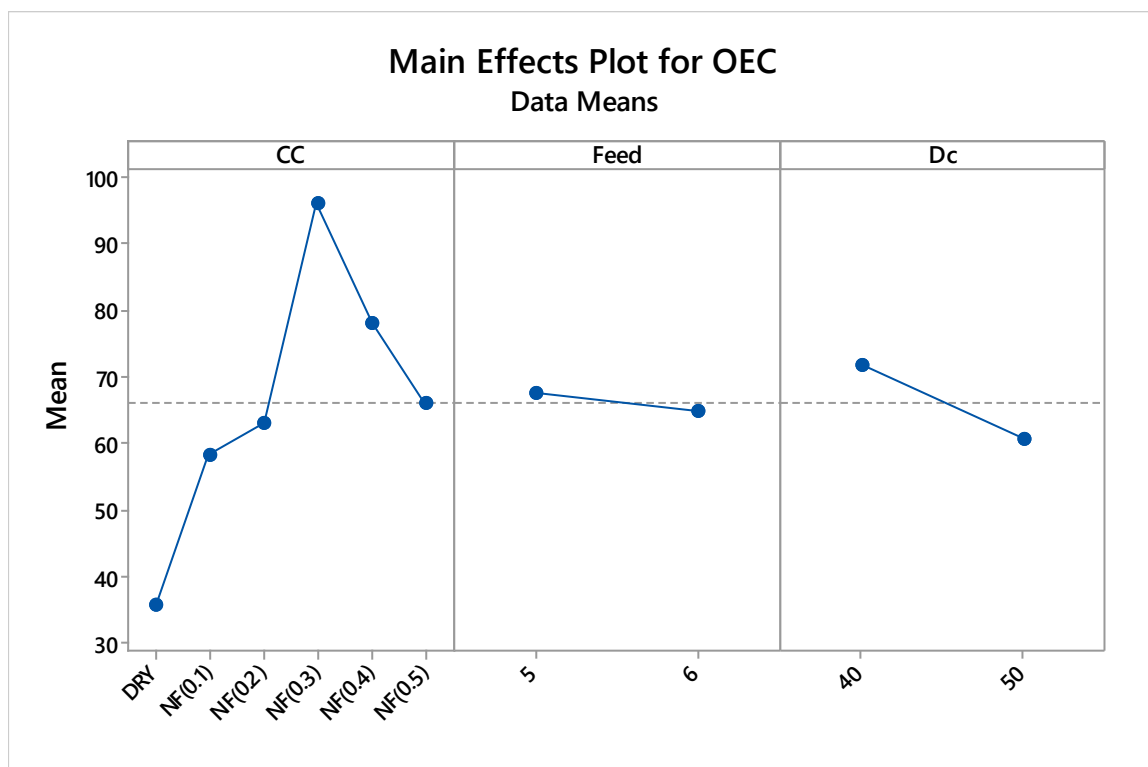


Figure 7.11: variation of OEC with input parameters

From the mean effect plot (as shown in Figure 7.11) of OEC, it is found that the optimal value of input parameters is CC: NF (0.3%), Depth of cut:40 μm , and feed: 5 $\mu\text{m}\cdot\text{tooth}^{-1}$. From the OEC Table 24, it has been seen that experiment number 24 gives the highest value of OEC. Figure 7.12 depicts the SEM image of the top burr at optimum condition.

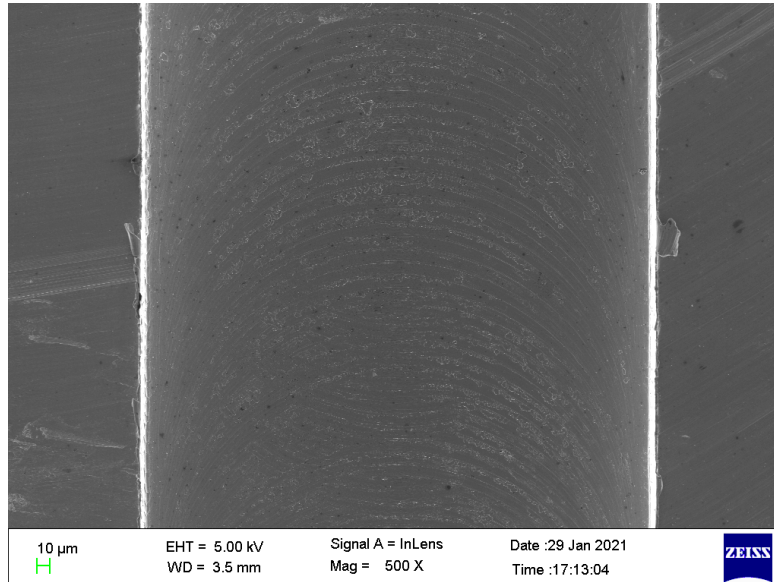


Figure 7.12: SEM image at optimum condition

Table 25: Optimal test results

Exp.	CC	Dc	Feed	Up Wb	Down Wb
OEC	NF (0.3)	40	5	12	11.18

7.5.3 Comparative analysis of the effect of emulsion and nanofluid:

The previous sections have dealt with the effect of the application of emulsion with different concentrations and the effect of nanofluid on burr minimization. In addition to the individual study, the effect of both the cutting fluids has been done with the best results obtained in each case. It is found that the emulsion is giving minimum burrs with an oil-water ratio of 1:20 whereas, the nanofluid gives the best result with 0.3%wt of nanoparticles. Results of the best conditions are shown in Figure 7.13. The table shows the percentage reduction in the burr size in up and down milling with EM and NF. EM is showing a reduction of 38 % and 28 % in up and down milling burrs. The NF is showing a 59 % reduction in up milling burrs and an 82 % reduction in down milling burrs. Therefore, it can be seen that the effectiveness of the NF is much higher in down milling burrs than in the application of EM. The high cooling and heat-dissipating characteristics of NF may be responsible for the more reduction of the burrs in the

NF application. In addition, qualitative analysis is shown in Table 26. It is found from this figure that nanofluid cooling is more effective in down milling.

Table 26: Comparison of output response of the two cutting fluids (optimum combination)

Cutting condition	Dry machining	Nanofluid	Emulsion	NF%	EM%
Up milling	44.62	18.41	27.61	59	38
Down milling	66.83	12.31	48.20	82	28

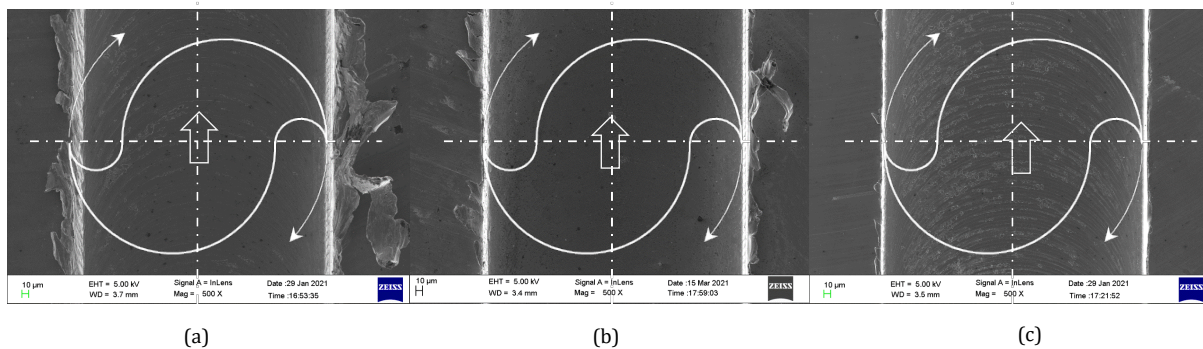


Figure 7.13: SEM image showing comparative analysis of equivalent top burr width with best (a) dry; (b) emulsion (1:20) and nanofluid (0.3%wt)

7.6 Summary

The effect of two types of cutting fluids of different strength has been seen on the size of top burrs in up milling and down milling in comparison with dry machining. The first cutting fluid is an emulsion or base lubricant (BL) with oil and water with four different ratios. The second cutting fluid used in this study is a nanoparticle (CuO) added nano lubricant with different wt% of nanoparticles at five levels. The lowest burr size is obtained using base lubricant, EM(1:20) cutting fluid while the larger burr is formed in dry machining. It was observed that based lubricant EM(1:5), EM(1:10), EM(1:20), and EM(1:30) reduces the burr sizes by 0.38%, 4.4%, 7.5%, and 2.1 % respectively in up milling operation while 23%, 31.98%, 37.14%, and 28.88% respectively in down milling with respect to dry machining. It showed that the effect of EM is very less in up milling burrs whereas it is effective in reducing the size of down milling burrs. Further Top burr size (equivalent burr width) increases with an increase in depth of cut (Dc) and feed while using water-based emulsion lubricant/ base lubricant. Optimum parameters at which the best output response obtained using base lubricant is-

CC: EM(1:20), Cutting speed: 25.13 m/min, feed: $6 \mu\text{m}\cdot\text{tooth}^{-1}$, Dc: 50 μm .

The lowest burr size is obtained using a nano-lubricant with 0.3wt.% CuO, while the larger burr formed in dry machining. 0.5%wt,0.4%wt,0.3%wt, 0.2%wt, and 0.1%wt of CuO reduces the burr sizes by 28.86%,43.7%,66.22%,18.07% and7.8% respectively in up milling operation while 44.68%,58.85%,79.11%,49.19% and 48.39% respectively in down milling. Therefore, similar to the EM the nano lubricants are less effective in the up milling burrs whereas effective in down milling burrs. Further Top burr size (equivalent burr width) increases with an increase in depth of cut (Dc) and feed while using nanofluid as cutting fluid. Further, a comparative analysis of the two cutting fluids i.e., water-based emulsion lubricant and nanofluid with the best results was done. It was found that 0.3% NF reduces the equivalent burr width by 59% and 82% in up and down respectively. Whereas, EM(1:20) decreases the equivalent burr width by 38.11% and 27.87 % in up and down respectively. Minimum quantity lubrication (MQL) using CuO-based nanofluid has shown very promising results in mechanical micromachining to set an alternative to the conventional coolant.

In the next chapter, overall results & discussions with future scopes have been discussed in detail.

Chapter: 8 CONCLUSION AND FUTURE SCOPE

Burr formation was always a challenge for the metal cutting domain. The removal of the burrs takes extra cost and time, therefore, increases the final cost of the product. The burr removal becomes more challenging if the size of the component is very small of orders few hundred microns. In micromachining fabrication is performed in the range of a few hundred micrometers. In micromilling when the feature size varies between microns to millimeters the small size burrs create issues with the quality of the surface and product. The removal of small size burrs is much more difficult than the removal of conventional size burrs. The problem added more difficulty if the workpiece material is a superalloy and difficult to cut material. Therefore, minimization of burrs may be a more beneficial task than the removal of the burrs in micromilling. Burrs can be of many types viz. top burr, entry burr, exit burr. The literature showed that many works are reported in the formation and minimization of entry and exit burrs in superalloys micromachining but very less work is reported for the top burrs. Therefore, the present work deals with the minimization of the top burrs in superalloys. Two super alloys Ti6Al4V and Inconel 718 have been selected as workpiece material. Initially, burr formation mechanism has been performed with Ti6Al4V with varying chip load in terms of the axial and radial depth of cut and the feed per tooth. This helped in understanding the mechanism of burr formation. Literature showed that the high-speed machining may help reduce the cutting forces and further reduction in the burr formation. Therefore, high-speed machining on Ti6Al4V was performed to see the effect of high cutting speed in burr formation and minimization. Further, the literature showed that cooling and lubrication may be helpful in the reduction of burr formation. The problem with the micromilling is the narrow gaps between the tool and chip, therefore, conventional cooling may not be helpful. Special arrangement has been done by MQL with two types of cutting fluids 1. Emulsion or base lubricant (BL) and 2. Nano lubricant. Micromilling has been performed on Ti6Al4V and Inconel 718 in a dry condition for comparison purposes and with different strengths of two cutting fluids. The results have been analyzed and the positive effect of lubrication and cooling has been observed. The detail of the main conclusion from the thesis is as follows:

8.1 The main conclusion of the thesis

8.1.1 Experimental setup

1. A high-speed micromachining center has been developed
2. The developed machining center has features of MQL and cryogenic lubrication
3. The motion accuracy in all three axes is achieved at $\pm 2.5 \mu\text{m}$ and the maximum spindle speed is 60,000 rpm.

8.1.2 Mechanism of top burr formation

1. The basic mechanism of top burr formation in down milling has been explained.
2. Down milling burr was formed mainly since the redeposition of material and side bulging action.
3. The effect of radial depth of cut on top burr width is insignificant.
4. ANOVA analysis confirms that feed per tooth and depth of cut has a significant effect on the top burr formation in down milling.
5. This mechanism may help in deciding the feasible parameters to reduce top burr formation.

8.1.3 High-speed micromachining

1. The measured width of the top burr illustrates that the up-milling burrs are bigger in HSMM and the down milling burrs are bigger in conventional speed. As in HSMM up milling burr formed due to increase in strain rate hardening of material while at conventional speed, down milling burrs are bigger due to squeezing and accumulation of uncut chip.
2. The equivalent burr width in down milling decreased by 33.02 % and 40.36 % as the cutting speed increased from 16 m/min to 79 m/min and from 79 m/min to 141 m/min respectively.
3. Increasing the depth of cut decreases the equivalent width of the up mill burr and vice versa occurs on the down mill side. It may be due to the effect of thermal softening at a higher depth of cut.
4. The influence of feed rate is negligible in up milling burr width. However, the width of the down milling burr is decreased by increasing the feed rate.
5. The equivalent burr width gets reduced in both cases up and down milling when tool diameter decreases and number of flutes increases. Smaller tool diameter has to reduce less material and hence, lesser burr formed. With the increase of the number of flutes, feed rate increases in the same proportion due to which uncut chip area get reduced; and hence less burr size formed.

8.1.4 Application of COOLANT and LUBRICANT in the machining of superalloys

Titanium alloys

1. The lowest burr size is obtained using base lubricant, EM(1:20) cutting fluid while the larger burr is formed in dry machining. It was observed that EM (1:5), EM (1:10), EM (1:20), and EM (1:30) reduces the burr sizes by 14.35%, 31.63%, 43.44%, and 7.79% respectively in up milling operation while 9.25%, 19.62%, 47.03 and 18.39% respectively in down milling with respect to dry machining. It showed that the effect of EM is very less in up milling burrs whereas it is effective in reducing the size of down milling burrs.
2. Optimum parameters at which the best output response obtained using base lubricant is- CC: EM(1:20), Cutting speed:25.13 m/min, feed: 6 $\mu\text{m}\cdot\text{tooth}^{-1}$, Dc: 40 μm .
3. The lowest burr size is obtained using nano-lubricant with 0.2 wt.% CuO, while the larger burr formed in dry machining. It was observed that 0.5%wt,0.4%wt,0.3 %wt, 0.2 %wt, and 0.1 %wt of CuO reduces the burr sizes by 8.02%,33.41%,35.10%,42.43% & 5.24% respectively in up milling operation while 5.24%,33.88%,28.14%,60.24% and 26% respectively in down milling.
4. Optimum parameters at which the best output response obtained using base lubricant is- CC: 0.2 wt.% CuO, Cutting speed:25.13 m/min, feed: 5 $\mu\text{m}\cdot\text{tooth}^{-1}$, Dc: 40 μm .
5. Further, a comparative analysis of the two cutting fluids i.e., water-based emulsion lubricant and nanofluid with the best results was done. It was found that 0.2% NF reduces the equivalent burr width by 45% and 70% in up and down respectively. Whereas, EM(1:20) decreases the equivalent burr width by 47% and 47 % in up and down respectively.

Inconel alloys

1. It was observed that base lubricant EM(1:5), EM (1:10), EM (1:20) and EM (1:30) reduces the burr sizes by 0.38%,4.4%,7.5% and 2.1% respectively in up milling operation while 23%,31.98 %,37.14% and 28.88 % respectively in down milling with respect to dry machining.
2. Optimum parameters at which the best output response obtained using base lubricant is- CC: EM(1:20), Cutting speed:25.13 m/min, feed: $\mu\text{m}\cdot\text{tooth}^{-1}$, Dc: 50 μm .
3. It was observed that 0.5%wt,0.4%wt,0.3%wt,0.2%wt, and 0.1%wt of CuO reduces the burr sizes by 28.86%,43.7%,66.22%,18.07% and 7.8% respectively in up milling operation while 44.68%,58.85%,79.11%,49.19% and 48.39% respectively in down milling.
4. Optimum parameters at which the best output response obtained using base lubricant is- CC: Cutting speed:25.13 m/min, feed: 6 $\mu\text{m}\cdot\text{tooth}^{-1}$, Dc: 40 μm .
5. 0.3 wt.% CuO, Cutting speed:25.13 m/min, feed: 5 $\mu\text{m}\cdot\text{tooth}^{-1}$, Dc: 40 μm .

6. Further, a comparative analysis of the two cutting fluids i.e., water-based emulsion lubricant and nanofluid with the best results was done. It was found that 0.3% NF reduces the equivalent burr width by 59% and 82% in up and down respectively. Whereas, EM(1:20) decreases the equivalent burr width by 38.11% and 27.87% in up and down respectively

8.2 Contribution

The presented work deals with a critical issue in micromachining. The issue is burr formation and its solution. The literature showed that the high-speed machining and lubrication in machining helped in a reduction in the burr formation. In micromachining, more precisely micromilling the high-speed machining is a difficult job due to small size of the diameter of the end milling tool. Therefore, high rotational velocity is required to move towards high-speed cutting. A high-speed machining center has been developed to achieve the high cutting speed by increasing the spindle speed to a very high level. It was found that the vibration in the high-speed machine was the main issue. The issue has been resolved in the present work and a high-speed micromilling center with maximum amplitude in the vibration of 4 nm is achieved.

Similar to the high-speed cutting lubricating a micromachining process is difficult due to the small size of the tool. It is difficult to approach the tool chip interface for a cutting fluid if it is in liquid form. Therefore, thin lubrication with low viscosity and high thermal capacity is required. Two types of cutting fluids have been developed by the authors and applied to the cutting zone in micromilling process. It is observed that the cutting fluid has shown their effect and burr size has been removed in superalloys. The thesis reveals that it is possible to minimize top burr size up to 70% and 82% using copper oxide nanofluid for titanium and Inconel alloys, respectively.

8.3 Future scope

The experimental investigation in this thesis for evaluating the performance of superalloys viz. Ti6Al4V & Inconel 718 may serve as a foundation for future research in micromachining. Future work suggestions include:

1. Optimization of machining parameters in micromilling for specific superalloys at specific conditions must be defined on standards.
2. Copper oxide nanofluid may be applied to other superalloys to minimize the burr, tool wear and enhance surface roughness.
3. Further, the effects of nanofluid (with nanoparticles containing higher conductivity from copper oxide) need to be explored in micromilling of superalloys.
4. Simulation of top burr formation at dry, MQL and Cryogenic needs to be characterized.

References

1. B.Z. Balázs, N. Geier, M. Takács, and J.P. Davim, "A Review on Micro-Milling: Recent Advances and Future Trends," *International Journal of Advanced Manufacturing Technology*, Springer Science and Business Media Deutschland GmbH, 2021, p 655–684.
2. S.L. Kumar, J. Jerald, ... S.K.-M. and, and U. 2014, A Review on Current Research Aspects in Tool-Based Micromachining Processes, *Taylor Fr.*, Taylor and Francis Inc., 2014, **29**(11–12), p 1291–1337.
3. C. Wang, R. Shao, G. Wang, J. Zhao, Z. Sha, and S. Sun, Controllable Wet Etching of Porous Anodic Alumina toward Highly Ordered Hierarchical Interfaces, *Surf. Coatings Technol.*, Elsevier, 2021, **412**, p 127016.
4. D. Serje, J. Pacheco, and E. Diez, Micromilling Research: Current Trends and Future Prospects, *Int. J. Adv. Manuf. Technol. 2020 1117*, Springer, 2020, **111**(7), p 1889–1916.
5. H. Shizuka, K. Okuda, ... M.N.-A.M., and U. 2011, Study on Surface Roughness in Micro End Milling of Mold Material, *Trans Tech Publ*, n.d.
6. B.Z. Balázs and M. Takács, Experimental Investigation and Optimisation of the Micro Milling Process of Hardened Hot-Work Tool Steel, *Int. J. Adv. Manuf. Technol.*, Springer, 2020, **106**(11–12), p 5289–5305.
7. T. Zhang, Z. Liu, and C. Xu, Influence of Size Effect on Burr Formation in Micro Cutting, *Int. J. Adv. Manuf. Technol.*, Springer London, 2013, **68**(9–12), p 1911–1917.
8. Y. Wang, B. Zou, G.Y.-C. International, and U. 2019, Wear Mechanisms of Ti (C7N3)-Based Cermet Micro-Drill and Machining Quality during Ultra-High Speed Micro-Drilling Multi-Layered PCB Consisting of Copper, *Elsevier*, n.d.
9. "Milling and Turning | Kugler Precision in Salem," n.d., <https://www.kugler-precision.com/en/expertise/milling-and-turning/>. Accessed 8 November 2021.
10. K. Zhu and X. Yu, The Monitoring of Micro Milling Tool Wear Conditions by Wear Area Estimation, *Mech. Syst. Signal Process.*, Academic Press, 2017, **93**, p 80–91.
11. L. Fernández-Robles, L. Sánchez-González, J. Díez-González, M. Castejón-Limas, and H. Pérez, Use of Image Processing to Monitor Tool Wear in Micro Milling, *Neurocomputing*, Elsevier, 2021, **452**, p 333–340.
12. R. Peng, J. Liu, X. Fu, C. Liu, and L. Zhao, Application of Machine Vision Method in Tool Wear Monitoring, *Int. J. Adv. Manuf. Technol. 2021 1163*, Springer, 2021, **116**(3), p 1357–

- 1372, doi:10.1007/S00170-021-07522-4.
13. L. O'Toole, C.W. Kang, and F.Z. Fang, Precision Micro-Milling Process: State of the Art, *Adv. Manuf.*, Shanghai University, 2021, **9**(2), p 173–205, doi:10.1007/S40436-020-00323-0/FIGURES/18.
 14. X. Zhang, T. Yu, P. Xu, and J. Zhao, An Intelligent Sustainability Evaluation System of Micro Milling, *Robot. Comput. Integr. Manuf.*, Pergamon, 2022, **73**, p 102239.
 15. Y. Wu, N. Chen, R. Bian, N. He, Z. Li, and L. Li, Investigations on Burr Formation Mechanisms in Micro Milling of High-Aspect-Ratio Titanium Alloy Ti-6Al-4V Structures, *Int. J. Mech. Sci.*, Pergamon, 2020, **185**, p 105884.
 16. "Micro Reactor Technology Market Professional Survey Report 2019 | PrnewsPrime," n.d., <https://www.prnewsprime.com/2019/09/micro-reactor-technology-market-professional-survey-report-2019/>. Accessed 6 June 2021.
 17. "Printed Circuit Board with Microprozessor Chip - Openclipart," n.d., <https://openclipart.org/detail/296380/printed-circuit-board-with-microprozessor-chip>. Accessed 6 June 2021.
 18. "Tooth Drilling Machine High Resolution Stock Photography and Images - Alamy," n.d., <https://www.alamy.com/stock-photo/tooth-drilling-machine.html>. Accessed 6 June 2021.
 19. E. Behroodi, H. Latifi, Z. Bagheri, E. Ermis, S. Roshani, and M. Salehi Moghaddam, A Combined 3D Printing/CNC Micro-Milling Method to Fabricate a Large-Scale Microfluidic Device with the Small Size 3D Architectures: An Application for Tumor Spheroid Production, *Sci. Reports 2020 101*, Nature Publishing Group, 2020, **10**(1), p 1–14.
 20. X. Wu, M. Du, J. Shen, F. Jiang, Y. Li, and L. Liu, Experimental Research on the Top Burr Formation in Micro Milling, *Int. J. Adv. Manuf. Technol. 2021 11711*, Springer, 2021, **117**(11), p 3477–3486, doi:10.1007/S00170-021-07916-4.
 21. "Helical Gear Manufacturing | AmTech - OEM Supplier Herringbone Gearing," n.d., <https://www.amtechinternational.com/helical-gears-manufacturer-supplier/>. Accessed 20 June 2021.
 22. A. Kale and N. Khanna, A Review on Cryogenic Machining of Super Alloys Used in Aerospace Industry, *Procedia Manuf.*, 2017, **7**, p 191–197.
 23. A. Shokrani, V. Dhokia, and S.T. Newman, Environmentally Conscious Machining of

- Difficult-to-Machine Materials with Regard to Cutting Fluids, *Int. J. Mach. Tools Manuf.*, Elsevier, 2012, **57**, p 83–101, doi:10.1016/j.ijmachtools.2012.02.002.
24. T.B. Sercombe, L.C. Zhang, S. Li, and Y. Hao, Additive Manufacturing of Cp-Ti, Ti-6Al-4V and Ti2448, *Titan. Med. Dent. Appl.*, Woodhead Publishing, 2018, p 303–324.
 25. G. Ul Rehman, S. Husain Imran Jaffery, M. Khan, L. Ali, A. Khan, and S. Ikramullah Butt, Analysis of Burr Formation in Low Speed Micro-Milling of Titanium Alloy (Ti-6Al-4V), *Mech. Sci.*, 2018, **9(2)**, p 231–243.
 26. S. Profile, A. Loureiro, C. Veiga, J.P. Davim, and A.J.R. Loureiro, Properties and Applications of Titanium Alloys: A Brief Review, *researchgate.net*, 2012.
 27. S. Gialanella and A. Malandrucolo, *Aerospace Alloys*, (Cham), Springer International Publishing, 2020, doi:10.1007/978-3-030-24440-8.
 28. A. Nowotnik, Nickel-Based Superalloys, *Ref. Modul. Mater. Sci. Mater. Eng.*, Elsevier, 2016.
 29. G.R. Thellaputta, P.S. Chandra, and C.S.P. Rao, Machinability of Nickel Based Superalloys: A Review, *Mater. Today Proc.*, Elsevier, 2017, **4(2)**, p 3712–3721.
 30. A. Pramanik, Problems and Solutions in Machining of Titanium Alloys, *Int. J. Adv. Manuf. Technol.*, 2014, **70(5–8)**, p 919–928.
 31. V. Bajpai, ... A.K.-I., and undefined 2013, Burr Formation and Surface Quality in High Speed Micromilling of Titanium Alloy (Ti6Al4V), *asmedigitalcollection.asme.org*, 2013, doi:10.1115/MSEC2013-1216.
 32. X. Yang, C.R.L.-M.S. and Technology, and U. 1999, *Machining Titanium and Its Alloys*, Taylor Fr., n.d.
 33. C. Bandapalli, B.M. Sutaria, D.V. Prasad Bhatt, and K.K. Singh, Tool Wear Analysis of Micro End Mills - Uncoated and PVD Coated TiAlN & AlTiN in High Speed Micro Milling of Titanium Alloy - Ti-0.3Mo-0.8Ni, *Procedia CIRP*, Elsevier, 2018, **77**, p 626–629.
 34. “Ultra-Precision and Micromachining | KUGLER Salem,” n.d.
 35. M. Aramesh, S. Montazeri, and S.C. Veldhuis, A Novel Treatment for Cutting Tools for Reducing the Chipping and Improving Tool Life during Machining of Inconel 718, *Wear*, Elsevier, 2018, **414–415**, p 79–88.
 36. M. Anthony Xavier, M. Manohar, P.M. Madhukar, and P. Jeyapandiarajan, Experimental Investigation of Work Hardening, Residual Stress and Microstructure during Machining Inconel 718, *J. Mech. Sci. Technol. 2017 3110*, Springer, 2017, **31(10)**, p 4789–4794,

- doi:10.1007/S12206-017-0926-2.
37. H.A. Kishawy and A. Hosseini, *Machining Difficult-to-Cut Materials*, (Cham), Springer International Publishing, 2019, doi:10.1007/978-3-319-95966-5.
 38. S. Pervaiz, A. Rashid, I. Deiab, and M. Nicolescu, Influence of Tool Materials on Machinability of Titanium- and Nickel-Based Alloys: A Review, *Mater. Manuf. Process.*, Taylor and Francis Inc., 2014, **29**(3), p 219–252.
 39. C.F. Consumption, Development and Evaluation of a Novel Supply System to Reduce Cutting Fluid Consumption and Improve Machining, 2019.
 40. Q. Gao, G. yan Guo, and M. Cai, Wear Mechanism and Experimental Study of a Tool Used for Micro-Milling Single-Crystal Nickel-Based Superalloys, *Int. J. Adv. Manuf. Technol.* **2021 1131**, Springer, 2021, **113**(1), p 117–129, doi:10.1007/S00170-020-06428-X.
 41. X. Lu, Z. Jia, H. Wang, L. Si, Y. Liu, and W. Wu, Tool Wear Appearance and Failure Mechanism of Coated Carbide Tools in Micro-Milling of Inconel 718 Super Alloy, *Ind. Lubr. Tribol.*, Emerald Group Publishing Ltd., 2016, **68**(2), p 267–277.
 42. D. Zhu, X. Zhang, and H. Ding, Tool Wear Characteristics in Machining of Nickel-Based Superalloys, *Int. J. Mach. Tools Manuf.*, Pergamon, 2013, **64**, p 60–77.
 43. M. Imran, P.T. Mativenga, A. Gholinia, and P.J. Withers, Comparison of Tool Wear Mechanisms and Surface Integrity for Dry and Wet Micro-Drilling of Nickel-Base Superalloys, *Int. J. Mach. Tools Manuf.*, Pergamon, 2014, **76**, p 49–60.
 44. SPINDLE SYSTEMS FOR THE DENTAL TECHNOLOGY, n.d.
 45. J. Luo, M. Li, W. Yu, and H. Li, The Variation of Strain Rate Sensitivity Exponent and Strain Hardening Exponent in Isothermal Compression of Ti–6Al–4V Alloy, *Mater. Des.*, Elsevier, 2010, **31**(2), p 741–748.
 46. L. O’Toole, C.W. Kang, and F.Z. Fang, Precision Micro-Milling Process: State of the Art, *Adv. Manuf.*, Shanghai University, 2021, **9**(2), p 173–205, doi:10.1007/S40436-020-00323-0/FIGURES/18.
 47. R. Y, V. K, and J. Mathew, Methodology for Prediction of Sub-Surface Residual Stress in Micro End Milling of Ti-6Al-4V Alloy, *J. Manuf. Process.*, Elsevier, 2021, **62**, p 600–612.
 48. H.H. Zeng, R. Yan, F.Y. Peng, L. Zhou, and B. Deng, An Investigation of Residual Stresses in Micro-End-Milling Considering Sequential Cuts Effect, *Int. J. Adv. Manuf. Technol.*, Springer London, 2017, **91**(9–12), p 3619–3634.

49. J.-C. Su, K.A. Young, K. Ma, S. Srivatsa, J.B. Morehouse, and S.Y. Liang, Modeling of Residual Stresses in Milling, *Int. J. Adv. Manuf. Technol.*, Springer Science and Business Media LLC, 2013, **65**(5–8), p 717–733.
50. W. Khaliq, C. Zhang, M. Jamil, and A.M. Khan, Tool Wear, Surface Quality, and Residual Stresses Analysis of Micro-Machined Additive Manufactured Ti–6Al–4V under Dry and MQL Conditions, *Tribol. Int.*, Elsevier, 2020, **151**, p 106408.
51. C. Bandapalli, K.K. Singh, B.M. Sutaria, and D.V. Bhatt, Experimental Investigation of Top Burr Formation in High-Speed Micro-End Milling of Titanium Alloy, <https://doi.org/10.1080/10910344.2018.1449213>, Taylor & Francis, 2018, **22**(6), p 989–1011.
52. K. Aslantas, L.K.H. Alatrushi, F. Bedir, Y. Kaynak, and N. Yilmaz, An Experimental Analysis of Minimum Chip Thickness in Micro-Milling of Two Different Titanium Alloys:, <https://doi.org/10.1177/0954405420933098>, SAGE PublicationsSage UK: London, England, 2020, **234**(12), p 1486–1498.
53. T. Özel, A. Olleak, and T. Thepsonthi, Micro Milling of Titanium Alloy Ti-6Al-4V: 3-D Finite Element Modeling for Prediction of Chip Flow and Burr Formation, *Prod. Eng.*, Springer Verlag, 2017, **11**(4–5), p 435–444.
54. E. Trent and P. Wright, “Metal Cutting,” 1956, <https://www.academia.edu>. Accessed 5 June 2021.
55. D. Hammond, D.M. Dimitrov Co-supervisor, and N.F. Treurnicht, “An Investigation of the Impact of Selected Cooling Strategies on Milling of Difficult-to-Cut Materials with an Emphasis on Titanium Alloys and Hardened Steel,” 2013, <http://scholar.sun.ac.za>. Accessed 5 June 2021.
56. J.C. Aurich, D. Dornfeld, P.J. Arrazola, V. Franke, L. Leitz, and S. Min, Burrs-Analysis, Control and Removal, *CIRP Ann. - Manuf. Technol.*, 2009, **58**(2), p 519–542.
57. A. Aramcharoen and P.T. Mativenga, Size Effect and Tool Geometry in Micromilling of Tool Steel, *Precis. Eng.*, 2009, **33**(4), p 402–407.
58. L.K. Gillespie and P.T. Blotter, The Formation and Properties of Machining Burrs, *J. Eng. Ind.*, 2010, **98**(1), p 66.
59. K. Nakayama and M. Arai, Burr Formation in Metal Cutting, *CIRP Ann. - Manuf. Technol.*, 1987, **36**(1), p 33–36.

60. M. Hashimura, J. Hassamontr, and D.A. Dornfeld, Effect of In-Plane Exit Angle and Rake Angles on Burr Height and Thickness in Face Milling Operation, *J. Manuf. Sci. Eng. Trans. ASME*, American Society of Mechanical Engineers Digital Collection, 1999, **121**(1), p 13–19.
61. T.R. Lin, Experimental Study of Burr Formation and Tool Chipping in the Face Milling of Stainless Steel, *J. Mater. Process. Technol.*, 2000, **108**(1), p 12–20.
62. G.L. Chern, Experimental Observation and Analysis of Burr Formation Mechanisms in Face Milling of Aluminum Alloys, *Int. J. Mach. Tools Manuf.*, 2006, **46**(12–13), p 1517–1525.
63. Z. Kou, Y. Wan, Y. Cai, X. Liang, and Z. Liu, Burr Controlling in Micro Milling with Supporting Material Method, *Procedia Manuf.*, 2015, **1**, p 501–511, doi:10.1016/j.promfg.2015.09.015.
64. P. Kumar, M. Kumar, V. Bajpai, and N.K. Singh, Recent Advances in Characterization, Modeling and Control of Burr Formation in Micro-Milling, *Manuf. Lett.*, 2017, **13**, p 1–5.
65. M.J. Chen, H.B. Ni, Z.J. Wang, and Y. Jiang, Research on the Modeling of Burr Formation Process in Micro-Ball End Milling Operation on Ti–6Al–4V, *Int. J. Adv. Manuf. Technol. 2012 629*, Springer, 2012, **62**(9), p 901–912, doi:10.1007/S00170-011-3865-6.
66. T. Özel, A. Olleak, and T. Thepsonthi, Micro Milling of Titanium Alloy Ti-6Al-4V: 3-D Finite Element Modeling for Prediction of Chip Flow and Burr Formation, *Prod. Eng.*, Springer Verlag, 2017, **11**(4–5), p 435–444, doi:10.1007/S11740-017-0761-4/FIGURES/10.
67. A. Davoudinejad, P. Parenti, and M. Annoni, 3D Finite Element Prediction of Chip Flow, Burr Formation, and Cutting Forces in Micro End-Milling of Aluminum 6061-T6, *Front. Mech. Eng.*, 2017, **12**(2), p 203–214.
68. A.K. Yadav, M. kumar, V. Bajpai, N.K. Singh, and R.K. Singh, FE Modeling of Burr Size in High-Speed Micro-Milling of Ti6Al4V, *Precis. Eng.*, 2017, **49**, p 287–292.
69. W. Chen, X. Teng, L. Zheng, W. Xie, and D. Huo, Burr Reduction Mechanism in Vibration-Assisted Micro Milling, *Manuf. Lett.*, Elsevier, 2018, **16**, p 6–9.
70. X. Zhang, N. Chen, J. Wu, J. Wei, B. Yan, L. Li, and N. He, Study on the Burr Formation Process in Micro-Milling of High Aspect Ratio Structures, *Int. J. Adv. Manuf. Technol.*, Springer Science and Business Media Deutschland GmbH, 2021, **115**(1–2), p 433–447, doi:10.1007/S00170-021-07203-2/FIGURES/20.

71. E. Kuram, B. Ozcelik, E. Demirbas, and E. Şık, "Effects of the Cutting Fluid Types and Cutting Parameters on Surface Roughness and Thrust Force," *iaeng.org*, n.d.
72. J.M. Vieira, A.R. Machado, and E.O. Ezugwu, Performance of Cutting Fluids during Face Milling of Steels, *J. Mater. Process. Technol.*, 2001, **116**(2–3), p 244–251.
73. X. Zhang, R. Shivpuri, A.S.-J. of M. Processing, and U. 2014, Role of Phase Transformation in Chip Segmentation during High Speed Machining of Dual Phase Titanium Alloys, *Elsevier*, n.d., 2021-06-03.
74. V.P. Astakhov, "Cutting Fluids (Coolants) and Their Application in Deep-Hole Machining," *viktorastakhov.tripod.com*, n.d., 2021-06-03.
75. S. Debnath, M. Anwar, A. Pramanik, and A.K. Basak, Nanofluid-Minimum Quantity Lubrication System in Machining: Towards Clean Manufacturing, *Sustainable Manufacturing*, Elsevier, 2021, p 109–135.
76. S. Paul and P. Kumar Pal, "STUDY OF SURFACE QUALITY DURING HIGH SPEED MACHINING USING ECO-FRIENDLY CUTTING FLUID," *mech-ing.com*, n.d.
77. Y. Yildiz, M.N.-I.J. of M.T. And, and U. 2008, A Review of Cryogenic Cooling in Machining Processes, *Elsevier*, n.d., 2021-06-17.
78. G. Krolczyk, R. Maruda, ... J.K.-J. of C., and U. 2019, Ecological Trends in Machining as a Key Factor in Sustainable Production—a Review, *Elsevier*, n.d., 2021-06-17.
79. M. Groover, "Fundamentals of Modern Manufacturing: Materials, Processes, and Systems," 2020.
80. M.E.B.-J. of materials processing technology and undefined 1996, Cutting Fluids: Part I. Characterisation, *Elsevier*, n.d., <https://www.sciencedirect.com/science/article/pii/0924013695018921>. Accessed 17 June 2021.
81. S. Lawal, I. Choudhury, Y.N.-I.J. of Machine, and U. 2012, Application of Vegetable Oil-Based Metalworking Fluids in Machining Ferrous Metals—a Review, *Elsevier*, n.d., 2021-06-01.
82. R.S. Revuru, N.R. Posinasetti, V.R. Vsn, and M. Amrita, Application of Cutting Fluids in Machining of Titanium Alloys—a Review, *Int. J. Adv. Manuf. Technol.*, Springer London, 2017, **91**(5–8), p 2477–2498, doi:10.1007/s00170-016-9883-7.
83. S. Saha, S. Deb, P.B.-J. of M. Processing, and U. 2020, An Analytical Approach to Assess the

- Variation of Lubricant Supply to the Cutting Tool during MQL Assisted High Speed Micromilling, *Elsevier*, n.d., 2021-06-17.
84. S. Debnath, M.M. Reddy, and Q.S. Yi, "Environmental Friendly Cutting Fluids and Cooling Techniques in Machining: A Review," *Journal of Cleaner Production*, Elsevier Ltd, 2014, p 33–47.
 85. M. Stanford, P.M. Lister, C. Morgan, and K.A. Kibble, Investigation into the Use of Gaseous and Liquid Nitrogen as a Cutting Fluid When Turning BS 970-80A15 (En32b) Plain Carbon Steel Using WC-Co Uncoated Tooling, *J. Mater. Process. Technol.*, Elsevier, 2009, **209**(2), p 961–972.
 86. W.B.-T. international and U. 1998, Lubricants and the Environment, *Elsevier*, n.d.
 87. Y.M. Shashidhara and S.R. Jayaram, Vegetable Oils as a Potential Cutting Fluid-An Evolution, *Tribol. Int.*, Elsevier, 2010, **43**(5–6), p 1073–1081.
 88. E. Benedicto, D. Carou, E.R.-P. Engineering, and U. 2017, Technical, Economic and Environmental Review of the Lubrication/Cooling Systems Used in Machining Processes, *Elsevier*, n.d.
 89. E.O. Ezugwu, J. Bonney, R.B. DA SILVA, A.R. Machado, and E. Ugwoha, High Productivity Rough Turning of Ti-6al-4v Alloy, with Flood and High-Pressure Cooling, *Tribol. Trans.*, 2009, **52**(3), p 395–400.
 90. E.O. Ezugwu, J. Bonney, R.B. DA SILVA, A.R. Machado, and E. Ugwoha, High Productivity Rough Turning of Ti-6al-4v Alloy, with Flood and High-Pressure Cooling, *Tribol. Trans.*, Taylor & Francis Group , 2009, **52**(3), p 395–400, doi:10.1080/10402000802687866.
 91. I. Ucun, K. Aslantasx, and F. Bedir, The Effect of Minimum Quantity Lubrication and Cryogenic Pre-Cooling on Cutting Performance in the Micro Milling of Inconel 718, *Proc. Inst. Mech. Eng. Part B J. Eng. Manuf.*, 2015, **229**(12), p 2134–2143.
 92. M. Perçin, K. Aslantas, I. Ucun, Y. Kaynak, and A. Çicek, Micro-Drilling of Ti-6Al-4V Alloy: The Effects of Cooling/Lubricating, *Precis. Eng.*, 2016, **45**, p 450–462.
 93. D. Biermann and M. Steiner, "Analysis of Micro Burr Formation in Austenitic Stainless Steel X5CrNi18-10," *Procedia CIRP*, 2012, p 97–102.
 94. E. Vazquez, J. Gomar, J. Ciurana, and C.A. Rodríguez, Analyzing Effects of Cooling and Lubrication Conditions in Micromilling of Ti6Al4V, *J. Clean. Prod.*, 2015, **87**(C), p 906–913.

95. C.H. Lauro, L.C. Brandão, S.L.M.R. Filho, and J.P. Davim, Behaviour of a Biocompatible Titanium Alloy during Orthogonal Micro-Cutting Employing Green Machining Techniques, *Int. J. Adv. Manuf. Technol.*, The International Journal of Advanced Manufacturing Technology, 2018, **98**(5–8), p 1573–1589.
96. K. Aslantas, A. ?icek, I. Ucun, M. Percin, and H.E. Hopa, “Performance Evaluation of a Hybrid Cooling-Lubrication System in Micro-Milling of Ti6Al4V Alloy,” *Procedia CIRP*, 2016, p 492–495.
97. S. Mekid, T. Laoui, and F. Patel, Exploring a Manufacturing Route to Produce WC-Based Micro-Cutting Tool With Nanostructured Material, *ASME 2011 Int. Mech. Eng. Congr. Expo. IMECE 2011*, American Society of Mechanical Engineers Digital Collection, 2012, **11**, p 171–176.
98. J. Chae, S.S. Park, and T. Freiheit, Investigation of Micro-Cutting Operations, *Int. J. Mach. Tools Manuf.*, Pergamon, 2006, **46**(3–4), p 313–332.
99. E. Kuram and B. Ozcelik, *Micro Milling*, Springer, Berlin, Heidelberg, 2014, p 325–365, doi:10.1007/978-3-642-45176-8_12.
100. J.C. Ziegert, An Ultrahigh Speed Spindle for Micro-Milling Mechanical Metamaterials View Project Artifact for Large-Scale Metrology View Project, n.d.
101. V. Bajpai, A.K. Kushwaha, and R.K. Singh, Burr Formation and Surface Quality in High Speed Micromilling of Titanium Alloy (Ti6Al4V), 2013, p V002T03A017.
102. S. Jahanmir, M.J. Tomaszewski, and H. Heshmat, “Ultra High-Speed Micro-Milling of Aluminum Alloy,” 2015.
103. P. Fallböhmer, C. Rodríguez, T. Özel, T.A.-J. of Materials, and U. 2000, High-Speed Machining of Cast Iron and Alloy Steels for Die and Mold Manufacturing, *Elsevier*, n.d., 2021-06-20.
104. R. Kuppuswamy and A. Yui, High-Speed Micromachining Characteristics for the NiTi Shape Memory Alloys, *Int. J. Adv. Manuf. Technol.*, 2017, **93**(1–4), p 11–21.
105. D. Huo and K. Cheng, A Dynamics-Driven Approach to the Design of Precision Machine Tools for Micro-Manufacturing and Its Implementation Perspectives, *Proc. Inst. Mech. Eng. Part B J. Eng. Manuf.*, 2008, **222**(1), p 1–13.
106. C. Brecher, P. Utsch, R. Klar, C.W.-I.J. of Machine, and U. 2010, Compact Design for High Precision Machine Tools, *Elsevier*, n.d.

107. H. Möhring, C. Brecher, E. Abele, J.F.-C. Annals, and U. 2015, Materials in Machine Tool Structures, *Elsevier*, n.d.
108. T. Chen, Y. Chen, ... M.H.-A. in M., and undefined 2016, Design Analysis of Machine Tool Structure with Artificial Granite Material, *journals.sagepub.com*, SAGE Publications Inc., 2016, **8**(7), p 1–14, doi:10.1177/1687814016656533.
109. ““Comparison of Bearings for the Bearing Choosing... - Google Scholar,” n.d.
110. “Newfangled Solutions Mach3,” n.d., <https://www.machsupport.com/software/mach3/>. Accessed 12 January 2022.
111. M. Kumar and V. Bajpai, Experimental Investigation of Top Burr Formation in High-Speed Micro-Milling of Ti6Al4V Alloy, *Proc. Inst. Mech. Eng. Part B J. Eng. Manuf.*, 2019, p 1–9.
112. A. Shokrani, V. Dhokia, and S.T. Newman, Investigation of the Effects of Cryogenic Machining on Surface Integrity in CNC End Milling of Ti-6Al-4V Titanium Alloy, *J. Manuf. Process.*, 2016.
113. R. M'Saoubi, D. Axinte, S.L. Soo, C. Nobel, H. Attia, G. Kappmeyer, S. Engin, and W.M. Sim, High Performance Cutting of Advanced Aerospace Alloys and Composite Materials, *CIRP Ann. - Manuf. Technol.*, CIRP, 2015, **64**(2), p 557–580, doi:10.1016/j.cirp.2015.05.002.
114. J. Cheng, Y. Jin, J. Wu, X. Wen, Y. Gong, J. Shi, and G. Cai, Experimental Study on a Novel Minimization Method of Top Burr Formation in Micro-End Milling of Ti-6Al-4V, *Int. J. Adv. Manuf. Technol.*, 2016, **86**(5–8), p 2197–2217.
115. P. Kumar, V. Bajpai, and R. Singh, Burr Height Prediction of Ti6Al4V in High Speed Micro-Milling by Mathematical Modeling, *Manuf. Lett.*, 2017, **11**, p 12–16.
116. X. Zhang, T. Yu, W. Wang, and J. Zhao, Improved Analytical Prediction of Burr Formation in Micro End Milling, *Int. J. Mech. Sci.*, Elsevier Ltd, 2019, **151**(December 2018), p 461–470, doi:10.1016/j.ijmecsci.2018.12.005.
117. F.B. De Oliveira, A.R. Rodrigues, R.T. Coelho, and A.F. De Souza, Size Effect and Minimum Chip Thickness in Micromilling, *Int. J. Mach. Tools Manuf.*, 2015, **89**, p 39–54.
118. “Burrs - Analysis, Control and Removal,” *Burrs - Analysis, Control and Removal*, 2010.
119. <https://www.iitism.ac.in/~vivek/varnica.pdf>
120. L.K. Gillespie and P.T. Blotter, The Formation and Properties of Machining Burrs, *J. Manuf. Sci. Eng. Trans. ASME*, 1976, **98**(1), p 66–74.

121. S.H.I. Jaffery, M. Khan, L. Ali, and P.T. Mativenga, Statistical Analysis of Process Parameters in Micromachining of Ti-6Al-4V Alloy, *Proc. Inst. Mech. Eng. Part B J. Eng. Manuf.*, 2016, **230**(6), p 1017–1034, doi:10.1177/0954405414564409.
122. M. Sima and T. Özel, Modified Material Constitutive Models for Serrated Chip Formation Simulations and Experimental Validation in Machining of Titanium Alloy Ti-6Al-4V, *Int. J. Mach. Tools Manuf.*, Pergamon, 2010, **50**(11), p 943–960.
123. X. Wu, M. Du, J. Shen, F. Jiang, Y. Li, and L. Liu, Experimental Research on the Top Burr Formation in Micro Milling, *Int. J. Adv. Manuf. Technol.*, Springer Science and Business Media Deutschland GmbH, 2021.
124. L. Chen, D. Deng, G. Pi, X. Huang, and W. Zhou, Burr Formation and Surface Roughness Characteristics in Micro-Milling of Microchannels, *Int. J. Adv. Manuf. Technol.*, 2020, **111**(5–6), p 1277–1290.
125. H.W. Park, S.Y. Liang, and G.W. Woodruff, “Analysis of the Scale Effect for Microscale Machine Tools,” *asmedigitalcollection.asme.org*, n.d., <https://proceedings.asmedigitalcollection.asme.org>. Accessed 11 April 2021.
126. S. Nadimi, B. Oliaei, and Y. Karpas, Influence of Tool Wear on Machining Forces and Tool Deflections during Micro Milling, *Int. J. Adv. Manuf. Technol.*, Springer-Verlag London Ltd, 2016, **84**(9–12), p 1963–1980, doi:10.1007/s00170-015-7744-4.
127. K.K. Singh and R. Singh, Chatter Stability Prediction in High-Speed Micromilling of Ti6Al4V via Finite Element Based Microend Mill Dynamics, *Adv. Manuf.*, Shanghai University Press, 2018, **6**(1), p 95–106.
128. R. Mittal, S. Kulkarni, R.S.-I.J. of Mechanical, and undefined 2018, Characterization of Lubrication Sensitivity on Dynamic Stability in High-Speed Micromilling of Ti-6Al-4V via a Novel Numerical Scheme, *Elsevier*, n.d., <https://www.sciencedirect.com/science/article/pii/S0020740318304752>. Accessed 11 April 2021.
129. J. Ning and S.Y. Liang, A Comparative Study of Analytical Thermal Models to Predict the Orthogonal Cutting Temperature of AISI 1045 Steel, *Springer*, Springer London, 2019, **102**(9–12), p 3109–3119, doi:10.1007/s00170-019-03415-9.
130. G. Kiswanto, D. Zariatn, T.K.-J. of M. Processes, and undefined 2014, The Effect of Spindle Speed, Feed-Rate and Machining Time to the Surface Roughness and Burr Formation of Aluminum Alloy 1100 in Micro-Milling Operation, *Elsevier*, n.d.,

- <https://www.sciencedirect.com/science/article/pii/S1526612514000450>. Accessed 11 April 2021.
131. R.W. Maruda, G.M. Krolczyk, M. Michalski, P. Nieslony, and S. Wojciechowski, Structural and Microhardness Changes After Turning of the AISI 1045 Steel for Minimum Quantity Cooling Lubrication, *J. Mater. Eng. Perform.*, n.d., **26**, doi:10.1007/s11665-016-2450-4.
 132. V. Kizhakken and J. Mathew, Modeling of Burr Thickness in Micro-End Milling of Ti6Al4V, *Proc. Inst. Mech. Eng. Part B J. Eng. Manuf.*, SAGE Publications Ltd, 2019, **233**(4), p 1087–1102.
 133. L.G.-P. Engineering and undefined 1979, Deburring Precision Miniature Parts, *Elsevier*, n.d., <https://www.sciencedirect.com/science/article/pii/0141635979900990>. Accessed 11 April 2021.
 134. A. Sidpara, Experimental and Theoretical Investigation into Simultaneous Deburring of Microchannel and Cleaning of the Cutting Tool in Micromilling, *Artic. Proc. Inst. Mech. Eng. Part B J. Eng. Manuf.*, SAGE Publications Ltd, 2018, **233**(7), p 1761–1771, doi:10.1177/0954405418798864.
 135. R. Lekkala, V. Bajpai, R.K. Singh, and S.S. Joshi, “Characterization and Modeling of Burr Formation in Micro-End Milling,” *Precision Engineering*, 2011, p 625–637.
 136. S.A. Niknam and V. Songmene, Factors Governing Burr Formation during High-Speed Slot Milling of Wrought Aluminum Alloys, *J. Eng. Manuf.*, 2013, **227**(8), p 1165–1179.
 137. R. Piquard, A. d’Acunto, and D. Dudzinski, Study of Burr Formation and Phase Transformation during Micro-Milling of NiTi Alloys, 2014, <https://au-193-34.rev.ensam.fr/handle/10985/10270>. Accessed 11 April 2021.
 138. F. Wang, J. Zhao, A. Li, N. Zhu, and J. Zhao, Three-Dimensional Finite Element Modeling of High-Speed End Milling Operations of Ti-6Al-4V, *Proc. Inst. Mech. Eng. Part B J. Eng. Manuf.*, SAGE Publications Ltd, 2014, **228**(6), p 893–902.
 139. M.J. Chen, H.B. Ni, Z.J. Wang, and Y. Jiang, Research on the Modeling of Burr Formation Process in Micro-Ball End Milling Operation on Ti-6Al-4V, *Springer*, 2012, **62**(9–12), p 901–912, doi:10.1007/s00170-011-3865-6.
 140. S. Oliaei, Y.K.-P. Engineering, and undefined 2017, Built-up Edge Effects on Process Outputs of Titanium Alloy Micro Milling, *Elsevier*, n.d., <https://www.sciencedirect.com/science/article/pii/S0141635916302975>. Accessed 11 April 2021.

141. S.L. Ko and S.W. Park, "Development of an Effective Measurement System for Burr Geometry," *Proceedings of the Institution of Mechanical Engineers, Part B: Journal of Engineering Manufacture*, 2006, p 507–512.
142. L. Gillespie, Burrs Produced by End Milling, 1976, <https://www.osti.gov/biblio/7259917>. Accessed 11 April 2021.
143. K. Vipindas, & B. Kuriachen, and J. Mathew, Investigations into the Effect of Process Parameters on Surface Roughness and Burr Formation during Micro End Milling of Ti-6AL-4V, *Springer*, Springer London, 2019, **100**(5–8), p 1207–1222, doi:10.1007/s00170-016-9210-3.
144. D. Biermann, M.S.-P. Cirp, and undefined 2012, Analysis of Micro Burr Formation in Austenitic Stainless Steel X5CrNi18-10, *Elsevier*, n.d., <https://www.sciencedirect.com/science/article/pii/S2212827112001904>. Accessed 11 April 2021.
145. H. Hassanpour, M.H. Sadeghi, H. Rezaei, and A. Rasti, Experimental Study of Cutting Force, Microhardness, Surface Roughness, and Burr Size on Micromilling of Ti6Al4V in Minimum Quantity Lubrication, *Mater. Manuf. Process.*, Taylor and Francis Inc., 2016, **31**(13), p 1654–1662.
146. "Azuddin M, Abdullah W. A Study on Surface Roughness... - Google Scholar," n.d., available: 2021-04-11.
147. H.B. Kulkarni, M.M. Nadakatti, S.C. Kulkarni, and R.M. Kulkarni, Investigations on Effect of Nanofluid Based Minimum Quantity Lubrication Technique for Surface Milling of Al7075-T6 Aerospace Alloy, *Mater. Today Proc.*, 2019.
148. B. Sen, M. Mia, G.M. Krolczyk, U.K. Mandal, and S.P. Mondal, "Eco-Friendly Cutting Fluids in Minimum Quantity Lubrication Assisted Machining: A Review on the Perception of Sustainable Manufacturing," *International Journal of Precision Engineering and Manufacturing - Green Technology*, 2019.
149. L. Sterle, D. Mallipeddi, P. Krajnik, F.P.-P. CIRP, and U. 2020, The Influence of Single-Channel Liquid CO₂ and MQL Delivery on Surface Integrity in Machining of Inconel 718, *Elsevier*, n.d., 2021-03-26.
150. R. Manimaran, K. Palaniradja, N. Alagumurthi, S. Sendhilnathan, and J. Hussain, Preparation and Characterization of Copper Oxide Nanofluid for Heat Transfer Applications, *Appl. Nanosci.*, Springer Nature, 2014, **4**(2), p 163–167,

- doi:10.1007/s13204-012-0184-7.
151. R. Zhou, S. Fu, H. Li, D. Yuan, B. Tang, and G. Zhou, Experimental Study on Thermal Performance of Copper Nanofluids in a Miniature Heat Pipe Fabricated by Wire Electrical Discharge Machining, *Appl. Therm. Eng.*, Elsevier Ltd, 2019, **160**, p 113989.
 152. F. Pashmforoush and R. Delir Bagherinia, Influence of Water-Based Copper Nanofluid on Wheel Loading and Surface Roughness during Grinding of Inconel 738 Superalloy, *J. Clean. Prod.*, Elsevier Ltd, 2018, **178**, p 363–372.
 153. S. Yi, J. Li, J. Zhu, X. Wang, J. Mo, and S. Ding, Investigation of Machining Ti-6Al-4V with Graphene Oxide Nanofluids: Tool Wear, Cutting Forces and Cutting Vibration, *J. Manuf. Process.*, Elsevier Ltd, 2020, **49**, p 35–49.
 154. J.S. Nam, P.H. Lee, and S.W. Lee, Experimental Characterization of Micro-Drilling Process Using Nanofluid Minimum Quantity Lubrication, *Int. J. Mach. Tools Manuf.*, Pergamon, 2011, **51**(7–8), p 649–652.
 155. J.S. Kim, J.W. Kim, and S.W. Lee, Experimental Characterization on Micro-End Milling of Titanium Alloy Using Nanofluid Minimum Quantity Lubrication with Chilly Gas, *Int. J. Adv. Manuf. Technol.*, Springer London, 2017, **91**(5–8), p 2741–2749, doi:10.1007/s00170-016-9965-6.
 156. A.S. Kumar, S. Deb, and S. Paul, Tribological Characteristics and Micromilling Performance of Nanoparticle Enhanced Water Based Cutting Fluids in Minimum Quantity Lubrication, *J. Manuf. Process.*, Elsevier Ltd, 2020, **56**, p 766–776.
 157. A. Haashir, T. Debnath, and P.K. Patowari, A Comparative Assessment of Micro Drilling in Boron Carbide Using Ultrasonic Machining, *Mater. Manuf. Process.*, Taylor and Francis Inc., 2020, **35**(1), p 86–94, doi:10.1080/10426914.2019.1697447.
 158. Ç.V. Yıldırım, M. Sarıkaya, T. Kivak, and Ş. Şirin, The Effect of Addition of HBN Nanoparticles to Nanofluid-MQL on Tool Wear Patterns, Tool Life, Roughness and Temperature in Turning of Ni-Based Inconel 625, *Tribol. Int.*, 2019.
 159. İ. Ucun, K. Aslantaş, and F. Bedir, The Effect of Minimum Quantity Lubrication and Cryogenic Pre-Cooling on Cutting Performance in the Micro Milling of Inconel 718, *Proc. Inst. Mech. Eng. Part B J. Eng. Manuf.*, SAGE Publications Ltd, 2015, **229**(12), p 2134–2143, doi:10.1177/0954405414546144.
 160. K. Aslantas and A. Çiçek, The Effects of Cooling/Lubrication Techniques on Cutting Performance in Micro-Milling of Inconel 718 Superalloy, *Procedia CIRP*, Elsevier, 2018,

77, p 70–73.

161. Ş. Şirin and T. Kivak, Performances of Different Eco-Friendly Nanofluid Lubricants in the Milling of Inconel X-750 Superalloy, *Tribol. Int.*, Elsevier Ltd, 2019, **137**, p 180–192.

Appendix: 1

Matlab code for the measurement of images

Note: This code is not generated by the candidate and it is borrowed by unknown source.

Acknowledgement: Unknown

```
function grabit(fname);
%GRABIT Extracts data points from an image file.
%
% GRABIT starts a GUI program for extracting data from an image file.
% It is capable of reading in BMP, JPG, TIF, and GIF files (anything that
% is readable by IMREAD). Multiple data sets can be extracted from a
% single image file, and the data is saved as an n-by-2 matrix variable in
% the workspace. It can also be renamed and saved as a MAT file.
%
% Following steps should be taken:
% 1. Load the image file.
% 2. Calibrate axes dimensions. You will be prompted to select 4 points
% on the image.
% 3. Grab points by clicking on points. Right-click to delete a point.
% Image can be zoomed during this stage.
% 4. Multiple data sets will remain in memory so long as the GUI is open.
% Variables can be renamed, saved to file, or edited in Array Editor.
%
% This code will also work for extracting data points from a tilted or a
% skewed image (even upside-down or mirrored). The calibration stage
% ensures that the imperfect orientation or quality of the image is
% accounted for.
%
% The types of files that will most likely work are BMP, JPG, TIF, and
% GIF (up to 8-bit) files. Basically, any format supported by the IMREAD
% is accepted.
%% GRABIT(FILENAME) will start the GUI program and open the image file
% FILENAME.
%
```

```
% Type GRABIT('-sample') to load a sample image.
%% Here are a few pointers when creating (saving) the image files:
% 1. Use RGB format.
% 2. For TIF files, use no compression, or PACKBITS compression.
% 3. Make sure the extension (*.bmp, *.jpg, *.tif, *.gif) agrees with the file
% forma
% VERSIONS:
% v1.0 - first version
% v1.1 - use imshow instead of image (takes care of colormap)
% v1.5 - convert to a GUI version
% v1.6 - added functionality to open a file from the command window and embedded a sample image
file to the function
%
% Created in Matlab R13. Tested in R13 & R14SP1
%
% Copyright 2003
% Jiro Doke
% Initialize
set(0, 'ShowHiddenHandles', 'on');

bgcolor = [1 1 .8];

%% close existing windows
im = findobj('type', 'figure', 'name', 'Grabit');
if ishandle(im)
    close(im);
end

im = figure;
set(im, 'units', 'normalized', ...
    'outerposition', [.01 .05 .98 .95], ...
    'doublebuffer', 'on', ...
    'name', 'Grabit', ...
    'numbertitle', 'off', ...
```

```
'menubar', 'none', ...
'color', bgcolor, ...
'defaultUicontrolUnits', 'normalized', ...
'defaultUicontrolBackgroundColor', [0.8 0.8 0.8], ...
'defaultUicontrolFontname', 'Verdana', ...
'defaultUicontrolInterruptible', 'off', ...
'defaultUicontrolBusyAction', 'cancel', ...
'defaultAxesUnits', 'normalized', ...
'pointershapedata', zoomPointer, ...
'pointershapehotspot', [8 8];
uicontrol('style', 'frame', ...
'position', [.01 .895 .8 .1], ...
'backgroundcolor', bgcolor);
uicontrol('style', 'pushbutton', ...
'string', 'Load Image...', ...
'callback', @LoadImage, ...
'position', [0.02 0.95 0.1 0.04], ...
'tag', 'Load Image Btn');
uicontrol('style', 'edit', ...
'string', '', ...
'position', [0.13 0.95 0.67 0.04], ...
'horizontalalignment', 'left', ...
'enable', 'inactive', ...
'tag', 'Image File Loc');
uicontrol('style', 'pushbutton', ...
'string', 'Calibrate', ...
'callback', @CalibrateImage, ...
'position', [0.02 0.9 0.15 0.04], ...
'enable', 'off', ...
'tag', 'Calibrate Image Btn');
uicontrol('style', 'pushbutton', ...
'string', 'Grab Points', ...
'fontweight', 'bold', ...
'callback', @GrabPoints, ...
```

```
'position', [0.19 0.9 0.15 0.04], ...
'enable', 'off', ...
'tag', 'Grab Points Btn');
uicontrol('style', 'listbox', ...
'callback', @SelectVariable, ...
'position', [0.825 0.12 0.165, 0.6], ...
'backgroundcolor', [.85 .85 .85], ...
'tooltipstring', sprintf('Double-click to edit\nvariable in Array Editor'), ...
'tag', 'Variable List');
uicontrol('style', 'pushbutton', ...
'string', 'Zoom Off', ...
'callback', @ZoomState, ...
'position', [0.36 0.9 0.15 0.04], ...
'enable', 'off', ...
'tag', 'Zoom State Btn');
uicontrol('style', 'text', ...
'string', 'Data in Memory', ...
'position', [.825 .72 .165 .02], ...
'backgroundcolor', bgcolor, ...
'fontweight', 'bold');
uicontrol('style', 'pushbutton', ...
'string', 'Save to file as...', ...
'position', [.825 .08 .165 .03], ...
'callback', @VariableManipulation, ...
'tag', 'SaveAs');
uicontrol('style', 'pushbutton', ...
'string', 'Rename...', ...
'position', [.825 .05 .165 .03], ...
'callback', @VariableManipulation, ...
'tag', 'Rename');
uicontrol('style', 'pushbutton', ...
'string', 'Delete from workspace...', ...
'position', [.825 .02 .165 .03], ...
'callback', @VariableManipulation, ...
```

```
'tag', 'Delete');

ah1 = axes('position', [0.01 0.01 0.8 0.8], ...
'visible', 'off', ...
'handlevisibility', 'on', ...
'tag', 'Image Axis');
axes('position', [.82 .01 .175 .985], ...
'box', 'on', ...
'color', bgcolor, ...
'hittest', 'off', ...
'xtick', [], ...
'ytick', []);
ah2 = axes('position', [0.85 0.8 0.13 0.14], ...
'box', 'on', ...
'handlevisibility', 'callback', ...
'tag', 'Preview Axis');

uicontrol('style', 'text', ...
'string', 'Preview Box', ...
'fontweight', 'bold', ...
'position', [.85 .95 .14 .02], ...
'backgroundcolor', bgcolor);

setappdata(gcf, 'I', []);
setappdata(gcf, 'map', []);
setappdata(gcf, 'savedVars', struct);
showAllVars(struct);

set(gcf, 'handlevisibility', 'callback');
set(0, 'ShowHiddenHandles', 'off');

if nargin == 1 & ischar(fname)
switch lower(fname)
case '-sample'
```

```
fname = SampleImage;
LoadImage([], [], fname);
try;
warning off;
delete(fname);
warning on;
end
otherwise
filename = which(fname);
if ~isempty(filename)
LoadImage([], [], filename);
else
errordlg(sprintf('%s\nnot found.', fname));
return;
end
end
end

function VariableManipulation(obj, edata);

set(0, 'ShowHiddenHandles', 'on');

listboxH = findobj('tag', 'Variable List');
savedVars = getappdata(findobj('type', 'figure', 'name', 'GrabIt'), 'savedVars');
vars = fieldnames(savedVars);
if isempty(vars)
set(0, 'ShowHiddenHandles', 'off');
return;
end
listboxVal = get(listboxH, 'value');
varName = vars{listboxVal};
switch get(obj, 'string');
case 'Save to file as...'
[fname, pname] = uiputfile('* .mat', sprintf('Save "%s" as:', varName), varName);
```

```

if ischar(fname)
[p, fname, e] = fileparts(fname); % strip off the extension
eval(sprintf('%s = savedVars.%s;', fname, varName));
save(fullfile(pname, fname), fname);
end
case 'Rename...'
answer = inputdlg({sprintf('Rename "%s" as:', varName)}, 'Rename...', 1, {varName});
if ~isempty(answer) & ~strcmp(varName, answer{1})
if ~(evalin('base', sprintf('exist("%s", "var")', answer{1}))) & isempty(strmatch(answer{1}, vars,
'exact'))
newVarNames = vars;
newVarNames{listboxVal} = answer{1};
for id = 1:length(vars)
tmp.(newVarNames{id}) = savedVars.(vars{id});
end
savedVars = tmp;
showAllVars(savedVars);
set(listboxH, 'value', listBoxVal);
assignin('base', answer{1}, savedVars.(answer{1}));
evalin('base', sprintf('clear %s;', varName));
else
errordlg('That name is already in use.');
```

```

set(0, 'ShowHiddenHandles', 'off');
return;
end
end
case 'Delete from workspace...'
btn = questdlg(sprintf('Delete "%s" from the workspace?', varName), 'Delete from workspace...', ...
'Yes', 'No', 'No');
switch btn
case 'Yes'
savedVars = rmfield(savedVars, varName);
showAllVars(savedVars);
evalin('base', sprintf('clear %s;', varName));
```



```
case 'No'
end
end

set(0, 'ShowHiddenHandles', 'off');
function SelectVariable(obj, edata);

set(0, 'ShowHiddenHandles', 'on');

sType = get(findobj('type', 'figure', 'name', 'Gragit'), 'SelectionType');
switch sType
case {'normal', 'open'}
savedVars = getappdata(findobj('type', 'figure', 'name', 'Gragit'), 'savedVars');
vars = fieldnames(savedVars);
if isempty(vars)
set(0, 'ShowHiddenHandles', 'off');
return;
end
listVal = get(obj, 'value');
varName = vars{listVal};
% check to see if the stored var is the same as the var in the
% workspace
if evalin('base', sprintf('exist("%s", "var")', varName))
if isnumeric(evalin('base', varName)) & ...
ndims(evalin('base', varName)) == 2

if size(evalin('base', varName)) == size(savedVars.(varName)) & ...
all(evalin('base', varName) == savedVars.(varName))
else % may have been modified in the workspace
btn = questdlg(sprintf('"%s" may have been modified in the workspace (e.g. Array Editor).\nUpdate
the variable?', varName), ...
'Modified Variable', 'Update Workspace', 'Update Gragit', 'Neither', 'Update Gragit');
switch btn
case 'Update Workspace'
```

```
assignin('base', varName, savedVars.(varName));
case 'Update Grabit'
savedVars.(varName) = evalin('base', varName);
setappdata(findobj('type', 'figure', 'name', 'Gorbit'), 'savedVars', savedVars);
showAllVars(savedVars);
set(obj, 'value', listVal);
case 'Neither'
end
end
else
btn = questdlg(sprintf('"%s" in the workspace is different from the one in Grabit.\nUpdate the
workspace variable?', varName), ...
'Wrong Variable', 'Update Workspace', 'Leave Untouched', 'Update Workspace');
switch btn
case 'Update Workspace'
assignin('base', varName, savedVars.(varName));
case 'Leave Untouched'
end
end
else
assignin('base', varName, savedVars.(varName));
end
switch sType
case 'normal'
axes(findobj('tag', 'Preview Axis'));
set(findobj('tag', 'PreviewLine'), 'xdata', savedVars.(varName)(:, 1), ...
'ydata', savedVars.(varName)(:, 2));
axis auto;
case 'open'
try
openvar(varName);
end
end
case 'alt' % right-click
```

```
%use contextmenu
end

set(0, 'ShowHiddenHandles', 'off');

function LoadImage(obj, edata, filename)

set(0, 'ShowHiddenHandles', 'on');

if nargin < 3
    [fname, pathname] = uigetfile({'*.bmp;*.jpg;*.jpeg;*.tif;*.tiff;*.gif', 'Image Files (*.bmp, *.jpg,
*.jpeg, *.tif, *.tiff, *.gif)';
    '*.bpm', 'BPM files (*.bpm)';
    '*.jpg;*.jpeg', 'JPG files (*.jpg, *.jpeg)';
    '*.tif;*.tiff', 'TIFF files (*.tif, *.tiff)';
    '*.gif', 'GIF files (*.gif)';
    '*.*', 'All files (*.*)'}, 'Select an image file');
    if ischar(fname)
        filename = fullfile(pathname, fname);
    else
        set(0, 'ShowHiddenHandles', 'off');
        return;
    end
end

set(findobj('tag', 'Image File Loc'), 'string', filename);

try
    warning off;
    [A, map] = imread(filename);
    warning on;
catch
    errordlg(sprintf('%s', lasterr));
    set(0, 'ShowHiddenHandles', 'off');
```

```
return;
end

if ndims(A) == 3 %some TIFF files have wrong size matrices.
if size(A, 3)>3
A = A(:, :, 1:3);
elseif size(A, 3)<3
error('This is a weird image file...possibly a bad TIFF file...');
set(0, 'ShowHiddenHandles', 'off');
return;
end
end

axes(findobj('tag', 'Preview Axis'));
cla;
line(NaN, NaN, 'color', 'blue', 'linestyle', '-', 'marker', '.', 'tag', 'PreviewLine');
imAxis = findobj('tag', 'Image Axis');
axes(imAxis);cla;
NP = get(gcf, 'nextplot'); % for compatibility with R14
iH = imshow(A, map);
set(gcf, 'nextplot', NP);
set(imAxis, 'tag', 'Image Axis', 'handlevisibility', 'callback');
line(NaN, NaN, 'color', 'red', 'linestyle', 'none', 'marker', '.', 'tag', 'ImageLine');

setappdata(gcf, 'I', A);
setappdata(gcf, 'map', map);
setappdata(gcf, 'CalibVals', []);
set(iH, 'ButtonDownFcn', '');

set(findobj('tag', 'Calibrate Image Btn'), 'string', 'Calibrate', 'enable', 'on');
set(findobj('tag', 'Grab Points Btn'), 'enable', 'off');
set(findobj('tag', 'Zoom State Btn'), 'enable', 'on', 'value', 0, 'string', 'Zoom Off');zoom off;

set(0, 'ShowHiddenHandles', 'off');
```

```

function CalibrateImage(obj, edata)
set(0, 'ShowHiddenHandles', 'on');
if isempty(getappdata(findobj('type', 'figure', 'name', 'GrabIt'), 'I'))
    set(obj, 'enable', 'off');
else
    axes(findobj('tag', 'Image Axis'));
    ht = title('Click on Origin of X-axis', 'fontsize', 20, 'color', 'red');
    [Xxo, Yxo] = ginput(1);
    if isempty(Xxo);set(0, 'ShowHiddenHandles', 'off');return;end;
    set(ht, 'string', 'Click on Maximum value of X-axis');
    [Xxm, Yxm] = ginput(1);
    if isempty(Xxm);set(0, 'ShowHiddenHandles', 'off');return;end;
    set(ht, 'string', 'Click on Origin of Y-axis');
    [Xyo, Yyo] = ginput(1);
    if isempty(Xyo);set(0, 'ShowHiddenHandles', 'off');return;end;
    set(ht, 'string', 'Click on Maximum value of Y-axis');
    [Xym, Yym] = ginput(1);
    if isempty(Xym);set(0, 'ShowHiddenHandles', 'off');return;end;
    set(ht, 'string', '');
    v1 = [Xxm - Xxo; Yxm - Yxo];
    v2 = [Xym - Xyo; Yym - Yyo];
    extreme_values = inputdlg({'Enter the value of the origin of x-axis', ...
    'Enter the value of the maximum of x-axis', 'Enter the value of the origin of y-axis', ...
    'Enter the value of the maximum of y-axis'}, 'Enter values', 1, {' ', ' ', ' ', ' '});
    if isempty(extreme_values) | isempty(extreme_values{1}) | isempty(extreme_values{2}) |
    isempty(extreme_values{3}) | isempty(extreme_values{4})
        error('Cancelled...');
    set(0, 'ShowHiddenHandles', 'off');
    return;
end
try;delete(findobj('tag', 'CalibPoints'));end
line([Xxo, Xxm, Xyo, Xym], [Yxo, Yxm, Yyo, Yym], 'color', 'red', 'marker', '*', 'markersize', 20,
'linestyle', 'none', ...
'tag', 'CalibPoints', ...

```

```
'HitTest', 'off');
Xo = eval(extreme_values{1});
Xm = eval(extreme_values{2});
Yo = eval(extreme_values{3});
Ym = eval(extreme_values{4});
Xlength = Xm - Xo;
Ylength = Ym - Yo;
% the basis vectors in the MATLAB domain
e1 = v1 / Xlength;
e2 = v2 / Ylength;
% rearrange axes
C = [e1 e2] \ [Xyo - Xxo; Yyo - Yxo];
blahX = [Xxo; Yxo] + C(2) * e2; Xxo = blahX(1); Yxo = blahX(2);
blahY = [Xyo; Yyo] - C(1) * e1; Xyo = blahY(1); Yyo = blahY(2);
calib.Xo = Xo;
calib.Xm = Xm;
calib.Yo = Yo;
calib.Ym = Ym;
calib.e1 = e1;
calib.e2 = e2;
calib.Xxo = Xxo;
calib.Yyo = Yyo;
setappdata(findobj('type', 'figure', 'name', 'GrabIt'), 'CalibVals', calib);
set(obj, 'string', 'Re-Calibrate', 'enable', 'on');
set(findobj('tag', 'Grab Points Btn'), 'enable', 'on');
end
set(0, 'ShowHiddenHandles', 'off');
function GrabPoints(obj, edata)
set(0, 'ShowHiddenHandles', 'on');
switch get(obj, 'string')
case 'Grab Points'
calib = getappdata(findobj('type', 'figure', 'name', 'GrabIt'), 'CalibVals');
axes(findobj('tag', 'Image Axis'));
zoom out;
```

```

set(findobj('tag', 'ImageLine'), 'xdata', NaN, 'ydata', NaN);
title({'Grab points by clicking on data points.', 'Right-click to delete previous point.'}, 'fontsize', 12, 'color', 'red');
set(findobj('tag', 'PreviewLine'), 'xdata', NaN, 'ydata', NaN);
set(findobj('tag', 'Preview Axis'), 'xlim', [min([calib.Xo calib.Xm]) max([calib.Xo calib.Xm])], ...
'yylim', [min([calib.Yo calib.Ym]) max([calib.Yo calib.Ym])]);
setappdata(findobj('type', 'figure', 'name', 'Grabit'), 'ImDat', []);
setappdata(findobj('type', 'figure', 'name', 'Grabit'), 'TrueDat', []);
set(findobj('type', 'figure', 'name', 'Grabit'), 'Pointer', 'cross');
set(findobj('type', 'image'), 'ButtonDownFcn', {@ImagePointClick, findobj('tag', 'Image Axis')});
set(obj, 'string', 'Finish Grabbing');
set([findobj('tag', 'Calibrate Image Btn'), ...
findobj('tag', 'Load Image Btn'), ...
findobj('tag', 'SaveAs'), ...
findobj('tag', 'Rename'), ...
findobj('tag', 'Delete')], ...
'enable', 'off');
case 'Finish Grabbing'
try
delete(findobj('type', 'text', 'tag', 'GrabTitle'));
end;
set(findobj('type', 'image'), 'ButtonDownFcn', "");
set(findobj('type', 'figure', 'name', 'Grabit'), 'Pointer', 'arrow');
set(obj, 'string', 'Grab Points');
set([findobj('tag', 'Calibrate Image Btn'), ...
findobj('tag', 'Load Image Btn'), ...
findobj('tag', 'SaveAs'), ...
findobj('tag', 'Rename'), ...
findobj('tag', 'Delete')], ...
'enable', 'on');
if ~isempty(getappdata(findobj('type', 'figure', 'name', 'Grabit'), 'TrueDat'))
savedVars = getappdata(findobj('type', 'figure', 'name', 'Grabit'), 'savedVars');
varNames = fieldnames(savedVars);
varNames{end + 1} = findNextVarName(varNames);

```

```

savedVars.(varNames{end}) = getappdata(findobj('type', 'figure', 'name', 'Grabit'), 'TrueDat');
assignin('base', varNames{end}, savedVars.(varNames{end}));
showAllVars(savedVars);
end
end
set(0, 'ShowHiddenHandles', 'off');
function showAllVars(savedVars)
set(0, 'ShowHiddenHandles', 'on');
varNames = fieldnames(savedVars);
if isempty(varNames)
    listBoxStr = {};
else
    for id = 1:length(varNames)
        [m, n] = size(savedVars.(varNames{id}));
        listBoxStr{id} = sprintf('%s [%dx%d]', varNames{id}, m, n);
    end
end
setappdata(findobj('type', 'figure', 'name', 'Grabit'), 'savedVars', savedVars);
set(findobj('tag', 'Variable List'), 'string', listBoxStr, 'value', length(listBoxStr));
set(0, 'ShowHiddenHandles', 'off');
function newVarName = findNextVarName(varNames)

wsVarNames = evalin('base', 'who');
vars = unique([wsVarNames(:);varNames(:)]);
idx = 1;
while 1
    if isempty(strmatch(sprintf('Data%d', idx), vars, 'exact'))
        newVarName = sprintf('Data%d', idx);
        return;
    else
        idx = idx + 1;
    end
end
function ImagePointClick(obj, edata, ah)

```



```

figH = get(ah, 'Parent');
ImDat = getappdata(figH, 'ImDat');
TrueDat = getappdata(figH, 'TrueDat');
calib = getappdata(figH, 'CalibVals');
xy = get(ah, 'CurrentPoint'); X = xy(1, 1); Y = xy(1, 2);
switch get(figH, 'SelectionType')
    case 'normal'
        ImDat(end + 1, :) = [X, Y];
        TrueDat(end + 1, :) = ([calib.Xo; calib.Yo] + [calib.e1 calib.e2] \ [X - calib.Xxo; Y - calib.Yyo]);
    case 'alt'
        if isempty(ImDat)
            return;
        else
            ImDat(end, :) = [];
            TrueDat(end, :) = [];
        end
    end
end

set(findobj('type', 'line', 'tag', 'PreviewLine'), 'xdata', TrueDat(:, 1), 'ydata', TrueDat(:, 2));
set(findobj('type', 'line', 'tag', 'ImageLine'), 'xdata', ImDat(:, 1), 'ydata', ImDat(:, 2));

setappdata(figH, 'ImDat', ImDat);
setappdata(figH, 'TrueDat', TrueDat);

function ZoomState(obj, edata)

set(0, 'ShowHiddenHandles', 'on');

switch get(obj, 'string')
    case 'Zoom Off'
        set(obj, 'string', 'Zoom On', 'enable', 'on');
        udata.titlestring = get(get(findobj('tag', 'Image Axis'), 'Title'), 'string');
        udata.btnstate = get([findobj('tag', 'Load Image Btn');...

```

```
findobj('tag', 'Calibrate Image Btn');...
findobj('tag', 'Grab Points Btn');...
findobj('tag', 'Variable List');...
findobj('tag', 'SaveAs');...
findobj('tag', 'Rename');...
findobj('tag', 'Delete')], 'enable');
udata.imgstate = get(findobj('type', 'image'), 'ButtonDownFcn');
udata.cursorstate = get(findobj('type', 'figure', 'name', 'GrabIt'), 'Pointer');
set(obj, 'userdata', udata);
set(get(findobj('tag', 'Image Axis'), 'Title'), 'string', 'Zoom In');
set([findobj('tag', 'Load Image Btn');...
findobj('tag', 'Calibrate Image Btn');...
findobj('tag', 'Grab Points Btn');...
findobj('tag', 'Variable List');...
findobj('tag', 'SaveAs');...
findobj('tag', 'Rename');...
findobj('tag', 'Delete')], 'enable', 'off');
set(findobj('type', 'image'), 'ButtonDownFcn', '');
set(findobj('type', 'figure', 'name', 'GrabIt'), 'pointer', 'custom');
zoom on;
case 'Zoom On'
zoom off;
set(obj, 'string', 'Zoom Off', 'enable', 'on');
udata = get(obj, 'userdata');
set(get(findobj('tag', 'Image Axis'), 'Title'), 'string', udata.titlestring);
set([findobj('tag', 'Load Image Btn');...
findobj('tag', 'Calibrate Image Btn');...
findobj('tag', 'Grab Points Btn');...
findobj('tag', 'Variable List');...
findobj('tag', 'SaveAs');...
findobj('tag', 'Rename');...
findobj('tag', 'Delete')], {'enable'}, udata.btnstate);
set(findobj('type', 'image'), 'ButtonDownFcn', udata.imgstate);
set(findobj('type', 'figure', 'name', 'GrabIt'), 'pointer', udata.cursorstate);
```

```
end
```

```
set(0, 'ShowHiddenHandles', 'off');
```

```
function fname = SampleImage;
```

```
str = [71, 73, 70, 56, 57, 97, 16, 2, 202, 1, 247, 0, 0, 0, 0, 0, 128, 0, 0, 0, ...
```

```
59];
```

```
fname = [tempname '.gif'];
```

```
fid = fopen(fname, 'w');
```

```
if fid > 0
```

```
    fwrite(fid, str');
```

```
    fclose(fid);
```

```
else
```

```
    error('Error trying to create sample image.');
```

```
end
```

Appendix: 2
List of publications:

Journal publications

1. **Kumar M** and Bajpai V. Experimental investigation of top burr formation in high-speed micro-milling of Ti6Al4V alloy. Proc Inst Mech Eng Part B J Eng Manuf 2020;234(4):730–738.
2. Yadav, A. **Kumar, M.**, Bajpai, V., Singh, N. K., and Singh, R. K. (2017). FE modeling of burr size in high-speed micro-milling of Ti6Al4V. Precision Engineering, 49, 287-292.
3. Kumar, P., **Kumar, M.**, Bajpai, V., and Singh, N. K. (2017). Recent advances in characterization, modeling and control of burr formation in micro-milling. Manufacturing letters, 13, 1-5.
4. Das, A., Bajpai, V., Shukal, S., Singh, C., **Kumar, M.** and Chandravanshi M. Development of a vibration free machine structure for high-speed micro-milling center. Adv. Man. Tech. (accepted)

Indian Patnet published:

1. A machine structure to reduce vibration of micro-milling machine
Inventors: Vivek Bajpai, Arnab Das, Shashank Shukla, Chitransh Singh, **Mohan Kumar** and Madan Lal Chandravanshi
Application number: 201931049978
Date of filling: 04-12-2019
Date of publication: 24-07-2020